N-Based s-Block Complexes: Synthesis and Application in Catalysis

Alexander C. A. Ried, MSci (Hons)

Thesis submitted to the University of Nottingham for the degree of Doctor of Philosophy

October 2017

Declaration

The work described in this thesis was carried out at the University of Nottingham between October 2013 and March 2017, under the supervision of Dr Deborah L. Kays. All of the work is my own unless stated to the contrary, and has not previously been submitted for any degrees at this or any other university.

Alexander Ried

Abstract

The history of organomagnesium chemistry spans over a century of research and discovery, during which alkaline earth coordination compounds and organometallics have seen more than one renaissance. They have proven valuable synthetic tools, widened our fundamental understanding of inorganic chemistry, and been applied to a growing number of catalytic transformations. Due to s-block bonding behaviour, advances in the latter two areas heavily draw on the stabilisation afforded by sterically demanding ligand systems, commonly featuring *N*-based donor sites. It is the development of such tailored supportive frameworks that has enabled the isolation and study of remarkable s-block species.

Reported herein is the exploration of the s-block chemistry of aminopyridinide and pyridylpyrrolide systems, as well as the conceptualisation of novel benzylanilide and tritylamide frameworks and their utilisation in the same.

Employing external donor entities enabled the isolation of the first heteroleptic alkaline earth halide supported by the above aminopyridinide system (**4**). An analogous pyridylpyrrolide complex (**11**) was synthesised, and the s-block chemistry of such frameworks considerably expanded with potassium compounds **5** and **6**, as well as a series of Ae coordination compounds obtained by transamination (**7**, **8**) and organoelimination reactions (**10**). Interheterocycle torsion angles and *N*-metal bond lengths revealed the pyridylpyrrolides to be a highly flexible set of ligands.

In the quest to synthesise sterically demanding benzylanilines, a facile method for the assembly of sterically congested imines (**13**, **14** and **15**) has been developed. Yields are higher or equal to those afforded in considerably more involved literature procedures. A series of novel proligands (**BzL**$^{1\text{-}4}$) have been synthesised and their s-block chemistry investigated, yielding lithium complex **20**. An array of novel tritylamine proligands (**TrL**$^{2\text{-}7}$) have been synthesised, and their ability to stabilise a series of highly reactive dilithium species (**23**-**27**) demonstrated.

Complex **4** showed considerable activity in the catalytic heterodehydrocoupling of amine-boranes, selectively affording $[Me_2NBH_2]_2$ from $Me_2NH{\bullet}BH_3$ under mild conditions.

Acknowledgements

First and foremost, I would like to thank my supervisor Dr Deborah L. Kays for her continued guidance, support and encouragement. I am grateful not only for the time she took to listen to my thoughts, but also the level of freedom I have been given over the research undertaken. Without the invaluable advice of Dr Ana Geer Chapter IV would not exist; to her and Dr Toby Blundell I am indebted for their guidance and friendship.

My thanks go to the stores and analytical staff of the University of Nottingham and those further afield; Dr William Lewis and Prof. Sandy Blake for X-ray crystallography training and discussions; Dr Huw Williams, Dr Adrienne Davis, Kevin Butler and Shazad Aslam for NMR spectroscopy; Dr Mick Cooper, Graham Coxhill and the NMSF (Swansea) for mass spectrometry as well as Dr Tong Liu and Stephen Boyer (LMU) for elemental analysis.

In the completion of my studies I count myself fortunate to have been surrounded by such fantastic friends and colleagues, my thanks go to past and present members of the Kays group. Whether it be our cheese and wine walks, Friday music sessions, or your tolerance for extravagant experimental procedures, I will treasure the memories that have made my time in B45 & B46 such an enjoyable one. Dr Kevan Grant deserves particular mention not only for his aid in plundering organic chemical supplies, but also in providing invaluable advice pertaining to their correct use, as well as being my partner in crime for lunch time running sessions.

I would like to thank my parents for giving me both the roots of home, and the wings of freedom. No son could ask for more than you have given, it is on your unshakable foundation I have been able to construct a life of happiness. Danke für alles.

The completion of a PhD can, at times, present itself as a seemingly insurmountable task. Whether by virtue of capricious reactions, or the

overwhelming exercise of collating three and a half years of laboratory work into a thesis, those who aim to lay testament to their love of wisdom will necessarily incur varying degrees of tribulations. In these, I have been fortunate to not only have the support of my friends and family, but also draw considerable strength from the outstanding natural beauty and challenges provided by the great outdoors. From Cornish bastions of granite, standing tall above the cauldron of the Atlantic, over Derbyshire with its organic gritstone outcrops and deep dales, to the heights of the magnificent Cullin traverse, the antidote to office stagnation is easily at hand. Lending perspective when needed, no decision left me in a position more anxious to progress than from the ledge of Brown's Eliminate, no journey out of personal lows more difficult than the path back to sunlight from the depths of King Pot, no environment less forgiving than the frozen Hardangervidda plateau. Being alive is not living, knowledge is not wisdom. For these lessons, I owe my unending admiration and awe to a world beyond the confines of civilisation.

Contents

Chapter 1 Introduction to Alkaline Earth Metal Chemistry.....I

1.1. The Beginning of Ae Coordination Chemistry.....3
1.2. Expansion.....5
1.2.1. Ae Cyclopentadienides.....5
1.2.2. Heavy Grignards.....8
1.2.3. Subvalency.....8
1.3. Synthesis of Alkaline Earth Metal Complexes.....13
1.3.1. The Schlenk Equilibrium.....17
1.3.2. Ether Cleavage.....19
1.4. Applications of Group II Complexes.....21
1.4.1. Synthetic Use.....21
1.4.2. Homogeneous Catalysis.....27
1.5. Ligands: The Backbone of Coordination Chemistry.....41

Chapter 2 Silylated Aminopyridines and Pyridylpyrroles.....44

2.1. Silylated Aminopyridines.....45
2.1.1. Results and Discussion.....48
2.1.2. Conclusions and Future Work.....55
2.1.3. Experimental.....57
2.2. Pyridylpyrroles.....61
2.2.1. Results and Discussion.....68
2.2.2. Conclusions and Future Work.....85
2.2.3. Experimental.....86

Chapter 3 Benzylanilines and Tritylamines.....92

3.1. Introduction.....93
3.2. Benzylanilides.....96
3.2.1. Results and Discussion.....99
3.2.2. Experimental.....112
3.3. Tritylamines.....120
3.3.1. Results and Discussion.....122
3.3.2. Experimental.....132
3.4. Conclusions and Future Work.....141

Chapter 4 Catalytic Heterodehydrocoupling of Amine-Boranes.....144

4.1. Introduction.....145
4.1.1. Global Energy Dynamics and Factors of Change.....145
4.1.2. The Hydrogen Energy Economy.....149
4.1.3. Hydrogen Storage.....151
4.1.4. Chemical Hydrides.....158
4.1.5. Principal Feasibility of a Boron Based Energy Carrier.....162
4.1.6. Thermal Dihydrogen Release from Amine-Boranes.....164
4.1.7. Catalytic Heterodehydrocoupling of ABs.....168
4.1.8. The Thermodynamics of Dehydrogenation and Reversibility.....179
4.1.9. AB Recycling.....181
4.2. Results and Discussion.....186
4.2.1. Initial Investigations on Catalytic Dehydrocoupling.....186
4.2.2. Investigations on the Effects of Catalyst Loading, Solvents, etc.....192
4.2.3. Identity of Reaction Intermediates.....205
4.2.4. Observations on a Possible Mechanism.....209
4.3. Conclusions.....212
4.4. Future Work.....213
4.5. Experimental.....215
4.5.1. Standard Procedures for Monitoring by NMR.....215
4.5.2. Standard Procedures for Monitoring by Hydrogen Evolution.....218

Chapter 5 General Experimental.....221

5.1. General Experimental Techniques.....222
5.1.1. Manipulation of Air- and Moisture Sensitive Compounds.....222
5.1.2. Solvents and Reagents.....223
5.2. Physical Measurements.....225
5.2.1. NMR Spectroscopy.....225
5.2.2. Mass Spectrometry.....225
5.2.3. Elemental Microanalysis.....225
5.2.4. Crystallographic Method.....226

List of Abbreviations

AB	Amine-borane
Ad	Adamantyl
Ae	Alkaline earth
aq.	Aqueous
Ar	Aryl
Ar*	2,6-Dibenzhydryl-4-methylbenzyl
$BAr^F{}_4$	Tetrakis(3,5-bis(trifluoromethyl)phenyl)borate
Bpin	Pinacolborane
br.	Broad
CAAC	Cyclic alkyl amino carbene
CCD	Charge coupled device
CHN	Carbon/ hydrogen/ nitrogen content (elemental analysis)
Cp	Cyclopentadienyl
Cp*	1,2,3,4,5-Pentamethylcyclopentadienyl
CSD	Cambridge structural database
CVD	Chemical vapour deposition
Cy	Cyclohexyl
d	Doublet (NMR)
DCM	Dichloromethane
DES	Deep eutectic solvent
DFT	Density functional theory
Dipp	2,6-Diisopropylphenyl
DMF	*N,N*-Dimethylformamide
DMSO	Dimethyl sulfoxide
ee	Enantiomeric excess
EPR	Electron paramagnetic resonance
eq.	Equivalents
ESI	Electrospray ionisation (mass spectrometry)
Et	Ethyl
FD	Field desorption (mass spectrometry)
FLP	Frustrated Lewis pair
HHV	Higher heating value
HMQC	Heteronuclear multiple quantum coherence
^{i}Pr	Isopropyl
J	Coupling constant (NMR)
K_i	Initial rate constant
L	Ligand, usually monoanionic
LDA	Lithiumdiisopropylamide
LHV	Lower heating value
m	Multiplet (NMR)
m	Meta

MAS	Magical angle spinning
Me	Methyl
Mes	Mesityl, 2,4,6-$Me_3C_6H_2$
Ms	Mesyl, CH_3SO_3
MS	Mass spectrometry
N''	Trimethylsylilamide
Nacnac	1,2-Diketiminide
nbp	Normal boiling point
^{n}Bu	Normal butyl
NHC	*N*-heterocyclic carbene
NMR	Nuclear magnetic resonance
NOESY	Nuclear overhauser effect spectroscopy (NMR)
o	Ortho
OLED	Organic light-emitting diode
p	Para
Ph	Phenyl
pmdta	N,N,N',N'',N''-Pentamethyldiethylenetriamine
ppm	Parts per million
PPSE	Polyphosphoric acid silyl ester
Priso	$(DippNCMe)_2CH$
PS	Polystyrene
q	Quartet (NMR)
R	Alkyl; Molecular fragment
ROP	Ring-opening polymerisation
s	Singlet (NMR)
SET	Single electron transfer
SHE	Standard hydrogen electrode
t	Triplet (NMR)
Tf	Triflate, CF_3SO_3
^{t}Bu	*tert*-Butyl
TEMPO	(2,2,6,6-Tetramethylpiperidin-1-yl)oxyl
thf	Tetrahydrofuran
TM	Transition metal
tmeda	N,N-Tetramethylethylenediamine
TMP	2,2,6,6-Tetramethylpiperidine
TMS	Trimethylsylil
^{t}Oct	*tert*-Octyl
Trip	2,4,6-Triisopropylphenyl
Trityl	Triphenylmethyl
Ts	Tosyl, *p*-Me-$PhSO_3$
XRD	X-ray diffraction
δ	Chemical shift (NMR)

Chapter 1

Introduction to Alkaline Earth Metal Chemistry

The alkaline earths derive their name from the medieval tradition of naming any element which could not easily be recognised, insoluble in water and not a metal "earth element". Additionally, elements which appeared to have properties similar to the most common alkaline compounds of the time, potash and soda, were referred to as alkali earth metals. Despite this classification, these compounds were not, in fact, Group II metals as we know them today, but rather their corresponding oxides as first postulated by Antoine Lavoisier. Following this, it was Sir Humphry Davy who first isolated a series of Group II metals by electrolysis in 1808.[1]

Since the discovery of alkylzinc compounds by Frankland in 1849, organometallic reagents have shown a continuous growth in importance and application.[2] Early milestones were set by Reformatsky, Barbier, Grignard, and later Gilman.[3–6] As the 20th century dawned, alkaline earth metal chemistry made its entrance. Now, Group II chemistry can look back on over a century of extensive synthetic use, catalytic application, and the discovery of remarkable species.

The following chapter aims to provide an overview of Group II coordination chemistry, from the discovery of organomagnesium compounds to recent developments. Whilst research into the heavier congeners is ever expanding, focus will be given to magnesium due to its popularity and wide application.

1.1. The Beginning of Ae Coordination Chemistry: Grignard Reagents

Despite their name, the birth of Grignard reagents can be traced back to Philippe Barbier's synthesis of dimethylheptenol at the end of the 19th century; reacting a mixture of methyl iodide, a methyl ketone and magnesium metal to yield a tertiary alcohol:

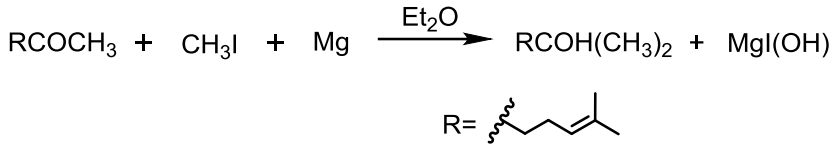


***Figure 1**: Formation of a tertiary alcohol via the Barbier reaction.*[4]

The involvement of an organomagnesium species was then postulated by Grignard, a pupil of Barbier.[7] Grignard's research culminated in his doctoral thesis in 1901, in which he elucidated the details of the aforementioned reaction as shown in Figure **2**.[5]

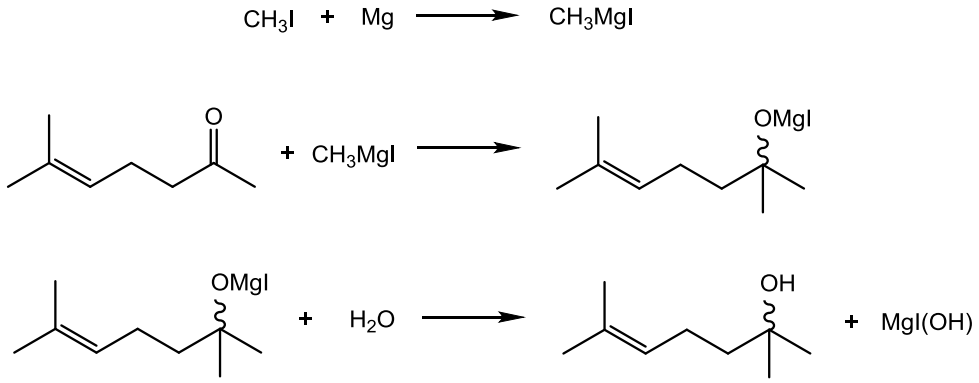


***Figure 2**: 3-step mechanism for the formation of a tertiary alcohol via the Barbier reaction, as proposed by Grignard.*[5]

As a result of his efforts, Grignard was awarded the Nobel Prize for his work on organomagnesium reagents, now eponymously referred to as "Grignard reagents" in his honour.[8]



***Figure 3**: Polarisation of a Grignard reagent versus a carbonyl.*

The widespread use of these reagents stems from their ability to afford nucleophilic carbon reagents, which are of great use to the synthetic chemist. In contrast to common electrophilic carbon centres polarised towards a heteroatom such as oxygen, *e.g.* in carbonyl groups, Grignard reagents are polarised towards a carbon (Figure **3**). The resulting importance of these compounds to organic and inorganic chemistry can hardly be overstated, with their use spanning from large scale industrial applications to the undergraduate laboratory.[9]

1.2. Expansion

Despite the development of a large library of Grignard reagents for synthetic applications, Group II chemistry has been limited to these classical Grignard reagents for the first half of the 20th century.[9] Whilst early attempts towards calcium analogues of Grignard reagents were made to no avail, a series of discoveries challenged traditional views of Ae chemistry on more than one occasion.

1.2.1. Ae Cyclopentadienides

The discovery of ferrocene by Kealy and Pauson in 1951 sparked research into this notable class of compounds; the use of cyclopentadienyl ligands quickly spread to early main group elements to give what may be considered the next evolutionary step in Group II chemistry: Ae metallocenes.[10]

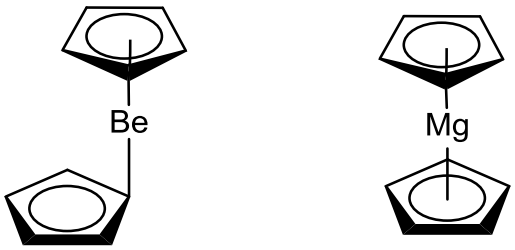


***Figure 4**: Monomeric Cp_2Be and Cp_2Mg.*

The tendency of alkaline earth metals to form heteropolar bonds and salt-like complexes render them an ideal bonding partner for the cyclopentadienyl ligand, and by 1961 all but the radium analogue of the Group II cyclopentadienides had been synthesised.[11] In 1979, the first resolved structure of non-polymeric alkaline earth metallocenes followed with Cp_2Be and Cp_2Mg (Figure **4**, Figure **5** ***a*** and ***b***).[12,13] Whilst beryllium is bonded to one Cp moiety in

an η^5 fashion and the other η^1-bound, both Cp rings act as η^5 ligands in Cp_2Mg, resembling a ferrocene-like structure. The variation in solid state structure signifies the changing metal characteristics, *i.e.* an increase in ionic radius and decrease in electronegativity,† resulting in both a larger coordination sphere and an increasingly ionic interaction.

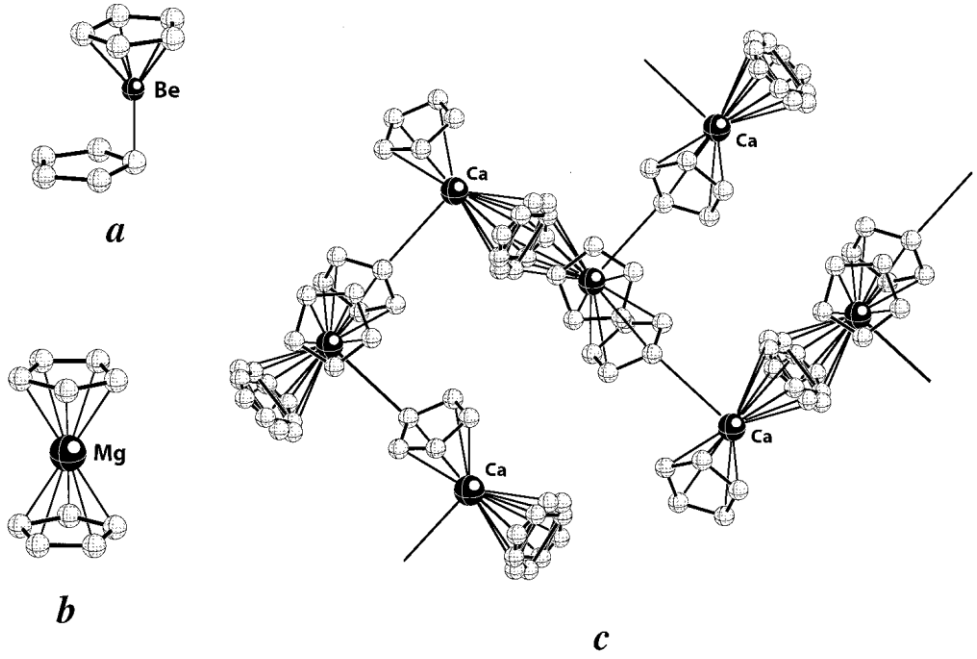


***Figure 5**: Structures of monomeric (a) Cp_2Be, (b) Cp_2Mg and (c) polymeric Cp_2Ca.*[11]

The polymeric structure of $[Cp_2Ca]_n$, as first resolved by Stucky and Zerger (Figure **5**), illustrates tendencies towards aggregate formation, particularly of the heavier Ae congeners; this stems from the large ionic radii of the metal centres, and has been partially overcome by ligand substitution to afford discrete molecules *via* increased steric bulk in later complexes.[14]

In addition to aggregate formation, the above structure also revealed non-coplanarity of the Cp rings; whilst this may be attributed to intermolecular

† Consequently a larger difference between, in this case, carbon (2.55 after Pauling) and the metal. *Cf.* Table **1**, pg. 13.

interactions in the aggregate, this geometry has also been observed in a series of Cp*-bound, discrete Group II metallocenes.[15]

By simple steric considerations, parallel Cp rings would appear to be the most favourable conformation. Early theories for this effect hypothesised a dipole induced by the negatively charged Cp rings (Figure **6**), whereas more recent approaches considered involvement of the d orbitals causing sp^3d or sp^3d^2 type hybridisation of the metal.[11]

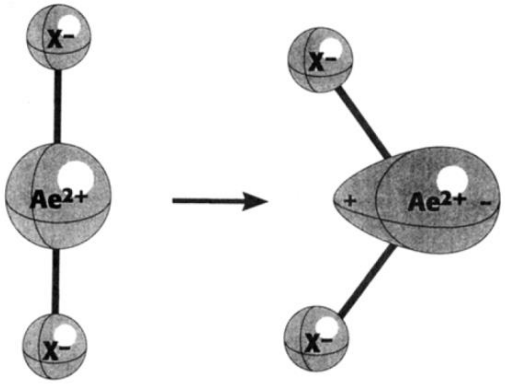


***Figure 6**: Polarisation-induced bending of an Ae compound.*[11]

The chemistry of Group II metallocenes has historically been limited to homoleptic complexes, which are of limited synthetic utility due to the poor solubility exhibited by this class of compounds. In addition, interchanging the Cp ligands for other functionalities has proven challenging. Despite this, Westerhausen *et al.* have recently expanded the synthetic applicability of calcocene to metathesis reactions in the formation of heteroleptic complexes.[16]

1.2.2. Heavy Grignards

Whilst continued research on main group metallocenes yielded a series of complexes with varying steric bulk, the fundamental Cp-system remained unchanged.[11,12] The general position of the scientific community towards the organometallic chemistry of the heavier Group II congeners was reflected by Cotton and Wilkinson in 1980, stating that "the organic compounds of calcium, strontium and barium are relatively obscure and of little utility [...]".[17] Indeed, an extension to non-Cp carbon-based systems was only made in 1991 with the synthesis of Lappert's benchmark $Ca[CH(SiMe_3)_2]_2(1,4\text{-dioxane})_2$ species, propelling Group II chemistry out of the metallocenes era.[18] Having been presented with proof for the synthetic accessibility of σ-bonded carbon-calcium compounds, the scientific community set out to synthesise a great variety of heavy Grignards, a detailed account of which has been provided by Hanusa and Westerhausen.[19,20]

1.2.3. Subvalency: The Ae – Ae Bond and the First Distinct Ae^0 Species

The expected valency of main group as well as Group III and XII elements is determined by the octet rule, according to which elements will accept or release electrons to achieve a noble gas configuration. Group II metals fulfil this rule by the release of two electrons, thereby becoming isoelectronic to the corresponding noble gas as a cation with a +2 charge (expected valency). Consequently, an oxidation state of +1 or 0 is considered subvalent; the subject of subvalent alkaline earth organometallics up to 2010 has been reviewed in detail by Westerhausen *et al.* [21] The following account is aimed at providing a brief overview of the now well-developed Mg^I systems, as well as the very first isolable molecular Ae^0 species.

(i) From Zn^I to Mg^I

Subvalency in the solid state is observed in heavy Group II subnitrides, represented by the general formula $[Ae_6N]$, and less common suboxides $[Ae_4O]$.[22] Subvalency is deduced from the formula by assuming nonmetal anion formation with electrons supplied by the metal, *i.e.* the formation of N^{3-} to give an anion isoelectronic to neon requires three electrons from a total of six surrounding metal atoms, resulting in an average oxidation state of +1. In addition to these formally subvalent species, Mg^I has also been isolated and studied in noble gas matrices.[23,24] Notwithstanding the existence of such species, it was long thought impossible to isolate stable, organically bound Mg^I complexes. This is not particularly surprising considering that a completely filled d shell exhibits neither acceptor nor donor character, and elements featuring these are commonly viewed as redox inactive. However, this view was challenged by Carmona's discovery of the first stable Zn^I–Zn^I compound in 2004 (Figure 7).

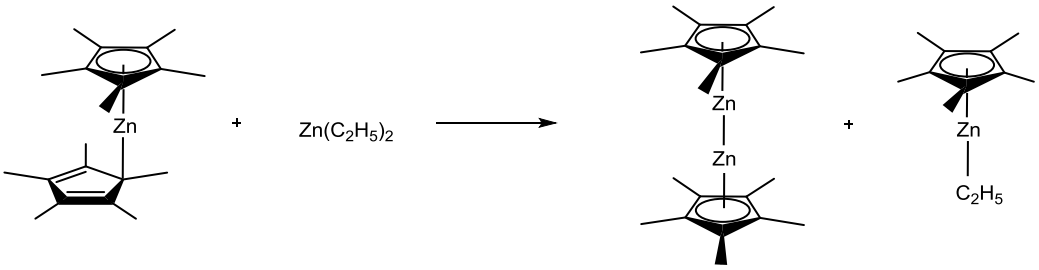


***Figure 7**: Synthesis of Cp*ZnZnCp*.*[25]

Given the similarities between Group II and Group XII metals, such as comparable ionic radii, prevalent +2 oxidation state, and lack of bonding d-electrons, it follows that the above discovery ignited research into yet another domain of Group II chemistry: the synthesis of subvalent, homodinuclear complexes.

Whilst all Group XII metals show similarity to the alkaline earths, zinc is by far the closest sibling to its Group II analogue, magnesium. Although the Group XII dications of Hg_2^{2+} and Cd_2^{2+} have long been known, Zn^I had only been reported

to exist under extreme conditions or locked in a matrix, comparable to Mg^{I}.[26] Consequently, the discovery of a Zn^{I}–Zn^{I} species suggested the synthetic accessibility of a stable, dimeric Mg^{I} analogue, an assumption supported by quantum chemical calculations.[27] Ultimately, the first successful synthesis and characterisation of a non-transient dimeric Mg^{I} species fell to Jones *et al.* in 2007.[28] Whilst efforts towards an Mg^{I} species taking a route analogous to the Zn^{I} equivalent were made to no avail, stabilisation with highly bulky, delocalised *N*-donor systems proved successful in the form of [{(Priso)Mg}$_2$] (Figure **8**).[28]

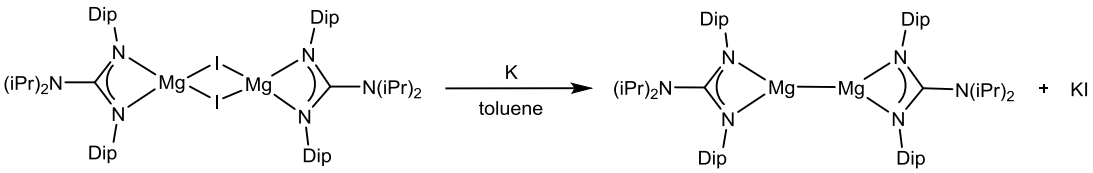


***Figure 8**: Jones's synthesis of [{(Priso)Mg}$_2$] by reduction of the corresponding organylmagnesium iodide.*[28]

Whilst similar calcium species have so far eluded isolation, Westerhausen *et al.* were recently successful in stabilising subvalent calcium in an inverse sandwich type complex by employing an extended π-system.[29] The energetic states of the arene lie between the first and second ionisation energy of calcium, allowing to capture it in its +1 oxidation state as shown below (Figure **9**). The line between the two Ca^{I} atoms does not denote a bond to each other, but rather to the aryl dianion.

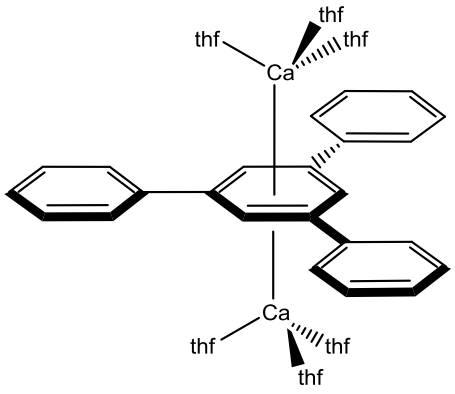


***Figure 9**: Inverse Ca^{I} sandwich complex.*[29]

(ii) Carbene-ligated Be: The first zero-valent alkaline earth complex

In contrast to the array of known L_nTM^0 (TM= transition metal) species, zero-valent monoatomic main group complexes have proven exceptionally difficult to access. However, the field of such p-block complexes is on the rise. A number of $L_2E^0_n$ compounds have been stabilised by strong σ-donor, sterically demanding *N*-heterocyclic carbenes (NHCs), *e.g.* for B, Sn and P.[30–32] All of the latter take the form of diatomic complexes, with monoatomic variants remaining rare; known examples rely on the use of cyclic alkyl amino carbenes (CAACs).[33,34]

Given that Be provides the highest tendency towards forming covalent, directional interactions, as well as a small coordination sphere, it presented a natural target for accessing a zero-valent alkaline earth. Previous work on subvalent Be complexes sought to stabilise these species employing diketiminate ligands, and despite the previous success in accessing Mg^I, these proved unsuccessful.[35,36] Ultimately, the prize of the very first molecular Ae^0 system fell to Braunschweig *et al.* in late 2016.[37] Given that previous computational studies had shown significant contributions in π backdonation towards stabilising an electron-rich Be^0 centre, it was reasoned that CAACs would provide superior stabilisation compared to NHCs; the latter are predominantly σ-donors and have poor π-acceptor qualities.

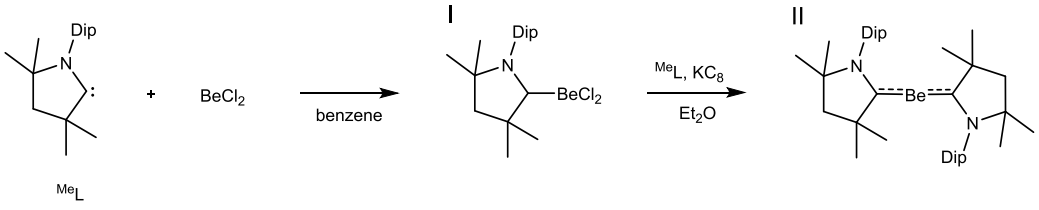


***Figure 10**: Synthesis of [(CAAC)$_2$Be^0].[37]*

As seen in Figure **10**, addition of the ^{Me}L ligand to $BeCl_2$ gave the corresponding adduct **I**, the reduction of which with KC_8 in the presence of a second equivalent of ^{Me}L gave **II** in good yield (78 %). Although cyclic voltammetry experiments hinted at the possibility of reducing **I** to Be^I or Be^0, attempts at chemical

reduction in the absence of another ^{Me}L equivalent yielded intractable mixtures. As the reactivity of **II** does not appear to differ from unbound ^{Me}L, it has been described as a bis(CAAC) adduct of elemental beryllium.

The aforementioned π-acidic qualities of the CAAC ligand appears to play a significant role in stabilising **II**, with a body of evidence pointing towards C–Be double-bond character. Combined with extensive computational investigation, the most accurate bonding description is that of a σ ligand-metal bond, as well as a three-centre, two-electron π-bond as displayed in Figure **II**. π-backdonation was found to be by far the strongest bonding contributor.

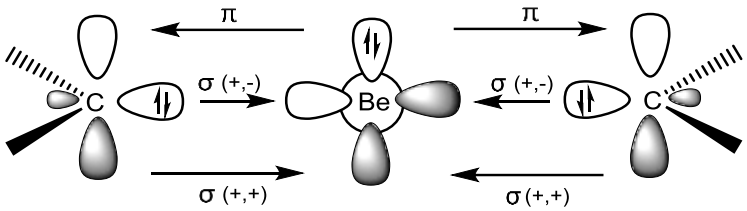


***Figure II**: Schematic orbital representation of [(CAAC)$_2$Be^0].[37]*

As main group elements are moving in on traditional TM territory, discoveries such as the above pave the way towards novel applications, *e.g.* for small molecule activation.[38] Given the infancy of this field, there is considerable scope for expansion.

1.3. Synthesis of Alkaline Earth Metal Complexes

The challenges encountered on the road to Group II complexes are considerable. These relate to the physical properties of the alkaline earths, which exhibit a strong electropositive character combined with negative redox potentials as well as large ionic radii (Table **1**). Such properties give rise to complexes that are highly reactive, and prone to association as well as various decomposition pathways, as discussed below.

***Table 1**: Ae^{II} ionic radii, electronegativity and redox potentials (vs. SHE) for Ae metals.*[39]

Element	r_{ionic} **(for M^{2+}, in Å)**	**Electronegativity (Pauling)**	**Redox potential (M^{2+}/ M, in V)**
Be	0.45	1.57	-1.97
Mg	0.72	1.31	-2.36
Ca	1.00	1.00	-2.84
Sr	1.18	0.89	-2.89
Ba	1.35	0.90	-2.92

The increase in ionic radius and decrease in electronegativity down the group results in considerable differences in bonding behaviour from magnesium to its heavier congeners, with a shift from highly covalent bonding in Be complexes, to increasingly ionic interactions as one moves down the group. Therefore, "heavy Grignards" in particular require carefully designed conditions to allow for the isolation of their thermodynamically labile heteroleptic complexes.

These properties have given rise to the development of a wealth of synthetic pathways, enabling the isolation of some highly reactive species. Figure **12** shows

an overview of traditional methodologies used to prepare σ-bound Group II complexes; whilst numerous π-bound† alkaline earth derivatives are now known, their description lies outside the scope of this brief overview. Synthetic approaches to early complexes have been reviewed by Hanusa.[11] Similarly, not all routes described herein are equally promising for different congeners; the merit of individual routes towards synthesising specific complexes is reviewed in detail elsewhere.[39,40]

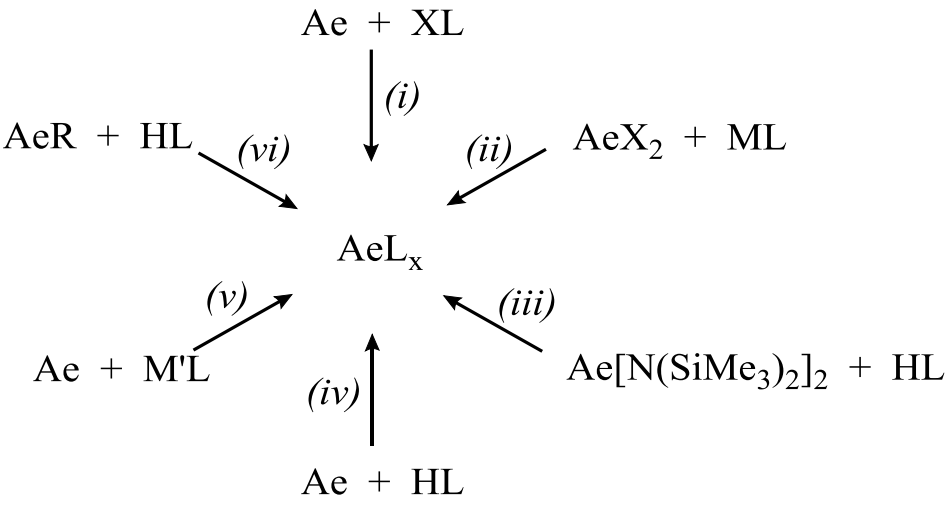


***Figure 12**: Synthetic methodologies for the isolation of Ae metal complexes. L is any ligand, X is a halogen, M is a Group I metal, R is a hydrocarbon, and M'L is either an organomercurial or organostannane.*

- Direct Synthesis (Route ***i***)

  The well-known formation of a Grignard reagent by direct insertion of the metal into a carbon-halogen bond. Despite its successful application in accessing of a wide array of synthetically useful Grignard reagents,[9] complex formation of heavier congeners requires a different approach.

† That is to say, the largely non-covalent interaction between Ae cations and electron rich π-system.

- Salt metathesis (Route ***ii***)

  One of the most common route to Group II complexes,[39] the formation of the alkali metal halide provides a strong driving force. The equilibrium nature of the reaction, which is affected by a variety of factors such as the solvent, the metal halide, the alkali metal and the ligand can prove problematic, reactions can yield a mixture of products and the outcome may be difficult to reproduce. Alkali metals may become incorporated to form a bimetallic species.[41]

- Transamination (Route ***iii***)

  Commercial availability of Group II amides, good solubility in a variety of solvents and easy removal of the formed protonated amide has made transamination an attractive synthetic pathway. However, the reaction is limited to ligands within a certain pK_a range. Whilst the acidity of the ligand needs to be higher than that of the formed amide, too acidic a ligand encourages side reactions.[40]

- Direct metalation (Route ***iv***)

  Despite the attractiveness of pure products and easy separation, direct metalation is not as commonly employed as one might assume, predominantly due to high dependency on ligand acidity. Mild solid-state synthesis has broadened the application of this method as reviewed by Ruhlandt-Senge *et al*.[39]

- Redox transmetalation (Route ***v***)

  Sacrificial organomercurial or organostannane complexes have been employed to yield the desired AeL_2 species in good yields in a variety of solvents. Despite these advantages, application of redox transmetalation is hampered by the high toxicity of reagents involved. The use of corresponding organobismuth reagents as reported by Ruhlandt-Senge *et al.* offers a less toxic alternative.[42]

- Organoelimination (Route ***vi***)

  The commercial availability of dibutylmagnesium and similar species has aided the popularisation of organoelimination in Ae complex synthesis, particularly for the synthesis of Hauser bases. The application to heavier congeners is inhibited by the very limited availability of equivalent precursors. However, recent developments have seen the use of dibenzyl derivatives of Ca, Sr and Ba in organoelimination reactions.[40]

As outlined above, a series of strategies have been developed for the synthesis of Group II complexes. Upon successful formation, there are two main decomposition pathways affecting their stability, as covered below.

1.3.1. The Schlenk Equilibrium

The Schlenk equilibrium, first hypothesised by Abegg in 1905,[9] affects all Grignard reagents in solution and describes their disproportionation from the heteroleptic RAeX complex to the diorgano species R_2Ae, and the dihalide AeX_2 (Figure **13**). The driving force is provided by the exothermic formation of the dihalide; provided the latter exhibits a degree of solubility in the employed solvent system (commonly ethereal), the equilibrium depicted below holds true. As Ae dihalides are insoluble in hydrocarbon solvents, such systems render the Schlenk equilibrium irreversible, forcing the conversion of LAeX to L_2Ae with concomitant removal of AeX_2 as a precipitate according to Le Chatelier's principle.

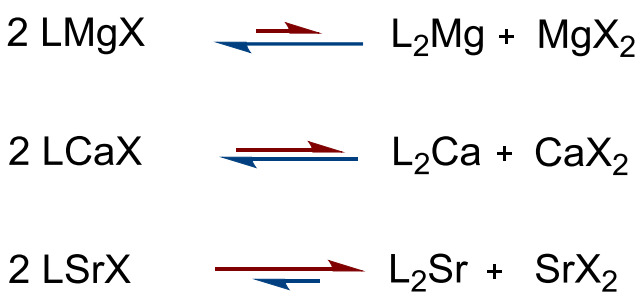


***Figure 13**: The Schlenk equilibrium.*

Whilst generally of considerable inconvenience, this equilibrium may also be exploited to obtain the diorgano species. In the presence of dioxane, the insoluble Group II halide-dioxane adduct precipitates quantitatively, affording the R_2Ae species. Although this equilibrium may appear simple enough, Figure **13** only gives a generalised overview. This does not account for the complex interplay of various associations and dissociations taking place. The fluxional nature of alkaline earth reagents is best described as shown in Figure **14**.



***Figure 14**: Alkaline earth reagent composition.*

Although this solution redistribution is usually described for heteroleptic halides, it principally applies to all heteroleptic Ae compounds. Depending on the nature of X, AeX_2 may be a salt or polymer, either resulting in poor solubility in non-coordinating solvents. In addition, the homoleptic L_2Ae species is usually kinetically stabilised and hence unreactive. Thus, redistribution is to be avoided from the beginning.

Strongly charge donating solvents generally shift the equilibrium to the right, as stabilisation by the solvent decreases from AeX_2 > RAeX > R_2Ae in accordance with Lewis acidity (*i.e.* AeX_2 – thf_n forms the strongest Lewis acid-base pair), as computationally investigated by Burk *et al.*[43] However, hydrocarbon solvents are not necessarily a better alternative, as alkaline earth metal halides are insoluble in non-coordinating solvents, resulting in the equilibrium being pushed to the right by removal of AeX_2. Consequently, solvent system effects are not always easily predictable.

Whilst all Grignard reagents are affected, the equilibrium position depends greatly on the metal. As the ionic radii increases down the Group, bonding interactions between metal and ligand become increasingly ionic, non-directional and more prone to dissociation. The equilibrium position is indicated in Figure **13**, with magnesium on the left hand side and its heavier congeners trending to the right.

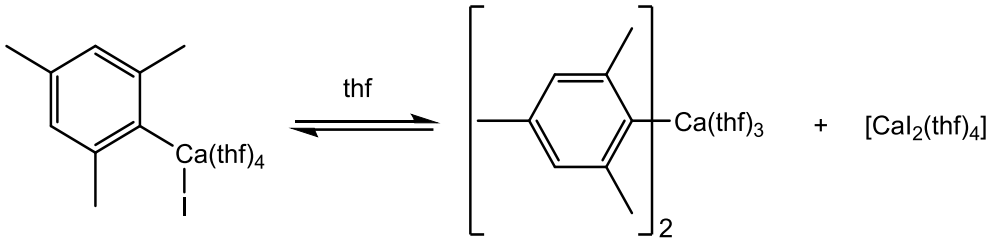


***Figure 15**: Schlenk equilibrium disproportionation of mesitylcalcium iodide.*[42]

Westerhausen *et al.* have studied the above equilibrium for solutions of 2,4,6-trimethylphenyl calcium iodide by NMR, and found two sets of resonance to be present, pointing to the equilibrium displayed above (Figure **15**). [44]

Due to its thermodynamic instability, kinetic stabilisation of LAeX is therefore required to avoid redistribution. This is commonly achieved with sterically demanding ligand systems, an overarching theme in Group II chemistry.

1.3.2. Ether Cleavage

The ionic character of Ae complexes, in particular the heavier congeners, results in poor solubility in non-coordinating solvents. As a result of this, ethers often present the only realistic solvent system. However, heavy Group II complexes in particular readily induce ether cleavage, causing degradation of the sample.[45] Whilst low temperatures and short reaction times may be employed to avoid such degradation, these are evidently conflicting in nature, as low temperatures slow reaction times not only of the degradation but also the desired reaction. Depending on the solvent and steric protection around the active centre, ether cleavage may occur by deprotonation in the α or β positions, as exemplified for phenylcalcium halides below (Figure **16**).

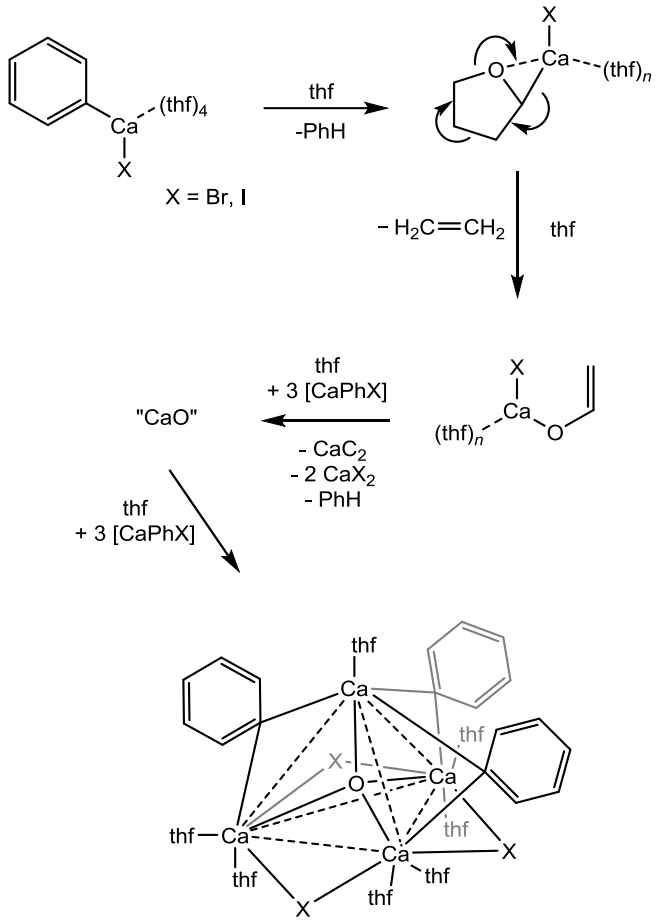


***Figure 16**: Ether cleavage reaction of phenylcalcium halides and formation of the CaO cage compound.*[44]

1.4. Applications of Group II Complexes

The rapid expansion of Ae chemistry has served to challenge previously held beliefs, deepen our fundamental understanding of bonding by providing a series of fascinating new compounds, and provided a multitude of sophisticated synthetic and catalytic avenues of pursuit. Furthermore, many of these complexes have been, and are, investigated for a series of applications, an outline of which will be given below.

1.4.1. Synthetic Use

Nucleophilic Grignard reagents have been applied to an enormous wealth of synthetic transformations; indeed, the extensive nature of this area renders the compilation of a comprehensive overview all but futile. To the best of my knowledge, the encyclopedic "Handbook of Grignard Reagents" by Silverman and Rakita presents the most exhaustive overview.[9] A more recent synopsis has been compiled by Richey; the use of Grignard reagents in conjunction with transition metal catalysts for the purpose of C–C cross-coupling has been covered by Cossy.[46,47]

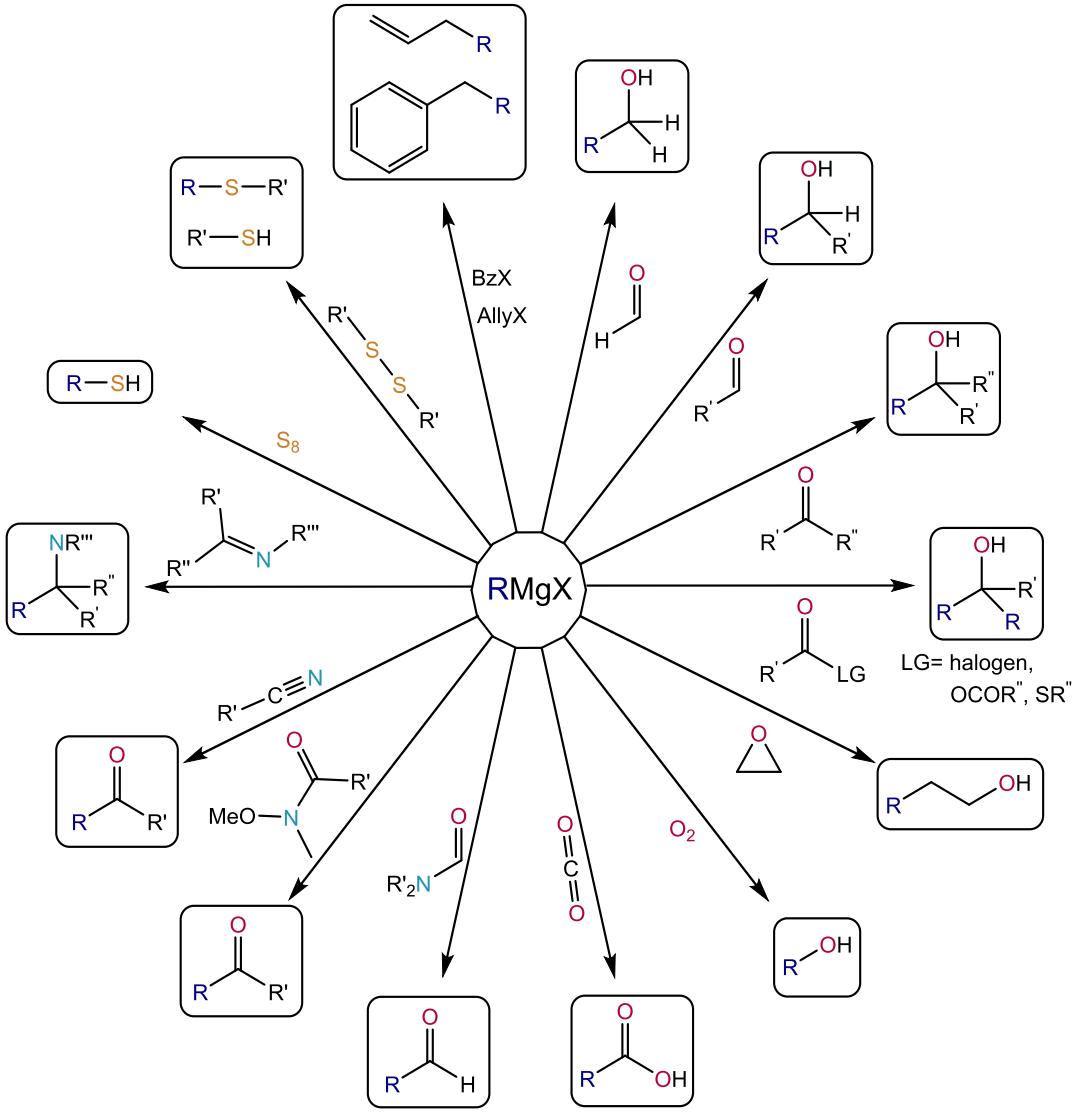


***Figure 17**: Reactions of Grignard Reagents,*
R is an alkyl or aryl, reactions assume an aqueous work-up.

Figure **17** is intended to outline some of the most common synthetic transformations. Invariably, most of these are centred around addition to a polarised carbon-heteroatom functionality to give a new C–C bond. Thus, Grignard reagents are commonly employed for the synthesis of primary, secondary, and tertiary alcohols as well as ketones and carboxylic acids. Nucleophilic substitution competes with action of R^- as a base, *i.e.* enolisation and reduction. Reactions involving nitrogen substrates frequently produce lower

yields as a result of decreased bond polarisation† and increased steric crowding. Although R can be an aryl or alkyl in general, its nature significantly influences the feasibility of a transformation, as the author found out to his own detriment (*v.s.* **3.2.1**(i), pg. 100). Grignards are not usually reactive towards alkyl or aryl halides, with the exception of activated allyl and benzyl halides. Broadly speaking, such C–C bond forming reactions continue to be dominated by transition metal catalysed reactions.

Whilst the reader is referred to the abovementioned books for excellent overviews of the vast field of Group II compounds in synthesis, two very different contemporary fields have been chosen for brief elucidation below. Even amongst recent developments, these are only two examples among many. The covered subjects do not reflect or imply an order of importance, and could just as easily be replaced by functionalisation through halogen-metal exchange as reviewed by Knochel, or the metalation of otherwise inert substrates by bimetallic species, as pioneered by Mulvey.[48,49]

(i) Grignards and Water: New Perspectives

By and large, moisture and oxygen are the bane of synthetic alkaline earth metal chemistry. Reactions are routinely carried out in anhydrous solvents under an inert atmosphere, for reasons mentioned above (*v.s.* Section **1.3**). To most s-block chemists, the thought of carrying out reactions in solvents known to react, sometimes violently, with these highly polarised organometallics would seem eccentric at best. This notwithstanding, recent developments suggest the potential for reactions to be carried out in protic solvents.

The key component of such transformation is that of speed. Long-known Barbier-type reactions, as reviewed by Li, present an early indication for the

† Electronegativities after Pauling: C 2.5, N 3.0, O 3.5. As a result, the azomethine carbon shows only moderate electrophilicity. Enolizable imines exhibit a tendency towards deprotonation rather than addition.

feasibility of Ae chemistry in the presence of air and moisture.[50] Another puzzle piece was provided by the competing rate of Li-halogen exchange *vs.* deprotonation (Figure **18**), which soon found further synthetic application.[51,52]

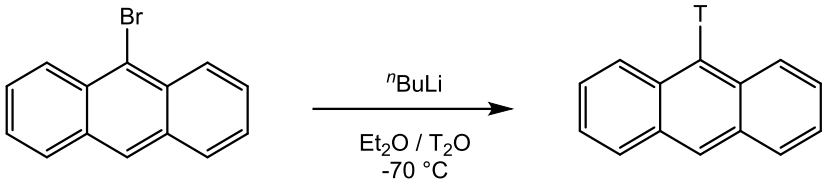


***Figure 18**: Synthesis of tritiated anthracene in T_2O-wetted diethyl ether.*

Just as Li-halogen exchange outcompeted deprotonation above, Grignards have potential in protic solvents and/ or aerobic conditions, provided nucleophilic addition is fast enough. To this end, the subject of polar organometallics in unconventional reaction media has recently been reviewed by Capriati *et al.*, which compiles evidence for the action of water as a polar ligand. In some cases, this increases the nucleophilicity of R^- to such a degree that addition outcompetes hydrolysis.[53]

Further work on the effect of quaternary ammonium salts by Song, as well as on deep eutectic solvents (DES) by Hevia *et al.,* suggest a kinetic activation. This is presumably due to the formation of a halide-rich magnesiate, as crystallographically identified in the latter publication (Figure **19**).[54,55] The nucleophilicity of these moieties is such that, again, addition outcompetes deprotonation.

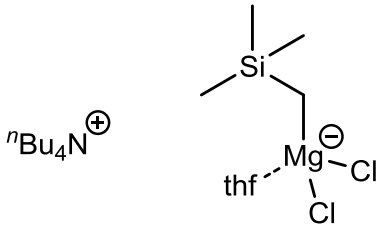


***Figure 19**: Monomeric and highly nucleophilic magnesiate as characterised by Hevia et al.*[54]

Such methodologies are far from academic curiosities, as recently demonstrated by Capriati *et al.* [56] A series of tetrahydrofurans were synthesised in good yields from alkyl and aryl Grignards and γ-chloroketone suspensions in water (Figure **20**).

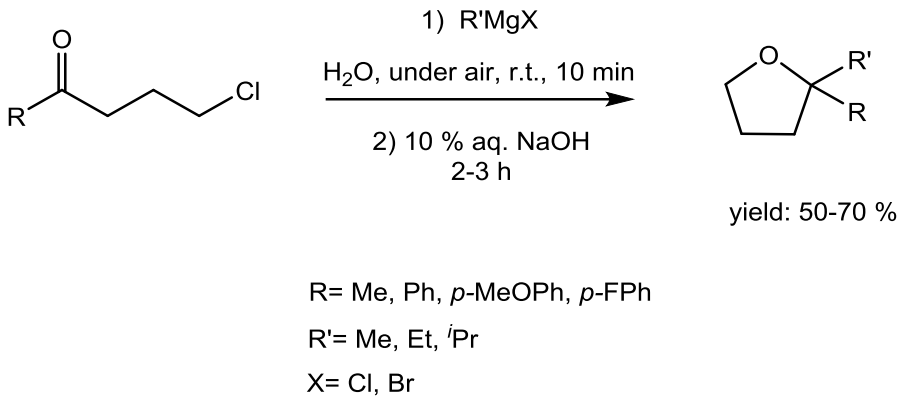


***Figure 20**: Tetrahydrofurans synthesised with Grignard reagents in water.*[56]

More than a hundred years after their conception and extensive use in organic synthesis, new aspects of Ae chemistry are still developing. An increasing understanding of Ae complex structure and its intrinsic link to reactivity is set to facilitate greener methods in s-block chemistry.

(ii) Applications of Subvalent Mg^{I}

On a rather different front to the above, subvalent Mg^{I} dimers have been investigated towards their potential as new synthetic reagents. Their thermal stability, good solubility in a wide range of solvents, and non-toxicity make them attractive alternatives to traditional reducing agents. A particularly systematic investigation of the reactivity homodinuclear Mg^{I} species exhibit towards a series of unsaturated organic substrates has been undertaken by Jones *et al.* (Figure **21**).

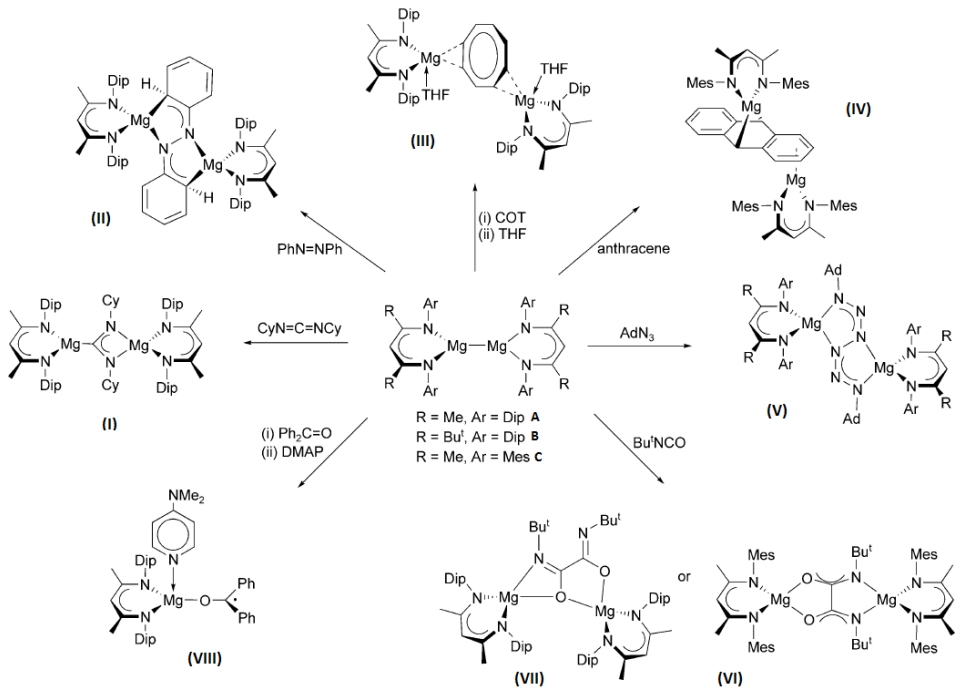


***Figure 21**: Reactivity of Mg^{I} dimers towards some unsaturated substrates.*[57]

The Mg^{I}–Mg^{I} dimer acts as a two-centre/two electron reductant as illustrated by reactions **I** to **IV**, with substrate insertion into the Mg–Mg bond leading to the formation of novel compounds. The synthetic application extends to reductive N–N and C–C bond formation, as demonstrated by reactions **V** to **VII**. However, exceptions to this type of reactivity exist, such as the formation of the stable magnesium ketyl complex **VIII**. Overall, the variety of novel compounds formed as described in Figure **21** hints at the potential of magnesium dimers for synthetic applications.

In addition to the more complex reactivity illustrated above, Mg^{I} species have also been investigated as reducing agents. Commonly utilised Group I and II metals, as well as potassium graphite, often pose issues in the form of side reactions due to their strongly reducing nature. Poor solubility further exacerbates the problem, resulting in suboptimal stoichiometric control. Additionally, their use is associated with a considerable fire hazard. In contrast, magnesium dimers exhibit good solubility, low handling hazard, and are comparatively selective, as reviewed by Jones *et al.*[57] Recently, Stasch has

demonstrated this applicability in the synthesising of a novel Zn^{I} dimer utilising Mg^{I} where classical reducing agents failed.[58]

1.4.2. Homogeneous Catalysis

Organometallic complexes have long provided the core of homogeneous catalysis, enabling remarkable substrate transformations through reactive metal sites, nested in a ligand framework. The latter not only provides a soluble, distinct, molecular species, it also allows for the tuning of steric surroundings, as well as altering electronics. Having given rise to no less than three Nobel prizes in the 21st century,† the importance of this ever-expanding field is difficult to overestimate.

At the heart of catalysis lies the expanse of transition metals. Availability of d-orbitals allows for rapid and reversible change in oxidation state, enabling the staple transformations of oxidative addition and reductive elimination. In contrast, such redox pathways are denied to d^0 species. This notwithstanding, such compounds are amongst the most active TMs, with Ziegler-Natta catalysts (Figure **22**) presenting the most prominent and industrially important examples amongst many.[59–61]

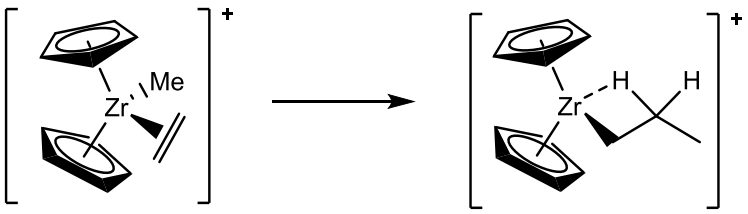


***Figure 22**: First steps in a Zr-metallocene catalysed ethylene polymerisation.*

† 2001: Enantioselective catalysis; Knowles, Noyori and Sharpless
2005: Metathesis in organic synthesis; Chauvin, Grubbs and Schrock
2010: Palladium-catalysed cross couplings; Heck, Negishi and Suzuki

Despite their activity, the downfall of such systems is frequently the limited scope of their applicability. Contrastingly, platinum group metals shine through their versatility, with Pd-catalysed cross-coupling reactions representing an invaluable part of any organic chemist's toolkit. However, their scarcity, and consequently considerable cost, provides a sizeable impetus for the development of alternative catalysts.

In light of their low cost, non-toxicity (excluding Be, and, to a lesser extent, Ba) and abundance, alkaline earths have received extensive attention for such a replacement. Although analogies between some d-block elements and Ae metals can certainly be drawn (*v.i.* Section **1.2.3**, pg. 8), f-block elements present a more fitting comparison. Lanthanides provide similar bonding and comparable ionic radii;† the similarities between Yb^{II} and Ca^{II} chemistry has been expounded upon by Harder.[62] As lanthanides have demonstrated their applicability to catalytic transformations, it should come as no surprise that alkaline earths, too, exhibit considerable potential for catalytic transformations.[63,64]

Indeed, this field has expanded sufficiently to warrant expansive book chapters by Crimmin and Hill as well as Arrowsmith.[65,66] Heavier Ae catalysis has previously been reviewed by Harder, Crimmin, amongst others; the most recent reviews have been compiled by Hill and Liptrot as well as Tsurugi and Mashima.[62,67–69] The reader is referred to these excellent works for detailed information. The section below aims to provide an outline of Ae reactivity in the context of catalysis, including some selected examples. It is by no means intended to be a comprehensive review of Ae catalysis.

† This is particularly true for trivalent 4f-metals, whereas Ln^{II} complexes exhibit a propensity for one-electron redox processes.

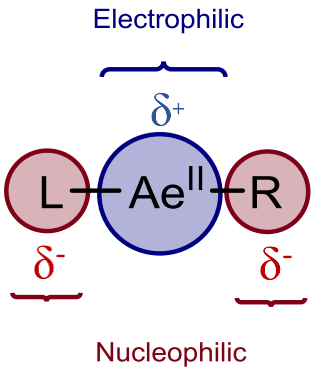


Figure 23: *Active sites in Ae complexes.*

It has been noted by Harder that Group II systems inhabit an advantageous position between late main group and Group I complexes; whereas the former's activity is based on electrophilic centres, and the latter's on a basic/nucleophilic organic fragment, Ae complexes provide both, as displayed in Figure **23**. Redox-inactivity in the context of catalysis results in transformations centred on Lewis-acidity of the metal site, basicity of the ligand, as well as, more conventionally, sterics and electronics around the active site. Thus, catalytic cycles of Ae complexes revolve around σ-bond metathesis,† and insertion into unsaturated substrates as seen below (Figure **24**).

A noteworthy exception is the TEMPO-aided hydrogen release from silanes first reported by Hill; such Group II SET processes are now comprehensively covered in a book chapter written by the same author.[70,71]

† This key transformation allows for the cleavage of strong bonds, was first proposed by Watson for Lutetium and Yttrium species (NB: a lanthanide and TM frequently compared to lanthanides), and has recently been reviewed by Waterman.[469,470]

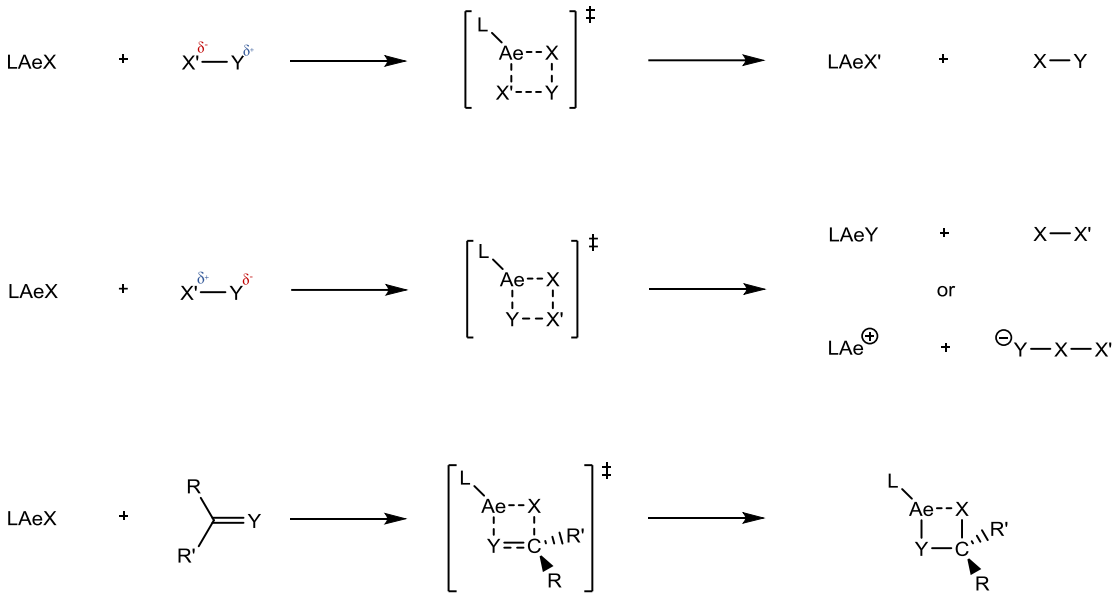


***Figure 24**: Catalytical pathways of Ae complexes.*
L is a monoanionic ligand, X is a monoanionic σ-bonded substituent

The first two reactions show σ-bond metathesis, where the substitution pattern depends upon polarisation of the substrate, *i.e.* the first shows a hydridic substrate, the second a protic substrate for X'= H. This naturally extends to Ae complex synthesis; transamination, for example, is merely a specific example of σ-bond metathesis in which the substrate is an acid with a lower pK_a than the conjugate acid of the metal base (*v.i.* **1.3**, pg. 15). The bottom reaction shows insertion into an unsaturated substrate, the basis of a plethora of Ae-catalysed heterofunctionalisations.

The applications of Ae catalysts may chiefly be divided into four categories: Heterofunctionalisation, polymerisation, dehydrogenative coupling, as well as di- and trimerisation of unsaturated substrates. All of these have been extensively reviewed in the abovementioned literature (*v.s.* pg. 28); consequently, when mentioned in a general context below, no specific reference will be given. Due to their particular importance, the first three will be outlined below. In line with work carried out, dehydrogenative coupling of ABs (amine-boranes) is covered more extensively in Section **1.4.2**(iii).

The "catalyst" employed in the processes listed below is not usually the active catalytic species, and therefore often referred to as a precatalyst in the literature on account of requiring activation. This does, however, appear to vary from publication to publication. In the interest of clarity, the term "catalyst" will be used throughout to refer to the organometallic species investigated for a given transformation. Its use does not imply knowledge (or a lack thereof) of the catalytically active species.

(i) Heterofunctionalisation catalysis

Heterofunctionalisation may be the most prominent domain of Ae catalysis, with an impressive wealth of functionalisations having been reported. Even more importantly, it is a relatively young discipline, with considerable potential for expansion.

Ae catalysts have been shown to catalyse hydroamination of unsaturated substrates, hydrophosphination, hydrosilylation, hydroboration, hydrogenation of activated alkenes and alkynes as well as hydroalkynylation. Figure **25** attempts to provide a general synopsis of these reaction pathways without claiming universal applicability.

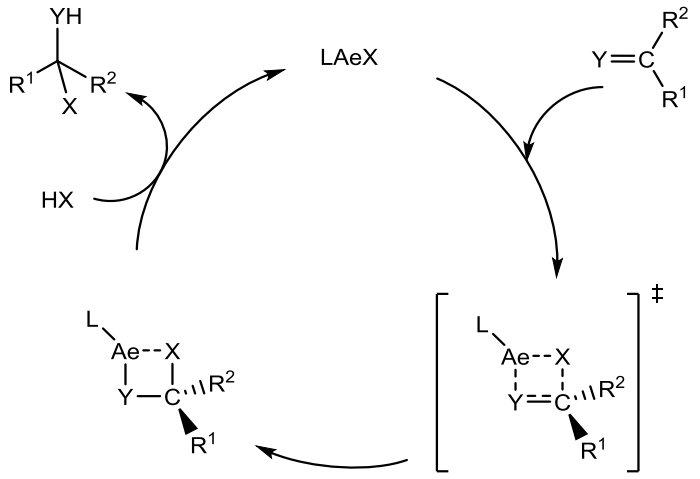


***Figure 25**: Hydro-heterofunctionalisation of unsaturated substrates.*
L is a monoanionic spectator ligand, X is a monanionic σ-bonded substituent, Y is commonly C or N.

Insertion of LAeX into an unsaturated bond yields a moiety activated towards addition of the desired substrate. LAeX is frequently generated from the reaction of LAeR with an equivalent of HX under elimination of RH (all in direct reference to Figure **25**). HX is therefore the amine, silane, phosphine, *etc.* added to the unsaturated moiety. The catalyst is then regenerated by σ-bond metathesis.

Maybe the most extensively utilised aspect of this chemistry is the intramolecular hydroamination of aminoalkenes, with the aforementioned reviews incorporating an impressive wealth of transformations. In addition to activating inert substrates, Ae catalysts have been shown capable of assembling asymmetric as well as complex structures. Three recent reports exemplifying each aspect are given below.

Hultzsch *et al.* demonstrated the enantioselective cyclisation of a variety of aminoalkenes; based on an earlier tetradentate ligand employed by the group, an altered, asymmetric variation afforded a series of cyclic amines in good enantiomeric excess (ee).[72] This was not limited to NMR scale experiments, the representative heterocyclic amine shown below (Figure **26**) was isolated on a preparative scale.

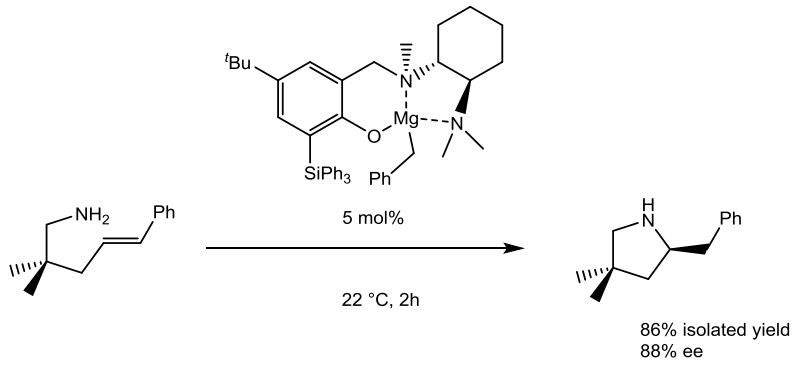


***Figure 26**: Enantioselective hydroamination by Hultzsch's Mg catalyst.*[72]

On the subject of complex systems, Hill *et al.* reported the remarkable 3-component assembly of a variety of imidazolidin-2-ones from inexpensive, commercially available materials and an easily accessible Ae catalysts in 2014

(Figure **27**).[73] This one-pot procedure afforded a series of heterocycles in excellent yields within hours. This is particularly noteworthy as terminal acetylenes are challenging substrates for Ae catalysis due to the formation of insoluble bisacetylides.

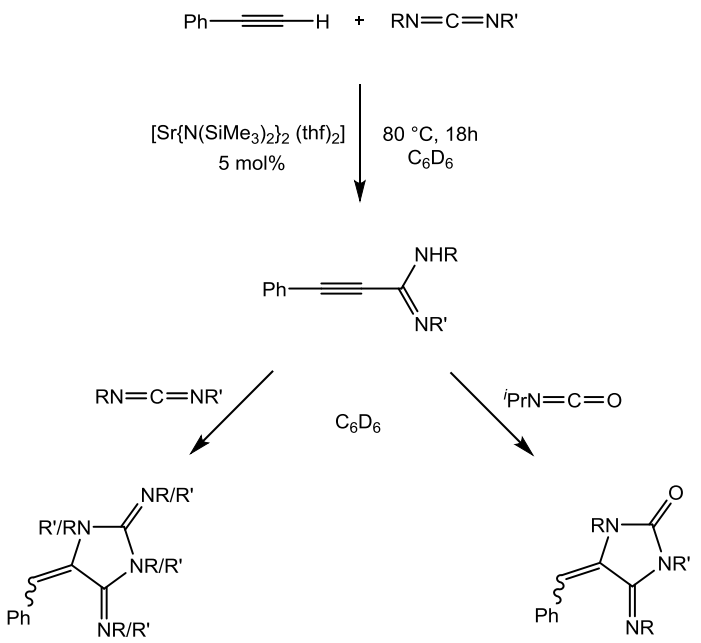


***Figure 27**: 3-component imidazolidin-2-one assembly by Hill et al.*[73]

Ae-catalysed hydrophosphination was first reported by Hill *et al.* in 2007, and has since been expanded from conjugated alkenes and alkynes to carbodiimides, aldehydes and ketones.[74]

Hydrosilylation has been reported for activated alkenes and ketones, in contrast to hydroamination this involves a hydridic rather than protic substrate (*cf.* Figure **24**). Hydroboration is of particular interest for the purpose of both reducing unsaturated substrates, as well as introducing boryl groups for further cross-coupling. A particularly remarkable achievement has been reported by Hill *et al.*, employing a $B(C_6F_5)_3$-activated Ae catalysts successfully enabled the selective reduction of CO_2 to a methanol equivalent (Figure **28**).[75] This type of chemistry is currently being expanded upon by the same group.[76]

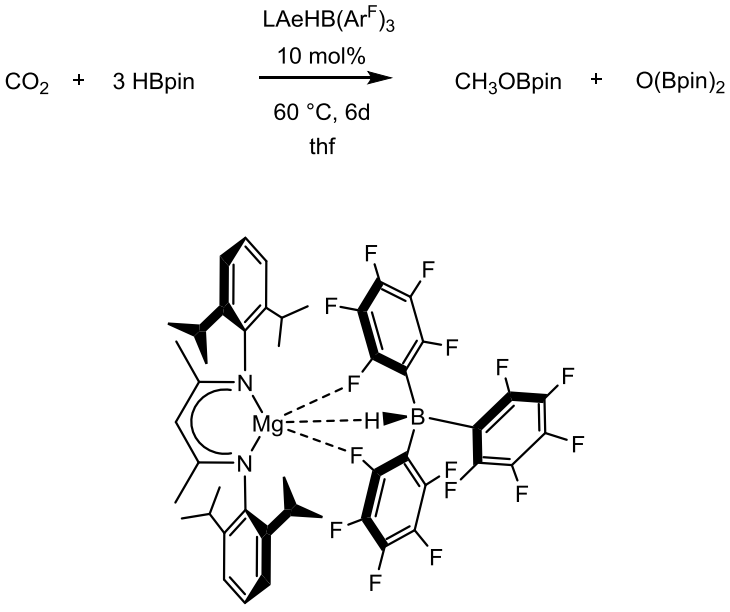


***Figure 28**: Ae-catalysed reduction of CO_2 with HBpin.*[75]

Variation of Ae catalytic activity towards heterofunctionalisation is not easily generalised; although the enthalpy of activation increases on descending the group, this is counteracted by a less negative entropy of activation. For the purpose of heterofunctionalisation, dication activity usually increases in the order of Mg << Ca < Sr. The fact that the reverse order is observed in the heterodehydrocoupling of ABs (*v.i.* Section **1.4.2**(iii), pg. 36) exemplifies the complex interplay of substrate and catalyst.

(ii) Polymerisation

Since its conceptualisation in 1956, the living anionic polymerisation of styrene has been applied to a vast number of alkenes, the polymerisation of which has yielded a diverse landscape of polymeric materials of considerable industrial importance.[77,78] Given the success of other d^0 systems (*cf.* Ziegler-Natta catalyst, pg. 27) in polymerisation catalysis, it will come as no surprise that alkaline earths have been investigated for, and show a propensity towards, the polymerisation of

a variety of substrates. This area has been comprehensively reviewed by Carpentier and Sarazin.[79]

Although Ae catalysed styrene polymerisation dates back to 1973, work in this area has predominantly been carried out by Harder *et al.* from 2000 onwards.[80,81] Initial work gave effectively atactic polystyrene (PS); however, further investigations led to a series of calcium catalysts capable of high syndiotactic selectivity.[82] The general motif of these fluorene systems is displayed in Figure **29**; it was determined that steric bulk in the 2- and 7-position was essential to selectivity in polymerisation.

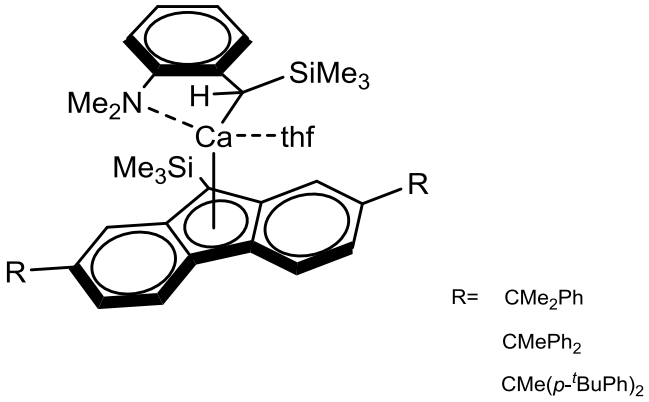


***Figure 29**: Styrene polymerisation catalysts as investigated by Harder et al.*[82]

The source of deviations from syndiotacticity is displayed in Figure **30** below, dissociation from the growing chain allows for stereocentre inversion, thus introducing an error. The simplified, boxed diagram on the left shows the mechanism of such an inversion. The barrier to carbanion dissociation thus presents a deciding factor; the fluorenyl ligand increases this by 2.5 kcal/mol compared to the homoleptic variant of the ligand displayed in Figure **29** and therefore is a crucial contribution to the performance of this calcium system. The presence of excess thf also has a detrimental effect, in both lowering the dissociation barrier and causing rapid disproportionation.[83]

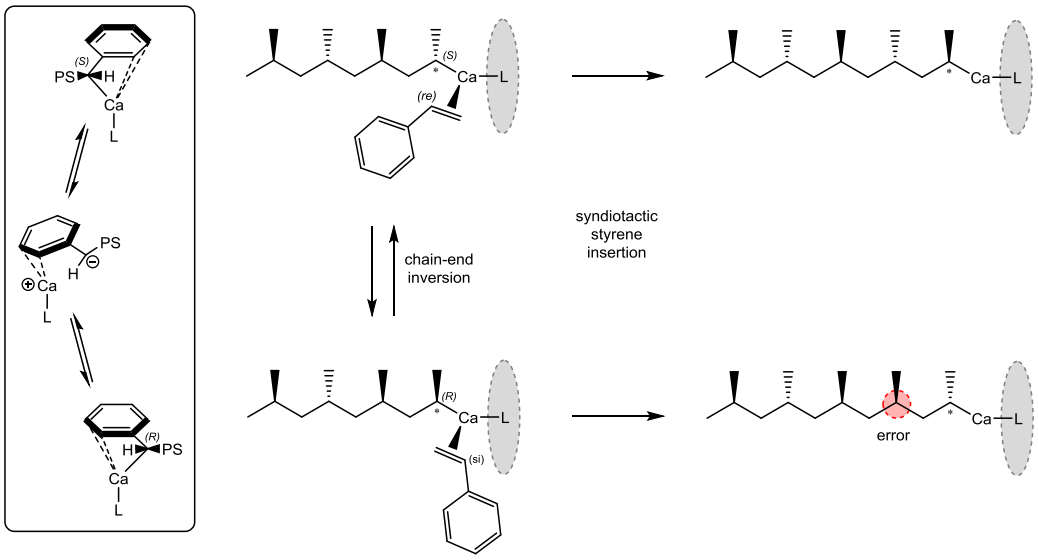


***Figure 30**: PS chain growth and source of errors.*[62]

In addition to the polymerisation of activated alkenes, single-site homogeneous calcium and magnesium catalysts have also proven highly active towards ring-opening polymerisation (ROP) of lactides, a field which has attracted enormous attention in recent years. [84–87] In light of depleting petrochemical feedstocks, the synthesis of a large range of biocompatible polymers from renewable resources presents and extremely enticing target. Given the non-toxicity and abundance of alkaline earths, Ae-catalysed lactide ROP is set for a natural partnership. Other than considerations of sustainability, an environmentally and biologically benign catalyst eliminates the need for its removal from the polymer.

(iii) Heterodehydrocoupling of Amine-Boranes (ABs)

With the growing field of Ae catalysis in general expounded on above, the subject of AB dehydrocoupling deserves particular attention in line with experimental work carried out. Whilst unsubstituted AB presents the most attractive substrate, the formation of insoluble product mixtures and unidentified catalyst deactivation pathways has so far precluded its use in Ae catalysed hydrogen storage. To the best of my knowledge, all reports as of mid-2017 make use of

N-alkylated or arylated substrates.

The first Group II catalysed dehydrocoupling of an AB was reported by Harder *et al.* in 2009,† preceded by investigations of a calcium amidoborane complex for hydrogen storage in the same group.[88,89] This chemistry was quickly, and substantially, expanded upon by Hill *et al.*[90] Although the dehydrocoupling of Me_2AB with $Mg[CH(SiMe_3)_2]_2$ proved a slow process,‡ it selectively yielded the cyclic aminoborane dimer $(Me_2NBH_2)_2$ *via* **1** (Figure **3l**).

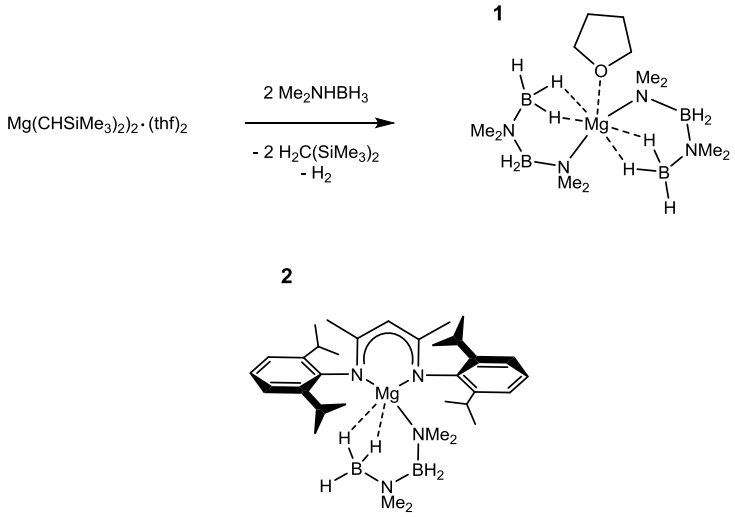


***Figure 3l**: Homo- and heteroleptic Me_2AB dehydrocoupling intermediates.*[90]

Stoichiometric reactions such as that visible above (Figure **3l**), undertaken to identify reaction intermediates, furnished the crystallographically identified **1**. Heating this to 60 °C then yielded the cyclic dimer as observed in catalytic dehydrocoupling. This was proposed to be formed *via* δ-hydride elimination; as the expected Mg hydride species was not observed in the decomposition of **1**, **2** was synthesised from Me_2AB and the corresponding Mg-Nacnac complex to obtain indirect evidence for the hydride. Indeed, decomposition of the former led to the formation of the expected cyclic dimer, with concordant formation of $[Dipp\text{-}Nacnac)Mg(\mu\text{-}H)\cdot(thf)]_2$. It is noteworthy that most AB-Ae systems

† In the form of a Mg-Nacnac catalysed dehydrocoupling of a bulky Dipp-substituted AB, the product of which has since been employed as an f-block ligand.[471]

‡ 3 days at 5 mol% and 60 °C

heavily feature Ae–H agostic interactions, the role of which has been expounded on by Hill *et al.*[91]

Thus, experimental results as well as later DFT studies by Sicilia *et al.* led to the general catalytic cycle displayed below (Figure **32**).[92]

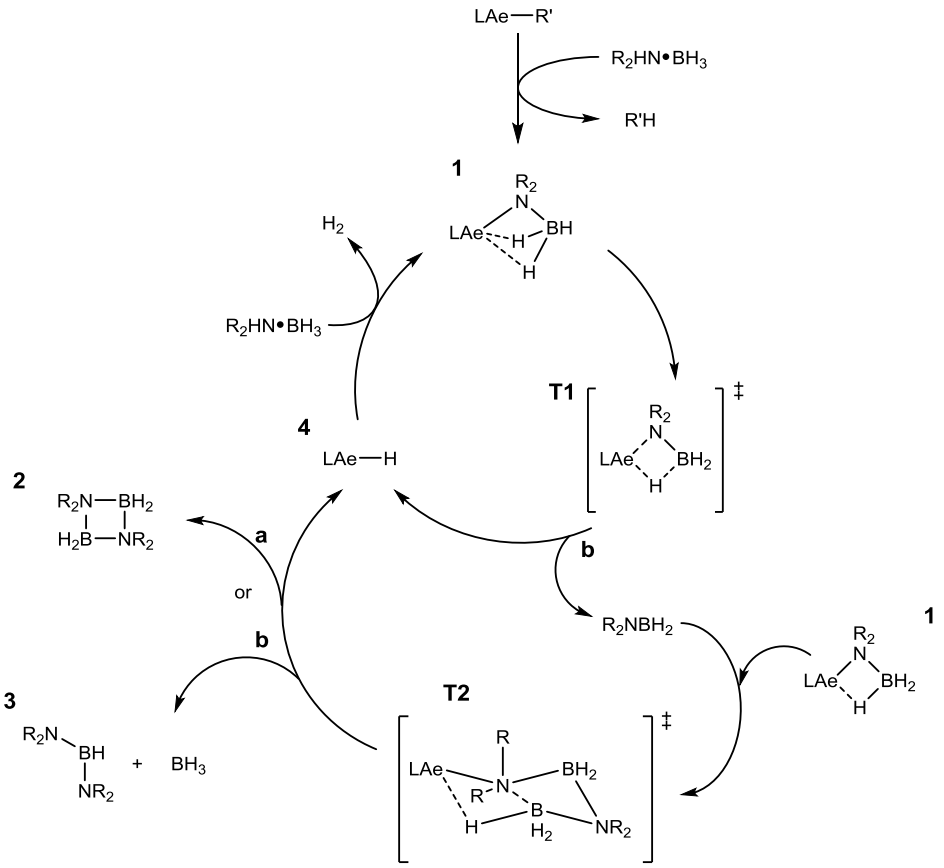


***Figure 32**: Proposed mechanism of Ae catalysed dehydrocoupling, combining the findings of Hill et al. and later DFT studies.*[90,92]

Reaction of LAeR' with AB liberates the protonated organic fragment R'H (*e.g.* $HN(SiMe_3)_2$, ^nBuH or H_2 in case of the hydride) under the formation of **1**. β-hydride elimination (**b**) from this *via* **T1** then forms the Ae hydride **4** (which releases H_2 from R_2AB to reform **1**) and iminoborane. Reaction with a further equivalent of **1** leads to the liberation of commonly observed reaction products such as **2** and **3**. Whilst the latter is formed by β-hydride elimination (**b**), the former takes its origin in an unusual δ-hydride elimination (**a**). **T2** thus offers insight into the formation of cyclic dimers, in a six-membered transition state, a

B–N interaction brings the BH moiety into spatial proximity of the Ae centre, setting it up for δ-hydride elimination and formation of the Ae hydride.

As a general observation on the differences between Ae and TM catalysis, the latter is based on low oxidation state and electron-rich active sites, resulting in catalytic cycles similar to that described for d-block dehydrocoupling in Section **4.1.7**, pg. 168. In contrast, Ae catalysis necessarily precludes mechanisms based around B–H oxidative addition (preceded by a M–BH σ-interaction as observed by Weller *et al.*) and/or B–N reductive elimination.[93]

A series of investigations on the relative activity of Ae complexes by the Hill *et al.* found a general decrease in activity on descending the group, and concluded that "the efficacy of these processes is dramatically affected by the identity of the alkaline earth cation and suggest that the individual kinetic barriers encountered are dependent upon a complex interplay of polarisation and steric effect".[94,95] As an example of either aspect, insertion of iminoborane into the Ae–N bond of **1** (Figure **32**) is significantly slower for Ca, leading to an accumulation of the latter (the self-dimerisation of which is dependent upon N substituents).[96]

Serving as an example of steric effects, the dehydrocoupling of $(Dipp)NH_2{\bullet}BH_3$ by [(Dipp-Nacnac)MgN$(SiMe_3)_2$] does not yield the cyclodimer observed for Me_2AB (*via* δ-hydride elimination), but the β-hydride elimination product $HB[NH(Dipp)_2]$ (Figure **33**; c.f. **3**, Figure **32**).

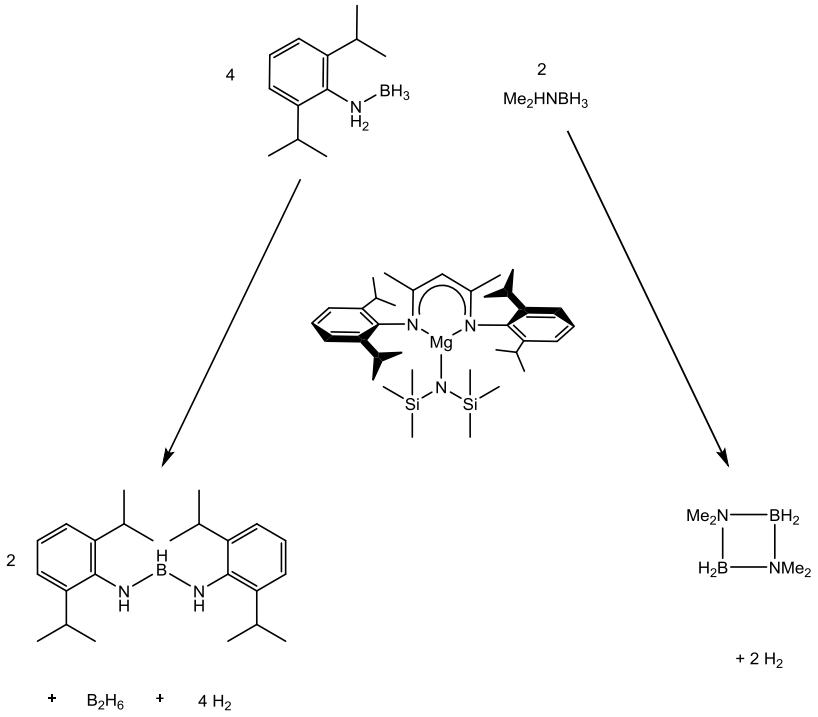


***Figure 33**: Steric effects on AB dehydrocoupling.*

In summary, a variety of s-block complexes are able to catalytically dehydrogenate *N*-substituted ABs. For the more common Group II precatalysts, this proceeds *via* the formation of an LAe(NR_2BH_3) moiety, which then thermally decomposes to liberate H_2. Product distribution depends on the Ae employed, as well as steric bulk, the transition state required for δ-hydride elimination (*v.s.* **T2**, Figure **32**) presumably being disfavoured in bulky systems.

1.5. Ligands: The Backbone of Coordination Chemistry

The term "ligand" takes its origin from the Latin *ligare*, that is to bind/ tie. Modern advances in the area of metal-organic moieties have been made possible by careful choice of these binding partners, allowing the isolation, study and application of distinct molecular species. These myriad of complexes† derive their properties not only from the metal site, but also the structure surrounding it. Complexes shown in Figure **34** exemplify how ligands have shaped this vast field, which inorganic chemists have successfully claimed as their own by virtue of the, predominantly, single metal site surrounded by sophisticated organic frameworks.

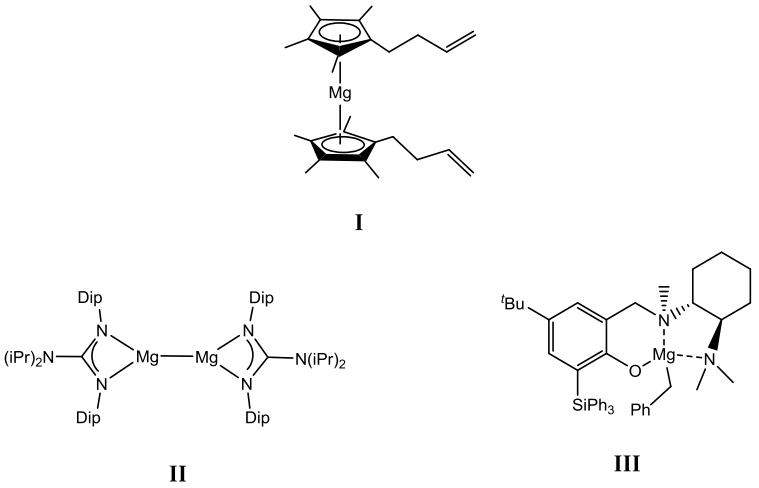


***Figure 34**: Three magnesium complexes bearing varied ligand systems.*

I is a monomeric, hydrocarbon-soluble magnesium metallocene investigated by Lentz *et al.* in the quest for Ae-olefin complexes, **II** the first Mg^{I} species synthesised by Jones *et al.*, and **III** a stereoselective hydroamination catalyst developed by Hultsch *et al.* (*v.s.* Sections **1.2.3** and **1.4.2**(i), pg. 32).[28,72,97] It is

† Somewhat arbitrarily divided into organometallic complexes, *i.e.* those featuring metal-carbon bonds, and coordination compounds, *i.e.* Brønsted base/ Lewis acid pairs. For an overview of the latter, the reader is referred to the weighty compendia Comprehensive Coordination Chemistry I and II.[472,473]

ligand design that has enabled all of the above, and continues to be the driving factor of new discoveries.

For more than a century, alkaline earths have predominantly found use for direct synthetic application. The separation between organometallics and coordination compounds is therefore comparatively well suited to Ae chemistry, with the former species featuring ligands as building blocks, and the latter providing an increasingly diverse amalgamation of catalysis, understanding of structure-reactivity relationships as well as breaking the paradigm of Ae redox inactivity. These fields are driven by the development of sterically demanding, multidentate spectator ligands. The task at hand is the stabilisation of highly reactive Ae mono- and dications: oxo- and hydrophilic, prone to aggregation and promoting ether cleavage, indisposed to form directional interactions.

A review by Hanusa summed up the *status quo* of Ae chemistry towards the end of the 20th century, and is revealingly focussed on Cp systems.[11] In the two decades since, Group II chemistry has undergone a renaissance, as outlined above. Figure **35** displays some of the monoanionic ligand systems commonly encountered in, and instrumental to the development of, modern main group chemistry.

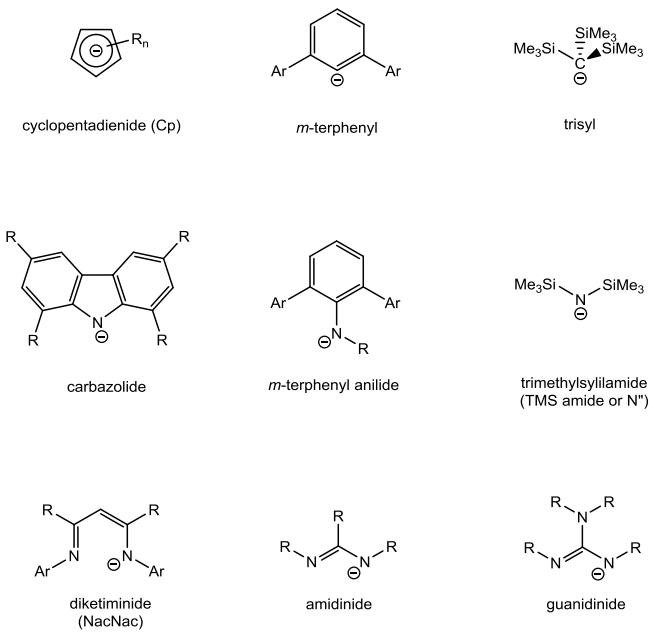


***Figure 35**: Common bulky monoanionic ligand systems in main group chemistry.*

The above ligands and their application in main group chemistry span an expansive field, and many variants on their general theme exist. For recent overviews of some systems, the reader is referred to these excellent reviews: Cyclopentadienides: Hanusa;[15] terphenyls: Clyburne and Mullen;[98] carbazolides and terphenyl anilides: Kays;[99] TMS amides: Coles;[100,101] diketiminides: Roesky *et al.*, Lappert *et al.*;[102,103] amidinides: Kilner an Barker as well as Edelmann (includes guanidinides);[104,105] guanidinides: Jones, with variations of the theme reviewed by Růžička and Chlupatý.[106,107]

Given that many of the well-developed ligand systems listed above have already found extensive use in Ae chemistry, the conceptualisation and investigation of uncommon and novel binding partners was chosen as an area of pursuit. In the course of this work, a total of four frameworks were probed towards their ability to stabilise Ae complexes. These may in turn be divided into two categories, pyridine-based bidentate proligands (**SiL** and **PyL**, Figure **36**), and monodentate benzylamines (**BzL** and **TrL**, Figure **36**).

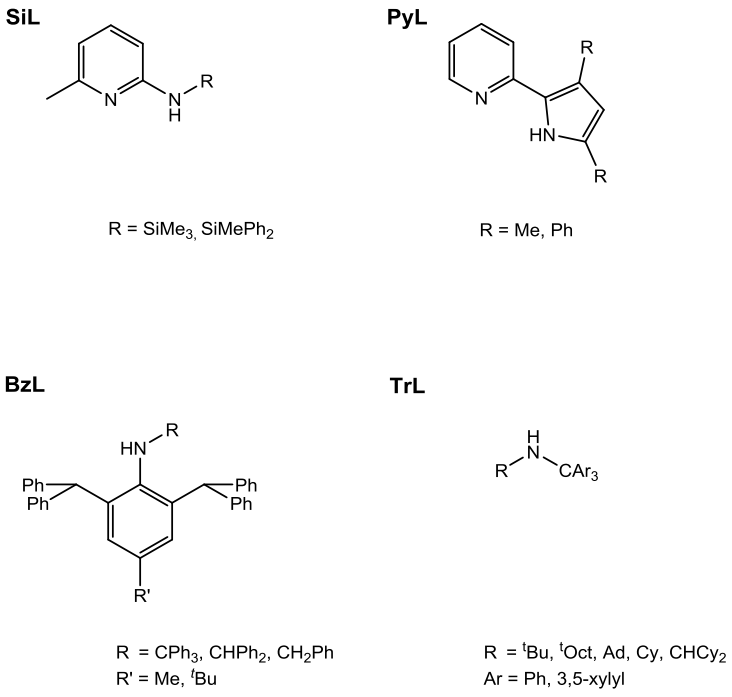


***Figure 36**: The four ligand systems investigated in this work.*

Chapter 2

Silylated Aminopyridines and Pyridylpyrroles

2.1. Silylated Aminopyridines

Amidopyridinides may be considered a cousin of the markedly more popular amidinides (*v.s.* Section **1.5**). They have been intensely studied by the group of Kempe; the application of their Group IV complexes has recently been reviewed.[108–112]

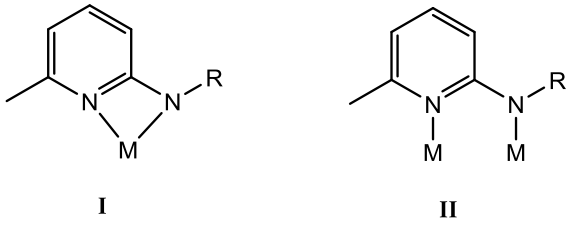


Figure 37: *Strained (***I***) and bridged coordination (***II***) modes of aminopyridinato ligands.*

Amidopyridinides commonly adopt a strained κ^2 binding mode; however, they are equally found to act as bridging ligands (**I** and **II**, respectively; Figure **37**). The former dominates in early TM and lanthanide complexes, whereas **II** is usually observed for late TM compounds.[113–115] Their flexibility within the κ^2 binding mode is a feature intrinsically linked with the accessibility of mesomeric forms, **A** and **B** in Figure **38**).

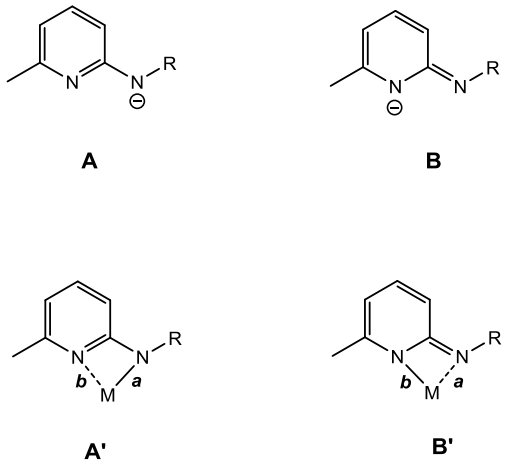


Figure 38*: Resonance forms and corresponding binding motifs of amidopyridines (***A** *and* **A'***) and iminopyridinides (***B** *and* **B'***).*

In the prevalent κ^2 mode, compounds originating from the deprotonation of 2-aminopyridines are collectively referred to as aminopyridinato complexes in the literature.[110] Given the two nitrogen-based resonance forms, this is a misnomer in either case: **A** is representative of amidopyridinide complexes, **B** of imidohydropyridinide systems.† Metal-nitrogen distances offer a convenient indicator to differentiate between the two, *i.e.* determine prevalence of one resonance form over the other. Metal–N_{amido} distances will be shorter than M–$N_{pyridine}$ for **A** (***a*** and ***b*** respectively, Figure **38**), with the reverse holding true for **B**. A comparative study by Kempe *et al.* found a considerably larger contribution of **A** in complexes featuring lanthanides or early TMs, with examples of coordination mode **B** being confined to a few late transition metals not adopting the bridged form (**II**, Figure **37**).[110]

With the first TM amidopyridinide complex reported by Cotton *et al.* in 1984, s-block examples followed in 1988, which were expanded to Group XIII complexes in 1990.[116–118] Out of the multitude of examples reported thus far, the stabilisation of an ultra-short, five-fold Cr–Cr interaction stands out as a particularly noteworthy achievement (Figure **39**).[119]

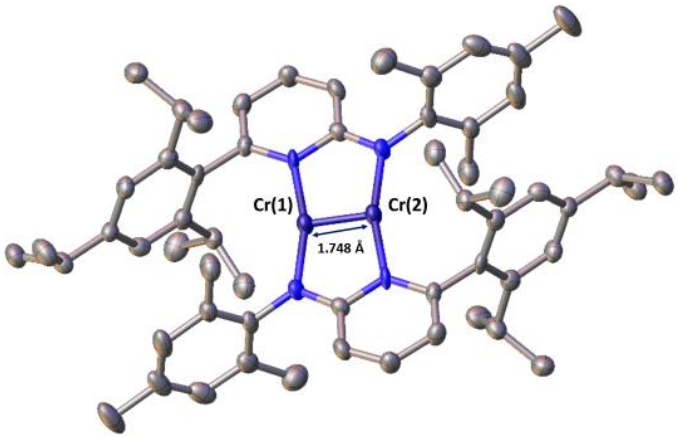


***Figure 39**: Molecular structure of [Tip(C_5H_3N)NCr(Mes)]$_2$ featuring an ultra-short Cr-Cr interaction (1.7489(18) Å), with ellipsoids set at at the 50% probability level; hydrogen atoms are omitted for clarity.*[119]

† Named here without a distinction between the binding nitrogen as both presumably have some contribution. Alternatively, if one were to base nomenclature strictly on the dominant nitrogen only, amidopyridines for **A**, and iminohydropyridinides for **B**.

As a subset of the above, silylated aminopyridines have formed an integral part of this generic ligand motif, with facile tuning and commercial availability of the incorporated silyl moiety offering easily accessible frameworks of varying steric bulk. From early Group I examples,[117] silylated aminopiridinide coordination chemistry has gone on to span the Periodic Table, from early to late transition metals,[113,115,120–122] main group,[118,123–125] and f-block complexes.[126,127] This class of ligand has shown a propensity towards stabilising heterobimetallic species, as reported for lanthanide-alkali metal complexes by Kempe and Lee *et al*.[127,128] A bimetallic magnesium complex has been isolated by Liu *et al.*, employing a terdentate aminosylil substituted amidopyridinide ligand.[129]

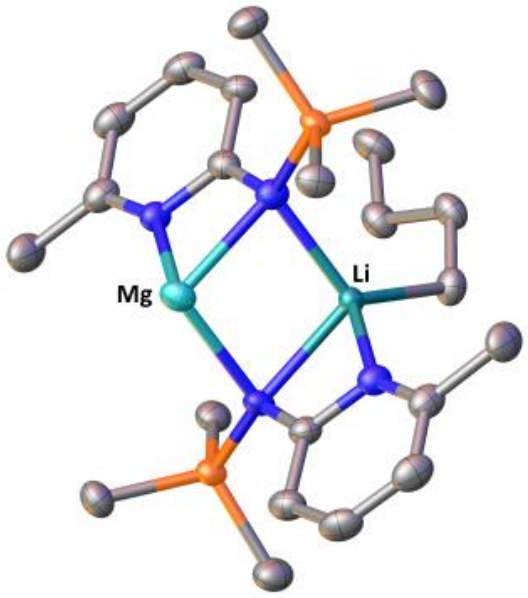


***Figure 40**: Monomeric unit of [**SiMeL**MgLi^{n}Bu]$_{\infty}$ with ellipsoids set at the 50% probability level; hydrogen atoms are omitted for clarity.*[41]

Notwithstanding some isolated examples, amidopyridinide alkaline earth complexes remain relatively rare; particularly in the case of heteroleptic species.[129–132] However, this area was substantially expanded upon by Kays *at al.*, who reported the first heavier Group II amidopyridinide, as well as a series of novel heterobimetallic s-block complexes.[41] Out of these, [**SiMeL**MgLi^{n}Bu]$_{\infty}$ as seen in Figure **40** stands out as a rare example of a mixed metal Li/Mg complex, the first structurally characterised example of an unsupported bridging alkyl

moiety between two metal centres. These advances notwithstanding, there is only a single literature example of a structurally authenticated heteroleptic amidopyridinide magnesium halide, employing the aforementioned terdentate aminosilyl substituted amidopyridinide.[129]

As halide fragments present valuable functional handles to allow the exploration of further reactivity, it was the aim of this work to synthesise **SiL**AeX species. Steric saturation was assumed to be a key component in stabilising the latter, thus attempts were made to synthesise a bulkier **SiL** framework. Whilst the synthesis and reactivity of **SiL** supported coordination compounds is discussed below, applications in dehydrocoupling form the basis of Chapter **4**.

2.1.1. Results and Discussion

(i) SiL Proligands and Work Towards Increased Steric Bulk

The silylated 2-aminopyridines **SiMeL**H and **SiPhL**H were synthesised according to literature procedures, with minor modification previously developed within our group as displayed in Figure **41**.[117,133]

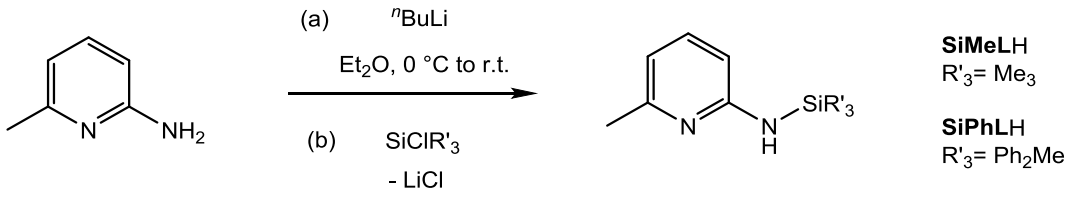


***Figure 41**: Synthesis of **SiMeL**H and **SiPhL**H.*

Although the introduction of a bulkier –$SiPh_3$ substituent has been attempted within our group, a reaction analogous to the above but incorporating $ClSiPh_3$

did not furnish the desired ligand, even at prolonged reaction times and elevated temperatures.† Attempts to synthesise a bulkier framework were therefore focused on the pyridine 6-position. Figure **42** outlines the path towards such proligands. A pyridine-R^2 disconnection of **B** was discounted due to the required amine protection prior to $C_{pyridine}$–C or $C_{pyridine}$–N bond formation. Amination (**C** to **B**) was considered either *via* the 6-H or 6-halo pyridines as discussed below (Figure **44**).

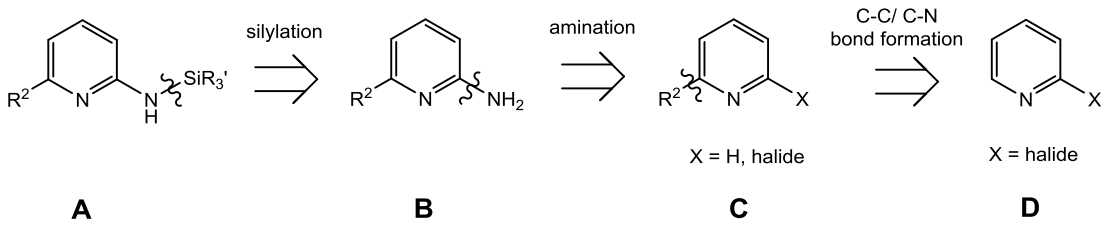


***Figure 42**: Retrosynthetic overview of **SiL** proligands.*

Two **C** precursors incorporating large aromatic R^2 substituents were previously synthesised within our group, two further carbazole-functionalised pyridines within this work according to Figure **43**.

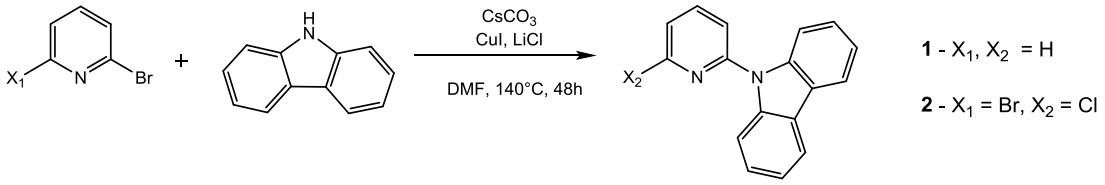


***Figure 43**: Synthesis of carbazole-functionalised pyridyls.*

Comparatively large amounts of reagents required necessitated the development of a work-up procedure not dependent upon column chromatography; fractional

† In contrast, the synthesis of $(Ph_3C)NH(C_5H_3N)NH(CPh_3)$ from the corresponding aminopyridine and trityl chloride has been reported to proceed smoothly in good yield, rendering electronic factors a likely culprit for the unavailability of a comparable $SiPh_3$ analogue.[293]

recrystallisation of **1** from pentane/chloroform afforded the pure title compound in significantly higher yield than previously reported (86% *vs.* 74%).[134] The novel chloropyridylcarbazole **2** was selectively obtained by an identical procedure in slightly lower yield. It is noteworthy that halide exchange occurred in the synthesis of the latter, as corroborated by mass spectrometry and XRD. Should 6-Br retention be required (*e.g.* for facile lithium-halogen exchange), this may be achievable by the use of LiBr instead of LiCl with uncertain effects on yield.

The synthesis of aminopyridines **C** was then attempted *via* (i) the Chichibabin reaction for **1** (Figure **43**), as well as mesityl- and triisopropylphenyl-substituted pyridine according to published procedures,[135,136] in addition to (ii) copper-catalysed amination of bromoarylpyridines according to Figure **44**.[137]

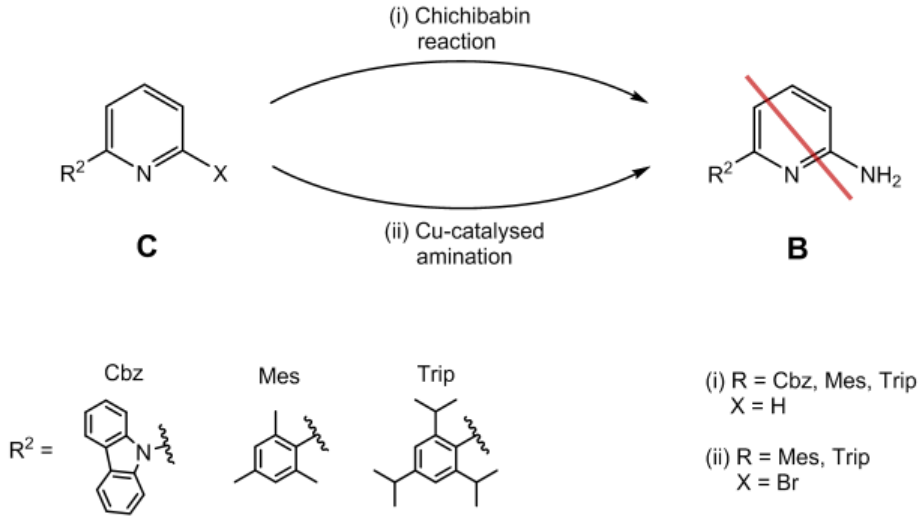


***Figure 44**: Attempted pathways to pyridine amination.*

Neither approach furnished the desired aminopyridine, with only unreacted starting material isolated from reactions involving Mes- and Trip-substituted pyridines regardless of methodology, and (i) with pyridinylcarbazole yielding an intractable mixture.

As all pyridines screened in the Cu-catalysed amination by Renaud and co-workers are considerably smaller and do not incorporate flanking aryl groups,

the lack of conversion for 6-Mes and 6-Trip bromopyridines may be attributed to insufficient solubility in the polar reaction medium. Electronic effects are unlikely to be the culprit, as substituents considerably more electron-donating than Mes and Trip (methoxy) only resulted in a slight decrease in conversion at 60 °C.[137] Conversely, electron-donating groups are known to inhibit Chichibabin amination, presumably rendering the α-$C_{pyridine}$ too electronegative for nucleophilic attack by $^{-}NH_2$.[138] Sodium amide quality is also know to significantly affect conversion to the amine.[139] Pyridylcarbazole did not tolerate the harsh reaction conditions. In light of the above difficulties, complex stabilisation by a secondary Lewis base, *i.e.* a donor entity, was considered a more promising avenue of pursuit.

(ii) Metalation

As metathesis reactions of **SiL** Group I salts with AeX_2 exclusively afforded homoleptic species or bimetallic complexes in previous work, organoelimination was chosen as an avenue to retain halide functionality. Although the heteroleptic zinc chloride of **SiMe**L has been reported, and the dimeric [**SiMeL**ZnEt]$_2$ is structurally known, comparable magnesium analogues remain absent from the literature.[121] Stabilisation of such species is achieved with steric as well as coordinative saturation, *i.e.* by internal solvation. Common donor moieties include those based on tertiary amines such as pmdta and tmeda, *e.g.* in the isolation of structurally verified PhCaI•(tmeda)$_2$.[140]

Thus, after a series of attempts to isolate **SiL**MgX from reacting proligands with MeMgX were frustrated by isolation of homoleptic complexes and magnesium dihalides, and attempts to increase steric bulk on the ligand were made to no avail (*v.s.* Section **2.1.1**(i)), addition of tmeda enabled the isolation of the heteroleptic magnesium iodide **4** (Figure **45**).

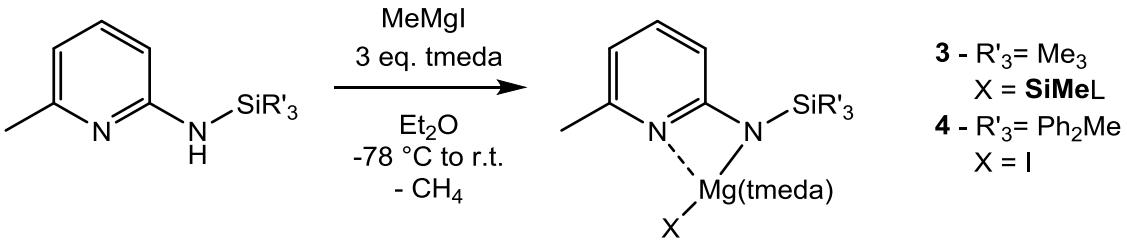


Figure 45: *Synthesis of **3** and **4** by organoelimination.*

In case of the less sterically demanding **3**, only the homoleptic (**SiMeL**)$_2$Mg(tmeda) could be isolated and structurally characterised (Figure **46**). In the absence of tmeda, spectroscopic data were consistent with homoleptic **SiMeL**$_2$Mg previously synthesised within our group by salt metathesis and organoelimination.[133]

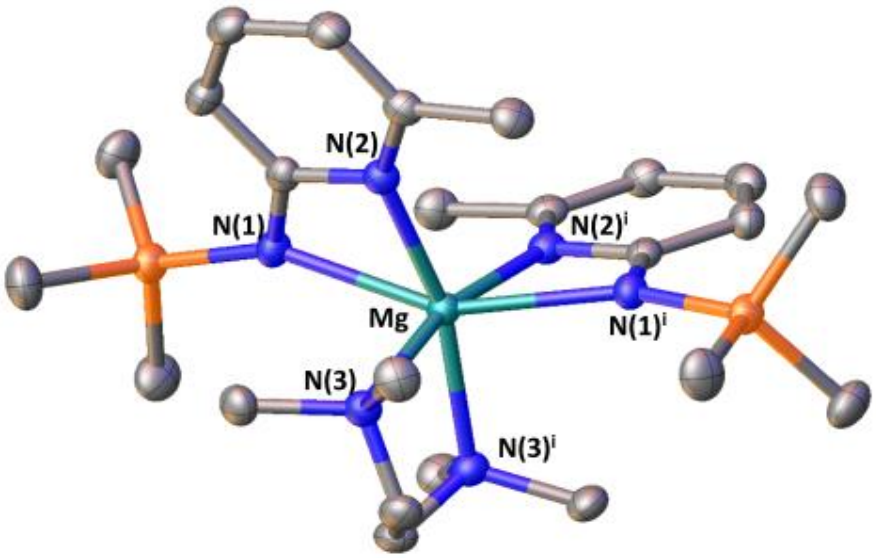


Figure 46*: Molecular structure of **3** with ellipsoids set at at the 50% probability level; hydrogen atoms have been omitted for clarity. Symmetry transformation used to generate equivalent atoms: (i)* $^3/_2$-x,$^3/_2$-y,-z.

Complex **3** adopts a pseudooctahedral geometry, in which magnesium is bound to two amidopyridinide ligands as well as one tmeda molecule in a *cis* MA_4B_2-type conformation. Deviation from an ideal octahedral geometry is the result of

acute bite angles as listed in Table **2**. tmeda exhibits an expectedly larger bite angle than the more constricted **SiMeL**.

***Table 2**: Selected bond distances (Å) and angles (°) in **3**.*
Symmetry transformation used to generate equivalent atoms: (i) $^3/_2$-x,$^3/_2$-y,-z.

N(1)–Mg	2.2677(12)	C(6)–Mg	2.6314(17)
N(2)–Mg	2.1509(12)	N(1)–Mg–N(2)	62.15(5)
N(3)–Mg	2.3205(13)	N(3)–Mg–N(3)^i	78.61(8)

Bond lengths indicate a slight preference towards an imidohydropiridinide binding motif, with the closest N–Mg contact observed at N(2), followed by N(1) and N(3). The latter are comparable to bond lengths observed in *e.g.* formamidine complexes such as [(tmeda)Mg{(*p*-MePh)NCHN(*p*-MePh)}].[141] Considerably shorter N_{tmeda}–Mg contacts (2.20-2.22 Å) have been reported in lower coordinate systems;[142,143] conversely, octahedral systems able to better meet the electrostatic demands of the metal centre whilst avoiding steric clash, *e.g.* acetylide ligands, exhibit longer N_{tmeda}–Mg interactions (2.38-2.39 Å) than those observed in **3**.[144,145]

In contrast to the above, employment of the bulkier **SiPhL** allowed for the isolation of the corresponding heteroleptic organomagnesium halide **4**,† the first example of the latter supported by a silylated amidopyridinide. Multinuclear NMR spectra are in excellent agreement with the desired [**SiPhL**MgI(tmeda)], with a slight downfield shift of most ^{1}H resonances observed in comparison to the free ligand, as well as disappearance of the N*H* signal. In an analogous comparison of ^{13}C{^{1}H} NMR spectra, the most pronounced diamagnetic shift was observed for $CH_3C(CH)_3CN$, which was shifted downfield from δ 157 ppm to 170 ppm. The identity of **4** was further ascertained by elemental microanalysis as

† Material isolated from an analogous reaction in the absence of tmeda showed highly congested spectra inconsistent with either the sample consisting solely of homoleptic **SiPhL**$_2$Mg or **SiPhL**MgI. Only the former could be isolated in purification attempts (previously synthesised within our group).[133]

well as single crystal X-ray crystallography. In the solid state, the pentacoordinate **4** adopts a distorted trigonal bipyramidal geometry, with both **SiPhL** and tmeda spanning an axial and equatorial positions, and iodine occupying the remaining equatorial site as visible in Figure **47** below.

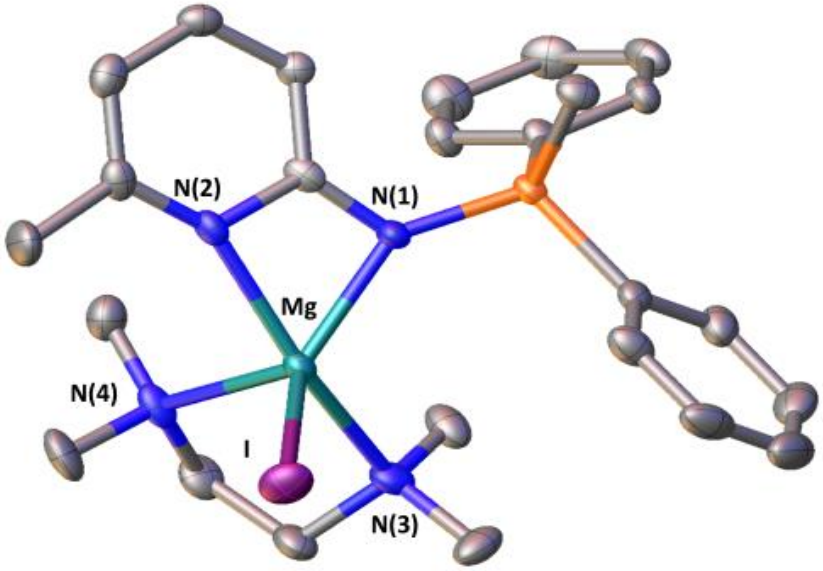


***Figure 47**: Molecular structure of **4** with ellipsoids set at at the 50% probability level; hydrogen atoms have been omitted for clarity. **4** crystallised with two distinct but chemically identical molecules in the asymmetric unit (labelled b in Table **3**).*

In contrast to **3**, the amide functionality is in closer proximity to the metal centre than pyridine by *ca.* 0.1 Å; poorer coordinative saturation in **4** results in shorter N–Mg distances compared to **3** (relevant bond lengths and angles are listed below in Table **3**). The variance in N_{tmeda}–Mg lengths is attributed to the proximity of, and resulting steric clash between, axial N(3) and N(7) positions with neighbouring phenyl rings. Such steric factors are also likely the root cause of N(2)–Mg(1) > N(1)–Mg(1); axial bond distances are longer than their equatorial counterparts for identical ligands in trigonal bipyramidal systems such as phosphorus pentahalides.[146] Observed bond lengths are comparable to those reported in the related diketiminide $[\{(Dipp)NCH_3CHCH_3N(CH_2CH_2N(CH_3)_2)\}MgI(Et_2O)]$.[35]

***Table 3**: Selected bond distances (Å) and angles (°) in **4**.*

$N(1)_{eq}$–Mg(1)	2.082(8)	N(1b)–Mg(1b)	2.076(8)
$N(2)_{ax}$–Mg(1)	2.178(8)	N(2b)–Mg(1b)	2.198(8)
$N(3)_{ax}$–Mg(1)	2.297(8)	N(3b)–Mg(1b)	2.269(9)
$N(4)_{eq}$–Mg(1)	2.218(8)	N(3b)–Mg(1b)	2.237(8)
C(6)–Mg(1)	2.561(9)	C(6)–Mg(1b)	2.551(9)
I(1)–Mg(1)	2.746(3)	I(1b)–Mg(1b)	2.744(3)
N(1)–Mg–N(2)	64.2(3)	N(1b)–Mg–N(2b)	64.2(3)
N(3)–Mg–N(4)	80.1(3)	N(3b)–Mg–N(4b)	79.8(3)

Efforts to exploit the halide functionality in **4** for halide abstraction with $NaBAr^F{}_4$, Mg–Fe bond formation with $KFeCp(CO)_2$, hydride formation with KH as well as reduction with potassium were made to no avail, with only unreacted **4** isolated from all of the above.† This passivity uncharacteristic of Grignard reagents extends to the thermal stability of **4,** which tolerated heating to 60 °C in C_6D_6 for several days without evidence of decomposition. However, **4** showed a remarkable activity towards the heterodehydrocoupling of aminoboranes, as discussed in detail in Chapter **4**.

2.1.2. Conclusions and Future Work

The silylated amidopyridinide ligand **SiPhL** has successfully been employed in the isolation of the first heteroleptic organomagnesium halide stabilised by such a framework, **4**. This required a combination of steric bulk and the presence of an external bidentate donor entity; absence of either resulted in the formation of homoleptic species or intractable mixtures. The divergence in N_{amide} and $N_{pyridinide}$ to magnesium bond distances observed across previously reported complexes and those synthesised within this work demonstrates the flexibility

† ^1H and ^{19}F NMR spectroscopy provided tentative evidence for the formation of **SiPhL**MgF in reactions with $NaBAr^F{}_4$, this could not be substantiated by mass spectrometry or structural data.

of the above ligand system towards adopting different binding motifs linked to available resonance forms (*v.s.* Figure **38**, pg. 45).

It is felt that although the introduction of bulkier pyridine α-substituents is unquestionably possible, and the resulting steric saturation would likely enable the stabilisation of otherwise ephemeral species, frameworks such as the related amidinides (**II**, Figure **48**) are better suited for such applications. These not only allow for facile installation of large flanking groups, but also buttressing to affect bite angles as displayed in Figure **48**.



I II

Figure 48: *Silylated amidopyridinides (I) and amidinides (II).*

This notwithstanding, it is the personal opinion of the author that the open nature of **I**, combined with appropriate semi labile donor entities, is better able to accommodate the equipoise between steric protection and availability of active sites for catalytic transformations as explored in Chapter **4**. A lack of C_2 symmetry further opens up avenues in asymmetric catalysis, as illustrated in the synthesis of metalachlor, an important herbicide produced on an industrial scale.[147] Here, a key iridium-catalysed hydrogenation was drastically improved by breaking C_2-symmetry of the previously employed phosphine ligand. The general benefits of such nonsymmetrical ligands have been reviewed by Pfaltz.[148]

2.1.3. Experimental

Synthesis of SiMeLH

To a colourless solution of 2-amino-6-methylpyridine (8.10 g, 75 mmol) in Et_2O (200 mL) was added drop wise ^{n}BuLi (30 mL, 2.5 M in hexane, 75 mmol) at 0 °C; the resulting yellow solution stirred for a further 2 h before slow addition of trimethylchlorosilane (9.9 mL, 78 mmol) causing the immediate formation of a LiCl precipitate. The mixture was stirred overnight, filtered, and solvent removed from the filtrate *in vacuo* to yield the crude product (12.75 g, 94%) which was distilled at 65 °C and $6x10^{-2}$ mbar to afford Si**L**^{1}H as a clear, free-flowing oil (15.49 g, 86%, d = 0.91 ±0.01 gcm^{-3} at 20°C) stored as a 1 M solution in hexanes.
Spectroscopic data matches those previously reported.[133]

Synthesis of SiPhLH

Following the same procedure as for **SiMeL**H. From 2-amino-6-methylpyridine (6.48 g, 60 mmol), ^{n}BuLi (2.5 M in hexane, 24 mL, 60 mmol) and diphenylmethylchlorosilane (13.2 mL, 63 mmol) was fractionally distilled at 140 °C and $3x10^{-2}$ mbar the title compound as a viscous clear oil (15.06 g, 82%) stored as a 1 M solution in hexanes.
Spectroscopic data matches those previously reported.[133]

Synthesis of pyridinylcarbazole [1]

According to a modified literature procedure:[134] To a suspension of carbazole (2.51 g, 15mmol), caesium carbonate (4.88 g, 15 mmol), lithium chloride (0.635 g, 15 mmol) and copper (I) iodide (0.285 g, 1.5 mmol) in dry degassed DMF (100 mL) was added 2-bromopyridine (2.52 g, 16 mmol) and the resulting mixture heated to 140 °C for 48 h. After being allowed to cool to room temperature, the brown mixture was charged with ammonium chloride (100 ml conc.), extracted with ethyl acetate (3*40 mL) and the combined organics washed with brine (20 mL), dried over magnesium sulfate and volatiles removed *in vacuo* to yield a free-flowing brown oil (11.11 g) further dried on high vacuum

(10^{-3} mbar). Fractional crystallisation from pentane/chloroform (1:1) yielded the title compound as brown crystals (3.15 g, 86%). Literature yield: 74%.

^{1}H NMR ($CDCl_3$, 298 K, 400 MHz): δ = 8.75 (dd, *J*=4.8, 1.2 Hz, 1 H), 8.11 - 8.18 (m, 2 H), 7.91 - 7.98 (m, 1 H), 7.86 (dt, *J*=8.3, 0.8 Hz, 2 H), 7.66 (d, *J*=8.0 Hz, 1 H), 7.46 (ddd, *J*=8.3, 7.1, 1.3 Hz, 2 H), 7.34 (td, *J*=7.5, 1.0 Hz, 3 H), 7.30 - 7.33 (m, 1 H) ppm.

^{13}C-{^{1}H} NMR ($CDCl_3$, 298 K, 101 MHz): δ = 151.9, 149.7, 139.6, 138.5, 126.2, 124.3, 121.2, 120.9, 120.2, 119.1, 111.1 ppm.

MS: (ESI) m/z $[M+H]^+$ Calc'd for $C_{17}H_{13}N_2$ 245.1073; Found 245.1074.

Synthesis of 6-chloropyridinylcarbazole [2]

In a an identical procedure to that listed above (**1**), carbazole (2.51 g, 15 mmol), caesium carbonate (4.88 g, 15 mmol), lithium chloride (0.635 g, 15 mmol), copper(I) iodide (0.285 g, 1.5 mmol) and 2,6-dibromopyridine (3.79 g, 16 mmol) were reacted in dry degassed DMF (50 mL) to obtain a brown oil (7.51 g) further purified by recrystallisation to obtain the title compound as brown crystals (2.4 g, 57%).

^{1}H NMR ($CDCl_3$, 298 K , 400 MHz): δ = 8.10 - 8.18 (m, 3 H), 8.05 (d, *J*=8.2 Hz, 1 H), 7.92 (d, *J*=8.4 Hz, 1 H), 7.87 (t, *J*=7.9 Hz, 1 H), 7.58 - 7.67 (m, 1 H), 7.41 - 7.51 (m, 3 H), 7.31 - 7.38 (m, 3 H) ppm.

^{13}C-{^{1}H} NMR ($CDCl_3$, 298 K, 101 MHz): δ = 151.6, 150.8, 140.7, 140.4, 139.5, 139.2, 126.5, 126.4, 124.6, 121.5, 121.3, 121.1, 120.2, 120.2, 116.6, 115.0, 112.0, 111.4 ppm.

MS: (ESI) m/z $[M+H]^+$ Calc'd for $C_{17}H_{12}ClN_2$ 279.0684; Found 279.0677. Chlorine isotope pattern match.

General Chichibabin amination protocol

According to literature procedure with minor modifications.[135,136] To the mono α-substituted pyridine in N,N'-dimethylaniline was added an excess of sodium amide (*ca.* 6-fold), the solution degassed with argon, and heated to 170 °C for 4 h under argon. Upon cooling to room temperature, the suspension was filtered and the residue washed with diethyl ether. The combined organic extracts were

quenched with potassium hydroxide (1 M aq.) at at 0 °C, the aqeous layer extracted with diethyl ether (3*30 mL). Combined ethereal extracts were washed with brine, dried over magnesium sulfate, and volatiles removed *in vacuo*.

General copper catalysed amination protocol

According to modified literature procedure.[137] The reaction vessel was charged with the relevant 6-bromopyridine (1.39 mmol), ammonia (1.53 mL, 35% / 18.1 M, aqueous), potassium carbonate (37 mg, 0.27 mmol), copper (I) oxide (10 mg, 0.07 mmol), *N,N*-dimethylethylenediamine (12 mg, 0.14 mmol) and ethylene glycol (5 mL), the resulting mixture briefly degassed with argon and heated to 60 °C for 16 h under argon. Upon cooling the biphasic mixture was filtered through glass wool and celite, which was subsequently flushed with ethyl acetate (2*15 mL). The blue aqueous layer was extracted with ethyl acetate (2*15 mL), the combined organic extracts then washed with water, brine, dried over magnesium sulfate, and volatiles removed *in vacuo*.

Reaction of of SiMeLH with MeMgI [3]

To a solution of MeMgI·$(Et_2O)_{1.5}$ (1.526 g, 5.5 mmol) in Et_2O (50 mL) at -78 °C was added drop wise **SiMeL**H (5 mL, 1 M in hexanes, 5 mmol) to result in the formation of a white precipitate. The mixture was stirred for 1 h, allowed to warm to room temperature causing the precipitate to dissolve, and stirred overnight. Filtration of the mixture and removal of solvent from the filtrate yielded a white powder (1.30 g, 78% based on **SiMeL**MgI).

NMR: Samples of sufficient concentration for NMR could not be prepared due to solubility issues, indicative of aggregate formation.

Reaction of of SiPhLH with MeMgI

Following the same procedure as for **3**. From MeMgI • 1.5 Et_2O (1.526 g, 5.5 mmol) and **SiPhL**H (5 mL, 1M in hexanes, 5 mmol) was isolated a white powder (2.21 g, 97%).

^{1}H NMR (C_6D_6, 298 K, 400 MHz): Multitude of overlapping signals, none of

which can definitively be attributed to a specific position.
$^{13}C\{^{1}H\}$ NMR (C_6D_6, 298 K, 100 MHz): δ = -1.66 (Si(CH_3), 14.13 (Et_2O), 24.38 (CH_3), 66.10 (Et_2O), 110.64 (CH), 129.17 (Ar-CH), 129.97 (Ar-CH), 134.69 (Ar-CH), 135.57 (CH), 139.33 (Ar-C), 140.00 (CH), 154.25 (C) ppm.

Synthesis of SiPhLMgI•(tmeda) [4]

To a suspension of MeMgI·$(Et_2O)_{1.5}$ (1.526 g, 5.5 mmol) in diethyl ether at -78 °C was added dropwise a solution of **SiPhL**H (10 mL, 0.5 M in Et_2O/hexanes, 5 mmol) over 45 min, stirred at -78 °C for a further 2 h, and allowed to warm to -30 °C. Subsequently, tmeda (2.25 mL, 15 mmol) was added, the resultant gel was allowed to warm to room temperature overnight. The milky suspension was filtered and volatiles removed from the filtrate *in vacuo*; washing of the residue with cold hexanes afforded the title compound as a white solid (1.80 g, 63%).
^{1}H NMR (C_6D_6, 298 K, 400 MHz): δ = 0.73 (s, 3 H, SiC*H*$_3$), 1.63 (s, 4 H, *tmeda*), 1.77 (s, 12 H, *tmeda*), 2.39 (s, 3 H, PyC*H*$_3$), 5.98 (d, *J*=7.15 Hz, 1 H, Py*H*), 6.21 (d, *J*=8.41 Hz, 1 H, Py*H*), 6.80 (overlapping d, *J*=8.41 & 7.15 Hz, 1 H, Py*H*), 7.19 (m, 2 H), 7.24 - 7.32 (m, 4 H), 7.87 (m, 4 H) ppm.
$^{13}C\{^{1}H\}$ NMR (C_6D_6, 298 K, 100 MHz): δ = -0.48 (Si(*C*H$_3$)Ph$_2$), 23.29 (Py*C*H$_3$), 46.75 (*tmeda*), 56.14 (*tmeda*), 109.69 (Py*C*H), 111.56 (Py*C*H), 128.94 (Py*C*H), 135.04 (Ar*C*H), 138.35 (Ar*C*H), 140.80 (Ar*C*H), 154.51 (Py*C*), 170.05 (Py*C*) ppm (quaternary Si*C*Ar obscured by solvent).
$C_{25}H_{35}IMgN_4Si$ (570.15): calc'd (%) C 52.60, H 6.18, N 9.81; found (%) C 52.49, H 6.03, N 9.72.

2.2. Pyridylpyrroles

Pyridylpyrrolides are a class of pyrrolide ligands derived from the deprotonation of 2-(2'-pyridyl)pyrroles. Ligands featuring the pyrrolide functionality have previously been employed in the stabilisation of heavy alkaline earth complexes, notably the calcium complexes of **I**, binding in an η^5 fashion, and **II**, in which a linker arm forces σ-N bonding (Figure **49**).[149–151] Pyridylpyrrolides may be seen as an extension or close relative of **II**, providing a linker functionality with an extended π-system (**III**, Figure **49**). They may equally be compared to the previously discussed amidopyridinides.

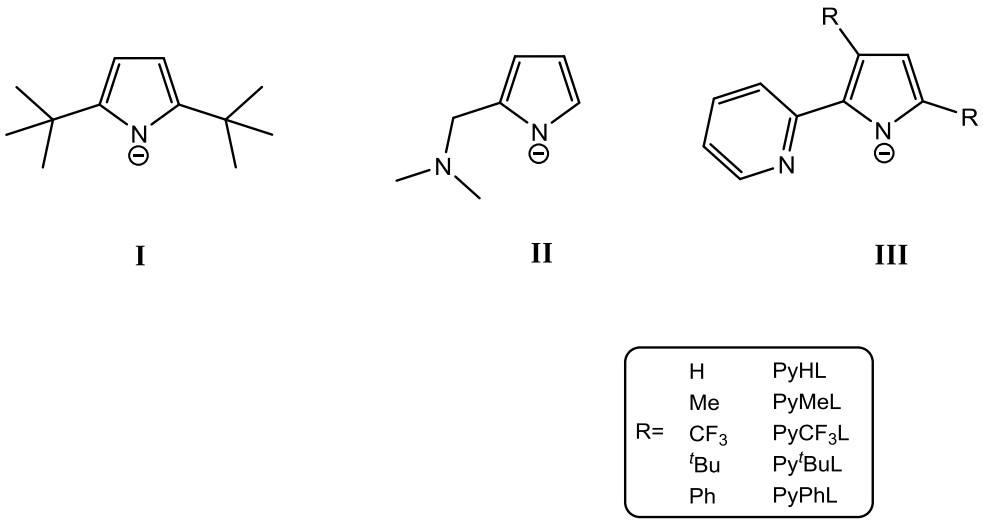


***Figure 49**: Pyrrolato ligands without (**I**) and with a linker arm (**II**) and the investigated pyrrolepyridinato.ligand* **III** with commonly used examples and their abbreviations.

The influence of pyridine as a donor in **III** is exemplified by the rarity of pyrrolide π complexation observed in the solid state. Known examples are confined to a coordination polymer, as well as a potassium ferrate and cobaltate reported by Searles.[152,153] Analogous to the Ca complex of **II**, the pyridyl linker forces σ-N bonding. Similar to the aforementioned aminopyridinato ligands (*v.s.* Figure **37**), pyridylpyrrolides can form five-membered metallacycles in a κ^2 binding motif, or act as a bridging binding partner (**III$_a$** and **III$_b$** respectively, Figure **50**).



III$_a$ **III$_b$**

***Figure 50**: Strained (**I**) and bridged coordination (**II**) modes of pyrrolepyridinato ligands.*

Although bridging pyrrolide has been described, the bridging pyridylpyrrolide (**PyL**) system **III$_b$** is extremely rare.[154] A comprehensive search of the Cambridge Structural Database (CSD) only revealed a single structurally known true example, shown below (Figure **51**).[155,156] The potassium salt of the same ligand exists as a coordination polymer, with both $N_{pyrrole}$ and $N_{pyridine}$ simultaneously coordinated to two potassium fragments.[152]

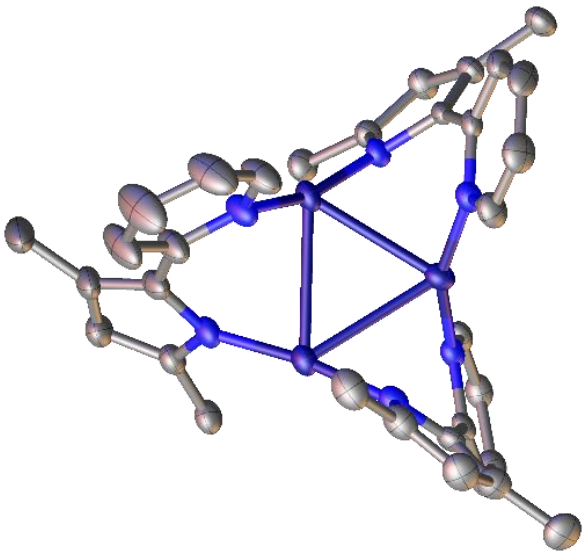


***Figure 51**: Molecular structure of [(**PyCF$_3$L**)Cu]$_3$ as reported by Caulton et al., with ellipsoids set at at the 30% probability level; hydrogen and fluorine atoms are omitted for clarity.*[156]

PyLs may adopt a wide range of conformations, as exemplified by the combination of tautomers (with a negative charge on nitrogen) and rotamers in Figure **52**.

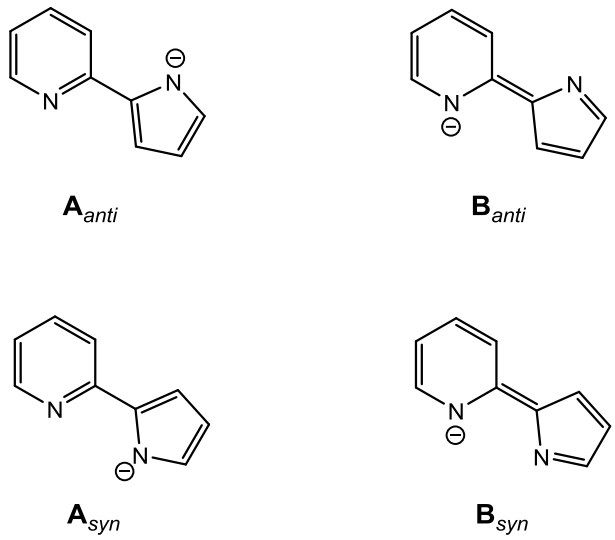


***Figure 52**: Tautomers and rotamers of **PyL** with a formal negative charge on nitrogen.*

In practice, all structurally known complexes adhere to a *syn* conformation, as opposed to **PyL**$_{anti}$ bridging in opposite directions. Free **PyHL**H proligands adopt the same conformation; calculations have shown the **PyMeL**H$_{syn}$ form to be energetically favourable over its *anti* counterpart by 4.3 kcal/mol, with a rotational barrier of 11.3 kcal/mol.[152,157–160] The *syn* confirmation of **PyMeL**H in solution was also demonstrated by ^{1}H NOESY NMR spectroscopy.[158] In contrast, in the related free ligand **PyCF$_3$L**$^-$, a coplanar *anti*-conformation is favourable by *ca.* 4.5 kcal/mol to **PyCF$_3$L**$_{syn}$ as a result of nitrogen lone pair repulsion in the gas phase.[152]

Bond lengths in **PyL** complexes are good indicators of the influence of one tautomer over another. In pyrrolides, the N$_{pyrrolide}$–M distance should be shorter than N$_{pyridine}$–M, with the reverse holding true for pyridinides (***a*** and ***b*** respectively, Figure **53**). The length of ***c*** serves as a further indicator.

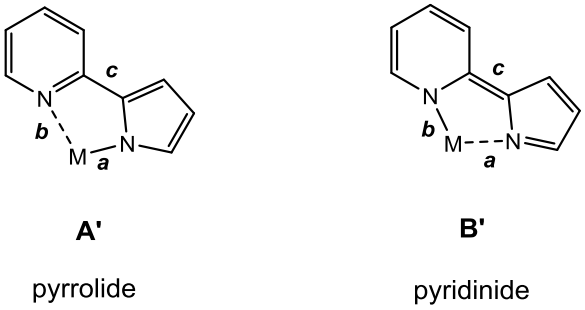


Figure 53**: Binding forms of tautomers* $\mathbf{A}_{syn}$ *(pyrrolide* **A') and* $\mathbf{B}_{syn}$ (pyridinide **B'**).

In order to address the question of binding mode prevalence and variation, a comprehensive survey of structurally known complexes was compiled. Table **4** does not include terdentate systems and mostly excludes larger conjugated systems, *i.e.* quinolides and indolides.

***Table 4**: Bond lengths (cf. Figure **53**) of pyridylpyrrolides (i: contains example(s) of indolide(s)).*

Bound element (# of examples)	***a*** $N_{pyrrole}$–$M_{(mean)}$ (Å)	***b*** $N_{pyridine}$–$M_{(mean)}$ (Å)	***b-a*** (Å)	**Absolute difference**† (as % of x̄ N–M bond length)	***c*** mean $C_{pyrr.}$– $C_{pyrid.}$ (Å)	**Ref.**
K (1)	2.819	2.972	0.153	5.284	1.477	[152]
Be (1) [i]	1.665	1.746	0.081	4.749	1.463	[161]
Ti (1)	2.119	2.256	0.137	6.262	1.437	[162]
Fe (1)	2.112	2.116	0.004	0.189	1.464	[153]
Ru (1)	2.082	2.108	0.026	1.241	1.446	[160]
Co (1)	1.981	2.040	0.059	2.934	1.457	[153]
Rh (1) [i]	2.074	2.134	0.060	2.851	1.440	[160]
Ir (3)	2.106	2.128	0.022	1.039	1.434	[160,163,164]
Ni (5)	1.934	1.972	0.038	1.955	1.435	[165,166]
Pd (3)	2.026	2.012	-0.014	0.693	1.432	[167,168]
Pt (5) [i]	2.036	2.082	0.046	2.243	1.427	[169–171]
Cu (3)	1.943	2.046	0.103	5.196	1.463	[152,156,172]
Au (3)	2.043	2.061	0.018	0.877	1.474	[173,174]
Zn (4) [i]	1.962	2.081	0.119	5.897	1.464	[159,161,175]
B (2)	1.538	1.624	0.085	5.407	1.445	[161,176]
x̄	2.029	2.092	0.062	3.122	1.454	

With the exception of Pd complexes, all $N_{pyrrolide}$–M distances are shorter than their pyridine counterparts. However, the difference in bond length is frequently small. It was felt that preference towards **A'** (or **B'** for Pd, Figure **53**) is best expressed as a percentage of the average N–M bond length within a complex or homologous series. For example, the above listed potassium complex (first

† $|\boldsymbol{a} - \boldsymbol{b}/\frac{\boldsymbol{a}+\boldsymbol{b}}{2}| \times \mathbf{100}$ (for **a** and **b** see Figure **53**)

entry, Table **4**) has a $N_{pyrrolide}$–K distance 5.28% shorter than $\overline{N–K}$, and thus a preference for **A'** (Figure **53**).

***Table 5**: Comparison of N-M bond lengths in selected amidopyridinides and pyridylpyrrolides (blue: shorter $N_{amide/pyrrolide}$ distance, red: shorter $N_{pyridinide}$ distance).*

Bound element	**Bonding mode preference** (as a function of % of mean N–M bond lengths)	
	Amidopyridinide[110]	***Pyridylpyrrolides***
Ti	7.52_{amide}	$6.26_{pyrrolide}$
Ni	1.98_{amide}	$1.95_{pyrrolide}$
Pd	$1.00_{pyridinide}$	$0.693_{pyridinide}$
Cu	$22.1_{pyridinide}$	$5.19_{pyrrolide}$
Zn	$0.469_{pyridinide}$	$5.89_{pyrrolide}$

The observed preference for $N_{pyrrolide}$ over $N_{pyridinide}$ binding stands in contrast to the more variable amidopyridinides as shown in Table **5**. This may be attributed to two comparatively "soft" binding sites in **PyL** *vs.* a "hard" and "soft" site respectively in amidopyridinides: Charge accrued on pyridine and pyrrole is more easily delocalised, consequently presenting a more polarisable/ softer site than the adjacent amide functionality. This factor is most strongly reflected in Cu amidopyridinides above (Table **5**), in which bond distances reflect the preference of a relatively soft metal centre to bind to pyridine.[177–179] Additionally, differences in ring strain between the five-membered metallacycles of **PyL** *vs.* the four-membered amidopyridinide system may further contribute to the observed variance.

As a general consideration of preference towards resonance forms in the protonated ligand, *i.e.* pyridylpyrrole or hydropyridylpyrrolylidene (**A**H and **B**H, respectively; Figure **52**), the length of $C_{pyridine}$–$C_{pyrrole}$ (***c***, Figure **53** and Table **4**)

may be used as a marker. This has an average value of 1.462 Å† with a standard deviation of 0.0103 Å.[152,157–160] There is no clear effect of electron withdrawing groups *vs.* electron donating groups on pyrrole, with both **PyCF$_3$L**H and **Py^{t}BuL**H exhibiting larger values of ***c*** (1.468 Å and 1.479 Å)[152,159] than the unsubstituted **PyHL**H (1.454 Å).[157] Instead, steric repulsion between pyrrole 2- and 3-substituents generally increases torsion angles between the aromatic rings, with a concomitant lengthening of ***c*** as described in Section **2.2.1(i)** below. All of the above values put $C_{pyridine}$–$C_{pyrrole}$ for **PyL** in the region of a conjugated C_{sp^2}–C_{sp^2} bond (Table **6**) well short of a true aromatic interaction.

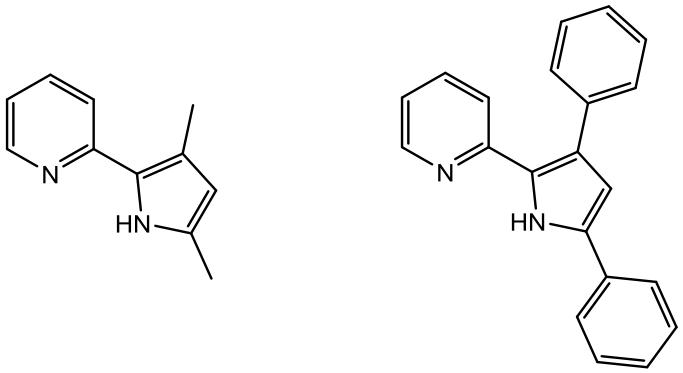
***Table 6**: Selected average bond lengths.[180]*

Bond	Bond length (Å)
C_{sp^3}–C_{sp^3}	1.53 - 1.55
C_{sp^3}–C_{sp^2}	1.49 – 1.52
C_{sp^2}–C_{sp^2} *non-conjugated*	1.47 – 1.48
conjugated	1.45 – 1.46
C_{Ar}≃C_{Ar}	1.38
C_{sp^3}–N_{sp^3} *amine*	1.46 – 1.48
C_{sp^2}–N_{sp^3} *1-H pyrrole*	1.37
C_{sp^2}–N_{sp^2} *imine*	1.35

It is in part this delocalisation which has made pyridylpyrrolides the focus of photophysical and electrochemical investigations for OLEDs, as well as being

† Compared to the slightly shorter 1.454 Å with a standard deviation of 0.0157 Å for **PyL** complexes (**Error! Reference source not found.**).

explored for gas sensing applications.[163,174,176,181,182] Although no Ae pyridylpyrrolide complexes are structurally known,† a series of Zn analogues have been synthesised and closely related compounds showed promising results in ε-caprolactone ROP.[161,175,176,183] The unexplored field of alkaline earth pyridylpyrrolide chemistry was therefore chosen as an attractive area of pursuit.



PyMeLH PyPhLH

***Figure 54**: Pyridylpyrrole proligands employed in this work.*

Towards this purpose, **PyMeL** and **PyPhL** were selected as ligands of varying steric protection, and their s-block chemistry probed by means of transamination, salt metathesis and organoelimination.

2.2.1. Results and Discussion

(i) Proligands

The syntheses of fused heteroaromatic systems such as pyrrolepyridines usually involve complex, many-step, low-yielding reactions, often employing transition metal catalysed coupling for the more recent examples.[184–189] A considerably

† There is a single structurally know example of a closely related Be pyridylindolide.[161] In addition to the CSD,[204] SciFinder® and Reaxys® searches have not revealed any additional references to **PyLAe** systems.

more facile approach to the synthesis of **PyL**H proligands was identified, involving the condensation of a diketone with 2-aminomethylpyridine (Figure **55**).[190]

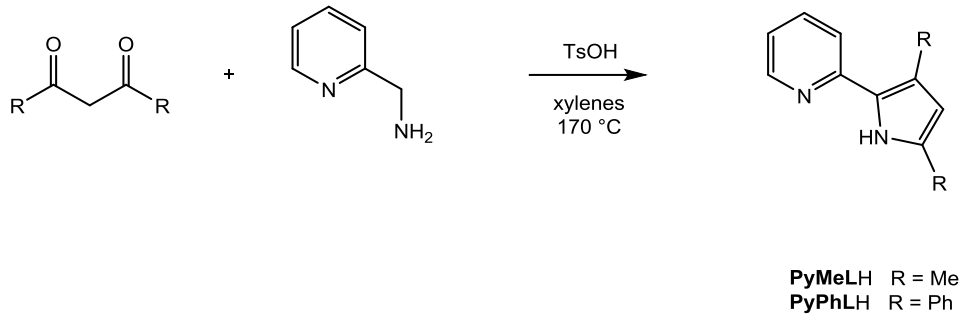


***Figure 55**: **PyL**H synthesis by condensation.*[190]

The known proligands **PyMeL**H and **PyPhL**H were synthesised according to the above literature procedure with minor modifications.[190] Purification was achieved by washing with sodium hydroxide solution, recrystallisation, and sublimation in contrast to column chromatography which was considered impractical for large scale work-up. As an interesting spectroscopic feature, ^{1}H ^{4}J W-coupling of pyrrole backbone C*H* to N*H* was observed in both proligands and verified by D_2O shake. As well as influencing steric crowding, the electronic alteration brought about by the introduction of phenyl groups is considerable. This is illustrated by the significant downfield shift of $CH_{pyrrole}$ from 5.8 ppm in **PyMeL**H to 6.5 ppm in **PyPhL**H. Additionally, whilst all formed complexes show fluorescence under UV light, **PyMeL**H shows none and **PyPhL**H weakly fluoresces. X-ray quality crystals were grown from cyclohexane/ ethanol and ethanol for **PyMeL**H and **PyPhL**H, respectively. Whereas the former adopts a hydrogen bonded dimer in the solid state, the latter is monomeric (Figure **56**). The presence of dimers in solution has been shown to be temperature as well as concentration dependent, with no **PyMeL**H dimers observed at low concentrations (10^{-8}-10^{-5} M, room temperature), although their presence at higher concentrations (0.06 M, -80 °C) has been confirmed by NOESY NMR studies.[191]

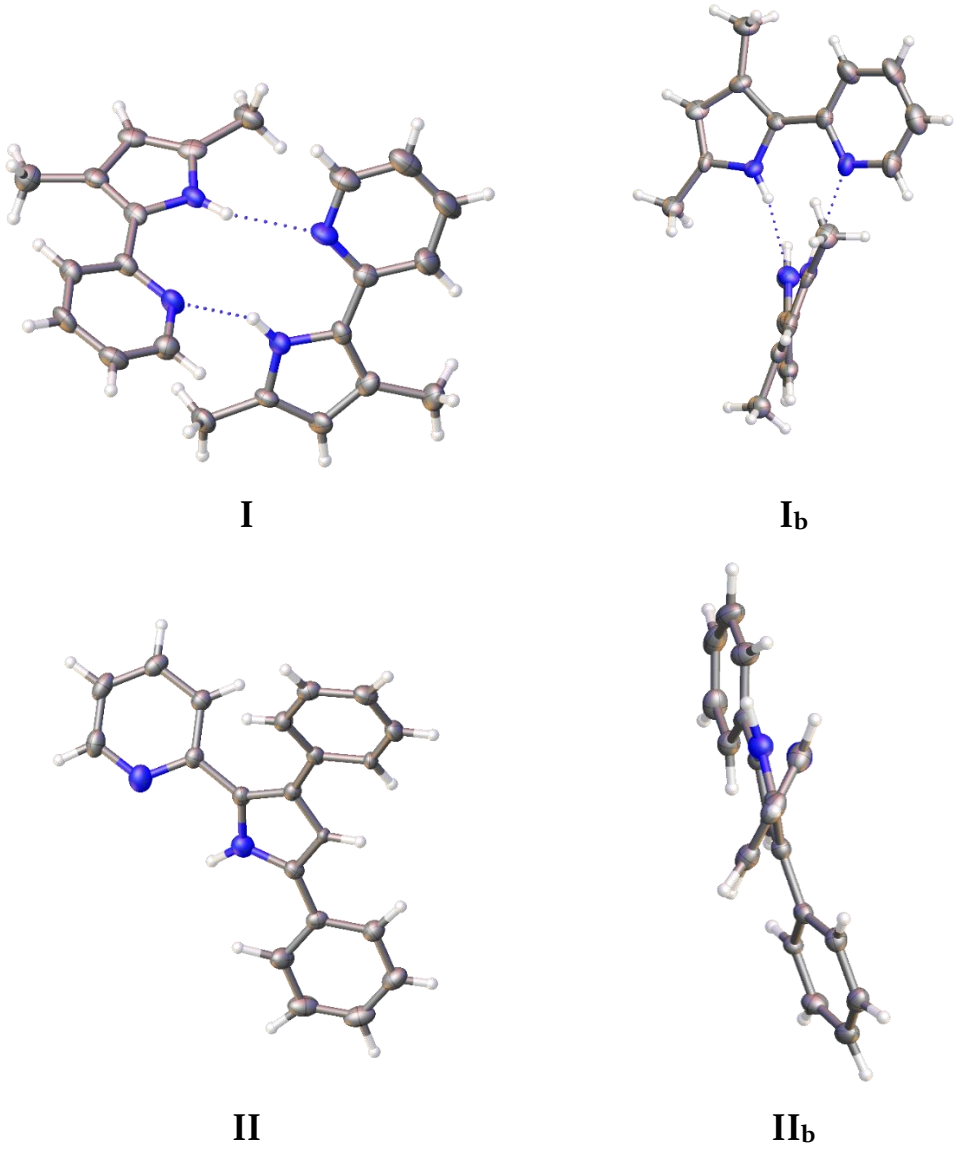
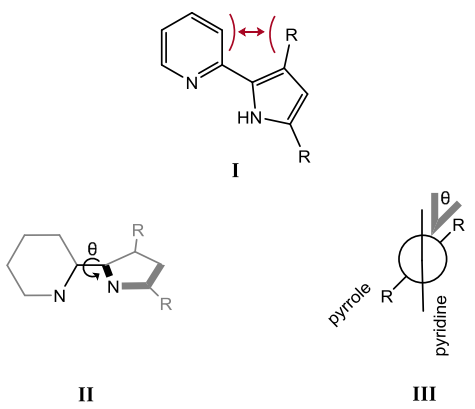


***Figure 56**: Molecular structures of (**PyMeL**H)$_2$ (**I**) and **PyPhL**H (**II**) with side-on views to demonstrate twist angles (**I$_b$** and **II$_b$**). H atoms drawn as spheres of arbitrary radius in calculated positions. Ellipsoids set at at the 50% probability level.*

Although a solid state **PyMeL**H dimer is known, the structure determined in this work is a polymorph with distinctively different features as displayed in, and discussed below Figure **57** (Me$^{(ii)}$ *vs.* Me$^{(i)}$).[158] Pyridylpyrrole proligands are known to exist as hydrogen bonded homodimers in the solid state, these frequently display different plane twist angles and $C_{pyridine}$–$C_{pyrrole}$ bond lengths between otherwise identical molecules as displayed in Figure **57**.[57–60] Interheterocycle π system overlap is dependent upon ring coplanarity, torsion angles therefore have a profound effect on properties intrinsically linked with

large delocalised systems, as exploited in a series of pyridylpyrrolide complexes (such as photophysical applications, *cf.* **2.2.1(ii)**). Although mainly investigated as their respective metallacycles, protonated **PyL**H systems have attracted interest in the area of intermolecular exited state proton transfer, the photoprotolytic activity of which is dependent upon delocalised systems.[158,191,192]



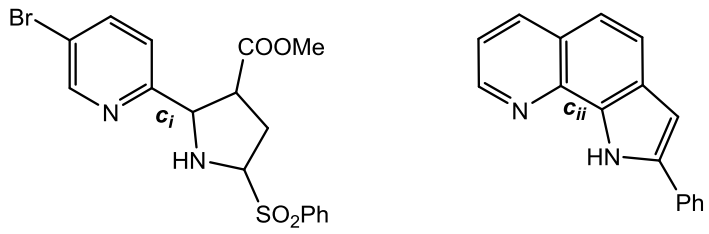
R	θ (°)	$C_{pyrrole}$-$C_{pyridine}$ (Å)
H$^{(i)}$	13.63(8)	1.454(2)
Me$^{(ii)}$	0.745(5) and 20.135(17)	1.437(8) and 1.458(7)
Me$^{(i)}$	10.92(6) and 16.71(8)	1.453(2) and 1.454(2)
CF$_3$ $^{(i)}$	32.1(3) and 36.6(3)	1.468(3) and 1.479(3)
Ph$^{(ii)}$	38.70(8)	1.475(3)
^{t}BuL$^{(i)}$	56.79(10) and 61.61(10)	1.463(3) and 1.479(3)

***Figure 57**: Proligands with their respective torsion angles and $C_{pyridine}$–$C_{pyrrole}$ bond lengths in the solid state.*
(i) literature values, (ii) determined within this work.
Those systems with two given lengths exist as dimers in the solid state. [152,157–160]

As R increases in size, steric repulsion (**I**) causes a larger twist angle θ between planes (**II** and **III**, all Figure **57**).† A larger deviation from coplanarity is concomitant with poorer π system overlap, and consequently $C_{pyridine}$–$C_{pyrrole}$ increases in length. Whilst these values unsurprisingly vary between different ligands, they also differ within the two molecules constituting a hydrogen bonded dimer. In this work, the (**PyMeL**H)$_2$ units display a significantly higher degree of anisotropy between each other in the solid state than that reported in the literature (Figure **57**, R = Me$^{(i)}$ & Me$^{(ii)}$).[158] Whilst one molecule is almost entirely coplanar, in the second pyridine and pyrrole rings are offset by 20°,

† For comparison of the less obvious Me *vs.* CF_3, their tetrahedra occupy 0.1135(15) and 0.341(2) Å^3, respectively.

whereas Blank *et al.* have reported offsets of 11° and 17°. In all of the above, an increase in θ correlates with a longer $C_{pyridine}$–$C_{pyrrole}$ distance from 1.437(8) to 1.458(7) Å. For comparison, these values lie between those of a system lacking conjugation, and one of an extended planar π-system, such as **I** and **II** in Figure **58** respectively.

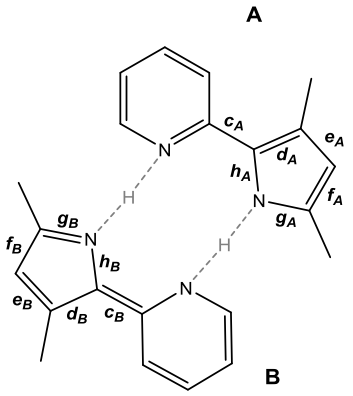


I **II**

c_i = 1.508 Å c_{ii} = 1.408 Å

***Figure 58**: Representative examples of a lower (**I**) and higher (**II**) degree of delocalisation.*[193,194]

As a measure of the flexibility towards tautomeric forms thus exhibited, Figure **59** shows selected bond lengths, providing a general agreement with (**PyMeL**H)$_2$ existing as an adduct of two molecules with respective tendencies towards one tautomer over the other in the solid state (Figure **52**).



Label	Bond lengths proposed **A** (Å)	Bond lengths proposed **B** (Å)	Δ (%)
c	1.458(7)	1.437(8)	1.44
d	1.373(10)	1.400(1)	1.97
e	1.424(9)	1.394(6)	2.16
f	1.360(8)	1.363(7)	0.232
g	1.357(7)	1.362(9)	0.352
h	1.376(7)	1.378(7)	0.0965

***Figure 59**: (**PyMeL**H)$_2$ dimer with corresponding bond lengths (blue: longer, orange: shorter).*

Whilst 1.44% may appear a negligible difference, the bond length variation of a non-conjugated C_{sp^2}–C_{sp^2} *vs.* C_{Ar}≃C_{Ar} is *ca.* 7% (Table **6**), the effect can therefore be described as significant. The variance observed in twist angles as well as bond lengths therefore lies testament to a highly flexible ligand system, theoretically capable of accommodating a range of electronic demands.

Attempts at pre- as well as post-heterocycle formation functionalisation of the **PyL** system, chiefly by pyridine α-substitution, were undertaken to no avail. Either required protection of the NH_x functionality prior to further substitution. For pre-heterocyle formation functionalisation, protection as a phthalimide was successful, whereas pyridine *N*-oxide formation was not. In attempted substitutions of formed **PyL**H systems, NH protection by tosylation or introduction of a *tert*-butyloxycarbonyl group yielded inseparable mixtures. By and large, pyridine substitution proved a fruitless and time consuming enterprise.[†]

(ii) Synthesis of s-Block Complexes

$KN(SiMe_3)_2$ was chosen as a metallating agent over previously employed KH due to the former's better solubility in a range of solvents and milder nature.[152,195] Reaction of the proligands with $KN(SiMe_3)_2$ thus afforded the solvent free potassium salts **5** and **6** (Figure **60**); the formed amine could easily be removed *in vacuo* and by washing residual material with hexane. ^{1}H NMR spectroscopy gave good evidence for the formation of the desired species, with a shift of all signals and disappearance of any NH signals, also manifested in the pyrrole backbone C*H* being observed as a singlet.

[†] Pyridine functionalization is a challenging area of pursuit, an excellent overview of which has been compiled by Comins *et al.*[209] *N*-oxide formation as reviewed by Yousif[474] gives access to improved nucleophilicity, which in turn has been employed in the synthesis of *e.g.* aminopyridines.[475–477] A variety of methods present themselves for pyridine α-lithiation as reviewed by Woltermann, the most recent advances being the use of LiDMAE.[478,479]

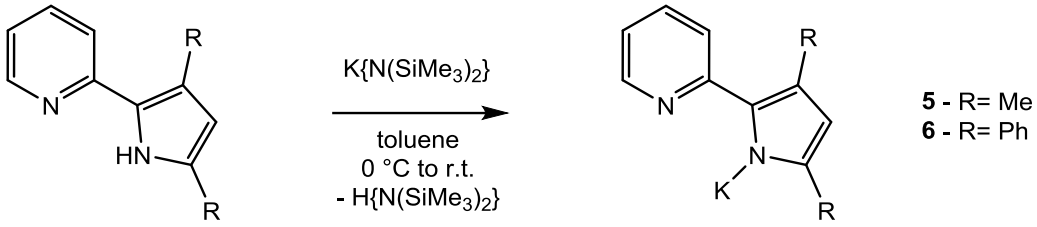


Figure 60: *Synthesis of potassium salts* ***5*** *and* ***6*** *by transamination.*

Both **5** and **6** displayed extremely poor solubility in hydrocarbon solvent systems, in 1:1 C_6D_6:D_8-thf, sample concentrations were not sufficient to obtain full $^{13}C\{^1H\}$ NMR data. The general broadness of spectroscopic features is indicative of dynamic aggregate formation; indeed, the structurally authenticated **5** revealed just such a polymeric array in the solid state, displayed in Figure **61**. Repeated attempts at obtaining X-ray diffraction grade single crystals of **6** were frustrated by challenging solubility as well as exceedingly poor crystallinity of the **PyL** system in general. Gas-phase diffusion and layering experiments at -30 °C frequently yielded amorphous material.

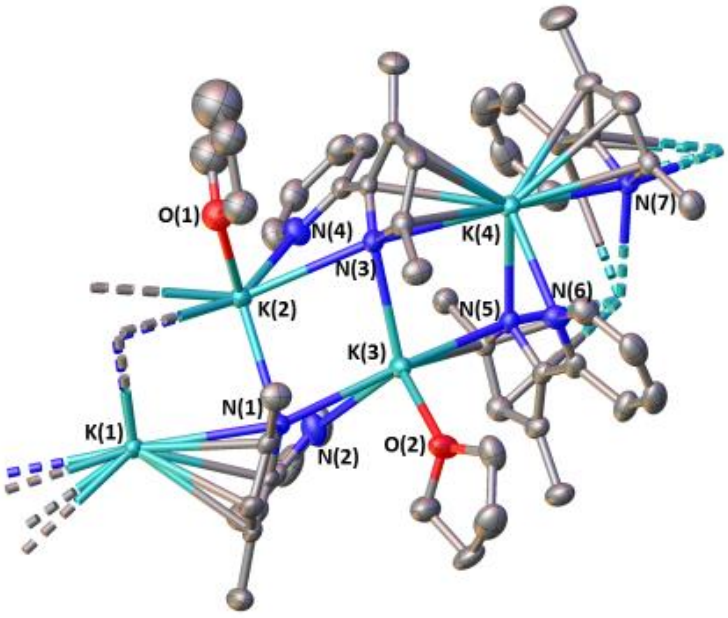


Figure 61: *Repeating unit of* ***5****,* ***[PyMeLK•thf$_{0.5}$]$_\infty$*** *with ellipsoids set at at the 50% probability level; hydrogen atoms are omitted for clarity.*

The ladder-esque coordination polymer **5** is schematically represented in **I,** (Figure **62**). **PyMeL** subunits adopt two binding motifs, shown as **A** and **B** in **II**. The repeating unit of **5** is comprised of three **A** and a single **B** subunit. Whereas $N_{pyrrole}$ bridge three potassium centres in either, **A** accomplishes this *via* an η^5 interaction as opposed to η^2 in **B**. The former is a very common feature of alkali metal complexes, particularly the heavier homologues.[196] $N_{pyridine}$ exclusively coordinate to single potassium centres.

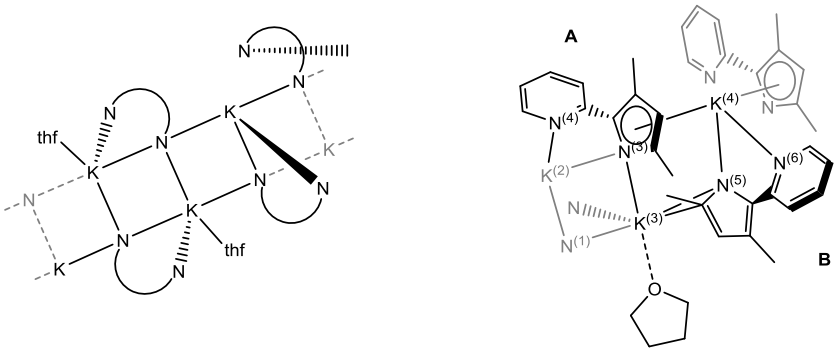
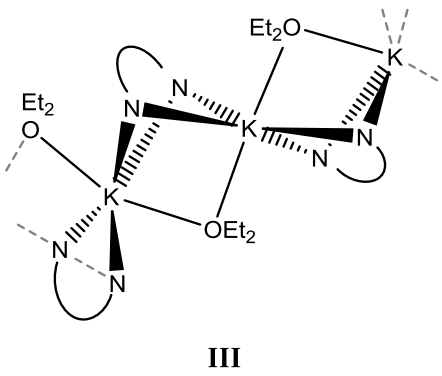


***Figure 62**: Schematic representation of **5** (**I**) and the two present binding motifs (**A** and **B**, **II**).*

The above stands in contrast to the only other structurally known **PyL**K complex, the repeating unit of which is schematically represented as **III** below**,** Figure **63**. Despite bond lengths between **5** and **III** generally being comparable (*e.g.* $N_{pyrrole}$–K lengths between 2.79-2.83 Å, see Table **7** for **5**), pyridine-pyrrole rings are nearly coplanar with twist angles of 5-10° compared to 20-32° in **5**.[152]



III

***Figure 63:** Schematic representation of $[PyCF_3LK{\bullet}Et_2O]_\infty$.*[152]

The difference in bonding motifs is presumably correlated with pyrrole electron densities, with potassium preferentially adopting η^5 interactions with the comparatively electron-rich $\{(CH_3)_2C_4HN\}$ π-system.

***Table 7**: Selected bond distances (Å) and angles (°) in **5**.*

$\{N(1)C_3\}_{pln}$–K(1)	2.830(3)	N(5)–K(3)	2.9131(9)
N(1)–K(2)	2.823(5)	C(31)–K(3)	3.262(6)
N(2)–K(2)	2.8378(10)	N(5)–K(4)	2.7527(9)
N(1)–K(3)	2.970(4)	N(6)–K(4)	2.8587(9)
N(1)–K(3)–N(2)	58.32(8)	N(5)–K(4)–N(6)	60.417(18)
C(5)–C(6)	1.458(8)	C(27)–C(28)	1.45384(3)
$Pyrr_{N(1)}$–$Pyrid_{N(2)}$	32.1(8)	$Pyrr_{N(5)}$–$Pyrid_{N(6)}$	20.795(5)
K(2)–N(1)–K(3)	78.69(11)	K(2)–N(3)–K(3)	77.88(3)
N(1)–K(2)–N(3)	95.26(9)	N(1)–K(2)–N(3)	96.94(9)

Salt-metathesis-type reactions of **5** and **6** with magnesium halides yielded intractable mixtures. Considering the success of transamination in the synthesis of **PyL**K complexes, the same procedure was thus adopted for their magnesium congeners, as shown in Figure **64** below.

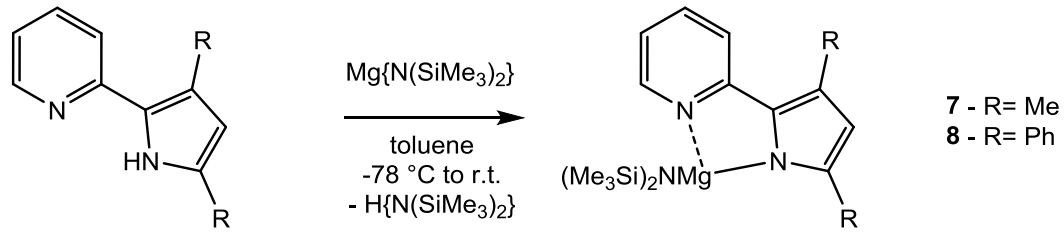


***Figure 64:** Synthesis of heteroleptic **PyLMg**N" complexes **7** and **8** by transamination.*

^1H, $^{13}C\{^1H\}$ and 2D-HMQC NMR spectroscopy gave good evidence for the formation of the desired species, although no signals were observed in the ^{29}Si NMR spectrum; the presence of silicon in **7** and **8** could indirectly be verified by ^{29}Si satellites in both $^{13}C\{^1H\}$ NMR spectra. Usefully, absence of protonated ligand

is not only verified by lack of an N*H* resonance often difficult to locate and integrate due to its broad nature, but also the transition of the pyrrole backbone to a singlet analogous to **5** and **6**. The latter was structurally characterised as the symmetry related dimer shown in Figure **65**.

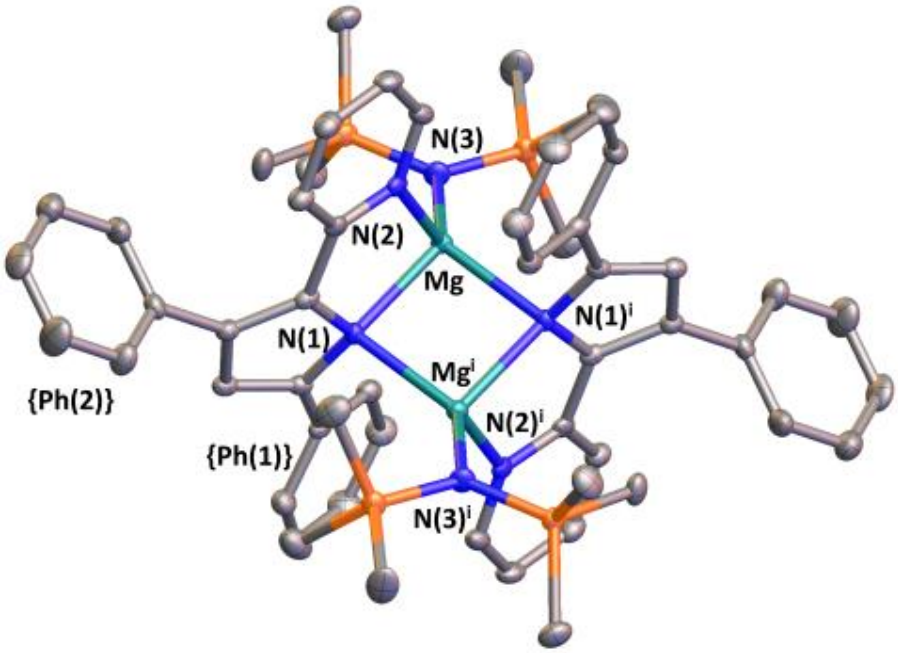


Figure 65: *Molecular structure of **8** with ellipsoids set at at the 50% probability level; hydrogen atoms have been omitted for clarity. Symmetry transformation used to generate equivalent atoms: (i) $^1/_2$-x, $^1/_2$-y,1-z.*

Dimerisation of heteroleptic magnesium systems is frequently observed in case of low steric demand of the spectator ligand and/ or substituents. This is exemplified in a series of bulky diketiminide complexes, [{(Dipp)NCHN(Dipp)}MgX]. For smaller X substituents such as Me, Cl and Br, the above are dimeric in the solid state. In contrast, larger substituents such as ^{t}Bu or $N(SiMe_3)_2$ give rise to monomers.[197] The dimeric nature of **8** (Figure **65**) is therefore an indication of the comparatively poor ability of **PyPhL** to sterically saturate a bonded metal; the motif of **8** is identical to that of the reported pyrrolide [{$C_4H_3N(CH_2NMe_2$}Mg{$N(SiMe_3)_2$}], a dimer bridged by μ^2 $N_{pyrrolide}$.[198] In contrast to the latter, the monodentate N(2)–Mg contact is shorter than its bridging N(1)–Mg counterpart by 0.16-0.05 Å (*ca.* 0.05 Å longer in the above

pyrrolide). The shortest N–Mg contact is observed between the silyl amide moiety and magnesium, a feature consistent with other MgN" systems featuring delocalised bidentate ligands such as diketiminides or amidinides.[197,199] Relevant bond lengths and angles are listed in

Table **8**.

Table 8: *Selected bond distances (Å) and angles (°) in* ***8****.*

N(1)–Mg	2.148(2)	C(5)–C(6)	1.463(3)
N(1)–Mg^{i}	2.258(2)	$Pyrr_{N(1)}$–$Pyrid_{N(2)}$	22.21(8)
N(2)–Mg	2.098(2)	$Pyrr_{N(1)}$–Ph(1)	35.82(6)
N(3)–Mg	1.985(2)	$Pyrr_{N(1)}$–Ph(2)	73.91(6)
N(1)–Mg–N(2)	81.38(8)	Mg···Mg	3.0830(14)
Mg–N(1)–Mg^{i}	88.78(8)	N(1)–Mg–N(1)^{i}	91.22(8)

Attempts at an analogous reaction with Ca(N")$_2$ (*v.s.* Figure **64**) yielded the adventitious **9**, presumably a hydrolysis product of **PyMe**LCaX, where X is **PyMeL** or N". Although hydrolysis of molecular Ae species is generally undesirable, the application of Ae oxides in ferroelectric $AeTiO_3$ type ceramics has attracted interest in elucidating intermediate species.[200]

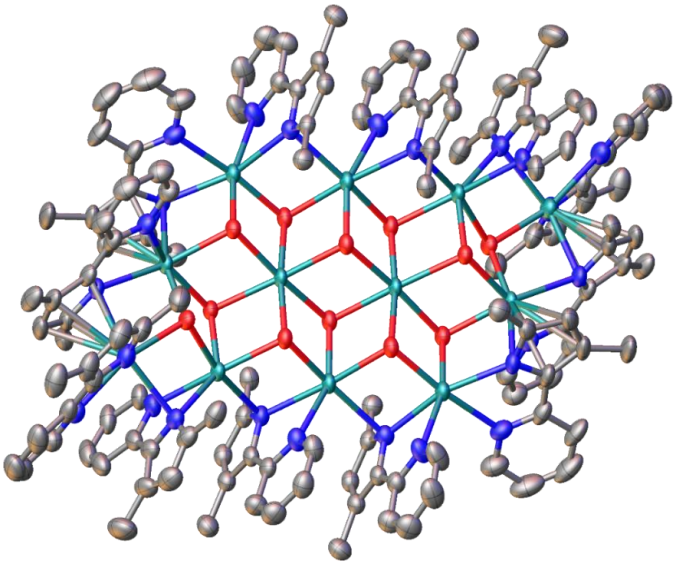


Figure 66: *Molecular structure of **9** with ellipsoids set at at the 50% probability level; hydrogen atoms and residual toluene have been omitted for clarity.*

9 takes the form of a rather aesthetic distinct dodecanuclear [**PyMeL**CaOH]$_{12}$ aggregate displayed in Figure **66**, in which [CaOH]$_x$ cage fragments are framed by a halo of ligands. The latter are observed to take three distinct forms, **A, B** and **C** as shown in Figure **67**.

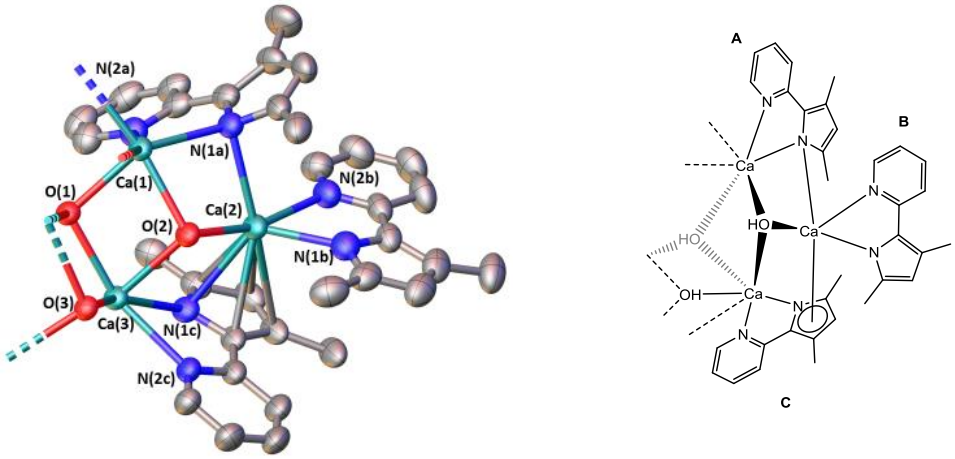


Figure 67: *The three ligand motifs observed in **9** and their schematic representation (**A**, **B** and **C**); hydrogen atoms and residual toluene have been omitted for clarity.*

A, **B** and **C** represent κ^2:μ^2, κ^2 and κ^2:η^5 ligands, respectively and have been given corresponding suffixes in Table **9** for ease of distinction, bond lengths are distinctive of a variation in binding mode, with the shortest N–Ca contact observed in the κ^2 **B**. **9** shares many structural features with tetranuclear calcium aryloxide and pyrazolide complexes obtained from the selective hydrolysis of their respective homoleptic congeners. These display a similar ring of ligands around calcium bridged by tricoordinate OH fragments; the same motif is observed in an isolobal F analogue.[200,201] A key difference between **9** and the above is the presence of two calcium atoms at the centre of the ring, lacking any Ca–N contacts and being entirely supported by surrounding hydroxyl groups.

Table 9: *Selected bond distances (Å) and angles (°) in* ***9****.*

N(1a)–Ca(1)	2.484(3)	$\{Pyrr_{N(1c)}\}_{pln}$–Ca(2)	2.5346(14)
N(1a)–Ca(2)	2.561(3)	N(1c)–Ca(3)	2.461(2)
N(1a)–Ca(1)	2.514(3)	N(2c)–Ca(3)	2.539(3)
N(2a)–Ca(1)	2.458(3)	N(2a)–Ca(2)–N(2a)	67.09(9)
C(5a)–C(6a)	1.447(5)	C(5c)–C(6c)	1.443(5)
N(1a)–Ca(1)–N(2a)	66.57(9)	Ca(1)–O(1)	2.340(2)
Ca(1)–N(1a)–Ca(2)	93.63(9)	Ca(1)–O(2)	2.365(2)
N(1b)–Ca(2)	2.369(3)	Ca(2)–O(2)	2.3199(18)
N(2b)–Ca(2)	2.500 (3)	Ca(3)–O(1)	2.367(2)
C(5b)–C(6b)	1.451(6)	Ca(3)–O(2)	2.390(2)
N(1b)–Ca(2)–N(2b)	69.02(11)	Ca(3)–O(3)	2.349(2)

Progressing onto the harsher organoelimination route, the latter provided mixed results in the metalation of **PyL**H proligands. Whilst the ^{1}H and ^{13}C{^{1}H} NMR spectra of material obtained from reacting the above with $^{n}Bu_2Mg$ were indicative of the formation of metalorganic species, a multitude of congested signals did not allow for definitive assignment. Purification was hampered considerably by the extremely high solubility of obtained material in hydrocarbons, combined with exceedingly poor crystallinity.

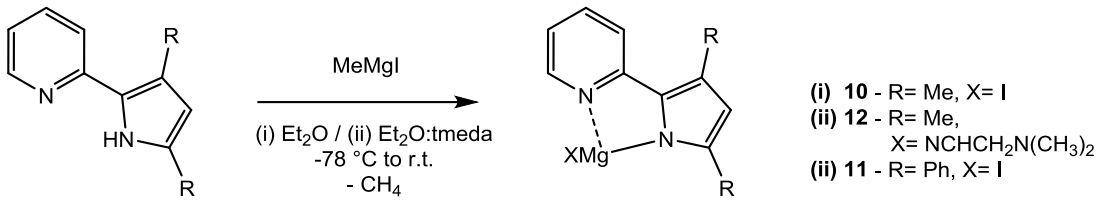


Figure 68: *Synthesis of **PyLMgI** complexes **10** and **12** by organoelimination.*

In contrast, the synthesis of heteroleptic organomagnesium halides by employment of MeMgI as shown in Figure **68** proved a more profitable undertaking. **10** was isolated in the absence of tmeda, and was characterised by multinuclear NMR spectroscopy as well as elemental microanalysis. The identity of **11** was analogously verified, as well as structurally authenticated (Figure **69**). In all cases, metalation resulted in the aforementioned disappearance of ^{4}J N*H*-C*H* coupling as well as a slight upfield shift of most ^{1}H NMR signals with concomitant downfield shift of ^{13}C{^{1}H} NMR resonances.

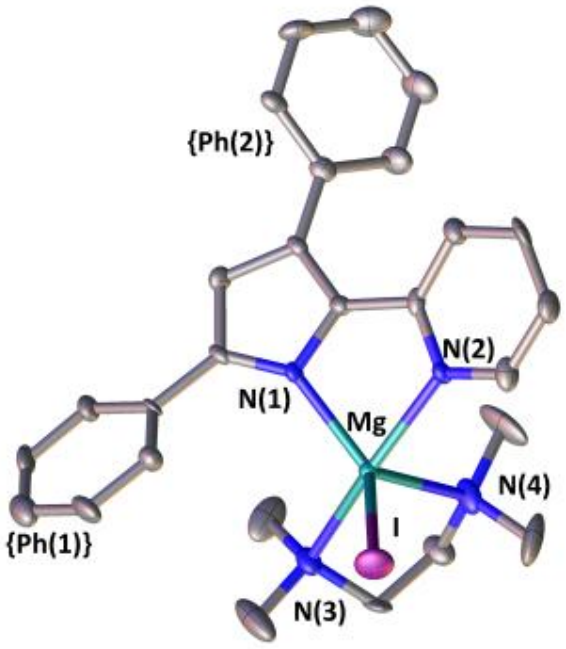


Figure 69: *Molecular structure of **11** with ellipsoids set at at the 50% probability level; hydrogen atoms have been omitted for clarity.*

In the solid state, **11** crystallises with two optical isomers in the asymmetric unit, as well as a residual Et_2O molecule with no apparent close contacts to either of the above complexes. The similarity with **4** becomes immediately apparent, **11** adopts a comparable distorted bipyramidal shape, with longer axial N–Mg distances compared to their equatorial counterparts, displayed in Table **10** below. Ligand bite angles in the 5-membered metallacycle **11** are expectedly less acute.

Table 10: *Selected bond distances (Å) and angles (°) in* ***11****.*

$N(1)_{eq}$–Mg	2.101(8)	N(1)–Mg–N(2)	76.9(4)
$N(2)_{ax}$–Mg	2.189(7)	N(3)–Mg–N(4)	79.3(5)
$N(3)_{ax}$–Mg	2.308(2)	$\{Pyrr_{N(1)}\}$–$\{Pyrid_{N(2)}\}$	16.6(4)
$N(4)_{eq}$–Mg	2.270(2)	$\{Pyrr_{N(1)}\}$–{Ph(1)}	29.2(5)
Mg–I	2.720(7)	$\{Pyrr_{N(1)}\}$–{Ph(2)}	41.3(4)
C(5)–C(6)	1.459(6)		

Attempts to isolate the **PyMeL** equivalent of **11** yielded crystals suitable for single-crystal X-ray diffraction, which did not yield data consistent with **PyMeL**MgI. Instead, the adventitious **12** was formed, comprised of the employed ligand and a deprotonated primary aldimine with its apparent origin in tmeda.

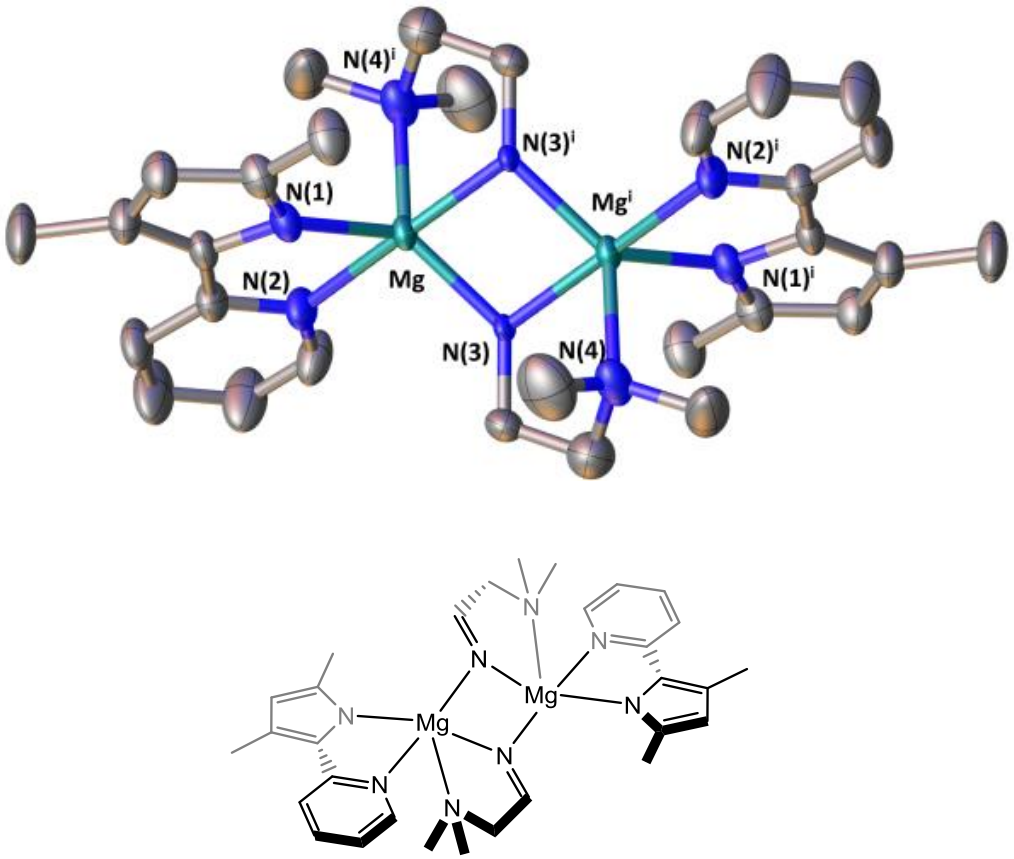


Figure 70: *Molecular structure of* ***12*** *and its schematic representation. Ellipsoids are set at at the 50% probability level; hydrogen atoms have been omitted for clarity. Symmetry transformation used to generate equivalent atoms: (i) 1-x,1-y,1-z.*

Bond lengths are consistent with the proposed structure, with a N(3)–C(12) distance of 1.40 Å and a considerably longer 1.56 Å for its N_{sp^3}–C_{sp^3} counterpart, N(4)–C(13) (*vs.* Table **6**, pg. 67). Due to the contiguousness with a standard O–C bond, occupation of the N(3) position was competitively refined *vs.* oxygen;† the data are more consistent with the former by $\Delta R_1 = 1.5\%$.[180] In contrast to the ubiquitous Schiff bases, structurally known Ae complexes featuring deprotonated primary aldimines are extremely rare, with a thorough search of

† Although relatively small anisotropic displacement ellipsoids point at the N(3) position being occupied by a heavier atom, this does not appear to be the case. Due to the small difference in electron density, distinguishing nitrogen from oxygen by X-ray crystallography is, however, problematic.

the CSD only revealing 3 examples, all of them bearing benzylic aldimides as opposed to the aliphatic imine fragment of **12**.[202–204] The above feature C=N bonds *ca.* 0.15 Å shorter than those observed in **12**, presumably due to the availability of keto-enol tautomerism in the latter. N_{sp^2}–Mg interactions in **12** are about 0.1 Å shorter than those of its diketiminide-supported congeners, even marginally shorter than the non-bridging N(1)–Mg, consistent with a "hard" electron donor. At 2.06 Å, N(1)–Mg was the shortest **PyL**-Mg contact observed in this work, even marginally shorter than N–Mg lengths in the "harder" **SiL** system (*v.s.* Table **3**, pg. 55).

Table 11: *Selected bond distances (Å) and angles (°) in* ***12****. Symmetry transformation used to generate equivalent atoms: (i) 1-x,1-y,1-z.*

N(1)–Mg	2.060(2)	C(5)–C(6)	1.428(4)
N(2)–Mg	2.185(3)	N(1)–Mg–N(2)	78.43(10)
N(3)–Mg	1.9552(19)	N(3)–Mg^{i}–N(4)	80.07(10)
N(4)–Mg^{i}	2.202(3)	N(3)–Mg–N(3)^{i}	81.76(9)
N(3)–C(12)	1.401(4)	Mg–N(3)^{i}–Mg^{i}	98.24(9)
N(4)–C(13)	1.563(8)	{Pyrr$_{N(1)}$}–{Pyrid$_{N(2)}$}	6.74(14)

The origin of **12** from a putative **PyMeL**MgI•tmeda complex is uncertain, particularly considering that the transformation of a tertiary amine to an imine by *N*-dealkylation is an oxidative process. Whilst alkali metal-induced C–N bond cleavage is a well-reported phenomenon, a similar cascade of deprotonation, β-hydride elimination, metal hydride attack and ultimately bond cleavage would produce fragments inconsistent with the above structure.[205–208] Instead, the latter should provide bridging NMe_2 units. Whether magnesium pyridylpyrrolides are capable of such a transformation appears dubious, considering no such process is observed even in PhSrI•$(tmeda)_x$.[140] tmeda starting material was therefore thoroughly screened by multinuclear NMR spectroscopy as well as mass spectrometry without obtaining evidence for a possible precursor to the incorporated fragment, be they nitrogen or oxygen-

derived. Persistent efforts towards a rational synthesis of **12** only saw the isolation of MgI_2•$tmeda_x$ and material tentatively assigned as **PyMeL**$_2$Mg•Et_2O.

2.2.2. Conclusions and Future Work

The palate of pyridylpyrrolide s-block chemistry has been expanded substantially, with **PyMeL** and **PyPhL** ligands successfully being employed in the stabilisation of a series of novel complexes. Many of these were structurally authenticated, affording insight into the binding characteristics of the above. **PyL** ligands adopt a variety of binding motifs, highlighting their flexibility. This notwithstanding, their exceedingly poor crystallinity significantly impeded the purification of materials synthesised, as well as growing crystals of sufficient quality for single crystal X-ray diffraction.

Intractable mixtures obtained from reactions with $^{n}BuMg_2$ may be attributed to nucleophilic attack by the carbanion; pyridines are known to react with nucleophiles in general and Grignard reagents specifically.[209] The poorer nucleophilicity of Me^- *vs.* Bu^- may serve as an explanation as to the more successful nature of reactions involving MeMgI.

Whilst such processes may be discouraged by pyridine substitution, attempts towards this proved non-trivial. **11** was briefly screened for a potential propensity in catalysing dehydrocoupling reactions analogous to **4,** but displayed a complete lack of activity.

Analogous to **SiL** ligands, work on the above system was discontinued in favour of the more sterically demanding **BzL** and **TrL**, as discussed in Chapter **3**.

2.2.3. Experimental

Synthesis of PyMeLH

A suspension of *p*-toluenesulphonic acid monohydrate (1.14 g, 6 mmol) in degassed xylenes (100 mL) was charged with pentane-2,4-dione (6.16 mL, 60 mmol) and 3-aminomethylpyridine (6.18 mL, 60 mmol) in a Dean-Stark apparatus. The mixture was heated to reflux at 170 °C for 8 h and subsequently allowed to cool to room temperature. Xylenes were removed from the orange mixture *in vacuo* at 80 °C to yield a yellow-brown solid which was dissolved in dichloromethane (50 mL), washed with $NaOH_{(aq)}$ (2 M, 3x30 mL) and water (2x20 mL), the solvent removed to yield 9.100 g (88%) of slightly brown solid. The crude was sublimed at 60 °C, $1x10^{-1}$ mbar to afford the title compound as a slightly yellow amorphous powder (7.53 g, 72%). Literature yield: 74% on 309 mg scale with chromatographic purification.

^{1}H NMR ($CDCl_3$, 298 K, 300 MHz): δ = 2.27 (s, 3H, C*H*$_3$), 2.41 (s, 3H, C*H*$_3$), 5.86 (d, J = 3 Hz, 1H, C*H*), 6.99 (ddd, 1H, C*H*, J = 7.3, 4.9, 1.1 Hz), 7.5 (dt, 1H, C*H*, J = 8.2, 1.2 Hz), 7.64 (m, 1H, C*H*), 8.49 (m, 1H, CH), 9.77 (br. s, 1H, N*H*) ppm.

$^{13}C\{^{1}H\}$ NMR ($CDCl_3$, 298 K, 75 MHz): δ = 12.72 (*C*H$_3$), 13.85 (*C*H$_3$), 111.30 (*C*H), 118.31 (*C*H), 118.98 (*C*H), 119.24 (*C*), 125.70 (*C*), 128.88 (*C*), 136.19 (*C*H), 148.72 (*C*H), 151.24 (*C*) ppm.

MS: (ESI) m/z 173.10 $[MH]^+$ 100%

Synthesis of PyPhLH

A suspension of p-toluenesulphonic acid monohydrate (1.14 g, 6 mmol) in degassed xylenes (100 mL) was charged with 1,3-diphenylpropane-1,3-dione (13.45 g, 60 mmol) and 3-aminomethylpyridine (6.18 mL, 60 mmol) in a Dean-Stark apparatus. The slightly yellow suspension was heated to reflux at 170 °C for 18 h and subsequently allowed to cool to room temperature. Xylenes were partially removed *in vacuo* to yield an orange slurry, which dissolved in dichloromethane (75 mL) to be washed with $NaOH_{(aq)}$ (2 M, 3x50 mL) and water (2x50 mL). Solvents were removed *in vacuo* to yield a highly viscous brown oil

recrystallised from hot ethanol/cyclohexane to afford the title compound as a slightly yellow, amorphous powder (11.11 g, 62%). Literature yield: 69% on 385 mg scale with chromatographic purification.

^{1}H NMR (C_6D_6, 298 K, 400 MHz): δ = 6.44 (ddd, 1H, C*H*, J = 7.4, 4.8, 0.9 Hz), 6.65 (d, J = 3.1 Hz, 1H, C*H*), 6.79 (td, 1H, C*H*, J = 7.8, 1.9 Hz), 6.98 (m, 1H, *p*-Ar*H*), 7.08 (t, 2H, Ar*H*, J = 7.6 Hz), 7.18 (m, 1H, *p*-Ar*H*), 7.26 (m, 2H, Ar*H*), 7.31 (d, 2H, Ar*H*, J = 7.2 Hz), 7.39 (br. d, 1H, C*H*), 7.56 (m, 2H, Ar*H*), 8.3 (m, 1H, C*H*), 10.42 (br. s, 1H, N*H*) ppm.

^{1}H NMR ($CDCl_3$, 298 K, 400.20 MHz): δ = 6.65 (d, J = 3 Hz, 1H, C*H*), 7.03 (ddd, 1H, C*H*, J = 7.3, 4.9, 1.1 Hz), 7.30 (m, 2H, C*H*), 7.38 (m, 6H, C*H*), 7.55 (m, 2H, C*H*), 7.66 (m, 2H, C*H*), 8.52 (m, 1H, C*H*), 10.15 (br. s, 1H, N*H*) ppm.

^{13}C{^{1}H} NMR ($CDCl_3$, 298 K, 100 MHz): δ = 110.15 (*C*H), 119.75 9 (*C*H), 120.55 (*C*H), 124.16 (Ar-*C*H), 126.60 (*C*), 126.74 (Ar-*C*H), 126.82 (Ar-*C*H), 127.49 (*C*), 131.97 (*C*), 132.87 (Ar-*C*), 136.05 (*C*H), 137.07 (Ar-*C*), 148.83 (*C*H), 150.42 (*C*) ppm.

MS: (ESI) *m*/*z* 297.13 $[MH]^+$ 100%

Synthesis of PyMeLK [5]

PyMeLH (1.033 g, 6 mmol) and K{$N(SiMe_3)_2$} (1.197 g, 6 mmol) were individually dissolved in toluene (2x30 mL), and the latter added drop wise to the former at 0 °C, resulting in an immediate deepening of the previously faint yellow and the formation of a precipitate. The mixture was allowed to warm to r.t., stirred overnight, and the solvent removed to yield a yellow solid washed with hexanes (1.192 g, 92%).

^{1}H NMR (C_6D_6 : D_8-THF, 298 K, 400 MHz): δ = 1.46 (m, 4H, CH_2-THF), 2.14 (s, 3H, CH_3), 2.39 (s, 3H, CH_3), 3.55 (m, 4H, CH_2-THF), 5.91 (s, 1H, C*H*), 6.52 (ddd, 1H, C*H*, J = 7.1, 5, 0.8 Hz), 7.21 (m, 1H, C*H*), 7.36 (d, 1H, C*H*, J = 8.2 Hz), 8.11 (br. d, 1H, C*H*, J = 4.1 Hz) ppm.

^{13}C{^{1}H} NMR (C_6D_6 : D_8-THF, 298 K, 75 MHz): δ = 25.12 (m, CH_2-THF), 67.33 (m, CH_2-THF), 112.42 (*C*H), 118.83 (*C*H), 136.17 (*C*H), 149.53 (*C*H) ppm. *A number of resonances are missing as a sample of sufficient concentration could not be prepared.*

Synthesis of PyPhLK [6]

Following the same procedure as for **5**. From **PyPhL**H (0.889 g, 3 mmol) and K{N(SiMe$_3$)$_2$} (0.598 g, 3 mmol) was isolated the title compound as a yellow solid (0.624 g, 62%).

^{1}H NMR (C$_6$D$_6$: D$_8$-THF, 298 K, 400 MHz): δ = 1.42 (br. s, 0.5H, C*H*$_2$-THF), 3.51 (br. s, 0.5H, C*H*$_2$-THF), 6.45 (ddd, 1H, C*H*, J = 7.2, 5, 1 Hz), 6.90 (m, 1H, C*H*), 6.93 (s, 1H C*H*), 6.97 (m, 1H, *p*-Ar*H*), 7.08 (br. m, 3H, Ar*H*), 7.22 (t, 2H, Ar*H*, J = 7.6 Hz), 7.38 (br. d, 1H, C*H*, J = 8.2 Hz), 7.57 (br. d, 2H, Ar*H*, J = 7 Hz), 7.83 (br. s, 1H, C*H*), 7.86 (br. s, 2H, Ar*H*) ppm.

A sample of sufficient concentration for ^{13}C{^{1}H} NMR could not be prepared.

Reaction of PyMeLH with ^{n}Bu$_2$Mg

PyMeLH (0.516 g, 3 mmol) and (^{n}Bu)$_2$Mg (0.207 g, 1.5 mmol) were individually dissolved in diethyl ether (2x20 mL), and the latter added drop wise to the pale yellow **PyMeL**H solution at -78 °C to give a neon-yellow solution allowed to warm to room temperature. Solvent was removed *in vacuo* to afford the title compound as a neon yellow foam (0.474 g, 86% based on **PyMeL**$_2$Mg).

^{1}H NMR (C$_6$D$_6$, 298 K, 300 MHz): δ = 0.78 (t, 1.5H, C*H*$_3$-Et$_2$O, J = 7 Hz), 2.19 (br. s, 3H, C*H*$_3$), 2.46 (br. s, 3H, C*H*$_3$), 3.2 (q, 1H, C*H*$_2$-Et$_2$O, J = 7.1 Hz), 6.08 (t, 1H, C*H*, J = 5.7 Hz), 6.22 (br. s, 1H, C*H*), 6.88 (t, 1H, C*H*, J = 7.4 Hz), 7.27 (d, 1H, C*H*, J = 8.2 Hz), 7.85 (br. s, 1H, C*H*) ppm.

^{13}C{^{1}H} NMR (C$_6$D$_6$, 298 K, 75 MHz): δ = 14.69 (*C*H$_3$), 15.48 (*C*H$_3$), 16.28 (*C*H$_3$), 66.39 (*C*H$_2$), 115.11 (*C*H), 118.93 (*C*H), 124.47 (*C*), 138.46 (*C*H), 148.29 (*C*H), 156.20 (*C*) ppm.

Reaction of PyPhLH with ^{n}Bu$_2$Mg

Following the same procedure as for **PyMeL**H above. From **PyPhL**H (0.444 g, 1.5 mmol) and (^{n}Bu)$_2$Mg (0.104 g, 0.75 mmol) was isolated a neon lime-yellow foam (0.394 g, 85% based on **PyPhL**$_2$Mg).

^{1}H NMR (C$_6$D$_6$, 298 K, 400 MHz): δ = 0.5-2 (br. m, 15H), 6.3-8.2 (br. m, 30H), 8.38 (br. s, 2H), 10.43 (br. s, 1H) ppm.

$^{13}C\{^1H\}$ NMR (C_6D_6, 298 K, 100 MHz): δ = 1.18 (*C*H_3), 14.30 (*C*H_3), 19.37 (*C*H_3), 22.55 (*C*), 23.15 (*C*H_2), 33.81 (*C*), 111.29 (*C*H), 119.63 (*C*H), 119.98 (*C*H), 124.39 (*C*H), 126.31 (*C*H), 126.75 (*C*H), 128.65 (*C*H), 128.83 (*C*H), 129.70 (*C*H), 136.11 (*C*H), 148.70 (*C*H) ppm.

Synthesis of PyMeLMg{N(SiMe$_3$)$_2$} [7]

To **PyMeL**H (0.344 g, 2 mmol) and Mg{N(SiMe$_3$)$_2$}$_2$ (0.690 g, 2 mmol) was added toluene at -78 °C, the resulting neon yellow milky suspension stirred for 1 h before being allowed to warm to room temperature. Removal of solvent *in vacuo* gave a neon grass green solid, residual amine was removed by gentle warming *in vacuo* and washing with cold pentane to yield the title compound (0.720 g, 101%).

^1H NMR (C_6D_6, 298 K, 400 MHz): δ = 0.03 (s, 18H, Si(C*H*$_3$)$_3$), 2.19 (s, 3H, C*H*$_3$), 2.87 (s, 3H, C*H*$_3$), 5.77 (t, 1H, C*H*, J = 6.3 Hz), 6.24 (s, 1H, C*H*), 6.72 (t, 1H, C*H*, J = 7.1 Hz), 7.02 (d, 1H, C*H*, J = 8.2 Hz), 7.23 (d, 1H, C*H*, J = 5.1 Hz) ppm.

$^{13}C\{^1H\}$ NMR (C_6D_6, 298 K, 100 MHz): δ = 4.79 (t, Si(CH$_3$)$_3$, $J_{(C,Si)}$ = 53.6 Hz), 13.50 (*C*H$_3$), 18.24 (*C*H$_3$), 118.36 (*C*H), 120.12 (*C*H), 121.11 (*C*H), 129.74 (*C*), 133.87 (*C*), 138.01 (*C*H), 144.67 (*C*), 145.99 (*C*H), 153.76 (*C*) ppm.

$^{29}Si\{^1H\}$ NMR (C_6D_6, 298 K, 79 MHz): displayed no visible signals.

Synthesis of PyPhLMg{N(SiMe$_3$)$_2$} [8]

Following the same procedure as for **7**. From **PyPhL**H (0.444 g, 1.5 mmol) and Mg{N(SiMe$_3$)$_2$}$_2$ (0.517 g, 1.5 mmol) was isolated the title compound as a dark green solid (0.63 g, 87%). Crystals for structural analysis were obtained by layering in toluene over pentane.

^1H NMR (C_6D_6, 298 K, 400 MHz): δ = 0.21 (s, 18H, Si(C*H*$_3$)$_3$), 2.11 (s, 1.3H, *tol.*) 5.82 (ddd, 1H, C*H*, J = 7.2, 5.4, 1.1 Hz), 6.03 (br. t, 1H, C*H*, J = 6 Hz), 6.56 (m, 2H, Ar*H*), 6.8 (tt, 1H, C*H*, J = 7.4, 1.1 Hz), 6.90 (s, 1H, C*H*), 6.95-7.4 (br. m, 18H, *tol.*), 7.55 (m, 5H, C*H*), 7.76 (m, 4H, Ar*H*), 7.9 (br. d, 2H, Ar*H*) ppm.

$^{13}C\{^1H\}$ NMR (C_6D_6, 298 K, 100 MHz): δ = 5.30 (Si(CH$_3$)$_3$), 21.76 (*C*H$_3$, *tol.*), 115.02 (Ar-*C*H), 115.65 (*C*H), 118.47 (*C*H), 118.86 (*C*H), 119.91 (Ar-*C*H), 120.24 (Ar-

*C*H), 125.04 (Ar-*C*H), 125.49 (Ar-*C*H), 126.03 (*C*H), 126.47 (Ar-*C*H, *tol.*), 127.13 (Ar-*C*H), 127.35 (Ar-*C*H), 129.24 (Ar-*C*H), 129.56 (Ar-*C*H), 129.79 (Ar-*C*H), 130.32 (Ar-*C*H), 130.46 (Ar-*C*H), 137.17 (*C*), 137.87 (*tol.*), 139.30 (Ar-*C*H), 139.89 (*C*), 140.42 (*C*), 145.26 (*C*), 145.40 (*C*), 146.42 (Ar-*C*H), 147.20 (*C*H), 156.47 (*C*), 156.91 (*C*) ppm.

$^{29}Si\{^{1}H\}$ NMR (C_6D_6, 298 K, 79 MHz): displayed no visible signals.

Synthesis of PyMeLMgI·$(Et_2O)_2$ [10]

Following the same procedure as for the reaction of PyMeLH with $^{n}Bu_2Mg$ above. From the addition of **PyMeL**H (0.516 g, 3 mmol) to MeMgI·$(Et_2O)_{1.5}$ (0.859 g, 3.1 mmol) was isolated the neon-yellow title compound (0.80g, 82%).

^{1}H NMR (C_6D_6, 298 K, 400 MHz): δ = 0.81 (t, 12H, C*H*$_3$-Et_2O, J = 7.1 Hz), 2.41 (s, 3H, C*H*$_3$), 2.43 (s, 3H, C*H*$_3$), 3.36 (q, 8H, C*H*$_2$-Et_2O, J = 7.1 Hz), 6.15 (t, 1H, C*H*, J = 6.2 Hz), 6.23 (s, 1H, C*H*), 6.92 (ddd, 1H, C*H*, J = 8.6, 7.1, 1.8 Hz), 7.26 (d, 1H, C*H*, J = 8.5 Hz), 7.87 (br. s, 1H, C*H*).

$^{13}C\{^{1}H\}$ NMR (C_6D_6, 298 K, 100 MHz): δ = 14.68 (*C*H$_3$), 15.82 (*C*H$_3$), 17.31 (*C*H$_3$), 66.67 (*C*H$_2$), 115.67 (*C*H), 116.21 (*C*H), 118.32 (*C*H), 125.67 (*C*), 131.88 (*C*) 138.99 (*C*H), 140.73 (*C*), 147.66, (*C*H), 156.79 (*C*).

$C_{12}H_{12}IMgN\cdot(C_{10}H_4O)_2$ (470.13): calc'd (%)C 48.49, H 6.64, N 5.95; found (%) C 48.36, H 6.51, N 5.72.

Synthesis of PyPhLMgI·(tmeda)·$(Et_2O)_{0.5}$ [11]

To a suspension of MeMgI·$(Et_2O)_{1.5}$ (0.444 g, 1.6 mmol) in diethyl ether at -78 °C was added dropwise a solution of **PyPhL**H (in Et_2O, 0.444 g, 1.5 mmol) over 1 h, stirred as a yellow suspension for 4 h, and allowed to warm to -30 °C. Subsequently, tmeda (0.9 mL, 6 mmol) was added, the resultant suspension stirred for a further 2 h, allowed to warm to room temperature and volatiles removed *in vacuo*; washing with cold hexanes afforded the title compound as a grass green solid (0.771 g, 86%).

^{1}H NMR (C_6D_6, 298 K, 400 MHz): δ = 1.12 (t, J = 7.02 Hz, 3 H, Et_2O), 1.70 (br. s., 12 H, tmeda) 1.90 - 2.34 (br. s, 4 H, tmeda), 3.26 (q, J = 6.92 Hz, 2 H, Et_2O), 6.19

(m, 1 H, Ar*H*), 6.55 - 6.61 (m, 1 H), 6.88 (s, 1 H, C*H*), 7.00 - 7.05 (m, 1 H, Pyr*H*), 7.17 - 7.36 (overlapping m, 6 H), 7.68 (dd, J = 8.11, 1.24 Hz, 2 H, Ar*H*), 8.05 (dd, J=8.18, 1.17 Hz, 2 H, Ar*H*), 8.61 - 8.64 (m, 1 H, Pyr*H*) ppm.

$^{13}C\{^{1}H\}$ NMR (C_6D_6, 298 K, 100 MHz): δ = 15.33 (Et_2O), 65.67 (Et_2O), 114.63 (Ar-*C*H), 117.27 (Ar-*C*H), 118.42 (Ar-*C*H), 125.97 (Ar-*C*H), 126.14 (Ar-*C*H), 126.50 (Ar-*C*H), 128.58 (Ar-*C*H), 129.18 (Ar-*C*H), 129.49 (Ar-*C*H), 131.76 (Ar-*C*), 134.00 (Ar-*C*), 137.55 (Ar-*CH*), 139.22 (Ar-*C*), 139.88 (Ar-*C*), 146.35(Ar-*C*), 147.67 (*C*H), 155.90 (Ar-*C*) ppm.

$C_{27}H_{31}IMgN_4 \cdot (C_{10}H_4O)_{0.5}$ (599.18): calc'd (%) C 58.07, H 6.05, N 9.34; found (%) C 57.93, H 5.95, N 9.26.

Chapter 3

Benzylanilines and Tritylamines

3.1. Introduction

By and large, systems employed in the stabilisation of Ae complexes feature polydentate binding motifs (*v.s.* Section **1.5**, pg. 41).[106] These profit from the chelate effect as well as the formation of a distinct steric pocket (**I**, Figure **71**), whereas flexibility in monodentate systems can expose the reactive metal site (**II$_a$**, **II$_b$**, Figure **71**).

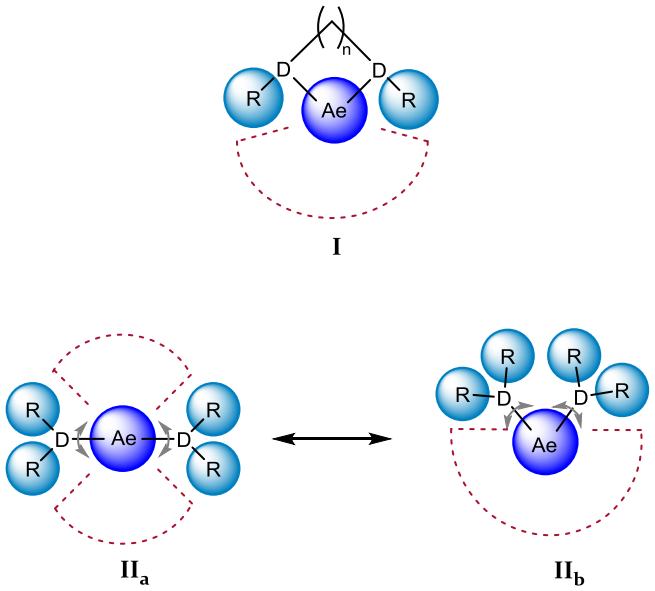
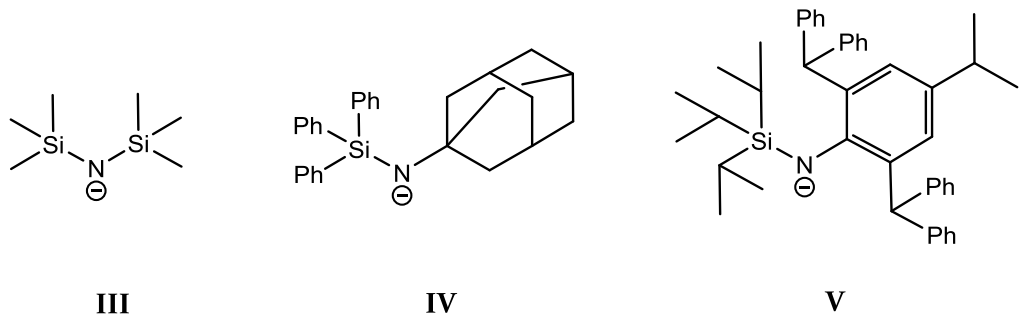


Figure 71: *Simplified representation of homoleptic bidentate (**I**) and monodentate ligand (**II$_a$**, **II$_b$**) systems. D = donor, R = sterically demanding moiety*†

As a consequence of the above, monodentate systems generally provide less protection from deleterious side reactions such as Schlenk-equilibrium type degradation, ether cleavage and aggregation than their multidentate congeners. The ability of the former to stabilise highly reactive metal centres relies entirely on steric crowding. The resultant quest for superbulky monodentate systems has, amongst others, brought forth the prolific silylamine framework. By virtue of

† Donor entities are kept identical to allow for consistency with a chelate effect argument, *i.e.* ligand I (Figure **71**) would be dianionic and individual ligands in II monoanionic (for D = N). In actuality, I is usually monoanionic and the remaining donor bears an additional R group, further increasing steric crowding. Additionally, the monodentate **II** equivalent would only feature one binding entity, leaving a large part of the metal coordination sphere open to attack.

being the most ubiquitously employed subset of the above, the role of bis-trimethylsilylamide in s- and p-block chemistry has been reviewed multiple times, most recently by Coles.[100,101] Success of the latter notwithstanding, work towards stabilising lower coordination numbers has given rise to ever more sterically demanding systems, as exemplified in Figure **72**. From the well-known bis-trimethylsilylamide **III**, to asymmetric silylamides featuring bulky aliphatic (**IV**) or aromatic (**V**) substituents, the stabilisation afforded by electronic saturation in multidentate systems is replaced with extreme steric crowding.[100,210–212]



III **IV** **V**

Figure 72: *From bulky to superbulky silylamides.*[100,210–212]

In contrast to internal solvation, the above do not adversely affect electrophilicity of bound metal centres, a key component of catalytic activity (*v.s.* Section **1.4.2**, *v.i.* Chapter **4**).[212] Despite the above listed drawbacks, monodentate systems consequently present an auspicious target. A treatise on the expansive field of s-block amide chemistry in general has been compiled by Lappert, as well as a more recent review on superbulky amide ligands in main group chemistry by Kays.[99,213]

Given the success of silylamides in particular, focus in this work was given to synthesising and employing R'_3CNR^2 congeners of the ubiquitous R'_3SiNR^2 systems, with both aryl and alkyl R^2 substituents examined in Sections **3.2** Benzylanilides and **3.3** Tritylamides, respectively. These may be seen as asymmetric, acyclic variants of the less bulky 2,2,6,6-tetramethylpiperidides (TMP), commonly employed in s-block chemistry.[214–216] Other than their

comparative novelty, the rationale behind exploring non-silyl frameworks is rooted in potential kinetic and thermodynamic advantages. The N–Si bond is both longer and more prone to dissociation than its N–C counterpart. N–Si Bond lengths in LAr* systems lie at 1.68 Å in comparison to 1.47 Å for N–C, thereby reducing the length by 13%.[217] This shortening brings steric bulk closer to the central metal coordination site, increasing steric protection. Furthermore, bond dissociation enthalpies clearly favour N–C at 750 $kJmol^{-1}$ compared to the 40% lower 439 $kJmol^{-1}$ for N–Si.[218†] Additionally, silicon incorporation precludes use in CVD, as even minor Si impurities are detrimental to electronic applications.[149,219]

† Whilst giving a good general indication of stability, the abovementioned values should be viewed with some caution as other factors may play considerable roles (*e.g.* ability of Si *vs.* C to stabilise radicals or tertiary cations).

3.2. Benzylanilides

The anilide functionality (**VI**, Figure **73**) features prominently in a series of s-block diketiminides (**VIII**), amidinides (**IX**) and guanidinides,[39,102,106,220–222] as well as dianionic diamide analogues of **VIII**, **X** in Figure **73**.[223,224] Monodentate anilide ligands have been employed in the stabilisation of alkali metal systems[225–227] as well homo- and heteroleptic Ae complexes[143,214] and heterobimetallic s-block aggregates.[228]

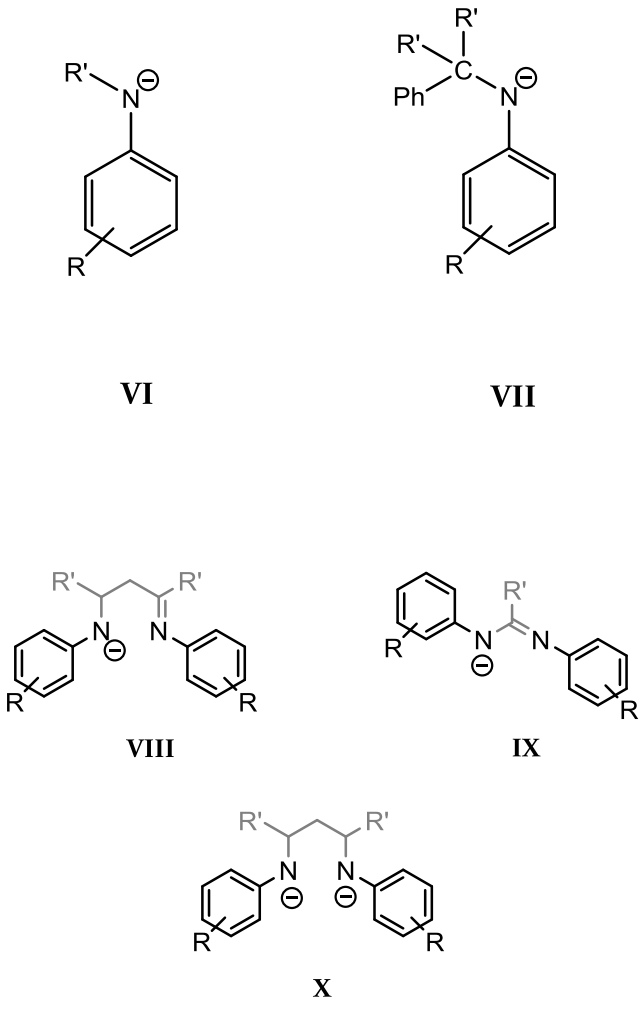


Figure 73: *The anilide framework and its incorporation in bidentate diketiminides (**VIII**) and amidinides (**IX**).*

Benzylanilides (**VII**) are less common, literature precedent extends to the stabilisation of a variety of lithium complexes,[229–233] whilst examples of structurally authenticated Ae species is confined to a single magnesium complex obtained from the reaction of [{(Dipp)NCH$_2$(Me)CHCH$_2$(Me)N(Dipp)}MgH] with triphenylmethanimine to obtain the heteroleptic complex shown below in Figure **74**, featuring an agostic interaction between Mg and C(38) at a distance of 2.66 Å.[234] There are, however, isolated examples of the benzylanilide motif in bidentate systems featuring phenyl or naphthyl bridging units.[235,236] Dibenzylic systems in particular are even rarer, aside from the Mg complex shown below main group examples are confined to the bis-amidogermylene [{(Dipp)N(CHPh$_2$)}$_2$Ge],[237] and two lithium complexes.[232,238] A thorough search of the literature revealed no trityl-bearing anilide complexes.

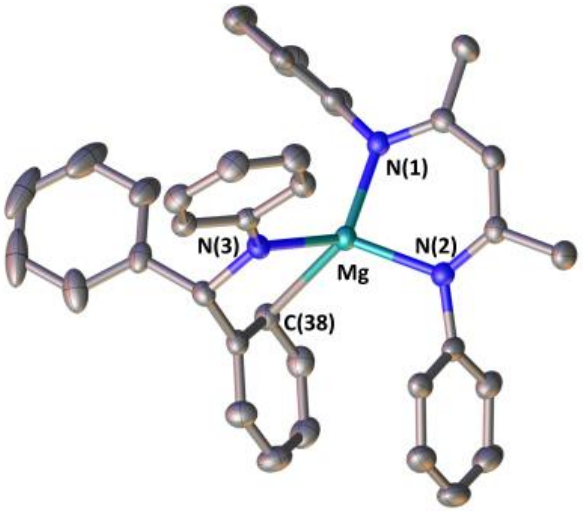


Figure 74: *[{(Dipp)NCH$_2$(Me)CHCH$_2$(Me)N(Dipp)}Mg{N(Ph)CHPh$_2$}reported by Hill et al., ellipsoids set at the 50% probability level; hydrogen atoms, residual solvent and ^{i}Pr groups are omitted for clarity.*[234]

Out of the existing monodentate anilides, silylated [(Ar*)N(SiR$_3$)] systems (Ar*= 2,6-{CHPh$_2$}-4-R-C$_6$H$_2$; R= Me, ^{i}Pr, ^{t}Bu)† stand out for their propensity in stabilising highly unusual main group as well as TM complexes.[239–243] This includes the first structurally authenticated two-coordinate terminal zinc

† The comparatively novel Ar* fragment featured in V, Figure **72** has attained considerable popularity since its conceptualisation in 2010.[480] As of September 2017 the CSD contains 194 structurally authenticated records of the [(Ar*)N(SiR$_3$)] motif alone.[204]

hydride, as well as the remarkable mixed-valence tri-zinc complex shown in Figure **75**.[212,244]

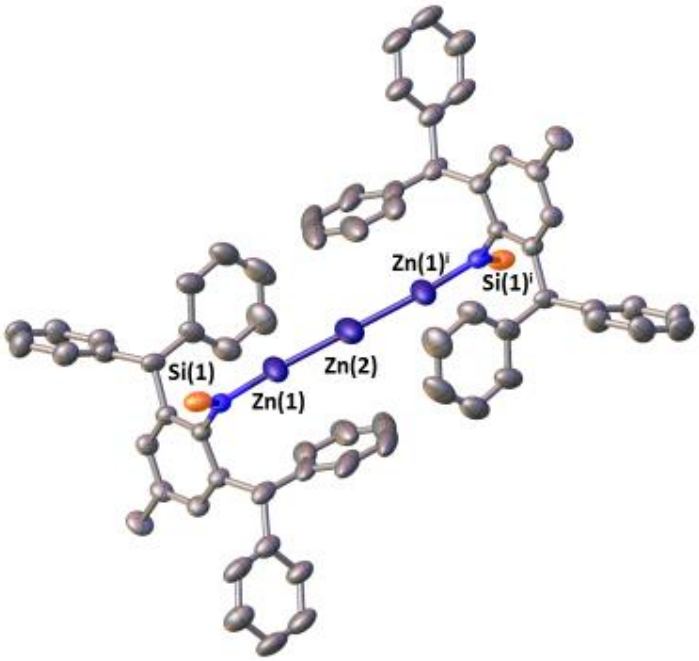


***Figure 75**: Molecular structure of [Zn$_3${(Ar*)N(Si^{i}Pr$_3$)}$_2$] featuring a linear chain of mixed valence Zn^{I}–Zn^{0}–Zn^{I} centres, ellipsoids set at the 50% probability level; hydrogen atoms, residual solvent and ^{i}Pr groups are omitted for clarity.*[244]

The success of these superbulky silylated anilides and comparative rarity of their alkylated analogues, specifically the absence of trityl substituted congeners, prompted interest in exploration of the latter. In addition to the rationale of N–C *vs.* C–Si provided above (*v.s.* pg. 95), it was envisaged that such a system might be accessible *via* air stable synthetic routes, allowing for facile purification and altering of aryl substituents.

3.2.1. Results and Discussion

Initial work on obtaining the desired proligands focused on obtaining *N*-tritylanilines, for which two synthetic routes were envisaged, displayed in Figure **76** below.

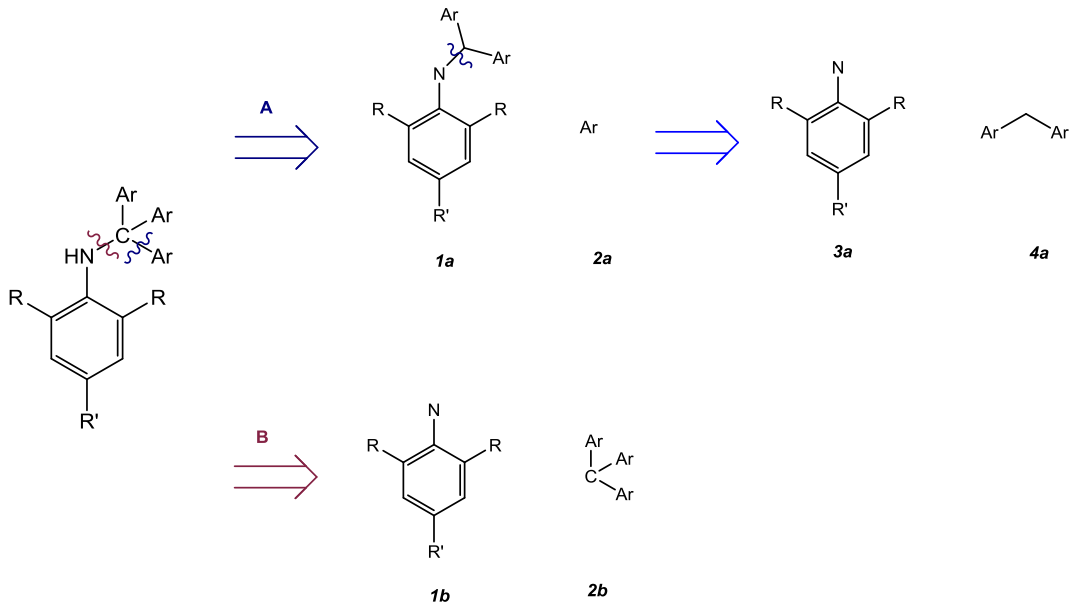


***Figure 76**: Retrosynthetic analysis of benzylanilines.*

Disconnection **A** was considered as a route to introduce asymmetric CAr'$_3$ functionalities from the reaction of an imine (***1a***) with an organometallic reagent (***2a***), the imine in turn being obtained from the condensation of a diarylketone (***4a***) with an aniline (***3a***, all Figure **76**). This is referred to as the imine route below. Whilst the latter is a well-developed methodology, imine substitution with organometallics is more problematic due to poor azomethine electrophilicity (compared to carbonyls). This inconvenient property has been the focus of some attention, as reviewed by Bloch.[245] Focus in this field over the past decades has mostly been dedicated to the development of stereoselective reactions for aldimines.[246–248] Whilst some limited research on the addition of alkyl halides to benzophenone anil dianions has been conducted, this pathway only results in *C*-alkylation in the case of isopropyl chloride. Additionally, to the

best of my knowledge no further work on this topic has been carried out since the 1970s.[249–251]

Disconnection **B** (Figure **76**) may be considered a straightforward approach analogous to the introduction of an SiR_3 functionality by reacting the corresponding chlorosilane with an anilide. In the carbogenic equivalent, ***1b*** is simply the desired aniline or anilide, and ***2b*** a variation of Ar_3CX, in which X denotes a good leaving group such as a halide, alcohol under acidic conditions, *etc*. This is referred to as direct alkylation below.

(i) Disconnection A: The Imine Route

The reaction of s-block organometallics with carbodiimide and nitrile substrates is a well-established route to amidinide and guanidinide complexes, amongst others (as displayed in Figure **77**).[221,252,253]

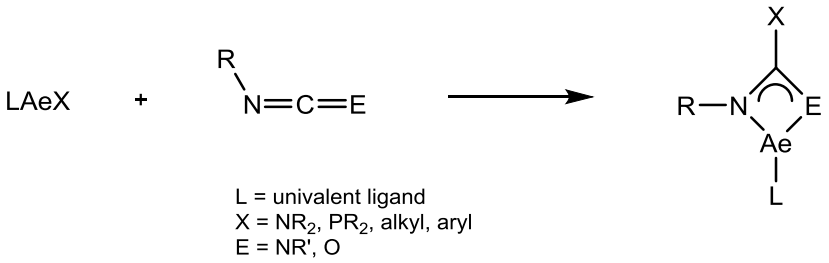


Figure 77: *Alkaline earth reagent insertion into heterocumulenic substrates.*

It was envisaged that an analogous reaction with imines may prove a convenient method to assemble benzylanilides as shown in Figure **78**. Comparable reactions have precedent in the synthesis of $(Me_3C)NHPh$,[254] $\{(C_6H_{11}N_3P)Ph_2C\}NHPh$,[255] and $(Ph_3C)NHPh$,[256] amongst others.[257,258]

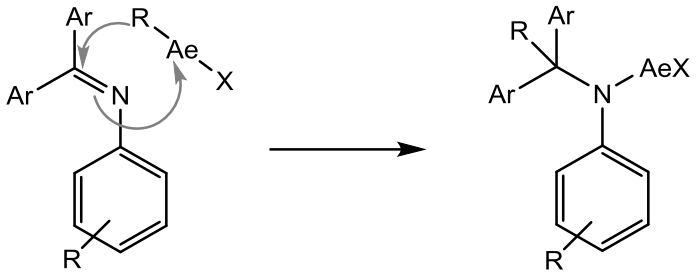
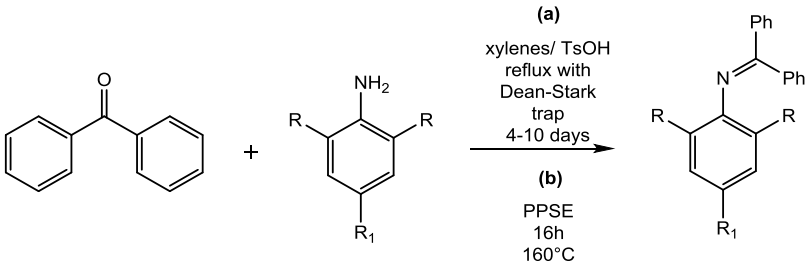


Figure 78: *Envisaged path to benzylanilides from benzylimines.*

Sterically undemanding aldimines and small ketimines may readily be synthesised from the condensation of their corresponding aldehydes or ketones;[259–261] however, analogous attempts at synthesising **13** and **14** (Figure **79**) employing mild reaction conditions† did not furnish the desired imines. Difficulties in the assembly of sterically congested diarylimines, particularly those involving *ortho*-substituted anilines, have been reported by Strekowski *et al.*,[262] common strategies to circumvent this involve the use of Lewis acids,[263] *p*-toluenesulfonic acid,[264] as well as zeolites or more exotic dehydrating reagents as reviewed by Love and co-workers.[265]



13 - R= Me, R_1= H	*via* (a): 68 %
14 - R= ^{i}Pr, R_1= H	*via* (a): 67 %; *via* (b): 71 %
15 - R= $CHPh_2$, R_1= Me	*via* (b): 32 %

Figure 79: *Synthetic routes to imines by aniline-diphenylketone condensation.*

† refluxing DCM, $MgSO_4$ as a desiccant and catalytic amounts of AcOH

Consequently, heating a solution of benzophenone and the corresponding aniline to reflux in xylenes over several days with a Dean-Stark trap gave good crystalline yields for **13** and **14**, whereas the considerably more bulky **15** could only be synthesised by employing polyphosphoric acid silyl ester (PPSE) in moderate yields (Figure **79**). Whilst **13** is a known compound, previously reported synthetic routes require precious metal-catalysed coupling reactions,[266] oxidation of the aniline with DDQ,[262] the use of tetraethyl orthosilicate and prolonged reaction times,[267] or Lewis acids affording much poorer yield.[268] The synthesis of **14** has previously been reported by Klingebiel in nearly identical yield to that obtained for method **a** in this work (Figure **79**), employing a considerably more involved methodology,[†269] as well as by tantalum-catalysed imidation of benzophenone with *N*-sulfinylamine under expulsion of SO_2 (again in nearly identical yield).[270] Spectroscopic data obtained for **13** and **14** match those reported in the literature. Whilst reflux in xylenes under removal of water successfully furnished the latter two imines, synthesis of the novel superbulky Ar*NCPh_2 **15** required the use of PPSE (method **b** in Figure **79**). ^{1}H and $^{13}C\{^{1}H\}$ NMR spectra are consistent with the formed imine; whilst the aromatic regions are expectedly crowded, C*H*Ph_2 (5.34 ppm) and Ph_2*C* azomethine (166.2 ppm) resonances proved valuable reporters.

With the desired imines in hand, their conversion to benzylanilides was attempted with a variety of organometallics, as displayed in Figure **80**.

[†] From the reaction of lithiated aminofluorosilane with benzophenone.

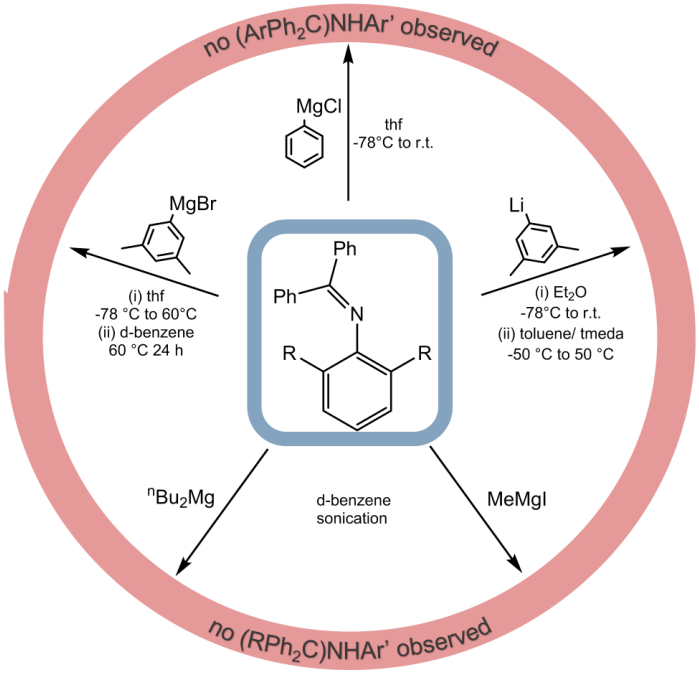


Figure 80: *Attempted imine metalation reactions. R = Me, ^{i}Pr (**13** and **14**, respectively).*

In my hands, the examined imines **13** and **14** proved impervious to functionalisation with a variety of aliphatic and aromatic organometallic reagents under a multitude of conditions. Reactions with organolithiums afforded completely opaque, blood-red solutions above -40 °C; multinuclear NMR spectra of isolated material were extremely congested. Upon aqueous work-up, 30-60% of unreacted imine could be recovered. The above characteristics point towards the formation of anil lithium radicals similar to those of sodium benzophenone ketyl.[250,251] Only unreacted imine could be recovered from the reaction of **12** and **14** with Grignard reagents; *in situ* NMR-scale experiments showed no evidence whatsoever for the desired azomethine substitution. Whilst this remarkable resilience is certainly desirable for Schiff-base type complexes, it presents a considerable inconvenience in benzylanilide assembly.

The undesirable characteristics displayed by imines investigated thus far were attributed to their propensity for radical stabilisation, steric bulk around the azomethine, and lacking electrophilicity. Whilst the former two properties are

inherently difficult to address, decreasing electron density of the imine system seemed a viable target. *N*-coordination to Lewis acids such as BF_3[271] and trimethylsilyl triflate[272,273] have previously been reported to improve azomethine electrophilicity, with the above in mind, **16-19** were synthesised to access species more vulnerable towards nucleophilic attack according to Figure **81**.

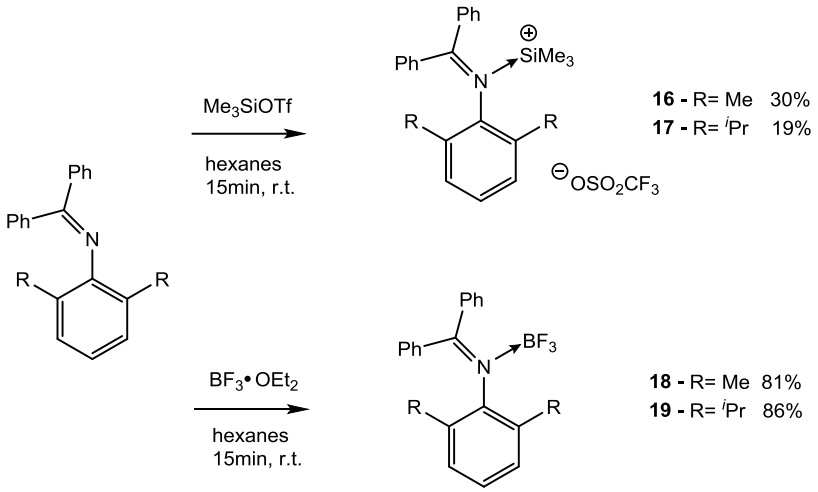


Figure 81: *Synthesis of imine-Lewis acid complexes.*

The identity of **16** and **17** could not be determined to an acceptable degree of certainty; despite the obvious physical changes such as colour and solubility compared to the free imine, multinuclear NMR spectra gave no evidence of Me_3Si resonances corresponding to a sufficient number of protons. Whilst considerable broadening of a multitude of resonances was observed, only a minor upfield shift of the azomethine *C*NPh_2 was observed in **17**.† Combined with low yields, this Lewis acid-base pair was seen as an unattractive target for further reactivity studies. In contrast, boron trifluoride adducts were isolated in good yields and excellent purity. **18** shows no more than 5% remaining BF_3•OEt_2 and no unreacted imine, whilst **19** was completely devoid of either. ^{1}H NMR spectra gave a good indication for the formation of the target adduct. A significant upfield shift of the azomethine resonance from around 166 pm into the aromatic region

† Poor solubility of **16** precluded the collection of $^{13}C\{^1H\}$ NMR data. No ^{29}Si resonances were observed in either **16** or **17**. "Air stable" mass spectrometry only gave evidence for the presence of the parent imines.

(120ppm-140ppm) is indicative of a disruption of nitrogen electron donation *via* the π-system, and thus increased electrophilicity. ^{19}F and ^{11}B NMR data further corroborated formation of the desired species. Whilst the former showed a marked downfield shift to $BF_3 \cdot OEt_2$ (-153 ppm *vs.* -139 ppm and -138 ppm in **18** and **19** respectively), ^{11}B resonances were scarcely affected. Signals in the aforementioned spectra are singlets not due to being run decoupled, but as a result of negative and positive components in the ^{19}F-^{11}B coupling cancelling each other out.

Reactions of **16** and **19** with organometallic reagents analogous to those undertaken for **12** and **14** (*cf.* Figure **80**, pg. 103) yielded only unreacted starting materials after aqueous work-up. Given the lack of success in imine functionalisation, this synthetic route was abandoned in favour of direct alkylation.

(ii) Disconnection B: Direct Alkylation

Generally, anilines are more difficult to alkylate than primary and secondary amines, which often readily react with alkyl halides in a standard nucleophilic aliphatic substitution. Whilst Buchwald-Hartwig amination has emerged as a prominent solution,[274] this palladium-catalysed cross-coupling reaction requires expensive reagents and often provides low yields for very bulky systems.[240] Despite aniline alkylation having received some attention in the literature, focus is usually given to the addition of small alkyl chains on *o,p*-unsubstituted anilines, an overview of which has been compiled by Salvatore *et al.*[275] Given the propensity of tritylic systems to form stable carbocations, *i.e.* readily available electrophilic fragments, and the limited information available on aniline *N*-trityl substitution, a variety of exploratory pathways were envisaged as depicted in Figure **82**.

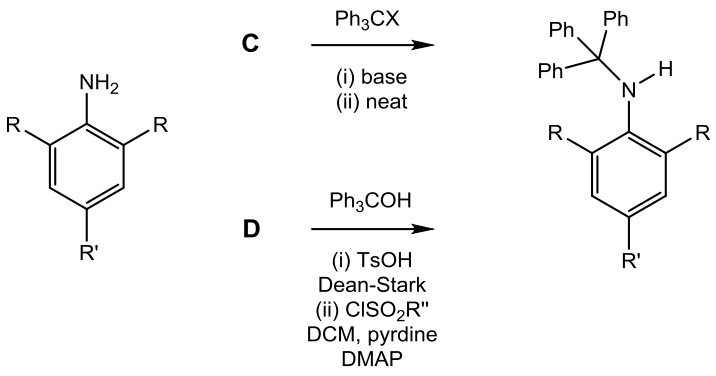


Figure 82: *Approaches to aniline N-alkylation.*
R = Me, ^{i}Pr, $CHPh_2$; R' = H, Me, R'' = Me, p-MePh, X = Cl, Br

These can be divided into those employing benzyl halides and trityl alcohol (**C** and **D** respectively, Figure **82**). The former were carried out under basic conditions to improve aniline nucleophilicity (**C**), whereas the latter employed acid to draw on improved trityl electrophilicity (**D**). Synthetic work and its results are summarised in Figure **83**. Whilst none of the below ultimately proved successful, a brief rationale for the employed methods and results thereof are given below.

For anilines with comparatively low melting points, neat reactions with tritylic chlorides and aniline as solvent, base and reagent have been reported with unsubstituted anilines.[276] The screened *o*-Me and *o*-^{i}Pr anilines exclusively yielded *p*-substituted *C*-trityls, with no *N*-alkylation observed (**E**, Figure **83**). The reaction most likely proceeds *via* the formation of an unstable anilinium salt, followed by Hofmann-Martius rearrangement, the acid catalyst being provided by HCl formed in the initial *N*-alkylation.[277]

In light of the observed undesirable side reactions, it was decided that a softer approach may be more fruitful. Considering the large amount of reasonable conditions and lack of literature procedures for the tritylation of *o,p*-substituted anilines, a base/solvent screen was undertaken, **F**(ii) in Figure **83**. Aprotic polar solvents appeared the best choice considering any reaction was most likely to proceed in an S_N1 fashion. As the alkylation of amines and anilines is known to

significantly profit from the use of caesium bases, both caesium carbonate and hydroxide were screened, amongst others, including organic bases.[278,279]

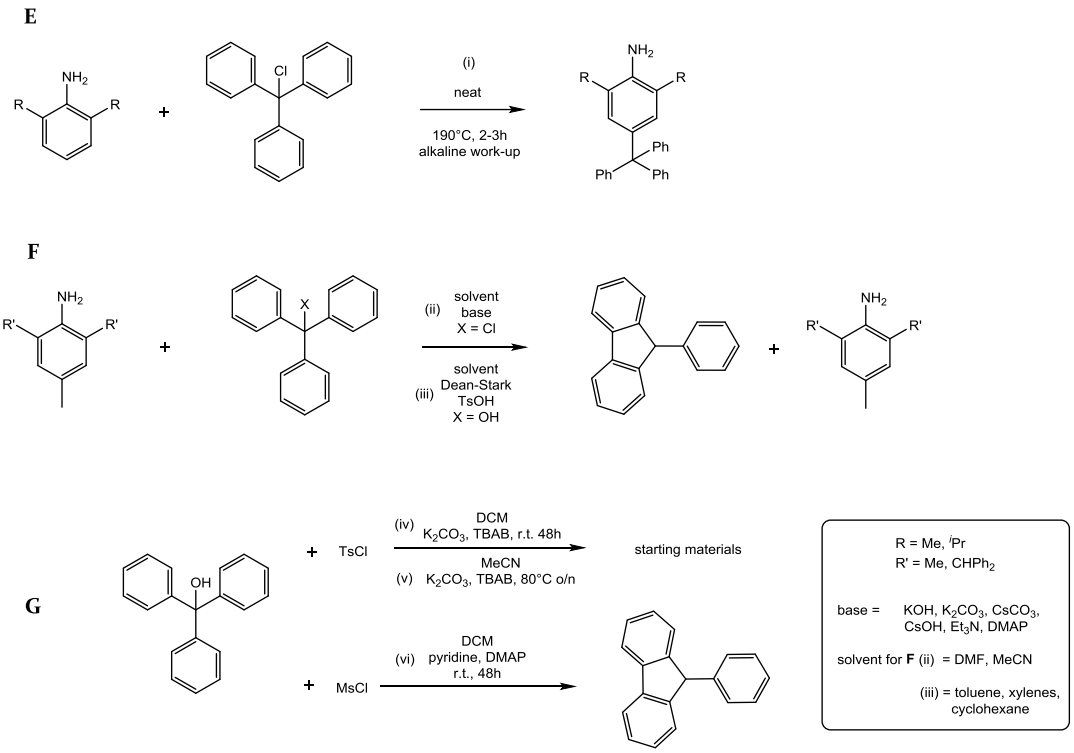


Figure 83: *Synthetic works towards the air-stable synthesis of N-trityl substituted anilines.*

Results of **E** (Figure **83**) have been discussed above. Approach **F**(ii) almost exclusively yielded unreacted starting materials, often with the concomitant formation of varying amounts of phenylfluorene.†

Reaction of trityl alcohol with anilines in three solvents forming a binary azeotrope with water did not yield any *N*-alkylated anilines (**F**(iii)).[280] Whilst isolable amounts of phenylfluorene (amongst unidentified side products of extreme coloration) were obtained from reactions employing toluene and xylenes, no reaction was observed in cyclohexane.

† Commonly observed as a by-product of the above reactions, the formation of phenylfluorene was first hinted at by ESI spectra, and ultimately ascertained by comparison to an authentic sample. Its non-polar nature and consequently high R^f value then facilitated identification in screening reactions by thin layer chromatography (TLC).

In an attempt to render the hydroxyl functionality in trityl alcohol a good leaving group without the need for elevated temperatures as above, conversion to corresponding alkyl sulfonates was attempted, reactions **G** in Figure **83** above. Reaction conditions were analogous to those successful in the sulfonation of comparable benzylic substrates.[281] Reactions with tosyl chloride under phase transfer conditions yielded starting materials, those with the less sterically demanding mesyl chloride afforded phenylfluorene in 83% yield.

The formation of phenylfluorene commonly observed within this work is rationalised in Figure **84**, a resonance form of the hyperconjugated carbocation is "conveniently" set up for an intramolecular cyclisation known to occur in tritylic systems.[282,283] Regrettably, the general reaction required in this Chapter, *i.e.* the intermolecular reaction of two sterically demanding fragments, will naturally favour the aforementioned intramolecular cyclisation.

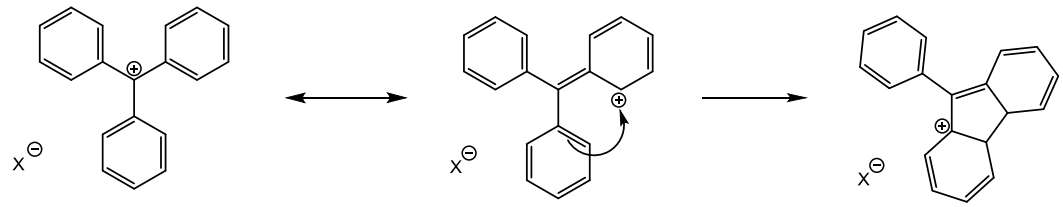


Figure 84: *Origin of phenylfluorene from trityl moieties. Radical pathways present another possibility.*[282,283]

The above displayed tendency of trityl moieties to undergo cyclisation thus precluded the air-stable synthesis of tritylanilines; even under basic conditions the desiccant properties of Group I carbonates and hydroxides often proved sufficient to produce at least some phenylfluorene, and no *N*-alkylated aniline. The cyclisation of a putative $MsOCPh_3$ even at room temperature further highlights the unsuitability of a trityl-focused approach to *N*-alkylation.† Thus,

† The synthesis of TrOTf has been demonstrated and employed in the synthesis of extremely bulky NHCs.[295,481] However, in contrast to the anilines employed above, imidazole precursors of the latter were not sterically congested before installation of the trityl group.

increasing aniline nucleophilicity by metalation was seen as the remaining avenue of pursuit.

A series of Ar*-based benzylanilines were thus synthesised by lithiation of the corresponding anilines, which were reacted with benzyl halides according to Figure **85**.

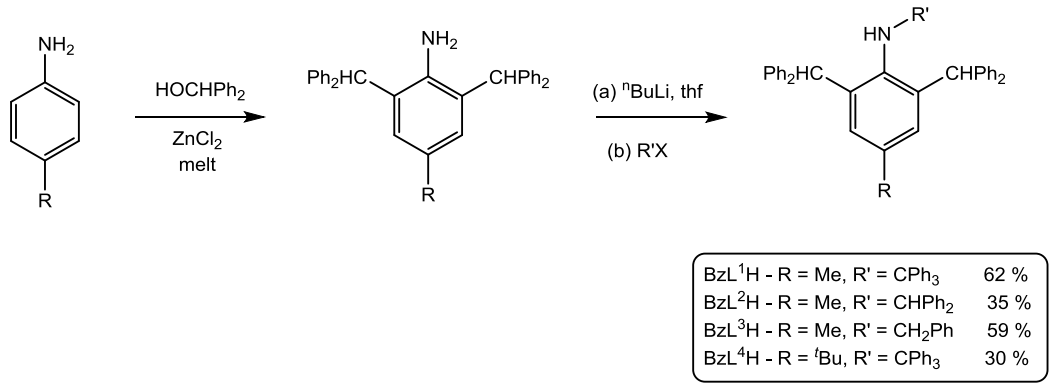


Figure 85: *Synthesis of benzylanilines.*

Whilst reactions of Ar*NHLi with trityl chloride provided poor yields and conversion, trityl bromide afforded significantly better results. This notwithstanding, a considerable variance in **BzL**[1]H yields was observed; additionally, separation of the latter from Ar*NH_2 starting material by recrystallisation proved problematic.[‡] The only consistently successful purification procedure required mixtures obtained from the above reaction to contain no more than 40% unreacted Ar*NH_2; from those recrystallisation from Et_2O afforded the pure ligand. Chromatographic separation was considered, but ruled impractical due to the multigram quantities required, as well as close R_f values obtained for a series of eluents (and mixtures thereof). **BzL**[2]H and **BzL**[3]H were primarily synthesised as proof of concept, their comparatively low steric bulk as well as presence of β-hydrogens renders them relatively poor candidates

[‡] The synthesis of BzL[1]H was repeated 16 times, conversions varied from 98 to 3%, and crystalline yields from 62% to none. No side products other than Ar*NH_2 starting material could be identified; the latter could be recovered in near quantitative yield from reactions which gave poor conversions.

for the stabilisation of s-block complexes. The introduction of a *p*-^{t}Bu functionality in **BzL**^{4}H was designed to investigate potential electronic effects of a more electron-rich ligand framework. The identity of all four proligands was ascertained by multinuclear NMR and mass spectrometry, as well as structural data displayed in Figure **86** below.

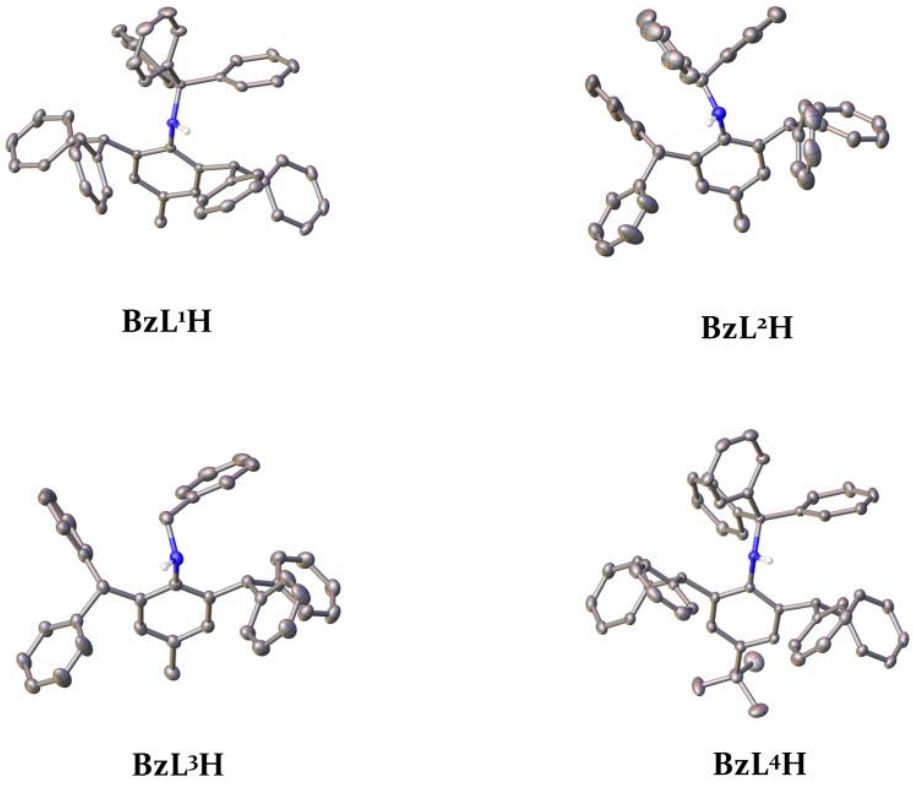


Figure 86: *Molecular structures of* ***BzL***$_x$*H proligands, ellipsoids set at at the 50% probability level; hydrogen atoms are omitted for clarity with the exception of NH.*

(iii) Benzylaniline Metalation

With the desired ligands at hand, metalation was attempted with a series of reagents as summarised in Figure **87**. Although all four ligands were investigated, the most extensive body of work was carried out on the displayed **BzL**^{1}H.

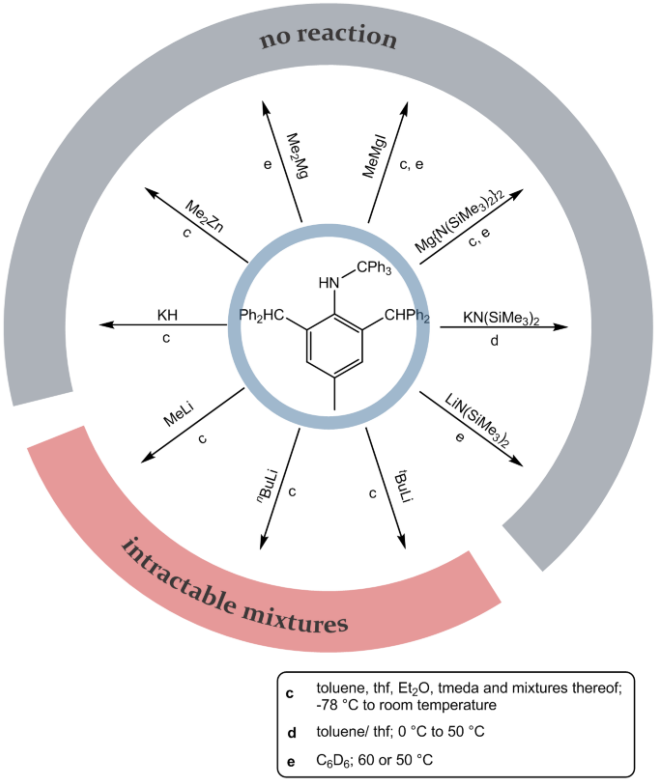


Figure 87: *Work towards* ***BzL****^{1}H metalation.*

Employing a variety of reagents and reaction conditions, **BzL**^{1}H was found to be unexpectedly inert towards metalation. Whilst lack of success in transamination may be attributed to an insufficient difference in pK_a for silylamines,[†] such arguments cannot be applied to the employed hydrocarbon organometallics. Steric factors may play a role, as the NH environment could be too crowded to accommodate a potential deprotonation transition state, particularly considering the propensity of s-block species to form larger aggregates.[196]

[†] The pK_a of HN(SiMe$_3$)$_2$ is *ca.* 30, that of unsubstituted aniline 30.6, likely higher for **BzL**^{1}H as electron donating ring substituents will destabilise the conjugate base.[482]

Reactions with organolithium reagents yielded intractable mixtures of extreme red colouration; this may be attributed to the former acting as a single electron donors towards the extended aromatic system, resulting in the formation of a putative trityl radical anion known to be prone to fragmentation.[282] **BzL**^{4}H and **BzL**^{3}H gave comparable results. In contrast to the above, multinuclear NMR spectra gave good evidence for the formation of **BzL**^{3}Li [**20**] by reacting the proligands with ^{n}BuLi. *m*-Ar*H* (of the central aromatic ring) and Ph_2C*H* resonances shift downfield as electron density is dissipated from nitrogen to the *ortho* and *para* positions, lithiation also resulted in PhC*H*$_2$ signals becoming anisochronous. Similar ^{13}C diamagnetic shifts of benzylic *C*H_2Ph and *C*HPh_2 resonances compared to the proligands (downfield by *ca.* 1 ppm in both cases) give a further indication of negative charge being heavily delocalised, with the former α and the latter γ to the deprotonated position.†

3.2.2. Experimental

Synthesis of Ph_2CNPh-2,6-Me_2 [13]

A light yellow suspension of benzophenone (7.28 g, 40 mmol), 2,6-dimethylaniline (4.84 g, 40 mmol) and tosic acid (0.76 g, 4 mmol) in xylenes was degassed with argon for 15 min and subsequently heated to reflux with a Dean-Stark trap for one week (reaction progress monitored by water formation). Xylenes were removed *in vacuo* to yield a brown oil which was recrystallised from hot hexanes (120 mL) to yield the title compound as large crystals of intensely yellow colour (7.761 g, 68%).

^{1}H NMR ($CDCl_3$, 400 MHz): δ = 2.10 (s, 6 H), 6.81 - 6.86 (m, 1 H), 6.93 (d, *J* = 7.5 Hz, 2 H), 7.13 - 7.18 (m, 2 H), 7.22 - 7.28 (m, 2 H), 7.28 - 7.34 (m, 1 H), 7.46 (t, *J* = 7.3 Hz, 2 H), 7.50 - 7.55 (m, 1 H), 7.85 (d, *J* = 7.0 Hz, 2 H) ppm.

† $^{13}CH_x$ resonances chosen for the above argument due to their intensity and correlation to ^{1}H in HMQC spectra as opposed to quaternary ^{13}C signals.

$^{13}C\{^{1}H\}$ NMR ($CDCl_3$, 101 MHz): δ = 18.5, 122.7, 125.8, 127.7, 127.8, 128.2, 128.4, 129.1, 129.4, 130.5, 139.8, 136.8, 148.9, 167.1 ppm.

Synthesis of $Ph_2CNPh\text{-}2,6\text{-}^{i}Pr_2$ [14]

Phosphorus pentoxide (11.3 g, 80 mmol) and hexamethyldisiloxane (51 mL, 240 mmol) were mixed in dichloromethane (50 mL), the mixture heated to reflux for 2 h, allowed to cool to room temperature and volatiles removed *in vacuo* to afford PPSE as a milky viscous oil. To this were added benzophenone (7.28 g, 40 mmol) and 2,6-diisopropylaniline (7.09 g, 40mmol) and the resulting mixture heated to 160 °C for 23 h. Onto the cooled mixture was poured sodium hydroxide (300 mL, 1 M) and the mixture homogenised by sonication and vigorous stirring. Extraction with dichloromethane (3*50 mL) gave a dark yellow solution washed with brine, dried over magnesium sulfate and reduced to a yellow sticky solvent *in vacuo* (12.63 g, 92%). Recrystallisation from hexanes afforded large crystals of intensely yellow colour (9.71 g, 71%).

The compound was also synthesised in a procedure identical to that of **13** from benzophenone (14.58 g, 80 mmol), 2,6-diisopropylaniline (14.18 g, 80 mmol) and tosic acid (1.5 g, 8 mmol) in xylenes (100 mL). Reflux for 10 days gave the title compound in comparable yield (18.18 g, 67%, analytical data identical).

^{1}H NMR ($CDCl_3$, 400 MHz): δ = 0.98 (d, *J* = 6.8 Hz, 6 H), 1.18 (d, *J* = 6.7 Hz, 6 H), 2.92 (spt, *J* = 6.8 Hz, 2 H), 6.98 - 7.05 (m, 3 H), 7.13 (d, *J* = 6.9 Hz, 2 H), 7.20 - 7.31 (m, 3 H), 7.43 - 7.55 (m, 3 H), 7.85 (d, *J* = 6.8 Hz, 2 H) ppm.

$^{13}C\{^{1}H\}$ NMR ($CDCl_3$, 101 MHz): δ = 21.9 24.0, 28.4, 122.7, 123.3, 127.7, 128.2, 128.9, 129.1, 129.4, 130.3, 135.8, 136.1, 140.0, 146.5, 165.7 ppm.

Synthesis of $Ph_2CN(4\text{-}Me\text{-}Ph\text{-}2,6\text{-}(CHPh_2)_2$ [15]

In a procedure identical to that of **14**, PPSE from phosphorus pentoxide (5.67 g, 40 mmol) and hexamethyldisiloxane (25 mL, 120 mmol) in dichloromethane (30 mL) was employed in the condensation of benzophenone (3.64 g, 20 mmol) and Ar^*NH_2 (8.79 g, 20 mmol) to obtain a yellow oil (11.90 g, 101%). Recrystallisation from hexane/ dichloromethane afforded the pure title

compound as crystals of intensely yellow colour (3.55 g, 32%).

^{1}H NMR ($CDCl_3$, 400 MHz): δ = 2.19 (s, 3 H) 5.34 (s, 2 H), 6.50 - 6.76 (m, 8 H), 6.91 - 7.47 (m, 26 H) ppm.

$^{13}C\{^{1}H\}$ NMR ($CDCl_3$, 101 MHz): δ = 51.7 126.0, 127.7, 128.1, 128.6, 129.1, 129.4, 129.5, 130.0, 131.6, 132.1, 145.4, 166.2 ppm.

Synthesis of [$Ph_2CNSiMe_3Ph$-2,6-Me_2][OTf] [16]

To a yellow solution of **13** (0.500 g, 1.75 mmol) in hexanes (15 mL) was added trimethylsilyl triflate (0.63 mL, 3.50 mmol) under argon. Solvent was removed from the formed milky yellow suspension by filtration and quenched into a sodium carbonate solution; the title compound remained as a white powder dried *in vacuo* (0.230 g, 30%).

^{1}H NMR ($CDCl_3$, 400 MHz): δ = 0.30 - 0.44 (m, 2 H) 2.18 (s, 6 H), 6.85 - 6.97 (m, 6 H), 7.03 (br. s., 2 H), 7.26 - 7.31 (m, 5 H), 8.02 (dd, *J* = 7.6, 1.7 Hz, 2 H) ppm.

Synthesis of [Ph_2CN $SiMe_3Ph$-2,6-$^{i}Pr_2$][OTf] [17]

In a procedure identical to that of **16, 14** (0.478 g, 1.40 mmol) and trimethylsilyl triflate (0.51 mL, 2.80 mmol) afforded the title compound as a light yellow powder (0.131 g, 19%).

^{1}H NMR ($CDCl_3$, 400 MHz): δ = 0.92 - 1.08 (m, 6 H), 1.13 - 1.30 (m, 6 H), 2.94 (spt, *J* = 6.8 Hz, 2 H), 7.06 (br. s., 3 H), 7.17 (br. s., 2 H), 7.27 (d, *J* = 3.9 Hz, 3 H), 7.50 (br. s., 3 H), 7.88 (d, *J* = 6.3 Hz, 2 H) ppm.

$^{13}C\{^{1}H\}$ NMR ($CDCl_3$, 101 MHz): δ = 22.3, 24.1, 28.5, 122.7, 129.0, 135.8, 139.9, 146.5, 165.8 ppm.

Synthesis of [Ph_2CNPh-2,6-Me_2][BF_3] [18]

In a procedure identical to that of **16**, **13** (0.500 g, 1.75 mmol) and boron trifluoride etherate (0.67 mL, 5.25 mmol) yielded the title compound as a white powder (0.501 g, 81%).

^{1}H NMR ($CDCl_3$, 400 MHz): δ = 2.36 (s, 6 H), 6.97 - 7.03 (m, 2 H), 7.07 - 7.12

(m, 3 H), 7.22 (t, *J* = 6.7 Hz, 2 H), 7.36 (br. s., 1 H), 7.53 (d, *J* = 7.0 Hz, 2 H), 7.61 (br. s., 1 H), 7.70 (br. s., 2 H) ppm.

$^{13}C\{^{1}H\}$ NMR ($CDCl_3$, 101 MHz): δ = 18.5, 128.1, ppm 132.4, 128.9, 128.5, 132.4 ppm.

^{11}B NMR ($CDCl_3$, 128 MHz): δ = 0.15 (s) ppm.

^{19}F NMR ($CDCl_3$, 376 MHz): δ = -139.1 (s) ppm.

Synthesis of [Ph_2CNPh-2,6-$^{i}Pr_2$][BF_3] [19]

In a procedure identical to that of **16**, **14** (5.00 g, 14.65 mmol) and boron trifluoride etherate (3.74 mL, 29.3 mmol) in hexanes (100 mL) yielded the title compound as a white powder (5.18 g, 86%).

^{1}H NMR ($CDCl_3$, 400 MHz): δ = 0.99 (d, *J* = 6.9 Hz, 6 H), 1.32 (d, *J* = 6.7 Hz, 6 H), 2.99 - 3.18 (m, 2 H), 7.03 (d, *J* = 6.9 Hz, 2 H), 7.13 - 7.23 (m, 4 H), 7.34 (d, *J* = 6.9 Hz, 2 H), 7.55 (br. s., 3 H), 7.66 (d, *J* = 4.8 Hz, 2 H) ppm.

$^{13}C\{^{1}H\}$ NMR ($CDCl_3$, 101 MHz): δ = 23.2, 24.7, 28.7, 124.4, 127.8, 128.0, 128.2, 128.7, 130.4, 130.8, 132.2, 135.2, 136.7, 141.9 ppm.

^{11}B NMR ($CDCl_3$, 128 MHz): δ = 0.06 (s) ppm.

^{19}F NMR ($CDCl_3$, 376 MHz): δ = -138.2 (s) ppm.

General Procedure for the Reaction of 18 and 19 with organometallics

To the Lewis acid-imine adduct (0.70 mmol) in toluene (5 mL) was added an excess of the organometallic reagent (1.0 - 1.4 mmol) at 0 °C. The resulting opaque yellow suspensions were allowed to warm to room temperature and left to stir overnight. Reactions were subsequently quenched by pouring into concentrated, ice-cold $NH_4Cl_{(aq)}$ (20 mL) and stirred for 1 h whilst warming to room temperature. After addition of water (30 mL) and separation of the organic layer, any remaining organics were partitioned into hexanes (2*10 mL), combined organic layers washed with conc. $NaCl_{(aq)}$ (2*10 mL), dried over $MgSO_4$ and solvents removed *in vacuo*.

*General Procedure for the Reaction of Neat Anilines with Ph_3CCl (**E**, Figure 83)*

According to modified literature procedure; anilines in this work are *o*-substituted (*vs.* not substituted) and trityl halide non-heterocyclic (*vs.* pyridine-containing), otherwise identical.[276]

*General Procedure for the Reaction of Anilines with Ph_3CCl in solution (**F,G** (ii), Figure 83)*

A suspension (inorganic base) or solution (organic base) of the desired aniline (0.45 mmol) and trityl chloride (0.5 mmol) in the relevant solvent (3 mL) were stirred at room temperature overnight, reaction progress and outcome was monitored by TLC/ MS and multinuclear NMR spectroscopy.

*General Procedure for the Reaction of Anilines with Ph_3COH, with water removal by azeotrope (**F** (iii), Figure 83)*

Procedure identical to that employed for **13**. Typically with 10 mmol of aniline, 10 mmol of Ph_3COH and 0.5 mmol TsOH.

General Procedure for the synthesis of benzylanilines

To a solution of Ar^*NH_2 in thf (*ca.* 15 mL per gram of aniline) was added dropwise ^{n}BuLi (2.5 M in hexanes) at -78 °C. The resultant orange solution was allowed to briefly warm to room temperature, the off-white suspension cooled down to -78 °C followed by addition of trityl bromide as a solid. Upon warming to room temperature, the reaction was left to stir overnight, quenched with a concentrated aqueous ammonium chloride solution. The separated aqueous layer was extracted with diethyl ether, and combined organics washed with water, brine, dried over magnesium sulfate and solvents removed *in vacuo*. The resultant mixture (typically containing 5-40% unreacted Ar^*NH_2) was recrystallised from diethyl ether (30 mL per gram of $\mathbf{BzL}_x$H/Ar^*NH_2 mixture) to afford the pure title compounds.

The use of trityl chloride generally gave poorer yields, reactions attempted in non-coordinating solvents (toluene and toluene/ hexane mixtures) did not

afford any tritylanilines. The reader is advised that trityl bromide solutions should not be added as solutions through stainless steel cannulae, this causes significant decomposition of the latter, manifest in light orange solutions turning deep red.

BzL¹H

From Ar*NH_2 (2.61 g, 5.93 mmol), ^{n}BuLi (2.37 mL, 2.5 M) and Ph_3CBr (1.94 g, 6 mmol) was obtained the title compound as a white microcrystalline solid (2.53 g, 62%).

The reaction was repeated a total of 16 times, conversions were subject to extreme variability under conditions kept identical to the best of my ability. Scale-up adversely affected conversion. The employment of catalytic amounts of CuCl gave more consistent yields, however resulted in the final product adopting a yellow-green tinge which could not be removed by recrystallisation, the use of active charcoal, or washing with aqueous triethylamine.

^{1}H NMR (C_6D_6, 400 MHz): δ = 1.78 (s, 3 H, C*H*$_3$), 3.74 (s, 1 H, N*H*), 5.68 (s, 2 H, C*H*Ph_2), 6.74 (s, 2 H, *m-Ar**), 6.81 - 6.90 (m, 8 H, CH-*o-Ph*$_2$), 6.98 - 7.07 (m, 13 H), 7.08 - 7.15 (m, 8 H), 7.27 - 7.36 (m, 6 H) ppm.

^{13}C{^{1}H} NMR (C_6D_6, 101 MHz) δ = 20.99, 52.64, 74.07, 126.25, 126.73, 127.70, 128.02, 130.09, 130.29, 130.44, 133.99, 141.84, 142.81, 144.73, 147.04 ppm.

MS: (FD) m/z $[M]^{+\bullet}$ Calc'd for $C_{52}H_{43}N$ 681.3390; Found 681.3397.

BzL²H

From Ar*NH_2 (2.20 g, 5 mmol), ^{n}BuLi (2 mL, 2.5 M) and Ph_2CHBr (1.24 g, 5 mmol) was obtained the title compound as a white microcrystalline solid (1.053 g, 35%).

^{1}H NMR ($CDCl_3$, 400 MHz): δ = 2.03 (s, 3 H, C*H*$_3$), 3.30 (s, 1 H, N*H*), 4.79 (s, 1 H, NHC*H*Ph*2*), 5.47 (s, 2 H, C*H*Ph_2), 6.41 (s, 2 H, s, 2 H, *m-Ar**), 6.80 - 6.88 (m, 2 H), 6.96 - 7.06 (m, 4 H), 7.06 - 7.15 (m, 12 H), 7.16 - 7.35 (m, 14 H) ppm.

^{13}C{^{1}H} NMR ($CDCl_3$, 101 MHz) δ = 30.30, 56.30, 125.80, 126.12, 126.62, 127.26, 128.11, 129.45, 129.74, 130.45, 143.44, 143.95, 144.24 ppm.

BzL³H

From Ar*NH_2 (2.20 g, 5 mmol), ^{n}BuLi (2 mL, 2.5 M) and $PhCH_2Br$ (1.03 g, 6 mmol) was obtained the title compound as a white microcrystalline solid (1.563 g, 59%).

In contrast to all other synthesised benzylanilines, addition of ^{n}BuLi resulted in a colour change from yellow-green to deep blue, as opposed to red.

^{1}H NMR ($CDCl_3$, 400 MHz): δ = 2.10 (s, 3 H, C*H*$_3$), 3.03 (br. s., 1 H, N*H*), 3.71 (s, 2 H, PhC*H*$_2$), 5.78 (s, 2 H, C*H*Ph_2), 6.59 (s, 2 H, *m*-Ar*), 7.04 (d, *J*=7.45 Hz, 8 H, CH-*o*-*Ph*$_2$), 7.10 (d, *J*=6.58 Hz, 2 H, CH_2-*o*-*Ph*), 7.16 - 7.23 (m, 4 H), 7.24 - 7.33 (m, 9 H) ppm.

^{13}C{^{1}H} NMR ($CDCl_3$, 101 MHz) δ = 21.32, 51.46, 54.56, 126.21, 127.15, 128.03, 128.28, 128.48, 129.49, 129.94, 132.01, 138.46, 140.30, 142.44, 144.09 ppm.

BzL⁴H

From ^{t}Ar*NH_2 (3.00 g, 6.22 mmol), ^{n}BuLi (2.49 mL, 2.5 M) and Ph_3CBr (2.01 g, 6.22 mmol) was obtained the title compound as a white microcrystalline solid (1.33 g, 30%).

^{1}H NMR ($CDCl_3$, 400 MHz): δ = 0.93 (s, 9 H, CC*H*$_3$)$_3$), 3.46 (s, 1 H, N*H*), 5.33 (s, 2 H, C*H*Ph_2), 6.47 (s, 2 H, *m*-Ar*), 6.55 - 6.64 (m, 8 H, CH-*o*-*Ph*$_2$), 7.08 - 7.15 (m, 6 H, C-*o*-*Ar*$_3$), 7.16 - 7.27 (m, 21 H, *m,p-Ar*) ppm.

^{13}C{^{1}H} NMR ($CDCl_3$, 101 MHz): δ = 30.54, 52.48, 127.75, 131.41 ppm.

BzL³Li [20]

To a colourless solution of **BzL**^{3}H (0.40 g, 0.755 mmol) in thf (15 mL) was added dropwise ^{n}BuLi (0.30 mL, 2.5 M, 0.755 mmol). The resulting intensely red solution was allowed to warm to room temperature overnight. Removal of solvent *in vacuo* and washing with hexanes (30 mL) afforded the title compound as a light orange microcrystalline powder (0.210 g, 52%).

^{1}H NMR (C_6D_6, 400 MHz): δ = 1.05 1.83 (s, 3 H, C*H*$_3$), 3.75 (s, 1 H, NC*H*$_2$Ph), 3.77

(s, 1 H, NC*H*$_2$Ph), 5.95 (s, 2 H, C*H*Ph$_2$), 6.86 (s, 2 H, *m*-Ar*), 6.92 - 6.98 (m, 6 H, CH$_2$-*m*-Ph, CH-*p*-Ph), 7.04 (m, 9 H, CH-*o*-Ph, CH$_2$-*p*-Ph), 7.08 - 7.13 (m, 10 H, CH-*m*-Ph, CH$_2$-*o*-Ph) ppm.

^{13}C{^{1}H} NMR (C_6D_6, 101 MHz) δ = 21.52, 52.52, 55.28, 126.96, 127.74, 128.72, 128.83, 129.04, 129.12, 130.34, 130.58, 130.91, 133.02, 139.70, 141.21, 143.63, 144.93, 145.06 ppm.

^{7}Li NMR (C_6D_6, 156 MHz) δ = 2.80 (br. s.) ppm.

3.3. Tritylamines

The generic motif of *N*-tritylamine proligands is displayed in Figure **88**, they consist of a CAr_3 umbrella complemented by an aliphatic or silyl moiety (R).

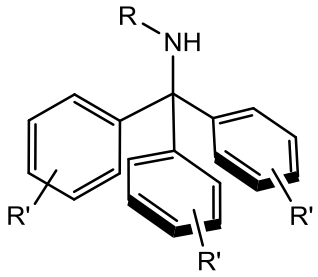


Figure 88: *General N-tritylamine motif, R= silyl or alkyl group.*

Analogous to the above mentioned anilides, silylated aliphatic analogues bearing $SiPh_3$ functionalities have seen use in the stabilisation of alkali,[284–286] alkaline earth,[287,288] as well as Group XIII complexes,[210,289] as well as some isolated transition metal and f-block species.[285,286,290] Although being widely employed as a protecting group for amines,[291,292] there only exists very limited precedent for the use of CPh_3 groups to impart steric crowding in coordination compounds. The latter has been employed in the isolation of titanium aminopyridinides,[293] on imino linker arms of Group I and II pyrrolides investigated for caprolactone polymerisation,[294] as well as very recently in extremely bulky *N*-heterocyclic carbenes allowing the isolation of monocoordinate Tl(I) as well as a $[GeCl]^+$ cation.[295] In addition, imido $NCPh_3$ units have featured in uranium complexes.[296] As a general observation, the negative charge of nitrogen introduced by metalation cannot be dissipated into an aromatic ring, consequently leading to more ionic complexes compared to their benzylaniline congeners.

In line with bulky lithium complexes such as LDA finding widespread use as synthetic reagents,[297] Corey *et al.* investigated a series of lithium salts generated *in situ* from the corresponding $RNHCPh_3$ proligands and ^{n}BuLi for their

propensity to form chiral enolates from achiral ketones.[298,299] Although no lithium salts were isolated, structural data of the employed proligands shown in Figure **89** gives an indication of the potential steric protection provided.

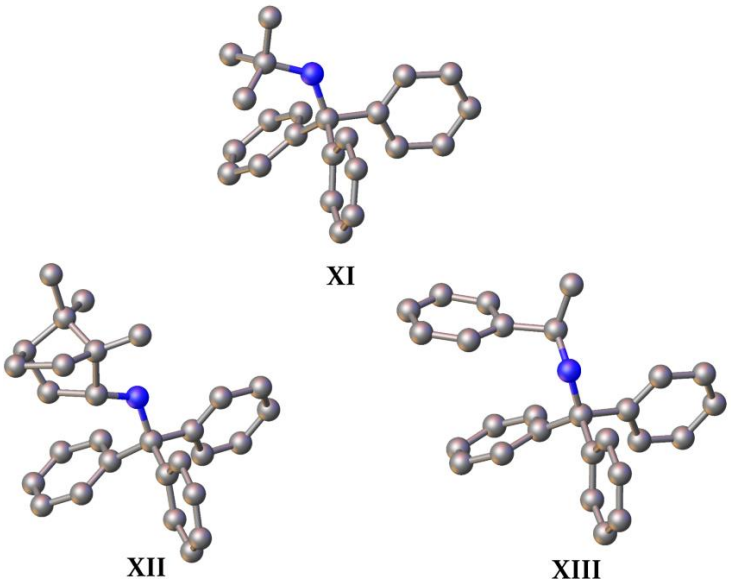


Figure 89: *Tritylamines investigated by Corey et al.*[298,299]

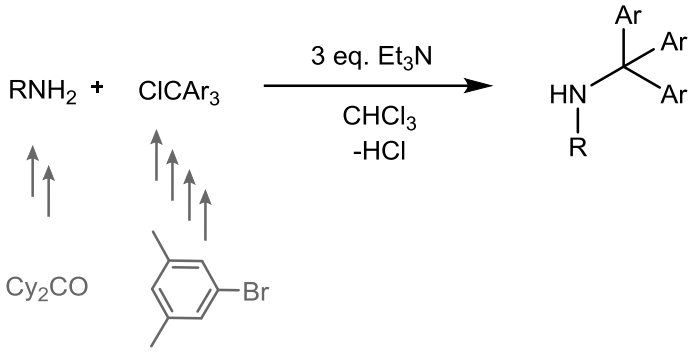
Lithium complexes of the above proved far superior to LDA and LiTMP in the stereoselective synthesis of silyl ketene acetals; whereas there is significant chelation control in the former (leading to poor *E*/*Z* ratios of 2/1 and 3/1, respectively), steric control imposed by [LiN(^{t}Bu)(CPh_3)] (*cf.* **XI**) resulted in a 14/1 *E*/*Z* selectivity for the same oxyacetate ester substrate. The desired *N*-tritylamines proligands were easily synthesised from commercially available precursors.[298]

3.3.1. Results and Discussion

Given both the underused nature of $RNHCPh_3$ systems and their facile synthesis, the exploration of this framework and its s-block complexes was identified as a propitious target.

(i) Proligands

In contrast to analogous attempts for the synthesis of tritylanilines (*v.s.* **3.2.1**(ii)), reacting a series of *t*- and *s*-alkylamines with trityl chloride yielded the desired ligands according to Figure **90**.



TrL^{1}H - R = ^{t}Bu, Ar = Ph	91 %
TrL^{2}H - R = Cy, Ar = Ph	76 %
TrL^{3}H - R = Ad, Ar = Ph	81 %
TrL^{4}H - R = Ad, Ar = 3,5-xylyl	69 %
TrL^{5}H - R = ^{t}Oct, Ar = Ph	98 %
TrL^{6}H - R = ^{t}Oct, Ar = 3,5-xylyl	67 %
TrL^{7}H - R = $CHCy_2$, Ar = Ph	64 %

Figure 90: *Synthesis of tritylamine proligands according to modified literature procedure.*[298]

TrL^{1}H-**TrL**^{7}H were obtained in excellent to good yields and characterised by multinuclear NMR spectroscopy, elemental analysis and single crystal X-ray crystallography (*v.s.* Figure **91**). In addition to proligands assembled from commercially available materials, sterically more demanding systems were

synthesised by incorporating tri(3,5-xylyl) as well as dicyclohexylmethyl functionalities. The highly modular nature of **TrL**H systems, combined with a facile synthesis, thus paves the way to a promising family of ligands.

^{1}H NMR spectra were well resolved, with δ N*H* resonances clearly visible in all ligands but **TrL**^{2}H;† these resonances shift downfield with increasingly electron donating adjacent groups. The extremely congested aliphatic region in ^{1}H NMR spectra of **TrL**^{7}H is in part due to the inequivalence of quasi-"*o*" and "*m*" positions, clearly visible in ^{13}C{^{1}H} NMR spectra, this property may be assumed to arise from rotational barriers of this very crowded proligand as seen in Figure **91**.

† Resolving the complex aliphatic multiplicities would require a higher field NMR machine which was unavailable at the time, ^{1}H-^{13}C HMQC data ascertained that chemical shifts of C*H* resonances are dependent upon spatial orientation, *i.e.* differ by up to δ0.5 ppm for "up" and "down" protons on isochronous carbons.

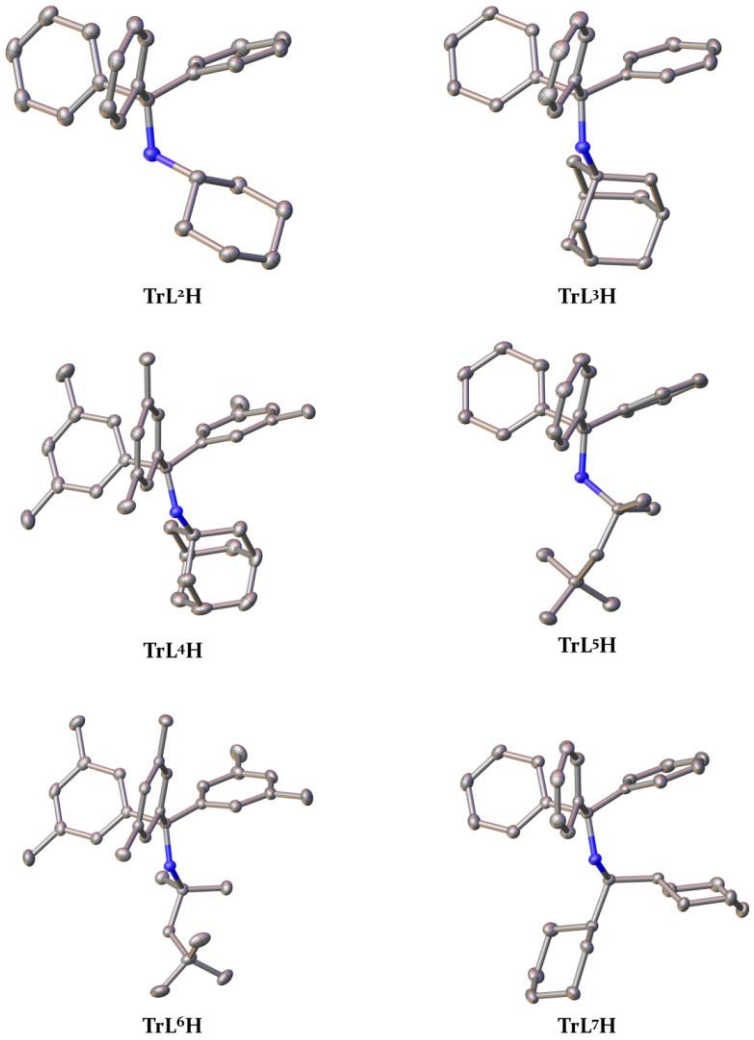
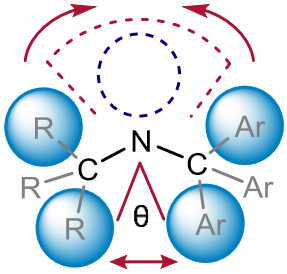


Figure 91: *Molecular structures of tritylamine proligands synthesised in this work, with ellipsoids set at at the 50% probability level; hydrogen atoms are omitted for clarity.*

Out of the plethora of available tertiary carbogenic substituents, trityl groups provide the largest "cone angle", the effect of which is demonstrated in Figure **92** below. As a result of repulsion between adjacent groups, θ increases and thus moves steric bulk closer to the binding site.



Me_3N[300]	110.9	$(Ph_3C)_2O$[301]	128
TrL^{1}H[298]	125.2(4)	$(Ph_3C)_2CH_2$[302]	129
TrL^{2}H	117.71(8)	**TrL**^{5}H	125.75(10)
TrL^{3}H	124.95(10)	**TrL**^{6}H	125.72(9)
TrL^{4}H	126.47(12)	**TrL**^{7}H	120.69(8)

Figure 92: *R'CNHCR angles θ (°) of novel proligands and known congeners.*

Whereas this angle is relatively small in *e.g.* triethylamine, the use of sterically demanding *t*-alkyl groups affords cone angles approaching those of ditrytilic systems, whilst ensuring good hydrocarbon solubility. The effect of steric bulk on cone angles is most noticeable in *s*-alkyl systems such as **TrL**^{2}H and **TrL**^{3}H, where exchanging a Cy group for $CHCy_2$ increases θ by 3°. Steric bulk also affects C_5H_5**C–C**Ph_2**–N** angles, aromatic rings pointing towards the less congested NH have angles of 107-108°, whereas those pointing towards aliphatics bend away at 109-111°.

(ii) Metalation

With the desired compounds in hand, the metalation of a series of proligands was explored with a multitude of reagents (Figure **93**). All numbering below refers to the displayed reaction, from **f** to **o**. **TrL**$_x$H systems proved completely inert towards organoelimination with magnesium alkyls (**i**, **j**) dimethylzinc (**h**) as well as redox transmetalation conditions (**g**). They were equally unreactive towards sodium amalgam (**o**) as well as sodium and potassium hydride (**f**). Reactions with the latter were undertaken in neat thf and with the addition of catalytic amounts of DMSO to overcome potential aggregate formation; neither approach furnished the desired species.[†]

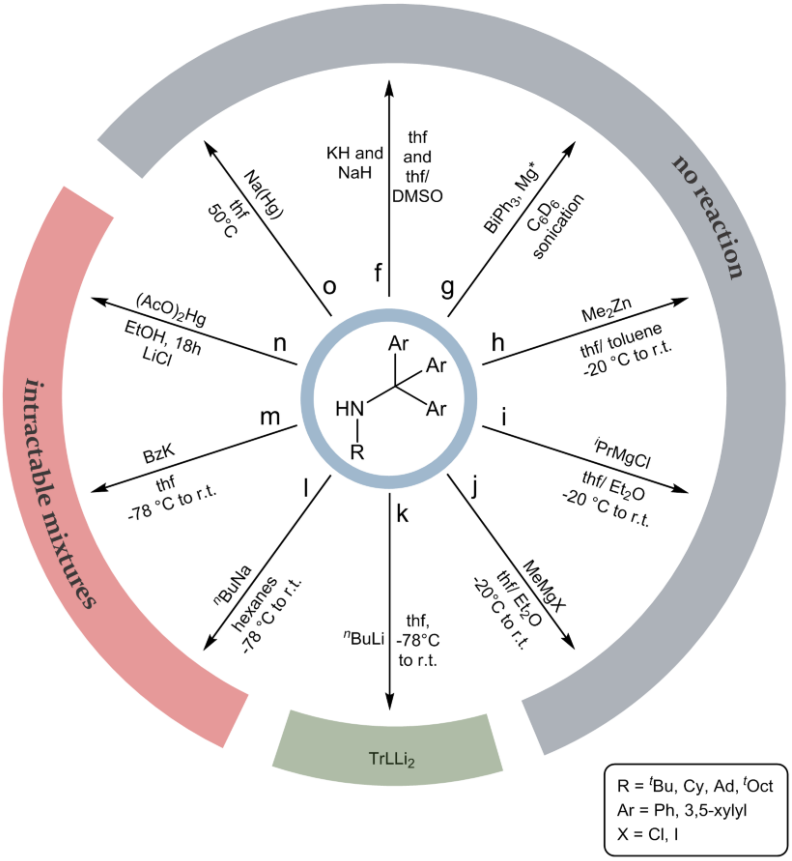
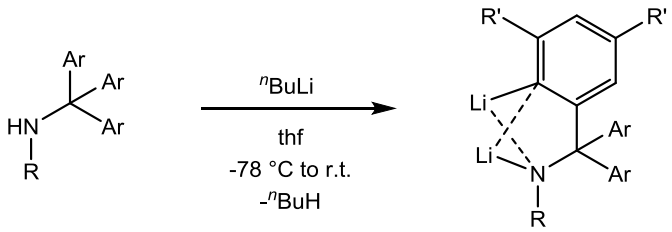


Figure 93: *Work towards* ***TrL****H metalation.*

[†] Although with a pK_a in the region of 35, the methylsulfinylmethylide generated *in situ* may not be sufficiently basic.[483]

Reactions with butylsodium (**l**), benzylpotassium (**m**) and mercury diacetate (**n**) yielded intractable mixtures. The latter was generated *in situ* from ^{t}BuONa and ^{n}BuLi.[303]

Out of the above, only reactions with butyllithium (**k**) afforded well-defined species. With the latter presenting the only recourse in a ligand system otherwise indisposed towards metalation, an array of lithium species were synthesised according to Figure **94**.



[23] TrL^{1}Li$_2$(thf)$_4$ -	R = ^{t}Bu, R' = H, Ar = Ph	91 %
[24] TrL^{2}Li$_2$(thf)$_4$ -	R = Cy, R' = H, Ar = Ph	79 %
[25] TrL^{3}Li$_2$(thf)$_{3.5}$ -	R = Ad, R' = H, Ar = Ph	86 %
[26] TrL^{5}Li$_2$(thf)$_3$ -	R = ^{t}Oct, R' = H, Ar = Ph	86 %
[27] TrL^{6}Li$_2$(thf)$_{2.5}$ -	R = ^{t}Oct, R' = Me, Ar = 3,5-xylyl	28%

Figure 94: *Synthesis of dilithium complexes.*

The lithiation of **TrL**^{l}H and *in situ* use of the obtained species has previously been reported by Corey;[298] however, no characterisation of the proposed lithium *t*-butyltritylamide was undertaken. Evidence collated in this work strongly suggests the formation of a dilithium compound regardless of the quantity of ^{n}BuLi employed (*v.i.* Section **3.3.2**, pg. 137).

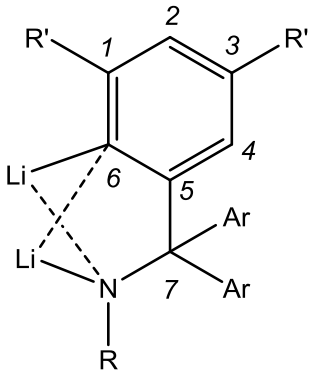


Figure 95: *Numbering scheme for the discussion of NMR spectra, positions refer for adjacent H for ^{1}H, and C for ^{13}C{^{1}H} NMR spectra.*

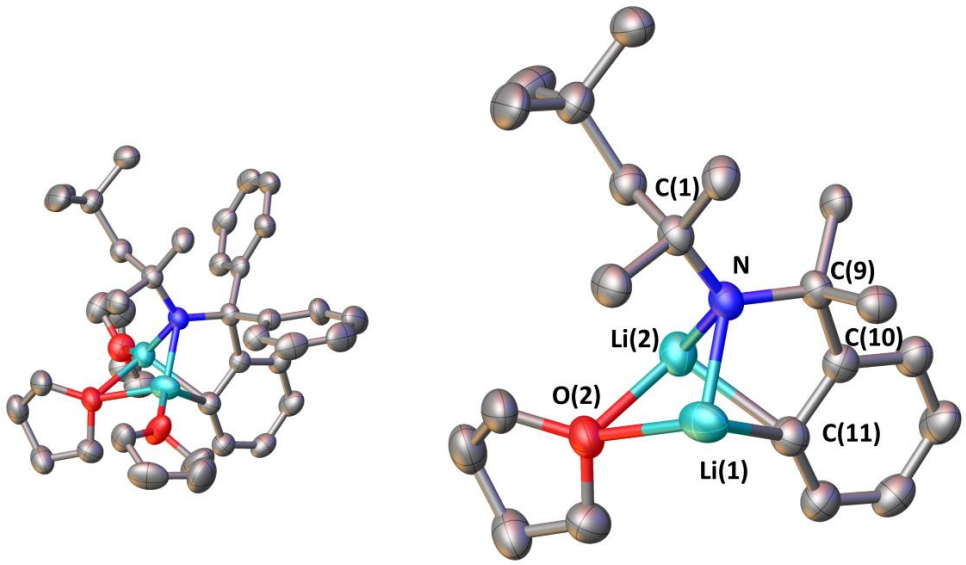
Metalation of **TrL**H proligands results in loss of the N*H* resonance in ^{1}H NMR spectra of **23**-**27**, in *s*-alkylamide **24** previously indistinct multiplicity of the CH_{Cy} signal resolves into a triplet. Integration of resonances assigned to thf indicate a direct effect of steric bulk on coordination number, as the number of bound solvent molecules decreases from **23** to **27** (from 4 to 2.5 solvent molecules). In general, aliphatic signals in the latter were shifted downfield respective to the corresponding proligand; resonances assigned to the lithiated aromatic ring are rendered inequivalent from the remaining two and integrate to 4 (**23**-**16**) or 2 protons (**27**). Whilst resonances of *2* and *3* overlap with *p*-Ar, *1* and *4* stand free of those and are well resolved. *2* displays significant downfield ^{1}H shifts of Δδ 0.6-1.3 ppm upon metalation of the adjacent position in all complexes. Inequivalence brought about by lithiation of one of the tritylic aromatics increases the number of ^{13}C{^{1}H} resonances observed, again, most signals are shifted downfield relative to the proligands, most notably in *7* with Δ δ~8 ppm. A resonance corresponding to *6* could not be observed, presumably due the inherent low intensity of quaternary ^{13}C signals, as well as being bound to a quadrupolar nucleus.

NMR chemical shifts of signals attributed to bound thf were shifted respective to free solvent, ^{1}H $CH_2(CH_2)$ resonances were consistently observed ~δ 0.1 ppm upfield, and $O(CH_2)$ ~δ 0.15 ppm downfield of unbound thf, with no ^{1}H signals corresponding to the latter observed after thorough drying.[304]

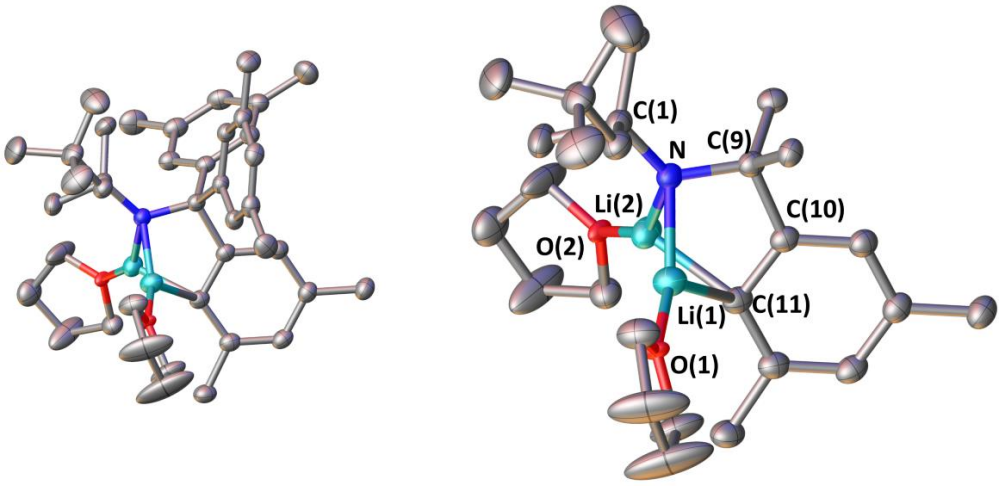
^{7}Li NMR resonances observed were substantially further downfield than those of

LDA, the latter lie in the region of δ = 1 ppm dependent upon solvent and concentration, whereas **TrL***Li*$_2$ signals of **23**-**27** resonated between δ2.8-3.5 ppm. The observed chemical shifts are comparable to those seen in lithium species deaggregated with PMDTA, and start to approach solvent separated ions.[305,306] In low temperature ^{6}Li NMR studies of $(PhLi)_n$, downfield shifts have also been shown to correlate with higher aggregate numbers, *i.e.* more Li atoms in spatial proximity to each other, although $(PhLi)_4$ resonances at δ2.4 ppm† are still upfield of any **TrL***Li*$_2$ signals.[307] ^{7}Li resonances are observed to shift downfield with increasing electron density of the ligand, with the *s*-alkyl, CPh_3 substituted species **24** at δ2.86 ppm, *t*-alkyl CPH_3 complexes **23**, **25** and **26** around δ3 ppm, and **27** displaying the least shielded resonance at δ3.46 ppm.

† $(PhLi)_2$ ^{6}Li resonance at δ1.6 ppm.[307]



[26] TrL^5Li_2



[27] TrL^6Li_2

Figure 96: *Molecular structures of **27** and **28**, with ellipsoids set at at the 50% probability level; non-bonding aryls and bridging thf are omitted for clarity on r.h.s., hydrogen atoms omitted in all.*

Despite persistent attempts, the extremely reactive nature of **23**-**27** only saw the isolation of single crystals suitable for X-ray diffraction for **26** and **27**. Relevant bond lengths and angles are listed in Table **12** below.

The binding geometry around Li presents itself as a heavily distorted tetrahedron in **26**, whereas **27** displays a trigonal planar environment. Li–N distances are comparable to those in the literature,[308] observed Li–C distances are *ca.* 0.1 Å

shorter than those found in the comparable $[Li_2(thf_2)N(C_6H_4)\{Si(NMe_2)_3\}]_2$ complex; **27** in particular displays considerably shorter Li–C contacts than those found in higher level aggregates (typically 2.2-2.3 Å) or even monomeric compounds (<2.2 Å).[306,309] The bridging thf in **26** is considerably closer to Li(2), presumable due to the more polarised nature of the N–Li moiety compared to N–C(11). The Li(1)···Li(2) distance in **27** is 0.235 Å longer than that of **27**, which may be due to the lack of a bridging thf molecule or an increased repulsion between a more strongly polarised metal atom, as indicated by ^{7}Li NMR shifts.

Increased steric bulk around the metal centres in **28** reduces the coordination number to three, although integration of ^{1}H NMR data suggests **28** to exist as a 1:1 mixture of **TrL**^{6}$Li_2(thf)_2$ and **TrL**^{6}$Li_2(thf)_3$.

Table 12: *Selected bond distances (Å) and angles (°) in **27** and **28**.*

26			
Li(1)–N	1.976(6)	Li(2)–N	2.001(6)
Li(1)–C(11)	2.131(7)	Li(2)–C(11)	2.220(7)
Li(1)–O(1)	1.907(7)	Li(2)–O(3)	1.948(6)
Li(1)–O(2)	2.313(8)	Li(2)–O(2)	2.051(6)
	Li(1)···Li(2)	2.255(9)	
Li(1)–O(2)–Li(2)	61.9(2)	Li(1)–N–C(9)	108.6(3)
C(1)–N–C(9)	122.6(2)	Li(2)–N–C(9)	104.0(2)
Li(1)–N–Li(2)	69.1(3)	Li(1)–C(11)–Li(2)	62.4(3)

27			
Li(1)–N	1.970(4)	Li(2)–N	1.975
Li(1)–C(11)	2.117(4)	Li(2)–C(11)	2.095(3)
Li(1)–O(1)	1.914(3)	Li(2)–O(3)	1.928(3)
	Li(1)···Li(2)	2.490(4)	
C(1)–N–C(9)	122.95(13)	Li(1)–N–C(9)	99.56(13)
Li(1)–N–Li(2)	78.26(14)	Li(2)–N–C(9)	101.58(14)
	Li(1)–C(11)–Li(2)	72.47(13)	

The rationale behind the formation of a dilithium complex as opposed to the expected monolithium species even with substoichiometric amounts of ^{n}BuLi is unclear. Whilst molecular dilithium complexes are very rare, in comparable known examples such as $[Li_2(thf_2)N(C_6H_4)\{Si(NMe_2)_3\}]_2$ monolithium complexes are obtained from reacting the corresponding proligands with ^{n}BuLi in a 1:1 ratio.[309–311] The pre-organisation of a putative monolithium species has been implicated in the regioselective outcome of vinylic lithiations,[311] and the agostic interaction between Mg and *o*-Ar observed in a comparable species (*v.s.* Figure **74**, pg. 97) may be considered a precursor to the observed dianion.[234] Whilst conjecture in the absence of an isolable transition state, monolithiation may serve to both weaken an adjacent C–H bond through agostic interactions, as well as further polarise an already electron rich nitrogen. This would then facilitate coordination of the latter to a second ^{n}BuLi equivalent, thereby brought into spatial proximity of the aforementioned CH functionality. An equilibrium between a monolithium and dilithium species at room temperature in non-coordinating solvents appears unlikely, as mixtures of **TrL**H and **TrL**Li_2 in C_6D_6 only showed sharp resonances belonging to either compound, without line broadening or the appearance of new signals.

3.3.2. Experimental

General Procedure for the Synthesis of aliphatic tritylamines

According to modified literature procedure.[298] To a degassed solution of the desired amine and trimethylamine (1.2 - 2 eq.) in chloroform (*ca.* 10 mL per gram of amine) was added dropwise a solution of trityl chloride and the resultant solution stirred at room temperature overnight. The solution was then diluted to *ca.* twice the original volume with dichloromethane, washed with sodium hydroxide solution, brine, followed by drying over magnesium sulfate and

removal of solvent *in vacuo*. Resultant solids were recrystallised from methanol or methanol/ chloroform and dried at 10^{-4} mbar overnight before transfer to the glovebox.

TrL1H

According to literature procedure, ^{1}H NMR spectrum in $CDCl_3$ consistent.[298] (15.55 g, 91%)

^{1}H NMR (C_6D_6, 300 MHz): δ = 0.84 (s, 9 H, (CH_3)$_3$), 1.53 (s, 1 H, N*H*), 6.92 - 7.01 (m, 3 H, *p*-C*H*$_{Ar}$), 7.04 - 7.13 (m, 6 H, *m*-C*H*$_{Ar}$), 7.67 - 7.76 (m, 6 H, *o*-C*H*$_{Ar}$) ppm.

^{13}C{^{1}H} NMR (C_6D_6, 75 MHz): δ = 32.59, 52.94, 70.80, 126.63, 128.12, 130.06, 149.25 ppm.

TrL^{2}H

From $CyNH_2$ (2.13 g, 21.52 mmol) and Ph_3CCl (6.00 g, 21.52 mmol) was obtained the title compound as a white microcrystalline solid (5.60 g, 76%).

^{1}H NMR (C_6D_6, 300 MHz): δ = 0.81 - 1.08 (m, 5 H, CyC*H*$_2$), 1.24 - 1.53 (m, 6 H, CyC*H*$_2$, N*H*), 2.29 - 2.46 (br. m, 1 H, CyC*H*), 7.00 (t, *J*=7.30 Hz, 3 H, *p*-C*H*$_{Ar}$), 7.11 (t, *J*=7.30 Hz, 6 H, *m*-C*H*$_{Ar}$), 7.66 (d, *J*=8.43, Hz, 6 H, *o*-C*H*$_{Ar}$) ppm.

^{13}C{^{1}H} NMR (C_6D_6, 75 MHz): δ = 26.37, 26.69, 36.45, 52.72, 72.14, 126.80, 128.39, 129.53, 148.38 ppm.

$C_{25}H_{27}N$ (341.49): calc'd (%) C 87.93, H 7.97, N 4.10; found (%) C 87.82, H 8.03, N 4.11.

TrL^{3}H

From $AdNH_2$ (2.00 g, 13.22 mmol) and Ph_3CCl (3.69 g, 13.22 mmol) was obtained the title compound as a white microcrystalline solid (4.19 g, 81%).

^{1}H NMR (C_6D_6, 400 MHz): δ = 1.42 (br. s., 12 H, AdC*H*$_2$), 1.49 (s, 1 H, N*H*), 1.77 (br. s., 3 H, AdC*H*), 6.98 (t, *J*=7.30 Hz, 3 H, *p*-C*H*$_{Ar}$), 7.10 (t, *J*=8.20 Hz, 6 H, *m*-C*H*$_{Ar}$), 7.78 (d, *J*=8.47 Hz, 6 H, *o*-C*H*$_{Ar}$) ppm.

^{13}C{^{1}H} NMR (C_6D_6, 101 MHz): δ = 30.05, 36.40, 44.80, 53.37, 69.67, 125.93, 127.36, 129.40, 149.11 ppm.

$C_{29}H_{31}N$ (393.57): calc'd (%) C 88.50, H 7.94, N 3.56; found (%) C 88.49, H 7.94, N 3.58.

Synthesis of (tri-3,5-xylyl)methyl chloride [21]

(i) Through a stirred solution of (3,5-dimethylphenyl)magnesium bromide in thf (0.36 M, 100 ml, 36 mmol) was bubbled carbon dioxide (*ca.* 40 g) for 1 h, temperature was controlled by keeping the reaction vessel in a water bath. The milky suspension was quenched with dilute sulfuric acid, extracted into diethyl ether (3*100 ml) and the combined organics washed with water (3*50 mL), brine (50 ml), dried over magnesium sulfate and volatiles removed *in vacuo* to afford 3,5-dimethylbenzoic acid in quantitative yield.
^{1}H NMR ($CDCl_3$, 300MHz): δ = 2.40 (d, *J*=0.5 Hz, 6 H), 7.26 (s, 1 H), 7.76 (s, 2 H), 12.11 (br. s, 1 H) ppm.
$^{13}C\{^{1}H\}$ NMR ($CDCl_3$, 75MHz): δ = 21.1, 127.9, 129.2, 135.5, 138.1, 172.9 ppm.

(ii) A solution of 3,5-dimethylbenzoic acid (6.00 g, 33.6 mmol) in methanol (100 mL) and sulfuric acid (few drops) was heated to reflux overnight. Volatiles were removed *in vacuo*, the remaining oil taken up in diethyl ether (100 mL), washed with sodium hydrogen carbonate (3*10 mL, 1 M), dried over magnesium sulfate and solvent removed *in vacuo* to afford methyl 3,5-dimethylbenzoate as a light yellow oil (5.15 g, 93%).
^{1}H NMR ($CDCl_3$, 300MHz): δ = 2.38 (s, 6 H), 3.92 (s, 3 H), 7.20 (s, 1 H), 7.67 (s, 2 H), ppm.
$^{13}C\{^{1}H\}$ NMR ($CDCl_3$, 75MHz): δ = 21.1, 52.0, 127.3, 130.0, 134.6, 138.0, 167.5 ppm.

(iii) To a solution of methyl 3,5-dimethylbenzoate (5.15 g, 31.36 mmol) in thf (50 mL) was added (3,5-dimethylphenyl)magnesium bromide (200 mL, 0.36 M in thf), the resulting solution was briefly heated to reflux and subsequently allowed to stir at room temperature over 48 h. The reaction was quenched with dilute sulfuric acid, the majority of ether removed *in vacuo* and the remainder extracted into diethyl ether (100 mL). The aqueous layer was further extracted with diethyl ether (50 mL), the combined organics washed with sodium

hydrogen carbonate (3*20 mL, 1 M) and brine (40 mL) to be dried with magnesium sulfate. Removal of solvent *in vacuo* afforded (tri-3,5-xylyl)methanol as a white powder (9.68 g, 89%).

^{1}H NMR ($CDCl_3$, 300MHz): δ = 2.37 (s, 18 H) 2.82 (s, 1 H), 7.00 (s, 9 H) ppm.

$^{13}C\{^{1}H\}$ NMR ($CDCl_3$, 75MHz): δ = 21.6, 82.0, 125.9, 128.9, 137.2, 147.2 ppm.

(iv) (Tri-3,5-xylyl)methanol (5.30 g, 15.38 mmol) was dissolved in acetyl chloride and the resultant orange solution briefly heated at reflux, then kept at 40 °C overnight. The formed precipitate was filtered off, washed with ice-cold methanol (2*30 mL) and dried *in vacuo* to afford the title compound as a white microcrystalline solid (4.29 g, 77%).

^{1}H NMR ($CDCl_3$, 300MHz): δ = 2.40 (s, 18H), 7.04 (s, 6H), 7.06 (s, 3H) ppm.

$^{13}C\{^{1}H\}$ NMR ($CDCl_3$, 75MHz): δ = 21.40, 82.05, 127.58, 129.29, 136.85, 145.44 ppm.

TrL^4H

From $AdNH_2$ (0.945 g, 6.25 mmol) and 21 (2.27 g, 6.25 mmol) was obtained the title compound as a white powder (2.06 g, 69%).

^{1}H NMR (C_6D_6, 400 MHz): δ = 1.47 (t, J=3.26 Hz, 6 H, AdCHCH2), 1.57 (d, J=3.39 Hz, 6 H, $AdCCH_2$), 1.63 (s, 1H, NH) 1.80 - 1.87 (br. s, 3 H, AdCH), 2.16 (s, 18 H, $ArCH_3$), 6.66 (s, 3 H, p-CHAr), 7.69 (s, 6 H, o-CHAr) ppm.

$^{13}C\{^{1}H\}$ NMR (C_6D_6, 101 MHz): δ = 21.36, 30.20, 36.66, 45.03, 53.47, 69.68, 127.52, 127.62, 136.31, 149.53 ppm.

TrL^5H

From $^{t}OctNH_2$ (16.1 g, 124.57 mmol) and Ph_3CCl (17.36 g, 62.29 mmol) was obtained the title compound as a white microcrystalline solid (19.06 g, 98%).

^{1}H NMR (C_6D_6, 400 MHz): δ = 0.85 (s, 6 H, $C(CH_3)_2$), 1.04 (s, 9 H, $C(CH_3)_3$), 1.45 (s, 2 H, CH_2), 1.88 (s, 1 H, N*H*), 6.97 (t, *J*=7.30 Hz, 3 H, *p*-CH_{Ar}), 7.09 (t, *J*=8.00 Hz, 6 H, *m*-CH_{Ar}), 7.76 (d, *J*=8.47, 6 H, *o*-CH_{Ar}) ppm.

$^{13}C\{^{1}H\}$ NMR (C_6D_6, 101 MHz): δ = 31.00, 32.33, 32.76, 57.76, 60.41, 71.35, 126.62, 128.11, 130.20, 149.58 ppm.

$C_{27}H_{33}N$ (371.56): calc'd (%) C 87.28, H 8.95, N 3.77; found (%) C 87.09, H 8.26, N 2.88.

TrL^6H

From ^{t}OctNH$_2$ (1.53 g, 11.82 mmol) and **21** (4.29 g, 11.82 mmol) was obtained the title compound as a white microcrystalline solid (3.36 g, 67%).

^{1}H NMR ($CDCl_3$, 300 MHz): δ = 0.80 (s, 6 H, C(C*H*$_3$)$_2$), 1.07 (s, 9 H, (C*H*$_3$)$_3$), 1.42 (s, 2 H, C*H*$_2$), 1.74 - 1.80 (s, 1 H, N*H*), 2.30 (s, 18 H, ArC*H*$_3$), 6.81 (br. s, 3 H, *p*-C*H*$_{Ar}$), 7.32 (s, 6 H, *o*-C*H*$_{Ar}$) ppm.

^{13}C{^{1}H} NMR ($CDCl_3$, 75 MHz): δ = 21.60, 30.36, 31.88, 32.24, 57.10, 59.83, 70.34, 127.33, 127.53, 136.26, 148.88 ppm.

Synthesis of Cy_2CHNH_2 [22]

General protocol for ketoximine synthesis adapted from Boudou.[312] A mixture of dicyclohexylmethanone (20.00 g, 0.103 mol), hydroxylamine hydrochloride (8.62 g, 0.124 mol) and sodium acetate trihydrate (16.87 g, 0.124 mol) in water (100 mL) was heated under vigorous stirring to 80 °C overnight. To the biphasic mixture was added dichloromethane (150 mL) and water (50 mL), the separated aqueous phase extracted with further dichloromethane (2*50 mL), and the combined organic layers washed with water (2*30 mL), brine (50 mL), dried over $MgSO_4$ and volatiles removed in vacuo (remaining Cy_2CO by short-path distillation under reduced pressure) to afford the ketoximine as a white solid (19.01 g, 88%, identity ascertained by multinuclear NMR). Dicyclohexylmethanone oxime (10.00 g, 47.7 mmol) was dissolved in thf (50mL), $LiAlH_4$ (5.40 g, 143.3 mmol) added in portions at 0 °C under considerable effervescence, and the resulting mixture allowed to warm to room temperature to be heated to 50 °C overnight. The mixture was cooled to 0 °C and sequentially quenched with water (5 mL), sodium hydroxide (5 mL, 15% aq) and further water (10 mL). To the grey suspension was then added diethyl ether (150 mL) and magnesium sulfate (10 g). Filtration, removal of solvents *in vacuo* and distillation from calcium hydride under reduced pressure afforded the title compound as a colourless oil stored over potassium hydroxide (5.24 g, 56%, 49%

overall).

Analytical data are consistent with the literature.[313]

TrL^{7}H

From **22** (5.24 g, 26.82 mmol) and Ph_3CCl (7.84 g, 26.82 mmol) was obtained the title compound as a faintly yellow crystals (7.56 g, 64%).

^{1}H NMR (C_6D_6, 300 MHz): δ = 0.93 - 1.35 (m, 12 H, CyC*H*$_2$), 1.40 - 1.74 (m, 10 H, CyC*H*$_2$), 1.91 (d, *J*=6.31 Hz, 1 H, NH), 2.13 (d, *J*=6.12 Hz, 1 H, C*H*(Cy_2)), 6.97 - 7.03 (m, 3 H, *p*-C*H*$_{Ar}$), 7.09 - 7.15 (m, 6 H, *m*-C*H*$_{Ar}$), 7.69 (dd, *J*=8.29, 1.04 Hz, 6 H, *o*-C*H*$_{Ar}$) ppm.

^{13}C{^{1}H} NMR (C_6D_6, 75 MHz): δ = 26.93, 27.10, 27.20, 30.60, 30.74, 40.63, 62.32, 71.29, 126.21, 127.73, 129.16, 148.04 ppm.

General Procedure for the lithiation of tritylamines

To a solution of **TrL**$_x$H in thf (~15 mL/g) was added ^{n}BuLi (3 eq.) at -20 °C. Solids, often crystalline, usually formed from the orange solutions within 20 min. The mixture was made up to three times the original volume by addition of pentane, liquids decanted and the remaining solid washed with further pentane, dried *in vacuo* and stored in the glovebox at -30 °C.

Dilithium species were obtained regardless of the quantity and concentration of ^{n}BuLi employed, attempts to isolate monolithium complexes by employing as little as 0.2 *eq.* ^{n}BuLi invariably yielded the former.

All **TrL**i$_2$ complexes are moderately light sensitive and unstable towards storage as solutions in thf or toluene for extended time periods (more than *ca.* 1 day at room temperature), solutions in diethyl ether or benzene show no significant signs of decomposition under absence of light. Solid materials were particularly pyrophoric, even by s-block standards.

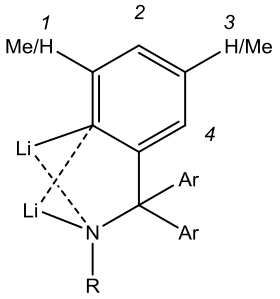


Figure 97: *Numbering scheme for ^{1}H NMR spectra of* ***23-27****.*

[(TrL^1)Li$_2$(thf)$_4$] [23]

From **TrL**^{1}H (5 mL, 0.5 M in hexanes, 2.5 mmol), and ^{n}BuLi (2.5 mL, 2.5 M) was obtained the title compound as yellow crystals (1.51 g, 91%).

^{1}H NMR (C_6D_6, 300 MHz): δ = 1.17 (s, 9 H, (C*H*$_3$)$_3$), 1.28 (dt, *J*=6.64, 3.27 Hz, 16 H, CH$_2$(C*H*$_2$)$_{thf}$), 3.40 (t, *J*=6.50 Hz, 16 H, O(C*H*$_2$)$_{thf}$), 7.01 - 7.29 (m, 8 H, *2,3*-C*H*$_{PhLi}$, *m,p*-C*H*$_{Ph}$), 7.47 - 7.54 (m, 1 H, *4*-C*H*$_{PhLi}$), 7.95 (d, *J*=7.35 Hz, 4 H, *o*-C*H*$_{Ph}$), 8.40 (dd, *J*=5.51, 2.50 Hz, 1 H, *1*-C*H*$_{PhLi}$) ppm.

^{13}C{^{1}H} NMR (C_6D_6, 75 MHz): δ = 25.86, 36.89, 53.60, 68.62, 79.00, 123.21, 125.00, 127.20, 127.44, 129.58, 131.38, 131.92, 141.79, 156.38, 168.05 ppm.

^{7}Li NMR (C_6D_6, 117 MHz) δ = 1.32 (br. s., weak), 2.99 (br. s., major).

[(TrL^2)Li$_2$(thf)$_4$] [24]

From **TrL**^{2}H (0.500 g, 1.46 mmol) and ^{n}BuLi (1.75 mL, 2.5 M) was obtained the title compound as a white powder (0.738 g, 79%).

^{1}H NMR (C_6D_6, 300 MHz): δ = 0.69 - 0.89 (m, 2 H, "*p*"-CyC*H*$_2$), 1.29 (dt, *J*=6.59, 3.20 Hz, 16 H, CH$_2$(C*H*$_2$)$_{thf}$),† 1.55 - 1.82 (m, 5 H), 2.72 (t, *J*=10.31 Hz, 1 H), 3.40 (t, *J*=6.45 Hz, 16 H, O(C*H*$_2$)$_{thf}$), 7.12 (t, *J*=7.1 Hz 2 H, *p*-C*H*$_{Ph}$), 7.17 - 7.30 (m, 6 H, *m*-C*H*$_{Ph}$, *2,3*-C*H*$_{PhLi}$), 7.58 (d, *J*=7.44 Hz, 1 H, *4*-C*H*$_{PhLi}$), 7.77 (d, *J*=7.35 Hz, 4 H, *o*-C*H*$_{Ph}$), 8.33 (d, *J*=4.80 Hz, 1 H, *1*-C*H*$_{PhLi}$) ppm.

^{13}C{^{1}H} NMR (C_6D_6, 75 MHz): δ = 25.46, 67.70, 124.29, 126.82, 130.15 ppm.

^{7}Li NMR (C_6D_6, 117 MHz) δ = 2.86 (br. s.) ppm.

† Overlaps with broad, indistinct multiplet, 1.15-1.40 ppm, CyC*H*$_2$ 18 H total.

[(TrL^3)Li$_2$(thf)$_{3.5}$] [25]

From **TrL**^{3}H (2.00 g, 5.08 mmol) and ^{n}BuLi (6.1 mL, 2.5 M) was obtained the title compound as a pale yellow powder (2.86 g, 86%).

^{1}H NMR (C_6D_6, 300 MHz): δ =1.23 - 1.36 (m, 16 H, $CH_2(CH_2)_{thf}$), 1.61 (br. s., 6 H, AdCCH_2), 1.66 (br. s., 8 H, AdCHCH_2), 2.01 (br. s., 3 H, AdC*H*), 3.47 (t, *J*=6.50 Hz, 16 H, $O(CH_2)_{thf}$), 7.05 - 7.15 (m, 4 H, *p*-CH_{Ar}, *2,3*-CH_{PhLi}), 7.19 - 7.29 (m, 4 H, *m*-CH_{Ph}), 7.50 (d, *J*=7.25 Hz, 1 H, *4*-CH_{PhLi}), 7.98 (d, *J*=7.44 Hz, 4 H, *o*-CH_{Ph}), 8.39 (br. s., 1 H, *1*-CH_{PhLi}) ppm.

^{13}C{^{1}H} NMR (C_6D_6, 75 MHz): δ = 25.92, 31.98, 38.26, 50.24, 54.34, 68.57, 123.40, 125.05, 127.16, 128.25, 128.56, 131.85, 157.06 ppm.

^{7}Li NMR (C_6D_6, 117 MHz) δ = 3.04 (br. s.) ppm.

[(TrL^5)Li$_2$(thf)$_3$] [26]

From **TrL**^{5}H (10 mL, 0.5 M, 5 mmol) and ^{n}BuLi (6 mL, 2.5 M) was obtained the title compound as a pale yellow powder (2.58 g, 86%).

^{1}H NMR (C_6D_6, 300 MHz): δ = 1.00 (s, 9 H, $(CH_3)_3$), 1.25 (s, 6 H, $(CH_3)_2$), 1.28 (dt, *J*=6.76, 3.26 Hz, 12 H, $CH_2(CH_2)_{thf}$), 1.42 (s, 2 H, CH_2), 3.36 - 3.50 (m, 12 H, $O(CH_2)_{thf}$), 7.05 - 7.16 (m, 4 H), 7.19 - 7.29 (m, 4 H, *p*-CH_{Ar}, *2,3*-CH_{PhLi}), 7.42 - 7.48 (m, 1 H, *4*-CH_{PhLi}), 7.94 (d, *J*=7.25 Hz, 4 H, *o*-CH_{Ph}), 8.35 - 8.43 (m, 1 H, *1*-CH_{PhLi}) ppm.

^{13}C{^{1}H} NMR (C_6D_6, 75 MHz): δ = 32.41, 32.95, 34.39, 58.14, 63.77, 68.77, 79.26, 123.01, 124.79, 126.57, 127.08, 129.62, 132.08, 142.01, 156.67 ppm.

^{7}Li NMR (C_6D_6, 117 MHz) δ = 2.98 (br. s.) ppm.

[(TrL^6)Li$_2$(thf)$_{2.5}$] [27]

From **TrL**^{6}H (300 mg, 0.658 mmol) and ^{n}BuLi (0.79 mL, 2.5 M) was obtained the title compound as colourless crystals (120 mg, 28%).

^{1}H NMR (C_6D_6, 300 MHz): δ = 1.06 (s, 9 H, $(CH_3)_3$), 1.24 - 1.30 (m, 10 H, $CH_2(CH_2)_{thf}$), 1.32 (s, 6 H, $(CH_3)_2$), 1.45 (s, 2 H, CH_2), 2.19 (s, 3 H, *3*-CH_3), 2.26 (s, 12 H, ArCH_3), 2.81 (s, 3 H, 1-CH_3), 3.50 - 3.60 (m, 10 H, $O(CH_2)_{thf}$), 6.78 (s, 2 H, *p*-CH_{Ar}), 6.96 (s, 1 H, *4*-CH_{PhLi}), 7.32 (s, 1 H, *2*-CH_{PhLi}), 7.60 (s, 4 H, *o*-CH_{Ph}) ppm.

^{13}C{^{1}H} NMR (C_6D_6, 75 MHz): δ = 22.37, 22.44, 23.06, 25.81, 32.38, 32.98, 34.53,

58.21, 63.52, 68.98, 77.35, 123.54, 126.37, 127.63, 129.65, 135.27, 135.80 ppm.

^{7}Li NMR (C_6D_6, 117 MHz) δ = 3.46 (br. s.) ppm.

3.4. Conclusions and Future Work

The synthesis of benzylanilide and tritylamine proligands as well as their s-block chemistry has been investigated. A facile method for the synthesis of highly sterically congested imines has been identified, providing equal or superior yields to significantly more involved literature procedures. Whilst benzylanilines were found not to be accessible *via* air-stable synthetic methodologies, tritylamines could be synthesised simply and in high yields. This underused proligands family proved a versatile and highly modular class of compounds, allowing for facile steric and electronic tuning.

Whilst metalation attempts of benzylanilines only afforded the single lithium complex **20**, **TrL** ligands were successfully employed in the stabilisation of a series of monomeric heterocoordinate dilithium species **23**-**27**, in **TrL** acted as a sterically demanding, dianionic C,N ligand. Steric congestion imparted by bulky alkyl and tritylic substituents was found to directly affect coordination numbers on the metal, either by direct evidence in the solid state (compounds **26** and **27**) or inferable from **TrL**Li_2-thf ratios. To the best of my knowledge, compounds **23**-**27** constitute the first structurally authenticated examples of non-aggregate, molecular dilithium complexes. Similar species have been employed as catalysts in the Tishchenko reaction,[314] the amidation of aldehydes with amines,[315] as well as in the synthesis of enantiomerically pure compounds.[316] Given the highly polarised and open nature of complexes **23**-**27**, these may prove particularly active in similar transformations, particularly given the close aggregate-activity relationship exhibited by s-block species in general, and organolithiums in particular.[305,306] The potentially fluxional nature of **23**-**27** in solution may be explored by means of variable temperature NMR spectra, particularly for ^{7}Li nuclei.[309]

Avoidance of steric saturation by thf either by synthesis in non-coordinating solvents, or systems of decreased Lewis basicity and increased volatility, may afford an exposed, highly electropositive site in **XIV** (Figure **98** below). The

availability of the latter could then be exploited for the coordination, and thereby activation, of weakly Lewis basic substrates such as aromatics displayed in **XV**. Additionally, **TrL**Li_2 complexes present an expedient starting point for the synthesis of heterobimetallic species, which have attracted considerable interest for synergic metal-hydrogen and metal-halide exchange.[49,317] Comparable Group I species **XVI** may be obtained from the reaction of dilithium complexes with Group I *t*-butoxide under elimination of LiO^tBu, whereas metathesis with RAeX is envisaged as a potential pathway to mixed group heterobimetallics **XVII**.

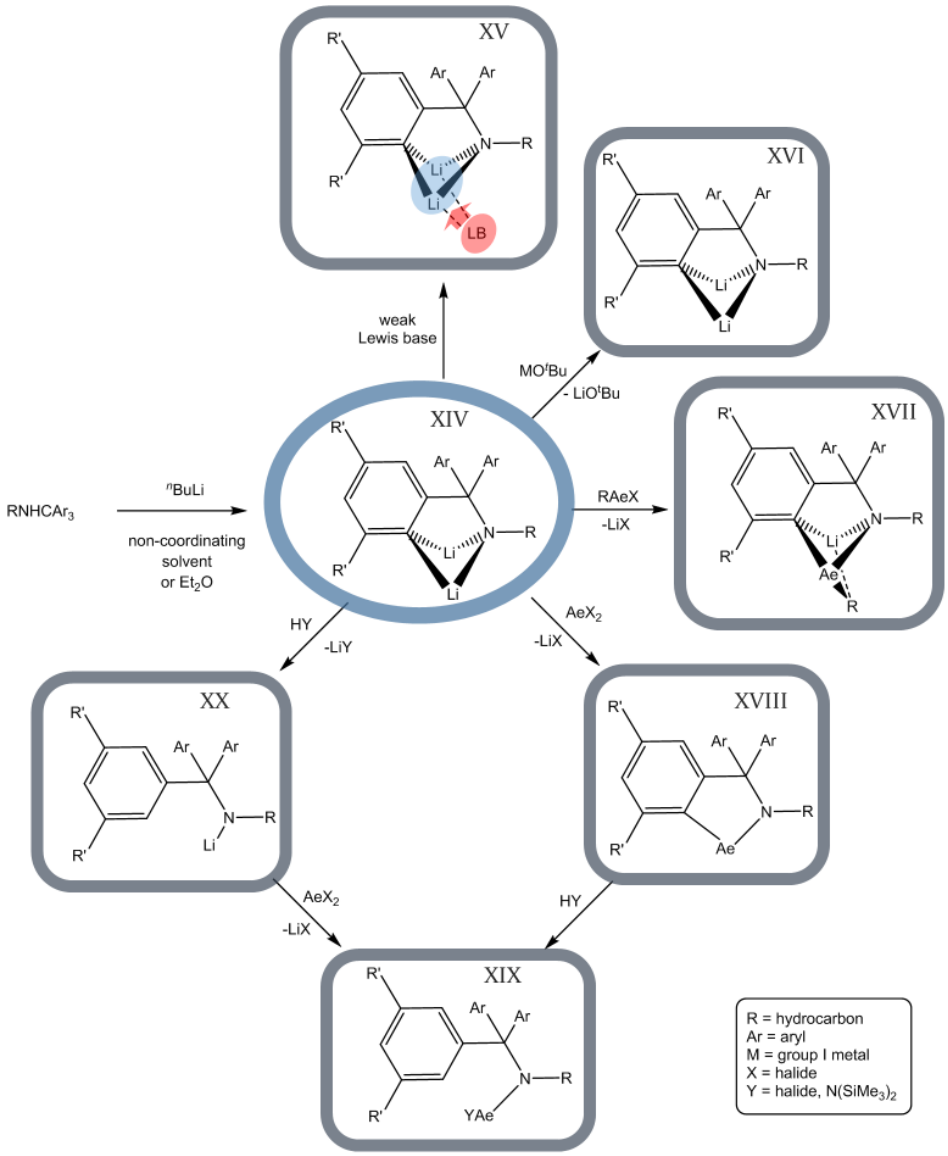


Figure 98: *Synthesis of solvent free* ***TrL****Li_2 and further functionalisation.*

In a similar vein, metathesis between **XIV** and AeX_2 is a plausible route to **XVIII**, completing the list of proposed compounds based on a dianionic framework. It may equally be feasible to obtain the originally envisaged monoanionic framework by selective protonation of **XVII** or **XIV** with HX, *e.g.* in the form of the easily handled triethylamine adduct at low temperatures and concentrations to avoid overprotonation. Equally, a weak acid, such as HMDS, may allow for selective removal of a single lithium to yield **XX**, or the heteroleptic complex **XIX** from **XVII**. Metathesis reactions between **XX** and AeX_2 present another synthetic route to **XIX**. The halide functionality of this would then allow the exploration of further reactivity, such as halide abstraction with $NaBAr^F$ and reduction to form metal-metal bonds, amongst others.

Chapter 4

Catalytic Heterodehydrocoupling of Amine-Boranes: Potential as Energy Carriers

4.1. Introduction

Global energy needs are currently being met primarily by fossil fuels, the extensive consumption of which is unsustainable and incurs serious environmental damage. In light of anthropogenic climate change, there is an immediate need to transition to alternative energy sources. Regardless of the primary source, the storage and transport of energy is a key technological challenge. A prominent emerging solution is the so-called "hydrogen economy". The required hydrogen poses challenges pertaining to storage and transport; amine-boranes (ABs) have emerged as highly promising carrier materials.

This section aims to provide a background of our current energy landscape, an argument for transitioning into a hydrogen economy, and technical aspects thereof. Hydrogen storage methods are discussed with a focus on ABs, with a comprehensive overview of hydrogen release methodologies presented.

This introduction thus provides the framework for experimental work carried out, *i.e.* the catalytic heterodehydrocoupling of dimethylaminoborane, expounded on in Sections **4.2** and **4.3** (pg. 186 and 212, respectively).

4.1.1. Global Energy Dynamics and Factors of Change

The ubiquitous utilisation of fossil fuels drives the engine of our economy, providing the energy to transport goods, propel personal vehicles, and sate an ever growing demand for electricity. They account for 81 % of the World's total primary energy supply as of 2014. Although this represents a 6 % decrease compared to 1973, the total energy demand has more than doubled from 71 PWh to 169 PWh *p.a.* in the same time (255 EJ and 608 EJ respectively).[318] This trend is likely to continue with the industrialisation of developing countries, with a predicted average growth rate of 1.8 % *p.a.* from 2000 to 2030.[319]

Notwithstanding the considerable progress fossil fuels have facilitated, their continued use is undesirable for a plethora of reasons. Despite new reserves being made available by advances in technology and a willingness to incur higher costs in their acquisition, fossil fuels are ultimately a finite resource. At current levels of extraction, proven reserves of coal would be exhausted by 2130, preceded by natural gas and oil by 2070.[320] In addition, reserves are geographically confined, thereby making supply reliant on political, economic and ecological factors. These detrimentally affect energy security and pricing, which is notoriously volatile in the case of crude oil, as depicted in Figure **99**.

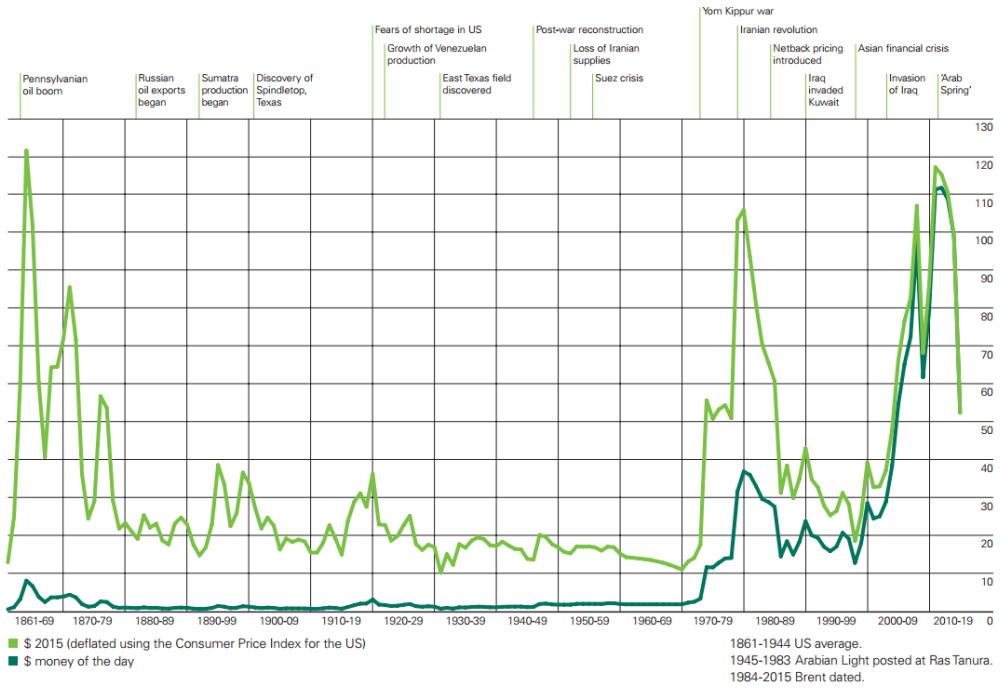


***Figure 99**: Crude oil prices from 1861-2015.*[320]

In addition, the combustion of fossil fuels is concomitant with the release of a variety of greenhouse gases, as well as other pollutants.[321] The release of these has caused widespread environmental and economic damage in the past, *e.g.* in the form of acid rain caused by sulfur dioxide emissions. Recognition of these adverse effects lead to the first international, legally binding treaty "Convention On Long-Range Transboundary Air Pollution" (CLRTAP), which came into force

in 1983, laying the groundwork for a series of further national and international conventions.[322] Whilst these greatly reduced non-carbon emissions, the continued increase of anthropogenic carbon dioxide concentrations lies testament to an unwillingness to transition away from fossil fuels. Despite an increase in sustainable energy production, fossil fuels still dominate worldwide energy production, as shown below (Figure **100**).

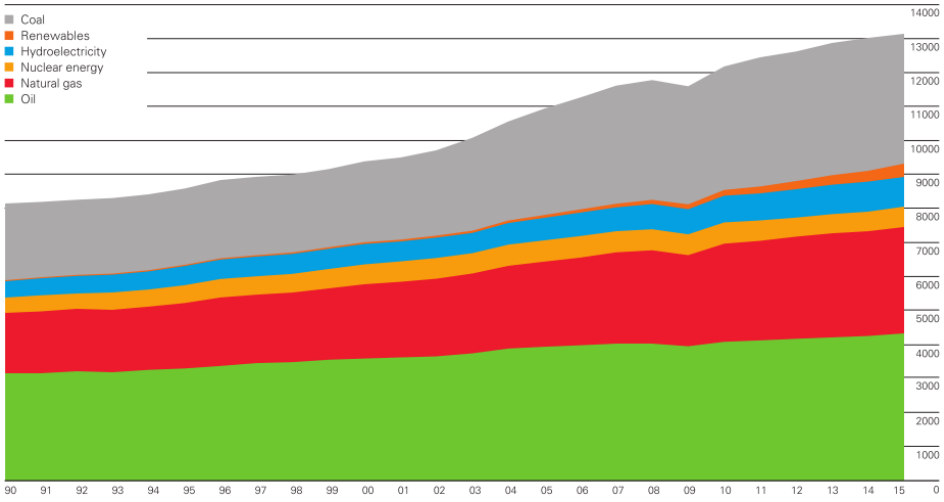


***Figure 100**: Worldwide primary energy consumption in Mtoe equivalents.*[320]

In summary, global energy demand currently depends on a set of rapidly depleting resources, the consumption of which produces compounds detrimental to human health as well as, by consensus of the vast majority of the scientific community, significantly and irreversibly altering the earth's climate. The latter issue can partially be addressed by carbon dioxide sequestration, as reviewed by Figueroa *et al.*[323] Whilst this technology would mitigate environmental impact for stationary application, *e.g.* power plants, it is not applicable to vehicular use.

In contrast to first appearance, this limitation may prove an advantage for transitioning into clean energy. As emission regulations are becoming increasingly strict, car manufacturers are struggling to meet current standards, as exemplified by the recent VW scandal.[324] Any technology reducing the adverse

effects of fossil fuel consumption ultimately only serves to delay the inevitable, *i.e.* a transition into alternative energy sources. Such developments are primarily driven by economic and legislative factors. The financially intensive, and increasingly unfeasible, removal of pollutants from small scale internal combustion (IC) engine applications therefore serve as a good impetus to move away from the *status quo*. This is particularly true for densely populated areas, in which air pollution is a major concern.[325,326] As light duty vehicles accounted for 11 % of global and 20 % of US fossil fuel emissions, respectively, in 2004, such a development would be far from symbolic and could provide critical technological advances for a complete transition to a sustainable energy economy.[327] If mobility and the current road infrastructure are to be retained, connecting vehicles to a continuous supply of energy is undesirable. The alternative is storing energy on board, ideally in the form of a high energy-density carrier system. In the case of automobiles, non-fossil fuel sources currently include battery-electric, biofuels, hydrogen as well as a variety of more exotic and hybrid systems.

Each of the above provides inherent challenges and advantages, very briefly summarised below:

> Battery-powered vehicles are already ubiquitously employed, and their application is a proven concept.[328] However, even the most advanced lithium-based batteries have a poor gravimetric energy density when compared with most other fuel types. In addition, worldwide lithium reserves are not sufficient for global market requirements. The considerable environmental damage caused by lithium mining also stands at odds with "green transport".[329]

> Biofuels are attractive due to their similarity with conventional fuels; they have a high energy density, are easily transported and tolerated either by existing IC engines or only slightly modified versions. This notwithstanding, their

relationship with food security has proven a contentious and complex issue, as reviewed by Bertini *et al.*[330] Their similarity to conventional fuel also extends to pollutants formed by their combustion, although levels are considerably lower.

Hydrogen may be utilised either directly in IC engines, or converted to electricity by means of a fuel cell. The latter process is entirely clean, producing only water and electricity, the former incurs the formation of low levels of NO_x. A high gravimetric energy density of 120 MJ/kg is offset by a relatively poor volumetric energy density of 10 MJ/m^3 at atmospheric pressure (still comparing favourably to Li-ion at 0.0026 MJ/m^3).[331] In contrast to the above, hydrogen is part of a more holistic system which has been described as the "hydrogen economy".

It is noteworthy that the thermodynamic efficiency of converting heat into work is limited by the Carnot cycle; for IC engines this implies a maximum attainable efficiency of *ca.* 30 % and actually lies at about 25 % for hydrogen combustion. In case of electric motors, an efficiency in excess of 90 % is attainable, with fuel cells providing energy at 50 - 60 % efficiency.[332] The latter therefore provides a significantly more attractive target.

4.1.2. The Hydrogen Energy Economy

In summary of the above, transitioning from fossil fuels to a sustainable global energy system is one of the key challenges of the 21st century. Diversification of power production is an increasing trend, as it appears unlikely that any one existing alternative power source has the potential to sate an ever-expanding, enormous global energy demand. However, regardless of their capacity, all sources face the issue of storage and mobility; *i.e.* how to utilise generated electricity for transportation or later use.

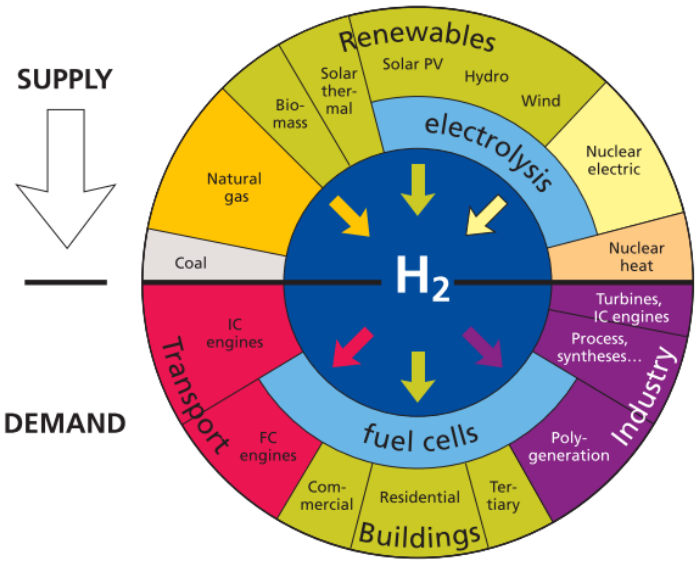


***Figure 101**: Primary energy sources, energy converters and applications.*[319]

Out of a variety of scenarios, the "hydrogen economy" has emerged as a dominant solution. The EU, US and Japan have all provided significant funding towards hydrogen and fuel cell technologies, with hydrogen-propelled busses already being trialled worldwide.[319,333,334] As depicted in Figure **101**, hydrogen acts not as a primary energy source, but an energy carrier. Possible sources include steam methane reforming (SMR), partial oxidation (POX), coal gasification, thermal cracking, biomass gasification and electrolysis. Individual merits and investment costs of these have been reviewed elsewhere.[335–337] Although SMR and POX are currently the most mature technologies, most hydrogen feedstocks are available virtually everywhere, thereby removing reliance on continued supply from potentially unstable regions. An ability to draw on a multitude of sources not only offers significant benefits to national energy security, it also provides economic advantages through a nationally closed system creating local employment.

However, the storage and transportation of hydrogen is inherently more involved than is currently the case for hydrocarbons. This indubitably poses one of the greatest barriers to a hydrogen economy, possible solutions are discussed below.

4.1.3. Hydrogen Storage

The 21st century has seen a considerable increase of interest in addressing the question of hydrogen storage, with an average of about 500 publications *p.a.* containing the term "hydrogen storage" in its title in the past ten years, as seen below (Figure **102**).

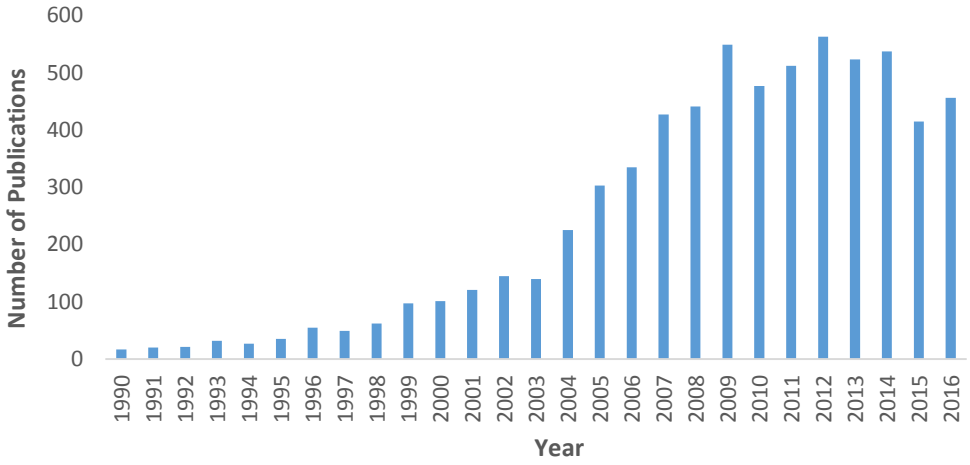


***Figure 102**: Number of publications containing "hydrogen storage" in its title.*[338]

Molecular hydrogen has the highest gravimetric energy density of any chemical fuel at 120 MJ/kg (or 59.4 kJ/mol), compared to 50 MJ/kg for methane and 43 MJ/kg for diesel fuel.[†] Its volumetric energy density, however, is relatively poor. This value varies from 10 MJ/m^3 (gas at 1 atm) to 8500 MJ/m^3 (liquid), compared to 20900 MJ/m^3 for liquid methane and 31400 MJ/m^3 for diesel.[339] This unfavourable property is a result of a strong repulsive interaction between hydrogen molecules, giving rise to a low critical temperature (T_c) of -240 °C. To increase storage density, this repulsion needs to be overcome or mitigated. The former can be achieved either by compression or cooling below T_c, the latter by forming an interaction with another material. This may be in the form of weak dispersive interactions, *i.e.* physisorption, or the formation of considerably

[†] All values stated as lower heating values (LHV) at 25 °C and 1 atm. In contrast to higher heating values (HHV), the former takes into consideration the enthalpy of vaporisation.

stronger chemical associations. Thus, six different storage methods present themselves.

(i) *High Pressure*

High pressure gas cylinders are ubiquitously employed for the storage of a wide variety of gases, commonly at a pressure of 20 MPa. As higher hydrogen pressures require thicker, and therefore heavier, cylinders, the storage systems gravimetric energy density thus decreases with increasing volumetric density, *i.e.* requires a compromise between the two. Pressures of up to 70 MPa are attainable with lightweight, composite cylinders such as shown in Figure **103**, allowing a hydrogen storage density of 36 kg/m^3 and system gravimetric capacities of 4.8 %.[340] A quoted figure of 28 wt % by Laurenczy *et al.* could not be substantiated by any other sources.[341] In addition to factors pertaining to size and weight of the storage medium, the energy required to convert feedstock hydrogen gas into the desired state is an important consideration. For the compression of hydrogen gas from atmospheric pressure to 35 MPa and 70 MPa, the energy costs represents 12 % and 15 % of the LHV, respectively.[342]



***Figure 103**: Composite material hydrogen tank.*[343]

(ii) *Cryogenic Liquid*

Hydrogen may be stored as a liquid in thermally insulated containers at -250 °C and a density of 70.8 kg/m^3, *i.e.* twice that of hydrogen at 70 MPa. This is offset by the weight of an inherently complex storage system as depicted below (Figure **104**), lowering *de facto* energy density. Ideal container parameters stand at odds with mobile applications, ideally being spherical and large. In addition, liquid hydrogen storage necessitates an open system to prevent very large overpressures (*ca.* 1 GPa), resulting in a boil-off in the region of 1.5 % per day. Lastly, liquefaction is an extremely energy-intensive process, requiring 55 MJ/kg of energy (46 % of the LHV).[344] For reference, a study on liquefaction efficiency has been conducted by Baker and Shaner.[345] The existence of two nuclear spin isomers causes further problems, as discussed under General Considerations (pg. 157).

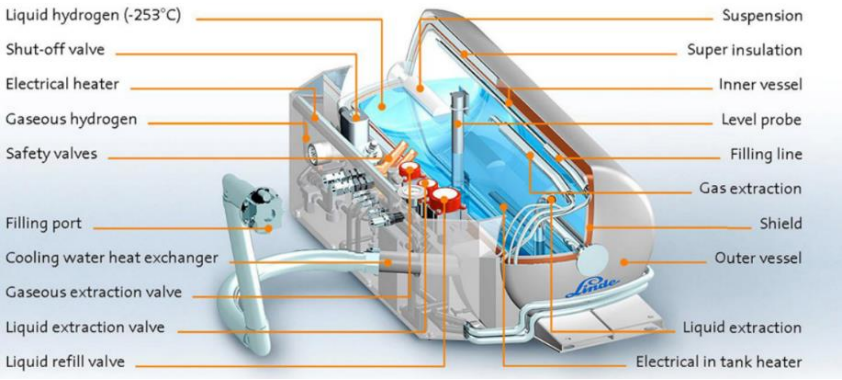


***Figure 104**: Liquid hydrogen storage vessel.*[342]

(iii) *Physisorption*

Hydrogen can be adsorbed onto highly porous materials, where the amount adsorbed is proportional to the surface area provided. As H_2 only provides two electrons, van der Waals interactions tend to be very weak, with isosteric heats of adsorption in the region of 4-7 kJ/mol.[346] Consequently, storage by physisorption requires low temperatures, and hydrogen uptake is usually

measured at -196 °C (77 K). Two classes of materials have emerged as particularly prominent for this application: metal-organic frameworks (MOFs) and carbon nanostructures. Research on the latter in particular has suffered from controversial reports; in one particular case, seemingly outstanding results by Dillon *et al.* could later be attributed to titanium alloy particles by Hirscher *et al.*[347,348] For the purpose of an overview, a survey of carbonaceous and silica-alumina based sorbents has been compiled by Nijkamp *et al.*, and more recently for carbon nanomaterials only by Ströbel *et al.*[349,350] The latter concluded that "the initial euphoria is over and we now have a realistic view of the possibilities for the storage of hydrogen in carbon materials", *i.e.* gravimetric uptakes in the region of 3 %.

Generally speaking, MOFs provide higher hydrogen uptake as reviewed by Long *et al.*; however, syntheses tend to be more involved, certainly for more complex linkers.[346,351] For comparison, the current target of 6.5 wt % H_2 adsorbed, set by the United States Department of Energy for automotive application, has been surpassed by a record 7.1 wt % by the Zn_4O(BDC) MOF (at 40 bar and -196 °C). Verified capacities of carbonaceous materials currently only reach 2.2 wt % for AC Norit 990293.[349,352]

In either case, appreciable hydrogen storage densities at room temperature are unlikely to be achievable.

(iv) *Hydrides for Chemical Storage*

Hydrogen may be stored in the form of a hydride, which can be divided into three categories as displayed in Figure **105**, providing an example of each. General advantages to the abovementioned methods include very high gravimetric capacities, as well as low cost.

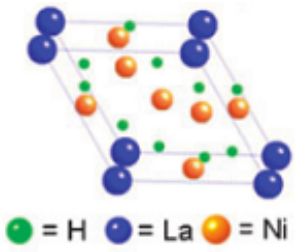
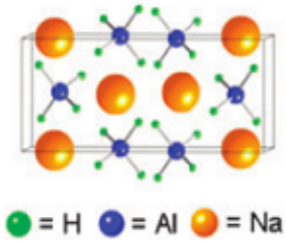
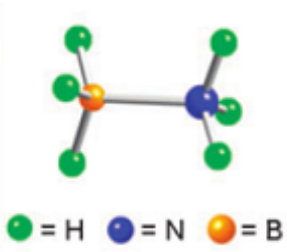
Conventional Hydrides	Complex Hydrides	Chemical Hydrides
$LaNiH_6$	$NaAlH_4$	$NH_3{\cdot}BH_3$
		
Hydrogen forms a metallic bond with the host metal atoms	*Hydrogen covalently bonded as stable "complex" anions*	*Hydrogen covalently bonded in material, utilised as single use "fuel"*

***Figure 105**: Classes of hydrides and examples thereof.*[327]

Conventional hydrides in themselves take the form of interstitial hydrides, such as PdH, and structural hydrides, such as MgH_2, the latter providing a 7.7 wt % H_2 capacity (*i.e.* 9.2 MJ/kg). For either, hydride formation proceeds *via* physisorption to the metal or alloy surface, chemisorption, formation of a solid solution (α-phase, H/M ratio <0.1) and finally formation of the hydride phase (β-phase, H/M ratio ≥1). The last two coexist to varying degrees dependent upon the metal, temperature and pressure.[353] Volume differences between phases cause internal stress at the phase boundary, leading to a phenomenon known as "hydrogen embrittlement", *v.i.* under General Considerations (pg. 157). This may cause complete structural failure within a few cycles, limiting reusability in case of non-powder systems.

Complex hydrides consist of a light cation, usually a Group I or II metal, and a multiatomic anion such as BH_4^-, AlH_4^-, or NH_2^-. High gravimetric and volumetric storage capacities make them an attractive target despite comparatively high ΔH_{des} values, *i.e.* a higher energy input in the form of heat is required to liberate hydrogen. For comparison, $LiBH_4$ provides a theoretical hydrogen content of 18.5 wt % and 120 kg/m^3 (13.9 wt % and 93 kg/m^3 in practice) compared to 7.5 wt % and 49 kg/m^3 for the high-performance MOF-177.[327] Despite these favourable properties, complex hydrides did not present an attractive storage medium due to their supposed irreversibility of hydrogen release, caused by unfavourable reaction thermodynamics. This paradigm was challenged in 1997 with the preparation of Ti-doped $NaAlH_4$, providing reversible hydrogen liberation under moderate conditions.[354] Complex hydrides thus became the focus of renewed interest, with a variety of methods developed to overcome thermodynamic and kinetic barriers; a more detailed overview can be found elsewhere.[340,341,355]

Chemical hydrides investigated for hydrogen storage chiefly consist of ammonia borane (AB) and derivatives thereof; out of all chemical storage media they provide the highest theoretical gravimetric capacity (19.5 wt % for $NH_3{\cdot}BH_3$). As these were the focus of experimental work carried out, chemical hydrides are discussed in detail below (Section **4.1.4**, pg. 158).

(v) *Oxidation of Reactive Metals*

Lastly, the least elegant method remains the oxidation of reactive metals with water, to form the corresponding hydroxide and hydrogen gas. In terms of storage, sodium potentially provides a gravimetric hydrogen density of 3 wt %, assuming water formed in the combustion process is recyclable. A reaction enthalpy of -197 kJ/mol (in the case of sodium) necessitates the management of a large exotherm, and recycling of the formed hydroxide requires very high

temperatures. The viability of such a process, based on zinc as the reactive metal, has been assessed in detail by Steinfeld.[356]

(vi) *General Considerations*

Regardless of the storage medium employed, there are some general considerations in utilising hydrogen as an energy carrier. As a result of its extremely small size, hydrogen may diffuse through materials otherwise considered gas-tight. Conveniently, this property also gives rise to an extremely high buoyancy, which presents an advantage compared to gasoline in case of a leak. Whereas the latter poses a long-term fire hazard due to lateral spreading and low diffusivity, hydrogen disperses rapidly, thereby only presenting a localised hazard.

Despite its non-corrosive nature, hydrogen poses a structural hazard towards many metals. This phenomenon is known as hydrogen embrittlement, and has frequently given rise to catastrophic material failures.[357] The issue is of great importance for industrial applications, as steel is particularly affected due to the high mobility of hydrogen in iron. Consequently, considerable research efforts have been undertaken to address the matter. Despite this, until recently, there existed no physically based mechanism to predict quantitative effects; designing resilient materials largely relied on a trial-and-error approach. This *status quo* was challenged by Song and Curtin in 2012, who have developed a model providing predictions in excellent agreement with experimental results for ferritic materials.[358] Further research building on these findings can be expected to form the basis of a variety of novel materials considerably more resistant to hydrogen embrittlement.

A further unique problem arises for the storage of liquid dihydrogen, owing to its two nuclear spin isomers *o*-H_2 and *p*-H_2. At room temperature, an equilibrated mixture contains 75 % of the former and 25 % of the latter. In contrast, for

hydrogen at its normal boiling point (nbp) this equilibrium lies at 0.2 % *o*-H_2. Liquefaction preserves the original 3:1 ratio; however, the excess of *o*-H_2 is now thermodynamically unstable and will convert to *p*-H_2, albeit rather slowly. This conversion is exothermic with a temperature-dependant heat of conversion, 523 kJ/mol at nbp, exceeding the latent heat of vaporisation of 452 kJ/kg. Thus, equilibration will release heat which can evaporate significant quantities of hydrogen. In practice, this is avoided by catalysing the aforementioned process before transfer to a storage vessel, *e.g.* with highly active charcoal or ferric oxides.[353]

4.1.4. Chemical Hydrides

Out of the abovementioned condensed phases, the boron-nitrogen (BN) family has attracted particular attention due to outstanding gravimetric and volumetric storage capacities. Although boranes, and adducts thereof, are now chiefly investigated for their ability to release hydrogen as a single use fuel and hydroboration, they previously received interest for military applications as a high energy fuel, also known as zip fuel.[359] Despite being ultimately unsuccessful, the cornerstone of boron chemistry had been laid.

Notably, research by Schlesinger *et al.* in the early 1950s spanned from the synthesis of the rather exotic uranium (IV) borohydride, to the preparation of a series of borohydrides by metathesis, and investigation on the effects of transition metal salts on hydrogen release rates from sodium borohydride solutions.[360–363] The latter was ahead of its time, as half a century passed before borohydrides regained attention as hydrogen storage materials.[364–367]

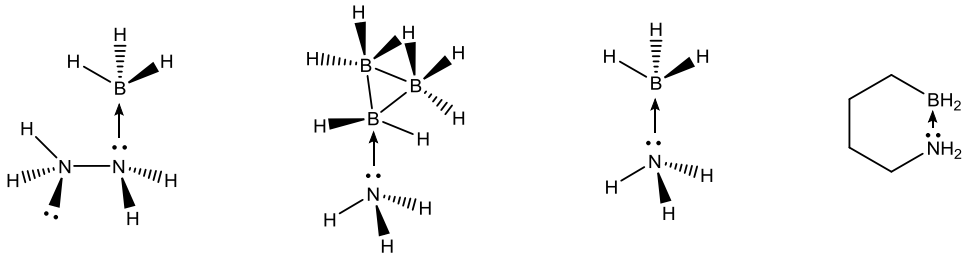


***Figure 106**: BN compounds.*

BN compounds may chiefly be divided into hydrazine boranes, amine triboranes, amine boranes (ABs)†, CBN heterocycles, as well as higher order polyboranes. Examples of the first four are given in Figure **106** (**1**, **2**, **3**, and **4** in the above listed order). An overview can be found elsewhere.[368]

Out of the above, AB and its congeners are emerging as particularly promising candidates.‡ This position was further strengthened in 2007, when an independent DOE report advised against the use of sodium borohydride as a hydrogen source for vehicular application in favour of AB.[369]

AB compares favourably with other storage materials, as it is non-hygroscopic, non-flammable, non-explosive, and has an exceptionally high theoretical gravimetric storage density of 19.4 %. The latter stems from low atomic weights, with A_r values of 14.0 and 10.8 for nitrogen and boron respectively. Relatively facile hydrogen release is rooted in ABs electronic structure, as discussed below.

AB bears multiple protic (N*H*) and hydridic (B*H*) hydrogens, resulting in intermolecular dihydrogen bonds clearly visible in the solid state, and a system

† For the purpose of this text, H_3NBH_3 is referred to as AB, and the family of derived compounds as ABs where grammatically sensible. Should AB refer to the family, it will be evident from context.

‡ A Web of Science™ search, conducted in May 2017 for the time period of 2000-2017, provides a rough comparison of the popularity of BN compounds. A combination of "hydrogen storage" (as Topic) and the following search terms returned (rounded): 1200 papers for "ammonia borane", 70 for "hydrazine borane", 20 for "triborane", 4 for "CBN" and "polyborane", respectively.

that is “set up” for hydrogen release, certainly in comparison to its hydrocarbon congener, ethane.[370] Considering the resonance structures shown below (Figure **107**), the hydrogen polarisation described above may at first appear counterintuitive, and therefore warrants consideration.

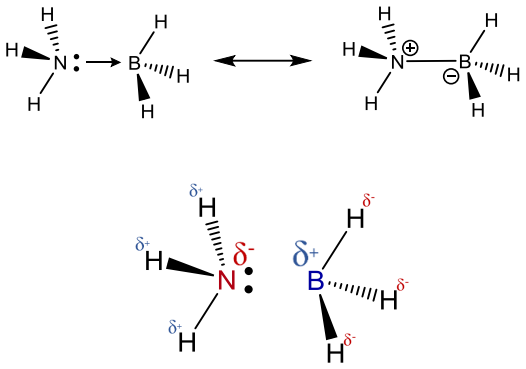


***Figure 107**: AB, resonance and charge distribution.*

At the two ends of the spectrum, AB may be considered as a Lewis acid-base adduct, or as formally bonded, with nitrogen and boron bearing positive and negative charges, respectively. This would imply a δ^- charge on N*H* and δ^+ on B*H*, whilst the reverse is actually the case. Although there is undoubtedly a charge transfer from nitrogen to boron, the dominant effect remains the electronegativity difference from 3.04 to 2.04 (Pauling) for N and B respectively; *viz.*, AB is polarised towards nitrogen which consequently bears protic hydrogens.[371]

Although altering the electronic properties of the system to impart favourable characteristics (such as more facile dehydrogenation) is an obvious avenue to pursue, the results may not be as predictable as one might anticipate, as demonstrated below.

Despite unsubstituted AB providing the highest hydrogen density, other factors such as dehydrogenation enthalpy and physical state of the AB in question, as well as reaction products formed, may make a substituted alternative more

attractive. A variety of substituted AB compounds were investigated by Nöth and Beyer (Table **13**), and evidently physical properties follow no obvious pattern.[372]

***Table 13**: Physical properties of selected amine boranes.*[368,372]

Alkylamine borane	Melting point/°C	Decomp. point/°C
H_3NBH_3	104	~100
H_2MeNBH_3	56	70
H_2EtNBH_3	19	30–40
$H_2{}^{n}PrNBH_3$	45	50–70
$H_2{}^{i}PrNBH_3$	65	90–100
$H_2{}^{n}BuNBH_3$	−48	10–15
$H_2{}^{t}BuNBH_3$	96	120–140
HMe_2NBH_3	37	150
HEt_2NBH_3	−18	200
$H^{n}Pr_2NBH_3$	30	140
$H^{i}Pr_2NBH_3$	23	250
$H^{n}Bu_2NBH_3$	15	120
$H^{i}Bu_2NBH_3$	19	150

One might assume, for example, that increasing the electron density on nitrogen increases the protic character of hydrogens attached, facilitating dihydrogen release. However, the decomposition temperature of diethylamino borane is twice that of unsubstituted AB. Sterics therefore appear to play a significant role, with decomposition temperatures for ^{n}Bu *vs.* ^{t}Bu substituted AB at 10 °C and 120 °C, respectively. This reflects a non-trivial hydrogen release mechanism as discussed in detail below (*v.i.* Section **4.1.5**, pg. 162).

Although seldom the focus of attention, AB substitution also affects physical properties. Most B-substituted ABs are liquids, and although they have thus far not been the centre of a concerted research effort, their liquid state clearly provides distribution advantages compared to their solid, *N*-substituted congeners. The synthesis and properties of such compounds has been reported by Hawthorne *et al.*[373,374]

4.1.5. Principal Feasibility of a Boron Based Energy Carrier

Any energy carrier has to face the ultimate test of feasibility. Beyond gravimetric capacity and recyclability, this extends to resource availability.

Boron is often seen as an abundant element from a researcher's perspective. Its annual production of nearly 1.9 million tonnes in 2012 (based on B_2O_3)†, or 27 Gmol, lies testament to its use in agriculture, ceramics and glass as well as detergents, to name but a few.[375,376] This notwithstanding, boron is a low abundance element.

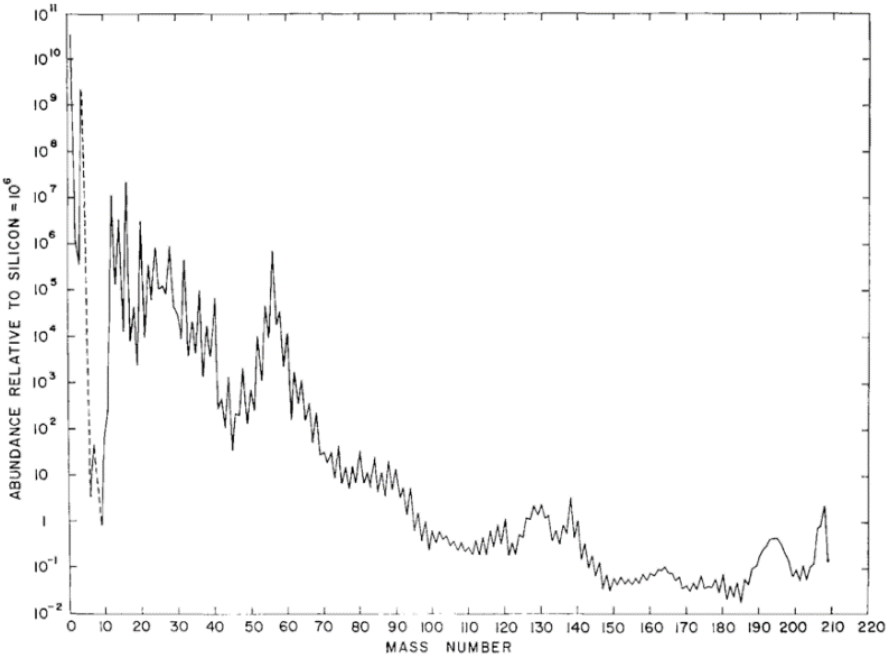


***Figure 108**: Cosmic abundance of the elements.*[377]

† Boron output and reserves are sometimes quoted as their primary minerals. These vary considerably in their boron content, leading to considerable discrepancies in quoted figures. All references herein are made relative to B_2O_3.

The low cosmic abundance of the stable isotopes of lithium, beryllium and boron is one of the most obvious trends visible in Figure **108**.‡ This carries through to terrestrial abundance, with a content of only 9 ppm in the earth's crust, lower than that of lithium (18 ppm) or lead (13 ppm). Boron deposits are highly localised, *i.e.* there is only a small number of commercially viable deposits, but these tend to be extensive in nature. Worldwide reserves are estimated at 380 million tonnes (5.45 Tmol).[378,379] Boron's relatively low abundance may well be the Achilles heel of an AB-based hydrogen economy, as demonstrated below.

As mentioned above (Section **4.1.1**, pg. 145), there is a current global energy demand of 608 EJ *p.a.* Roughly a tenth of this is accounted for by transportation. Given that each mol of boron can realistically be utilised to release 2 mol of H_2 (*v.i.* pg. 165) with an energy density of 120 MJ/kg, one can very crudely estimate the feasibility of an AB-based hydrogen economy by availability of resources (Equation **1**).

$$5.45 \times 10^{12}\ mol \div \left(\frac{60.8 \times 10^{18}\ Jyr^{-1}}{120 \times 10^{3}\ Jg^{-1} \div 2.02\ gmol^{-1}} \div 2 \right) = 5.29 \times 10^{-3} yr$$

***Equation 1**: Duration of potential energy supply by worldwide boron reserves.*

Therefore, the entirety of currently estimated boron reserves have an energy capacity of 322 PJ in the form of AB, which would cover automotive demand for *ca.* 2 days before complete recycling was necessary. To the best of my knowledge, this has not been addressed in any publication to date. It must be highlighted

‡ The scarcity of stable isotopes of the abovementioned elements is rooted in their creation. The vast majority of nuclei were either formed within minutes after the Big Bang, in stellar fusion, or through neutron capture (in order of increasing atomic number); however, this is probably not the case for ^{6}Li, ^{7}Li, ^{9}Be, ^{10}B and ^{11}B. Lithium occupies a non-trivial position better described elsewhere.[484] Beryllium and boron are bypassed entirely in standard thermonuclear synthesis, and their origin is thought to lie in galactic cosmic-ray bombardment, *i.e.* the fragmentation of heavier nuclei in a process known as spallation.[485,486] This is assuming an isotropic universe immediately after the Big Bang, an anisotropic concentration of protons and neutrons opens another avenue to the genesis of light elements as described by Croswell.[487]

that this is an extremely crude calculation, and critically does not take into account boron demands for any other industry.
An often overlooked factor are the economic implications of increased boron demand. Rendering boron a high-demand, low-abundance resource would lead to a considerable price increase, exerting financial pressure on a hypothetical AB-based hydrogen economy.

Thus, AB cannot be the sole energy source of vehicular transport. Analogous to a prospectively facetted energy production landscape, it appears likely that multiple energy carriers will replace fossil fuel derived products. This notwithstanding, AB has the potential to play a key role in the hydrogen economy given efficient recycling of spent fuel. Aforementioned storage characteristics give AB an edge over pressurised or liquefied H_2, particularly for applications in which space and weight come at a premium (*e.g.* small personal vehicles).

In conclusion, AB is a key puzzle piece of future transport; time and technological advances will reveal the entire picture. Looking beyond storage capacity, the challenge of hydrogen release from AB becomes apparent. This addresses release rates, product distribution, and possible recycling directly tied to thermodynamic considerations. All of the above are discussed in the forthcoming Sections.

4.1.6. Thermal Dihydrogen Release from Amine-Boranes

Hydrogen may be released from ABs by solvolysis (most commonly hydrolysis), thermolysis, or by action of a catalyst. The first generates borates, the recycling of which is difficult due to the formation of very strong B–O bonds (ΔH_f = 806 kJ/mol; *v.i.* Section **4.1.9**, pg. 183).[218] These methods have been the focus of concerted research efforts described elsewhere.[380,381] Whilst thermolysis is

outlined below, focus will be given to catalytic dehydrocoupling, in line with experimental work carried out (*v.i.* Sections **4.1.7**, pg. 168).

Comprehensive reviews of hydrogen release methods have been compiled by Staubitz *et al.,* and more recently by Paul *et al.*[382,383]

(i) AB Thermolysis in the Solid State

Out of all hydrogen release mechanisms, thermolysis stands out in its seeming simplicity. On closer investigation, this process is not entirely trivial, with implications for products formed as well as decomposition temperatures.

Reaction rates and products formed by dehydrogenation upon heating were found to be highly dependent upon N/B substitution (*v.s.* Table **13**, pg. 161) as well as reaction conditions. Out of the AB family, the decomposition of ammonia-borane is doubtlessly the most investigated one, and is detailed below. The release of hydrogen occurs in three stages:

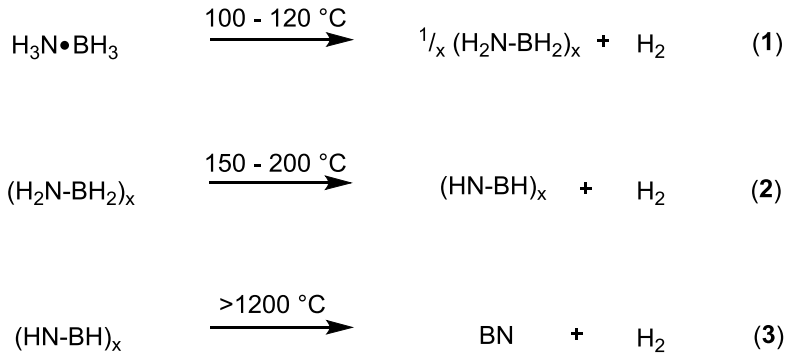


***Figure 109**: Generalised AB thermolysis and hydrogen loss onset temperatures in the solid state.*

From Figure **109**, it is apparent that steps (**1**) and (**2**) occur at feasible temperatures, whereas (**3**) not only occurs at very high temperatures, but also produces highly inert boron nitride. For the purpose of practical application,

gravimetric storage potential is therefore two thirds of the commonly quoted 19.5 %.†

Processes (**2**), and (**1**) in particular, have been investigated in detail. Solid state dehydrogenation temperatures have been shown to exhibit a considerable dependency on heating rates. Slow heating rates generally resulted in a lower onset of (**1**), *e.g.* as low as 82 °C for a rate of 0.05 °C/min, where previous investigations had determined decomposition to start at 120 °C at 5 °C/min.[384,385] At 60 °C, the half-life of AB is in the order of weeks. Products formed tend to be non-uniform, and their characterisation challenging.

The understanding of AB solid state thermolysis was considerably expanded upon by solid state ^{11}B and $^{11}B\{^{1}H\}$ MAS NMR by Autrey *et al.*, optical microscopy and high temperature X-ray diffraction by Bowden *et al.*, as well as emission thermophotometry by Wendlandt and Geanangel.[386–388]

(ii) AB Thermolysis in Solution

Thermal AB decomposition has also been studied in solution; Shaw and Autrey employed *in situ* multinuclear NMR, notably finding that decomposition followed second order kinetics in respect to AB.[389] Hydrogen release rates were therefore highly concentration dependant. In addition, observed species allowed for the postulation of a decomposition pathway as described below (Figure **110**). It has been noted that the mechanism stands at odds with the second order kinetics described in the same paper.[382] Borane, formed by AB dissociation, may also act as a Lewis acid catalyst, a factor not considered in the proposed mechanism.

† Figure **109** is a generalisation, different release methods can give rise to a cross-linked BN material liberating *e.g.* 2.5 eq. H_2, *v.i.* Section **4.1.7(i)**, pg. 25).

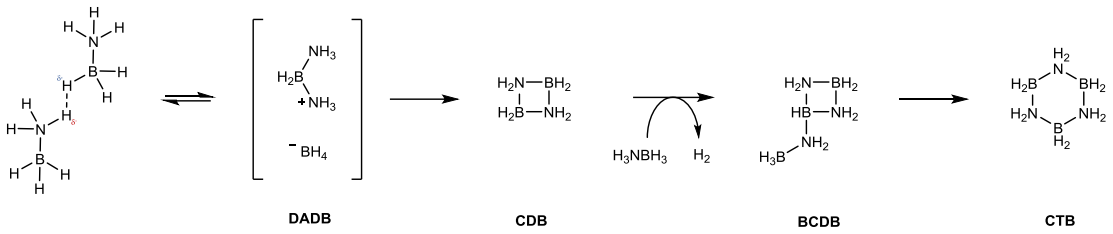


***Figure 110**: Decomposition pathway of AB as postulated by Audrey and Shaw.*[389]

The abovementioned concentration-dependence was later investigated by Mertens *at al.* by ^{11}B NMR spectroscopy; in summary, decomposition pathways appear to vary significantly with AB concentration.[390] The relative amounts of both DADB and BCDB were found to increase at high [AB]. Artificially increasing [DADB] resulted in yet a higher [BCDB]. Given the relation between DADB and BCDB, as well as the fact that no DADB was detected below 1.5 M [AB], the mechanism postulated by Audrey and Shaw was concluded to be an unlikely contributor at high concentrations.

Although Autrey and Mertens employed different solvents in their studies (dimethoxyethane and triethylene glycol dimethyl ether, respectively), both are glycol ethers and may be considered sufficiently similar to allow for quantitative comparison between the two publications.

It is evident from the above that AB dehydrocoupling is non-trivial, with rates and likely decomposition pathways dependent upon a multitude of factors. The control of hydrogen release rates, as well as products formed, remains an ambitious prospect of considerable importance; borazine, for example, is particularly undesirable, as it poisons fuel cells.[382] Thus, the indiscriminate nature of thermolysis renders AB dehydrogenation a challenge better addressed by the employment of catalysts (*v.i.* Section ***4.1.7***).

4.1.7. Catalytic Heterodehydrocoupling of ABs: Across the Periodic Table

The catalytic dehydrocoupling of main group compounds is an elegant method for obtaining E–E or E–E' bonds. Aside from applications in organic synthesis and materials chemistry, concomitant release of hydrogen renders this process a viable method of energy storage.†

The most ubiquitous catalysts employed for AB dehydrogenation are based on transition metals (TM). Although first reported with 5th period precious metals, base metals have recently gained ground. Section **(i)** discusses the genesis of these TM catalysts, from beginnings to contemporary advances.

Notwithstanding the prevalence of TM catalysts, main group systems have more than demonstrated their suitability for AB dehydrocoupling. These provide an extremely diverse panorama, from organic acids to s-block silyl amides as summarised in Sections **(ii)** and **(iii)**. The variety of systems shown to be active may partially be explained by the small difference in B–H and N–H bond enthalpies (389 kJ/mol and 386 kJ/mol, respectively); *i.e.,* there is equal merit in weakening one or the other to effect hydrogen release.

Mechanistic details of the above are an intense field of ongoing research, an area so substantial it has been reviewed by Waterman in 2013.[391]

(i) d-Block

The first dehydrocoupling of ABs by a TM catalyst reported in the open literature dates back to 2001 by Manners *et al.*†[392] Contrary to later investigations, efforts

† The below is focused on dehydrocoupling for the purpose of hydrogen storage, for information on main group element bond formation, recent reviews by Manners *et al.* and Melen present a good starting point.[488,489]

† Preceded by a patent by Laine and Blum in 1989, describing the use of $Ru_3(CO)_{12}$ at 60 °C.[490] Manners *et al.* employed Rh^{I}, Rh^{III} and less active Ir^{I} precatalysts at 5 - 0.5 mol% to convert a series of ABs into their cyclic hydrogen depleted congeners at timescales of 24 - 72h at 45 °C.

were initially focused on catalytic main group (E–E) bond formation, to supplement or replace classical reactions such as salt metathesis. Despite the original aim of synthesising novel AB-derived oligomers and polymers, attention quickly shifted to hydrogen release as the potential of AB as a carrier material became apparent.

The performance of the above was surpassed, with considerable margin, by an iridium pincer complex five years later (**1**, Figure **III**).[393] Originally employed for transfer dehydrogenation by Brookhart *et al.*, Goldberg *et al.* found [Ir(POCOP)H_2] (POCOP = μ^3-1,3-(OP^{t}Bu$_2$)$_2$$C_6H_3$) to liberate one equivalent (eq.) of hydrogen from AB at 0.5 mol% in 14 min at room temperature.[394] In contrast to Manners Rh system, the iridium catalyst was found to stay intact, *i.e.* no metal aggregate was formed and added mercury did not inhibit catalytic activity.[395]

Hydrogen release is concomitant with the formation of a black solution and precipitate. Later investigations suggested the formation of a Rh^0 colloid.[368]

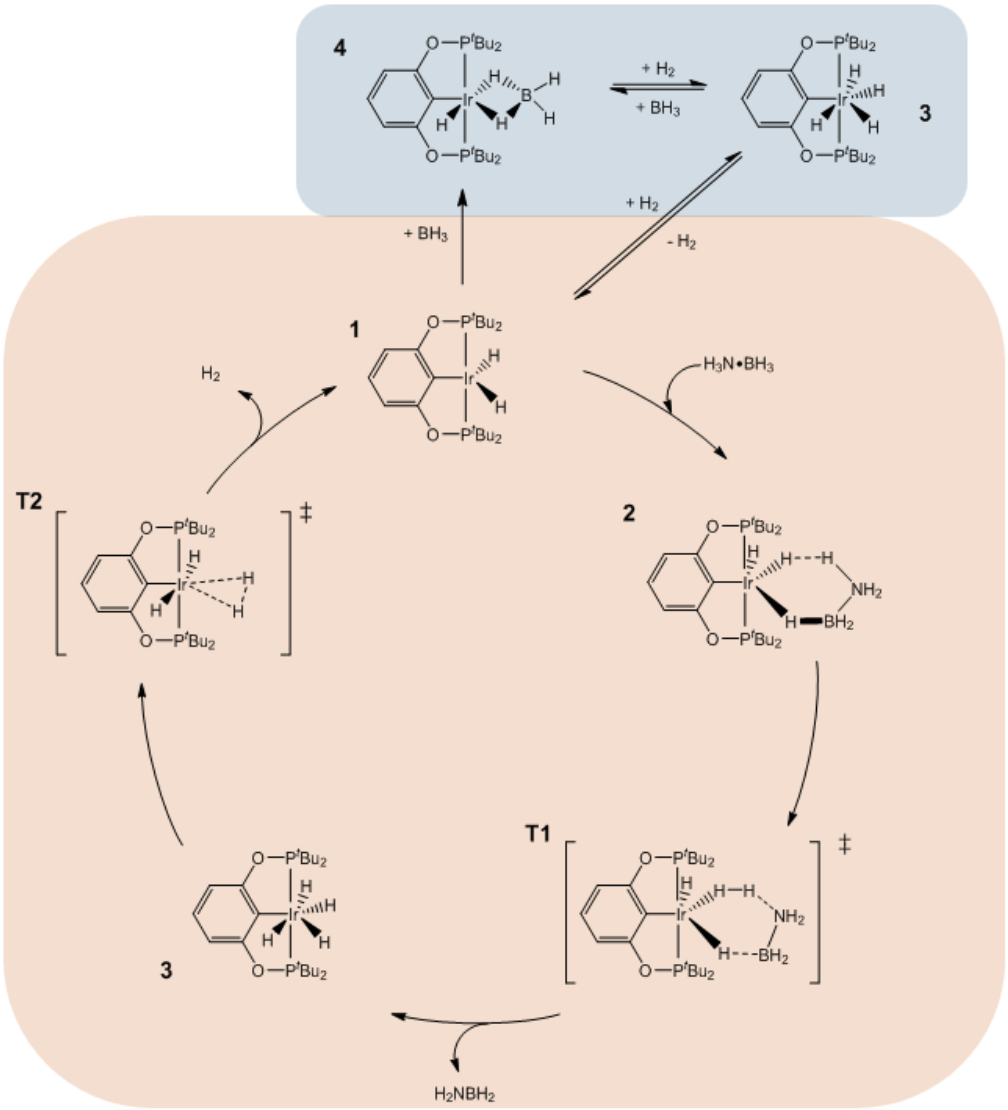


***Figure 111**: Theoretically proposed Ir(POCOP)H_2 catalytic cycle (red) and experimentally observed deactivation (blue).*[393,396]

The employed catalyst **1** (Figure **111**, blue section) was found to transform into **4** over time, from which **1** could be regenerated by passing H_2 through the solution (proceeds *via* the formation of **3**). Aiming to delineate mechanistic details of AB dehydrogenation by Ir(POCOP)H_2, Paul and Musgrave carried out DFT calculations to arrive at the catalytic cycle shown above (Figure **111**, red section). A competing catalytic cycle, based on a 14-electron iridium species, was concluded to be implausible at room temperature. It was postulated that H_2NBH_2 (aminoborane, AOB) is released by a concerted proton and hydride transfer (**T1**), followed by hydrogen release from tetrahydride complex **3** *via* **T2**.

It has to be noted that **1** only appears capable of releasing a single equivalent of H_2 from AB; this has been attributed to steric crowding around the catalytic centre.[382]

These advances notwithstanding, the use of precious metals is undesirable due to their scarcity and hence high cost; homogeneous base-metal catalysts present a more attractive target. The first application of the above in an AB dehydrogenation was reported by Manners *et al.* in the same year as the above iridium-based system, 2006.[397] The active catalyst is presumed to be a Ti^{II} species, formed in situ from Cp_2TiCl_2 and $^{n}BuLi$ as shown below (Figure **112**). The electron deficient nature of Ti^{II} is likely the driving factor behind its activity, particularly considering the inactivity of Ti^{IV} towards catalysing dehydrocoupling. In contrast to Manners previous Rh system, the below was found to be a heterogeneous catalyst.

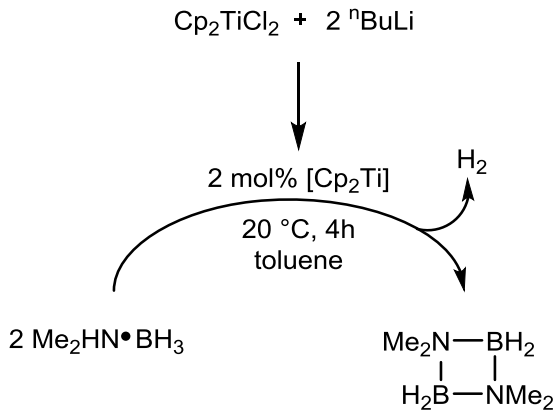


***Figure 112**: Ti^{II} catalysed dehydrocoupling.[397]*

However, hydrogen release was only investigated for Me_2AB and $^{i}Pr_2AB$, both followed by ^{11}B NMR; Manners makes no mention of unsubstituted AB.

The first dehydrocoupling of the latter, by a homogeneous base metal catalyst, was published in early 2007.[398] Baker *et al.* set out to provide a stable, cost-effective system. Given the propensity of strong donor ligands to promote B–H bond activation, three Ni^0-NHC systems were investigated, all generated in situ from $Ni(cod)_2$ and 2 equivalents of the selected carbene. Out of the these, the

nickel complex of Ender's NHC was found to be the most active, with a release of 2.5 eq. of H_2 at 1 mol% catalyst concentration and 60 °C.[399] Notably, both Ru and Rh-NHC complexes showed poorer performances. A kinetic isotope effect (KIE) of 2.3 and 1.7 was observed for ND_3BH_3 and NH_3BD_3, respectively. ND_3BD_3 exhibited a KIE of 3.0, implying that the rate determining step(s) involve the breaking of both an N–H and B–H bond.

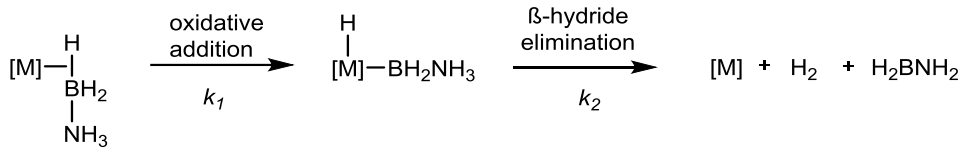


***Figure 113**: Proposed initial steps of $Ni(NHC)_2$ catalysed AB dehydrocoupling.*[398]

It was postulated that the first dehydrogenation step proceeds by initial σ-complex formation, B–H bond activation, and β-hydride elimination (Figure **113**). Given the KIEs, k_1 and k_2 can be assumed to exhibit competitive rates.
Baker *et al.* therefore provided two important milestones on the road to AB as a hydrogen source: An inexpensive catalyst, and the release of nearly all hydrogen available from AB.

As depicted above, the beginning of the 21st century saw the development of robust AB dehydrogenation catalysts, capable of releasing varying amounts of hydrogen, as well as first studies aimed at delineating catalytic cycles. The last ten years or so saw a considerable expansion of all the above aspects, the breadth of which defies description here. The reader is referred to three expansive reviews, recently compiled by Manners *et al.*, Rossin and Peruzzini, as well as Paul *et al.*[382,383,400] A brief summary of recent developments is given below.

Considerable advances towards elucidating mechanistic details were made by Baker *et al.*; employing cyclohexene as a trapping reagent for free AOB revealed significant differences between Rh, Ni and Fe catalysed systems. It has been suggested that the release of more than one equivalent of hydrogen is linked to

the presence of free AOB, an important step towards rational catalyst design.[401,402]

5th and 6th row based catalysts continue to be investigated, *e.g.* Ru by the groups of Fagnu and Schneider; the latter reported a Ru-PNP complex capable of releasing 0.8 eq. of H_2 from AB at room temperature and 0.01 mol% catalyst loading.[403,404] Williams *et al.* demonstrated the ability of Shvo's catalyst (Figure **114**) to release 2 eq. of H_2 from AB at 70 °C with the addition of catalytic amounts of ethanol. To the best of my knowledge, this is the first Ru catalyst to extract over 1 eq. of H_2 from AB.[405]

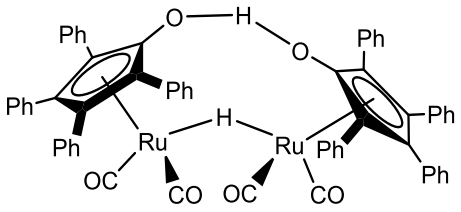


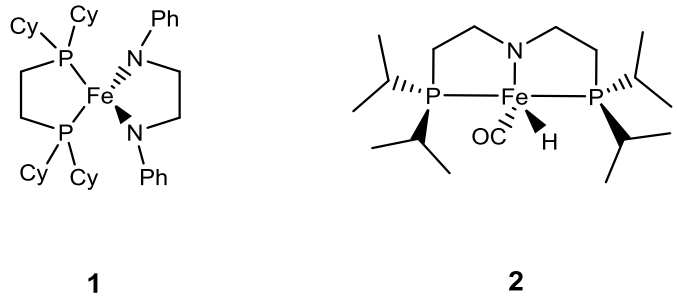
***Figure 114**: Shvo's catalyst as employed by Williams et al.*[405]

Recent examples of Os and Rh hydride catalysts have been reported by the group of Esteruelas.[406,407]

The above advances notwithstanding, base metals present a more attractive target from a sustainability perspective. Given the intrinsic link between this and AB as a future energy carrier, concerns over environmental aspects and resource availability (*v.s.* Section **4.1.5**, pg. 162) extend to catalysts employed in hydrogen release.

Thus, the aforementioned Ti catalysis was significantly expanded upon by the same group, finding that catalyst activity decreased on descending Group IV and with increased steric bulk on the ligand. Further evidence for an active Ti^{II}

species was unearthed.[408†] The first series of Fe-based catalysts were published in 2012 by Baker *et al.*, with **1** (*v.i.* Figure **115**) capable of releasing 1 eq. of H_2 at 60°C and 2 mol% within 2h.[409] A considerably more active Fe catalyst was subsequently reported by Schneider *et al.*, liberating 1 eq. of H_2 at room temperature and 0.5 mol% within 8h (**2**).



1 **2**

***Figure 115**: Fe precatalysts as employed by Baker (**1**) and Schneider (**2**).*[409,410]

A Co^{I} hydride catalyst employed by Lin and Peters further expanded the base metal palette.[411] Initially investigated with a focus on transfer hydrogenation, it was very recently superseded by a significantly more active system.[412]
The abovementioned review by Rossin and Peruzzini gives an excellent overview organised by chemical group.[400]

Although base metals catalysts have been shown to exhibit lower activity than their precious metal counterparts, they are certainly gaining ground. The fine tuning of steric bulk and electronic environment has brought about significant advances, rendering them a competitive option; particularly in light of their lower cost.

† Although Manners *et al.* have suggested the involvement of a Ti^{III} species in the catalytic cylce, the same publication concluded that "The lack of reactivity of [...] Ia and Ib with either Ti^{III} or Ti^{0} species supports the presence of a catalytically active Ti^{II} complex.".[408] However, a Ti^{III} moiety is both part of the catalyst and present throughout the catalytic cycle in some Ti-phosphinearyloxide FLPs, as demonstrated by EPR.[420]

(ii) p-Block

The above section lies testament to the pervasiveness of TMs in AB dehydrogenation. Whilst base metals have economic benefits, their use still poses challenges. Catalysts thereof are frequently air sensitive, their use is also likely to impede the recycling of spent material in the hydrazine process (*v.i.* Section **4.1.9**, pg. 184).[413] This notwithstanding, metal-free systems are still relatively rare. These can be divided into three categories: acid catalysed, base-catalysed and frustrated Lewis pairs (FLP). Some Group XIII complexes also show activity, and a mechanism similar to TM catalysts as described elsewhere.[414,415]

Given the hydridic nature of B–*H*, strong acids can effect protonolysis, leading to the loss of dihydrogen. This has been investigated for Brønsted acids such as trifluoromethanesulfonic acid (TfOH), as well as Lewis acids.[413] Wegner *et al.* found 9,10-dichlorodiboraneanthracene (**1**, Figure **116**) to be an exceptionally active example of the latter.[416] Remarkably, **1** was shown to be capable of releasing 2.46 eq. of H_2 from AB at 5 mol% and 60 °C in 7h. The studied bis(borane) also proved robust, no loss of activity was observed within 15 cycles (even without removal of any formed products).

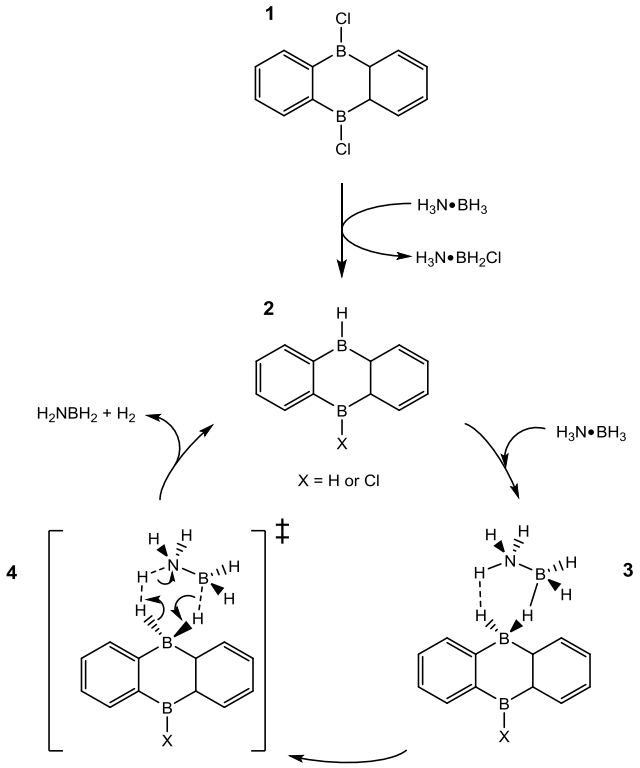


***Figure 116**: AB dehydrocoupling by a bis(borane).*[416]

The proposed dehydrogenation mechanism involves a chloride-hydrogen exchange between **1** and AB (catalyst activation), followed by coordination of a further equivalent of AB to give **3**. A concerted dehydrogenation (**4**) liberates hydrogen with concomitant formation of AOB, recovering the active catalyst **2**.

Analogous to acids, AB dehydrocoupling can be initiated with strong bases. The addition of strong bases, such as LiH or $LiNH_2$, only effects the release of 1.5 eq. of hydrogen, whereas strong non-nucleophilic bases such as bis(dimethylamino)naphthalene have been shown capable of releasing over 2 eq., also avoiding borohydride formation.[367,417] Deprotonation of AB yields the $[H_2NBH_3]^-$ anion, which then initiates dehydropolymerisation in the solid state and ionic liquids.

Finally, the role of free NHC in dehydrogenation (*cf.* [398]), and their similarity to FLPs, has given rise to an investigation of the latter for the purpose of AB dehydrocoupling.[418] Regrettably, most FLPs form stable FLP-H_2 systems, thereby deactivating the catalyst (*i.e.* reactions are stoichiometric). This has been overcome with FLPs featuring electrophilic TM centres such as Zr^{IV} and the abovementioned Ti^{III} (*v.s.* footnote pg. 1).[419,420] Although the Zr^{IV} complex investigated by Wass *et al.* is exceptionally active towards Me_2NHBH_3,† it performs poorly with AB as the substrate. These are, of course, no longer metal-free dehydrocoupling catalysts, and cannot formally be assigned to either d- or p-block catalysis in their own right.

(iii) s-Block

Homogeneous Group I and II catalysis in solution is currently one of the least explored avenues to AB dehydrocoupling. Their use is driven by considerations of cost, and inherently low toxicity (barring Be). A_r values of the lighter congeners are around a tenth of some of the precious metals mentioned above, an important factor given the issue of gravimetric capacity.

Currently, the strongest link between the s-block and a hydrogen economy is the proposed use of its hydrides and amides as storage materials (*v.s.* **(iv)**, pg. 154). The first association with ABs in particular was formed in the late 2000s; efforts towards "destabilised" AB were undertaken both physically by ball milling with MgH_2, and chemically in the form AB's calcium salt $[Ca(NH_2BH_3)_2(thf)_n]$.[421,422] Although providing lower hydrogen release temperatures, dehydrocoupling of these solid state systems remains mechanistically ambiguous. The latter is a considerable drawback, given that mechanistic understanding paves the way to rational catalyst design. In line with work carried out, the below therefore focuses on solvated species.

† 1 eq. H_2 released after 10 min at room temperature and 1 mol% catalyst loading[419]

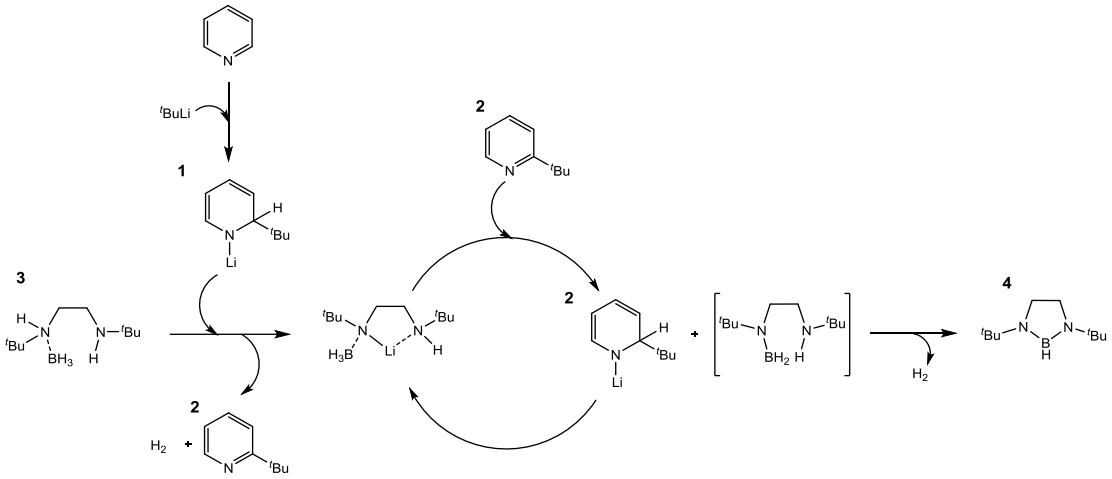


***Figure 117**: Soluble "LiH" catalysed diamine borane cyclisation.*[423]

Reports of s-block catalysed, heterogeneous AB dehydrocoupling in solution is predominantly confined to Group II complexes, with notable exceptions reported by the groups of Hill.[†], Panda and, very recently, Mulvey (*v.s.* Figure **117**).[423–425] The latter reported an elegant cyclisation of diamine boranes, previously achieved with a ruthenium catalyst. The easily accessible, hydrocarbon soluble, "LiH carrier" **1** effects the cyclisation of diaminoborane adducts, such as **3,** to obtain the corresponding diazaborolidine (**4**, all Figure **117**) in high yields.

Both Ae catalysis in general, and Ae-catalysed dehydrocoupling in particular, are expounded on above (*v.s.* Section 1.4.2, pg. 27).

[†]Bellham, Hill and Köhn investigated the propensity of Group I bis(trimethylsilyl)amides to catalyse Me_2HNBH_3 dehydrocoupling. Reaction times were long (124 h) even at elevated temperatures (80 °C) and yielded a mixture of products.

4.1.8. The Thermodynamics of Dehydrogenation and Reversibility

The thermodynamics of any hydrogen releasing reaction fundamentally dictates the suitability of a carrier material for storage applications. This section aims to provide a ground-up perspective on thermodynamic background and its implications for dehydrogenation.

Whilst not a necessity, a reversible medium is desirable. For the purpose of a chemical reaction, a system that is reversible under reasonable conditions will have a low free energy difference between the initial and final state, *i.e.* starting materials and products respectively. Thus, ΔG should roughly equal 0. This results in an equilibrium sensitive to temperature and concentration, which may be exploited to drive the reaction either way.

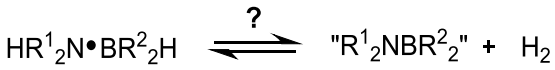


***Figure 118**: AB dehydrogenation.*

As is clear from Figure **118**, there is an entropic drive for AB dehydrogenation, *i.e.* ΔS will have a positive value. In addition, gaseous hydrogen is constantly removed, further driving the equilibrium.

$$\Delta \mathbf{G} = \Delta \mathbf{H} - \mathbf{T}\Delta \mathbf{S}$$

***Equation 2**: Gibbs free energy, enthalpy and entropy.*

Given that ΔG should ≈0 and ΔS will have a positive value, a moderately endothermic ΔH_{des} is required for a system reversible under desirable conditions (*cf.* Equation **2**).

Whilst an enormous variety of catalysts have been investigated for their propensity to increase dehydrogenation reaction rates, considerably less focus has been given to determining an AB system with desirable thermodynamic parameters.[400] These have been examined experimentally by the groups of Wendlandt and Wolf, employing differential scanning calorimetry and thermogravimetric measurements, respectively.[384,426] This lay the foundation for detailed computational studies by Dixon *et al.*, which concluded that the release of the first equivalent of hydrogen from AB is thermoneutral, *i.e.* potentially reversible. However, this is not the case for the remaining two equivalents.[427]

The above research was not aimed towards determining a reversible system, but rather to increase our understanding of AB dehydrogenation in general. To the best of my knowledge, the first concerted effort towards determining a reversible AB system was undertaken by Manners *et al*. in 2008. In brief summary, computational studies determined that reversible hydrogen removal may be possible for some amine-borane adducts. Thermodynamic parameters for such systems appeared to be governed by the strength of dative bonds, both in starting materials and products; electron-donating groups on nitrogen and electron-withdrawing groups on boron, respectively, were found to be favourable. In addition, steric strain differences between products and starting materials materialized as a further contributor.[428] It has been remarked that the complex nature of AB decomposition, as well as differences between computational studies (*e.g.* DFT *vs. ab initio*), make a comparison between individual reports very difficult, if not impossible.[382]

All considerations above focus purely on a chemical reaction, and assume constant pressure and temperature. A more engineering-based approach, equally rooted in thermodynamics, is to consider whether the supplied pressure of hydrogen is sufficient to drive *e.g.* a fuel cell. Heat requirements for desorption also determine whether on-board application is realistic. Thus it is important to acknowledge the equilibrium between gas phase hydrogen and the condensed

phase as given by the van't Hoff equation below (Equation **3**). P_{H_2} is the equilibrium pressure, and P_0 a reference pressure, normally 1 atm.

$$P_{H_2} = P_0^{(\frac{-\Delta H}{RT}+\frac{\Delta S}{R})}$$

***Equation 3**: Van't Hoff equation.*

Applying the 2009 DOE target for hydrogen fuel cell pressures of 0.3 MPa, vehicle operating constraints can be translated to thermodynamic reaction parameters. Thus, an ideal ΔH_{des} at a typical operating temperature of 80 °C lies at around 20-30 kJ/mol, as described in detail elsewhere.[327]

4.1.9. AB Recycling

A major factor determining the viability of any hydrogen storage system is its recyclability. This is a given for physisorbed hydrogen, but much less so for chemically bonded systems, the thermodynamic side of which has been discussed above (Section **4.1.8**). Ideally, an AB recycling process would utilise molecular hydrogen, and not rely on the use of any other stoichiometric reagents. Such a system has been outlined by Mertens *et al.* (Figure **119**), and although holding true to a "closed loop", it describes an enormously energy intensive set of processes.[429]

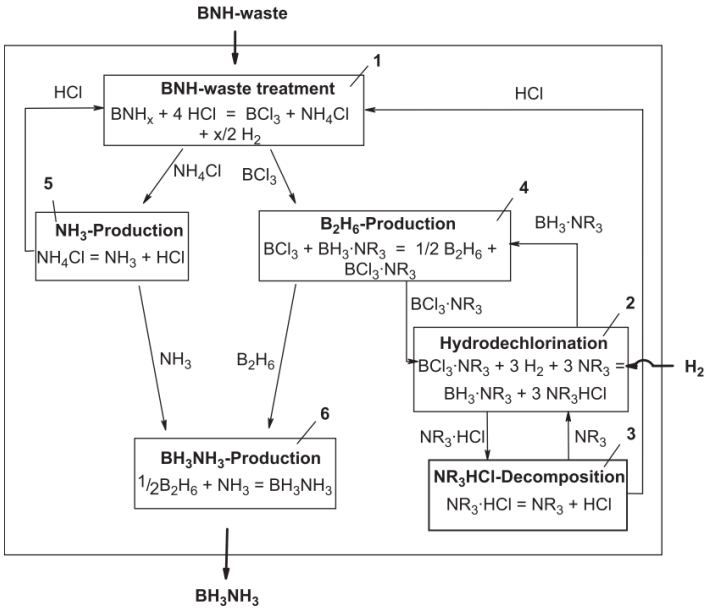


***Figure 119**: AB regeneration according to Mertens et al.*[429]

In summary, whilst steps such as the digestion of spent AB to a corresponding boron halide (**1**) is reasonably facile, BX_3 hydrodehalogenation (**2**) remain a very challenging prospect. This either requires the use of very high temperatures (600 – 750 °C), or the employment of hydride reagents.[430] These include sodium borohydride, tributyltin hydride or organosilanes. However, this does not truly address the issue of recycling, merely moving the problematic step further down the line to generating the abovementioned reagents.[429] Again, none of the above can be directly hydrogenated with molecular H_2, all leading back to the generation of sodium hydride. This is synthesised from the elements at 250 °C to 300 °C.[431] Although such conditions appear more favourable than direct hydrodehalogenation, the generation of metallic sodium is highly energy intensive in itself.

A later publication improved on the above process by lowering energy requirements, this employed an HCl/ $AlCl_3$/ CS_2 system for spent fuel digestion and Ni_3B as a hydrogenation catalyst.[432]

The above and other promising avenues of pursuit have been summarised by Huang and Autrey, as well as Staubitz *et al.*[382,433] These can principally be divided

into regenerating either borate esters formed by solvolysis, or species not containing B–O bonds such as those formed in thermal decomposition of AB. Efforts on the former have been focused on matching the hydride affinity of a boron ester to the hydride donor ability of transition metal hydrides, and despite the considerable strength of B–O bonds, these species are not a thermodynamical dead end.[434,435] However, generally speaking, these processes still suffer from low efficiencies or merely shift the thermodynamical burden onto a different species, such as $LiAl(OMe_4)$, the recycling of which has not yet been realised.[436] Out of the thus far published regeneration protocols, two fundamentally different approaches stand out, remarkably both published by Sutton *et al.*

The first process utilises a tin reagent for hydride transfer, from which *o*-benzenedithiol and tributyltin chloride, respectively, are recovered by digestion in ethereal HCl. The latter is transformed back to the hydride by formylation, followed by thermal decarboxylation.[437,438] Although not mentioned in the original paper, the carbon dioxide generated may be hydrogenated, *e.g.* employing $RuCl_2(PTA)_4$, to generate formic acid. This creates a "closed loop", with the latter part shown in blue on Figure **120** below.[439]

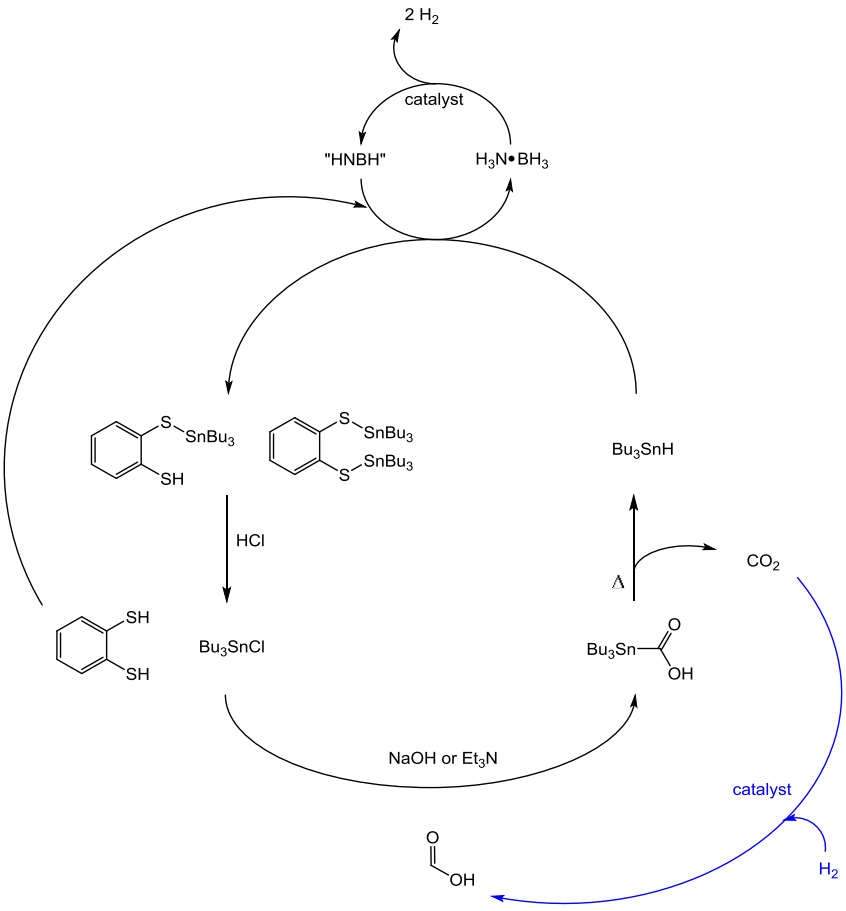


***Figure 120**: AB regeneration with tin thiolate and CO_2 recycling.*[437,439]

Despite its elegance, the above process is highly complex and involves a multitude of steps, thereby reducing overall efficiency. The same group reported a remarkably simple AB regeneration procedure in 2011, only one year after the benzenedithiol protocol. This employs hydrazine in ammonia, and proceeds at 40 °C with an overall yield of 95%, notably in the absence of any catalyst as displayed below (Figure **121**).[440]

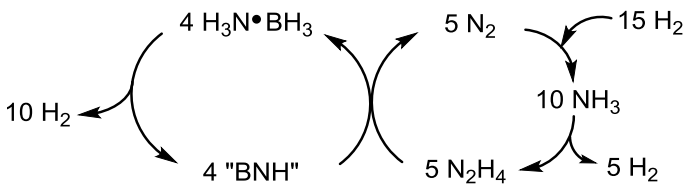


***Figure 121**: Ideal AB regeneration with hydrazine.*[440]

Hydrazine production is without a doubt the key bottleneck for the implementation of such a system. Direct synthesis of hydrazine from nitrogen and hydrogen is not thermodynamically feasible, and its productions is predominantly realised in the Olin Raschig process from NaOH, Cl_2 and NH_3.[441]

The number of promising approaches developed for AB dehydrogenation lie testament to its importance. The merit of individual approaches now needs to be determined by on basis of economic desirability, as well as applicability for large-scale, industrial application.

4.2. Results and Discussion

4.2.1. Initial Investigations on Catalytic Dehydrocoupling

A series of novel complexes synthesised (*v.s.* **Chapter 2**) were investigated for their ability to act as precatalysts in the dehydrocoupling of $Me_2NH{\bullet}BH_3$. By far the best performance was observed in employing complex **4** (*v.s.* Section **2.1.1(ii)**, pg. 54), which showed complete conversion of $Me_2NH{\bullet}BH_3$ to the dimeric dehydrocoupling product $[Me_2NBH_2]_2$ at 60 °C, with concomitant formation of very small amounts of other coupling products (*v.i.* Figure **126** & Table **14**). The structurally similar complex **11** showed no activity whatsoever under analogous reaction conditions (Figure **122**).

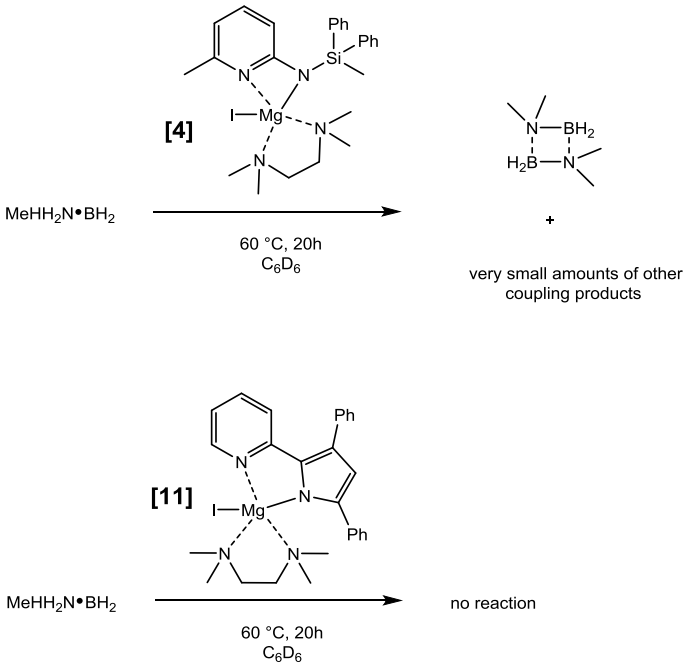


***Figure 122**: Initial investigation of **4** and **11** as dehydroupling catalysts.*

Conversion was monitored by ^{1}H and ^{11}B NMR spectroscopies. **4** proved robust towards both elevated temperature in general, and dehydrocoupling conditions

in particular. Figure **123** shows a typical ^{1}H NMR spectrum for the experiments undertaken (**1-3** and **9-11**, Table **18**).

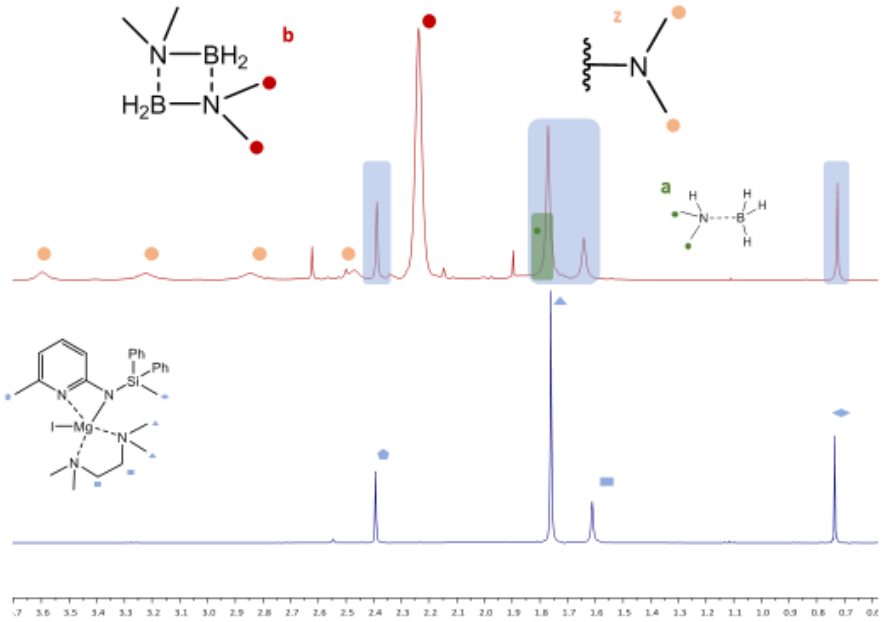


***Figure 123**: Aliphatic region of **4** (bottom) of catalytic dehydrocoupling experiment, after 6h at 60 °C (entry **1**, Table **18**; 20% catalyst loading).*

As visible from the blue regions, **4** remains unaffected. This is equally true for lower catalyst loadings, a representative 20 mol% loading was chosen for clarity of scale. Hydridic protons were too broad for observation; however, the integration of amine-borane methyl groups provide good indicators of reaction progress. Whilst **b** stands clear of other signals, the starting material's $Me_2NH{\bullet}BH_3$ (**a**, shown in green) overlaps with H_3C-tmeda. This was corrected for by subtracting the latter from the overall integration (known by relative ratio of the uncongested H_2C-tmeda). Signals **z** (Figure **123**) do not correlate to starting material, and can be assumed to originate from other dehydrocoupling products. The identity of those are more conveniently assigned by ^{11}B NMR (see below).

Although plotting progress by ^{1}H NMR is certainly feasible, ^{11}B spectra provide a less cluttered outlook. The triplet visible slightly upfield from the dimeric dehydrocoupled dimer **b** (Figure **124**) is discussed in Section **4.2.3**.

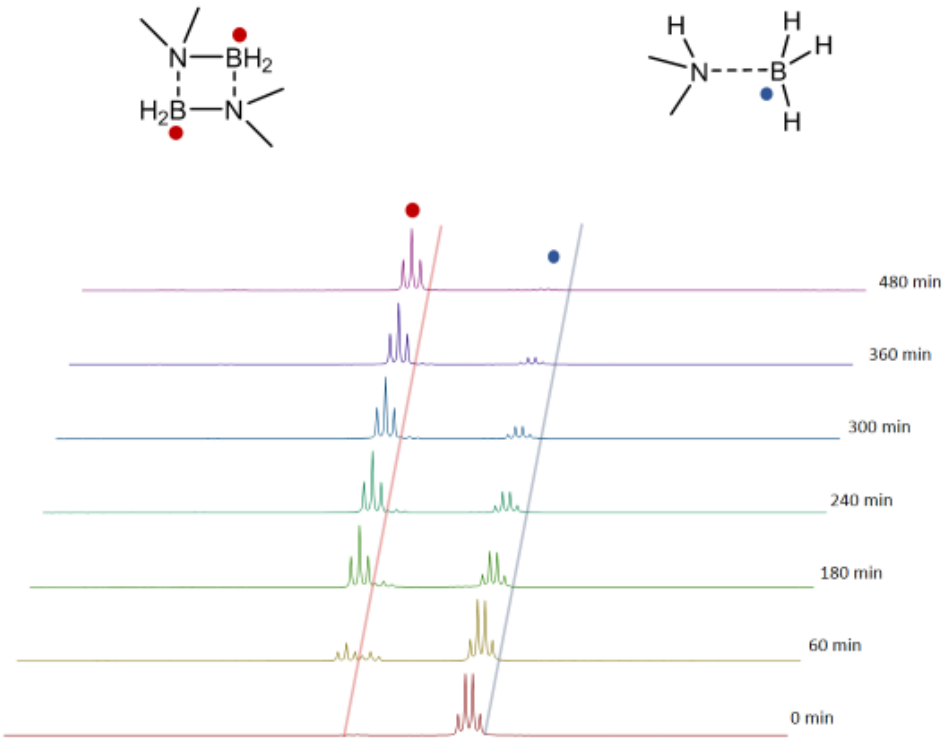


Figure 124: Reaction progress by ^{11}B NMR; entry 2, Table 18 (spectra offset by 10°).

The validity of ^{11}B integration ratios was ascertained by comparison to conversion by ^{1}H NMR, as displayed in Figure **125**. Consequently, data listed below were obtained by integration of ^{11}B NMR spectra.

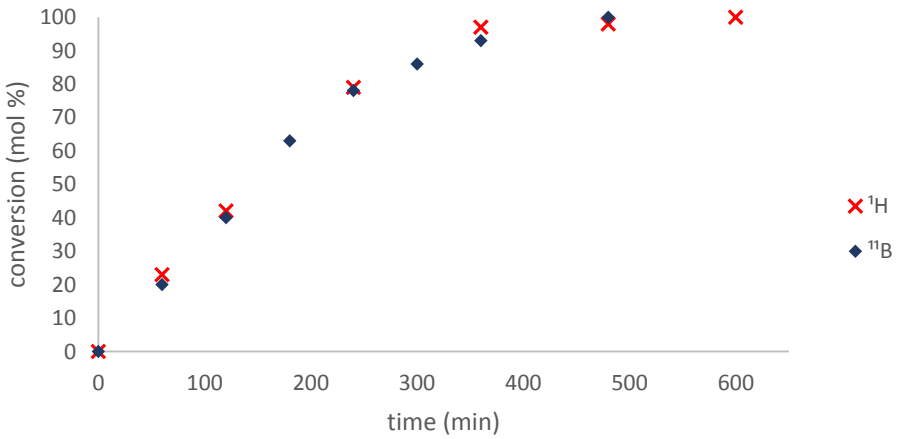


Figure 125: Progress by ^{1}H vs. ^{11}B NMR (entry 1, Table 18).

By and large, the dehydrocoupling of $Me_2NH{\bullet}BH_3$ by complex **4** yields the hydrogen-depleted dimer in excellent selectivity under a multitude of conditions (as compared in Section **4.2.2**). As a demonstration of possible side products, Figure **126** shows the poorest selectivity observed out of all experiments conducted.

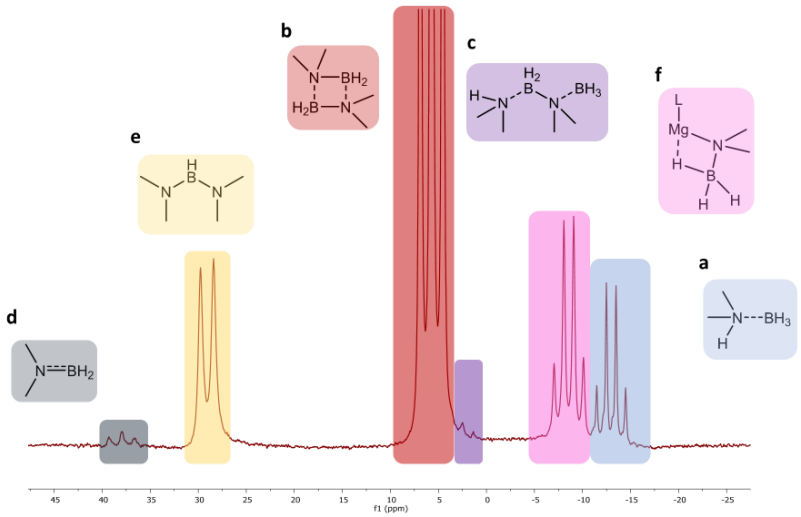


***Figure 126**: ^{11}B NMR for 20 mol% catalyst loading in thf, after 22h at 60 °C (entry **4**, Table **18**).*

The assignment of **c** is discussed in Section **4.2.3**. In contrast to Figure **126**, most reaction conditions provided excellent selectivity similar to that shown in Figure **127**. A comparison between ratios of side products formed for a reaction in C_6D_6 *vs.* thf is given in Table **14** below.

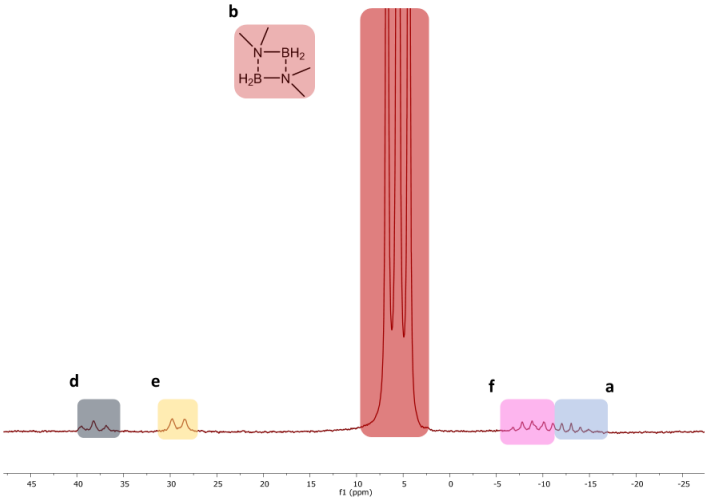


***Figure 127**: ^{11}B NMR for 10 % catalyst loading in C_6D_6 after 10h (entry **2**, Table **18**).*

Shifts and multiplicities for above signals (Figure **126**) are shown below, arranged in order of increasing field. Starting material **a** is highlighted in blue, the dehydrocoupled dimer **b** in red.

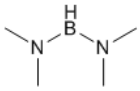
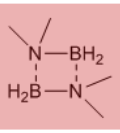
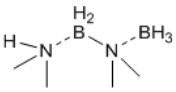
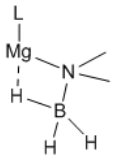
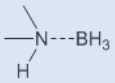
Label	Compound (*cf.* Figure 126)	^{11}B NMR δ (ppm)	Relative amount (%) for entry 2, Table 16, 10 h (in C_6D_6)	Relative amount (%) for entry 4, Table 16, 22 h (in thf)
d		37.9 (t, ^1J B,H) = 128.2 Hz, BH_2)	0.67	0.56
e		29.1 (d, ^1J (B,H) = 130.9 H, BH)	0.89	10.3
b		5.7 (t, ^1J (B,H) = 112.7 Hz, BH_2)	97.9	71.3
c		2.3 (t, ^1J (B,H) = 110 Hz, BH_2)	0.09	1.4
f		-8.6 (q, ^1J (B,H) = 98.1 Hz, BH_3)	0.01	10.8
a		-13.0 (q, ^1J (B,H) = 96.5 Hz, BH_3)	0.40	5.6

***Table 14**: Overview of products formed, their ^{11}B assignment and representative ratios.*

4.2.2. Investigations on the Effects of Catalyst Loading, Solvents, Halide Abstraction, and Substrate

(i) Catalyst Loading and Rate Differences between Measurement Methods

Investigations on the effect of catalyst loading revealed a non-linear dependence, *i.e.* doubling catalyst concentration did not halve reaction times (Figure **128**). Presumably, the formed dehydrocoupling product blocks active catalyst sites. At higher [**4**], this process becomes more pronounced, disproportionally affecting the overall rate of dehydrocoupling. Additionally, as the Schlenk equilibrium is concentration dependant, higher [**4**] may result in an increased presence of the homoleptic species, which is likely less active due to steric crowding around the magnesium centre. As visible below (Figure **128**, C_6D_6 *vs.* Figure **129**, thf), conversion rates also differ significantly by solvent, *v.i.* Section **(iii)**.

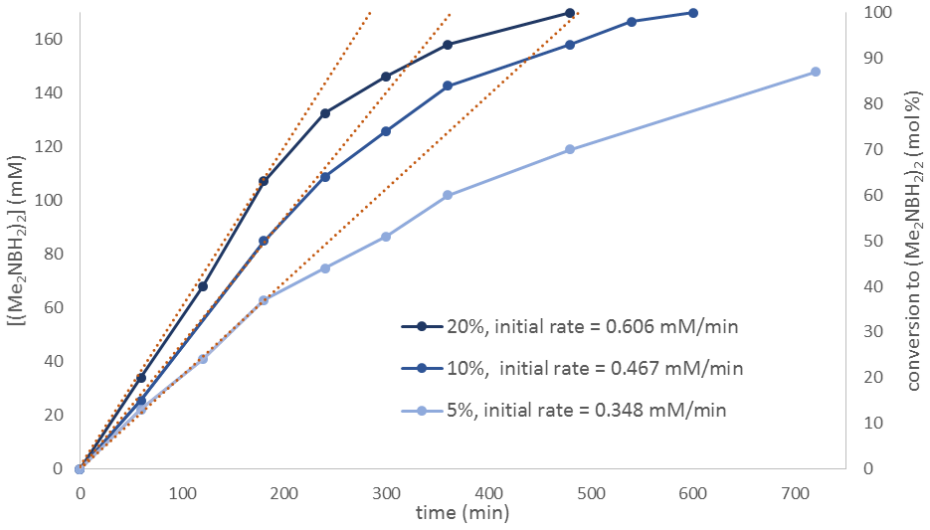


***Figure 128**: Conversion by catalyst loading (in C_6D_6, entries **1-3**, Table **18**).*

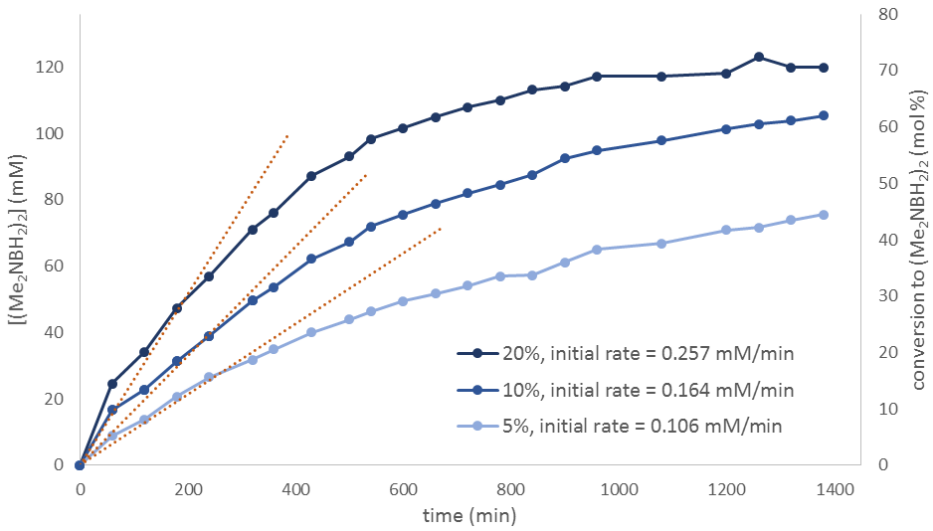


Figure 129: *Conversion by catalyst loading (in thf, entries **4-6**, Table **18**).*

Quantitatively, differences in conversion speed are well represented by comparison of initial rate constants (K_i, by $[(Me_2NBH_2)_2]$) to catalyst loadings and solvents as seen below in Table **15**.

Table 15: *Catalyst loadings and solvents vs. initial rate constants obtained from stop-and-go as well as in situ measurements of NMR spectra.*

	Stop-and-go		*In situ*
[4] (%)	in C_6D_6 (mM min^{-1})	in thf (mM min^{-1})	in C_6D_6 (mM min^{-1})
20%	0.606	0.257	
10%	0.467	0.164	2.72
5%	0.348	0.106	1.64

In contrast to the above "stop-and-go" data, experiments conducted *in situ* showed a much faster reaction rate. Indeed, initial hydrogen evolution for 10 % catalyst loading rendered the sample too heterogeneous for accurate

shimming.[442] This resulted in the first reliable data for entry **12** (Figure **130** and Table **18**) being obtained after 19 min, at which point 50 % of the starting material had already been consumed.

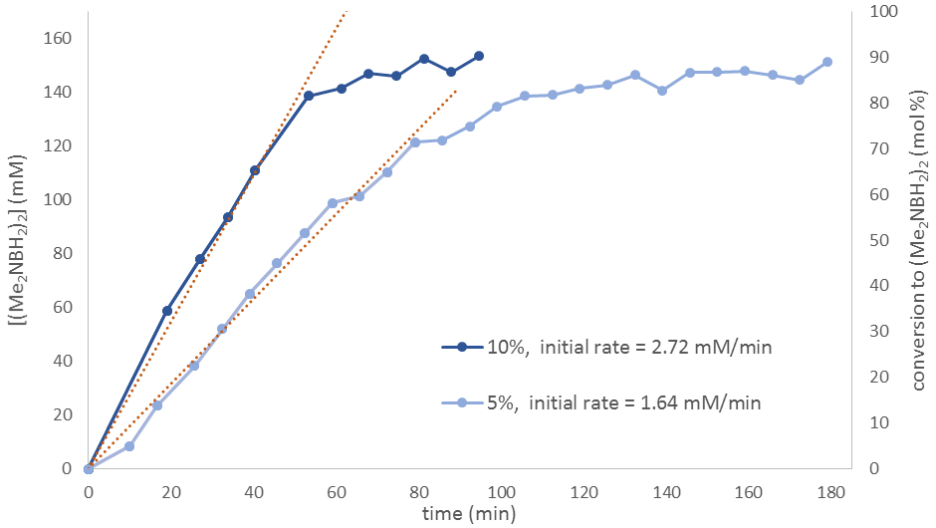


Figure 130: *Conversion by catalyst loading, monitored by in situ NMR (in C_6D_6, entries **12** and **13**, Table **18**).*

This represents a roughly five-fold increase in K_i from stop-and-go to continuous *in situ* measurements as seen in Table **15**. Whilst the causality of this extreme change is not known, possible explanations include:

The presence of an induction period. An equilibrium between "activated" and "deactivated" catalyst, with removal of the iodo fragment yielding the true catalytic species. Upon cooling, the latter then requires reactivation, slowing down the overall rate. Similar effects have been observed in transformations catalysed by molecular TM complexes (as opposed to nanoparticles).[443,444]

Decoordination of the tmeda fragment (entropically favoured) at higher temperatures, creating a more active species. Similar to the above argument, a less active form might be predominant at room temperature. A broadening of ^{1}H resonances assigned to tmeda during the course of catalysis (including spectra recorded at room temperature) provides evidence towards a dynamic process. Upon full conversion, signals sharpen to their original state.

Although this accounts for differences as observed in Figure **128** *vs.* Figure **130**, the same cannot be said of deviations compared to volumetric experiments. Figure **131** shows a comparison between conversions for three different measurement methods, all at 10 % catalyst loading. Although volumetric experiments (*v.s.* Figure **132**) were carried out in toluene rather than C_6D_6, this is unlikely to account for the observed ΔK_i of 1.69 mM min^{-1} from *in situ* NMR to volumetric measurements (*v.i.* Section **(iii)**, ΔK_i between non-coordinating solvents of 0.165 mM min^{-1} max.).

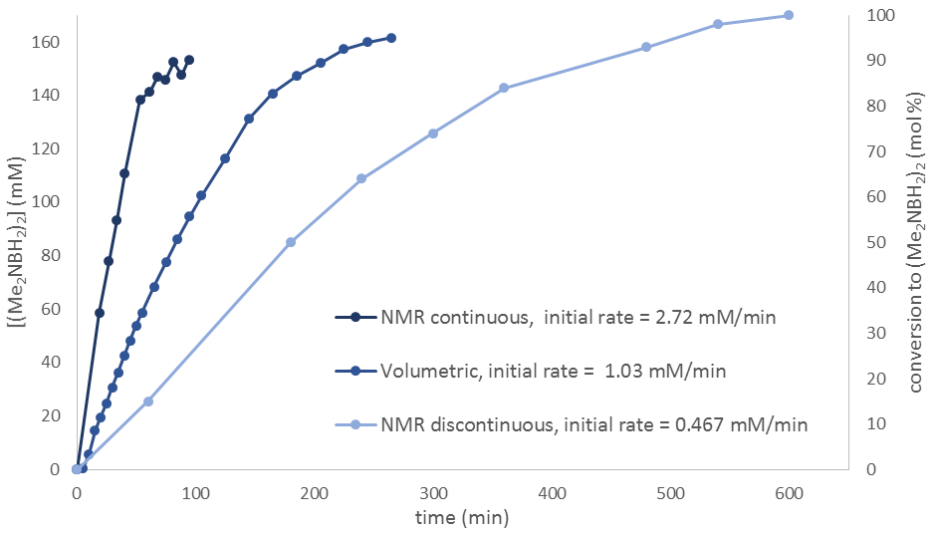


***Figure 131**: Conversion by measurement method at 10 % catalyst loading (entries **2**,**12** and **14**, Table **18** and Table **19**).*

The above suggested causality for rate differences between "stop-and-go" measurements and *in situ* NMR should equally apply to volumetric experiments, *i.e.* rates between the latter two should be similar. As seen in Figure **131** above and Table **16** below, this is clearly not the case.

Table 16: *Comparison of K_i values over a range of measurement methods and catalyst loadings.*

	NMR, in C_6D_6		Volumetric,
[4] (%)	Stop-and-go (mM min^{-1})	*In situ* (mM min^{-1})	in toluene (mM min^{-1})
10%	0.467	2.72	1.03
5%	0.348	1.64	0.614

The above variance may be attributed to one or more of the following factors:

The open nature of volumetric experiments, *i.e.* the possible presence of trace moisture or oxygen, which may lead to catalyst deactivation.

Freeze-thaw effects: *in situ* NMR experiments were the only ones subjected to this process. Upon thawing, localised pockets of high substrate and catalyst concentration could facilitate rapid conversion of **4** to the hypothetical active species. Surface effects similar to those observed in ice/ water systems are possible, but unlikely due to the weak nature of interactions between electropositive species and the C_6D_6 quadrupole.[445,446] This does not account for continued high rates once one catalyst equivalent of substrate has been transformed (*i.e.* beyond 10 % conversion).

Figure **132** below provides an overview of varying catalyst loading in volumetric experiments.

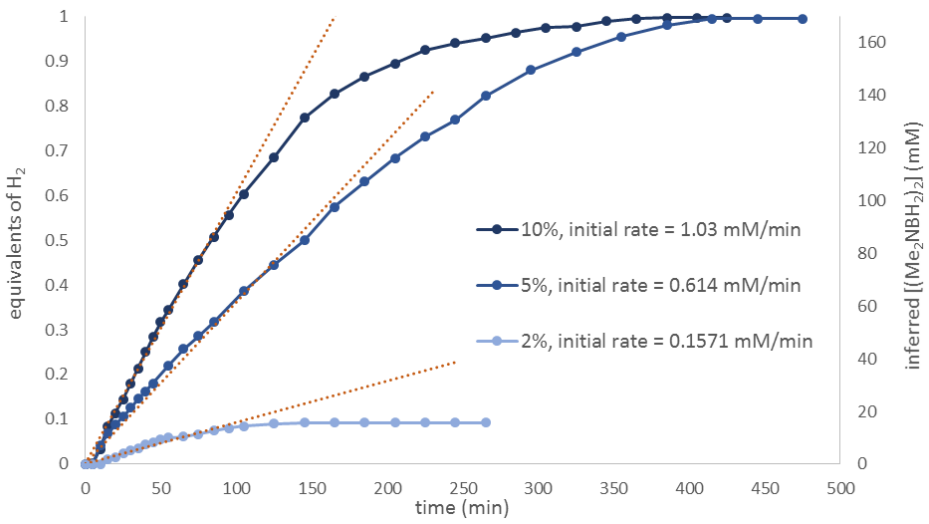


***Figure 132**: Conversion by catalyst loading, monitored by hydrogen evolution (in toluene, entries **14-16**, Table **19**).*

In the 2 % catalyst loading experiment above (Figure **132**), **4** was likely deactivated either by an unknown mechanism (*e.g.* borohydride formation),[447] or reaction with residual moisture or oxygen. Generally, 80 % conversion is reached approximately twice as fast in volumetric experiments compared to discontinuous NMR measurements.

(ii) Recyclability and Reproducibility

4 was investigated for reusability by multiple precursor injections, without removal of formed products. At 10 % catalyst loading, **4** was found to tolerate two consecutive injections before considerable deterioration of activity, as seen in Figure **133**.

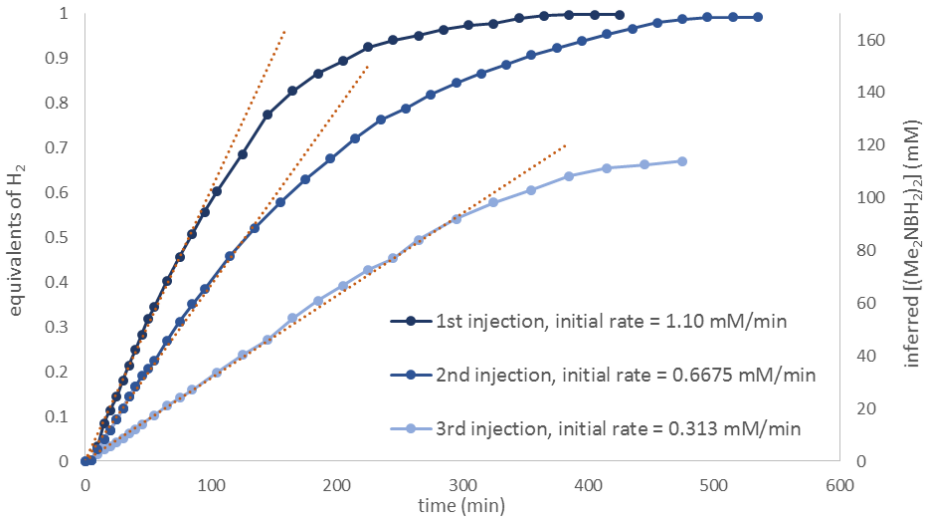


***Figure 133**: Repeated injections of $Me_2NH{\cdot}BH_3$ without removal of formed products (in toluene, 10 % catalyst loading, entry **14**, Table **19**).*

To the best of my knowledge, no such experiment has previously been reported for any Ae dehydrocoupling catalyst, or many other catalysts for that matter. A resilient bis(borane) reported by Wegner *et al.* presents a notable exception (*v.s.* Section **4.1.7**(ii), pg. 175).[416]

Experiments at 5 % catalyst loading were repeated to ascertain reproducibility. The deviation of the 5 % loading shown in light blue (dip) correlated with a random decrease in oil bath temperature by 5 °C at around 25 min.

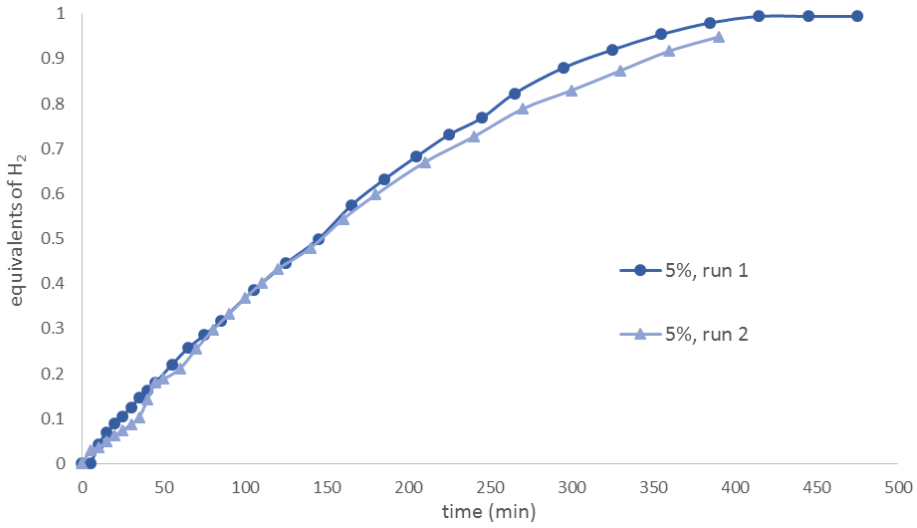


***Figure 134**: Repetition of 5 % catalyst loading experiment (in toluene, entry **15**, Table **19**).*

(iii) Solvent Effects

Dehydrocoupling experiments were carried out in a series of solvents, as summarised in Figure **135**. With reactions in thf yielding inferior rates compared to non-coordinating systems, focus was given to the latter group (*v.s.* Figure **128** and Figure **129**). In addition to C_6D_6, toluene and benzotrifluoride were examined as an electron rich and electron poor system, respectively.

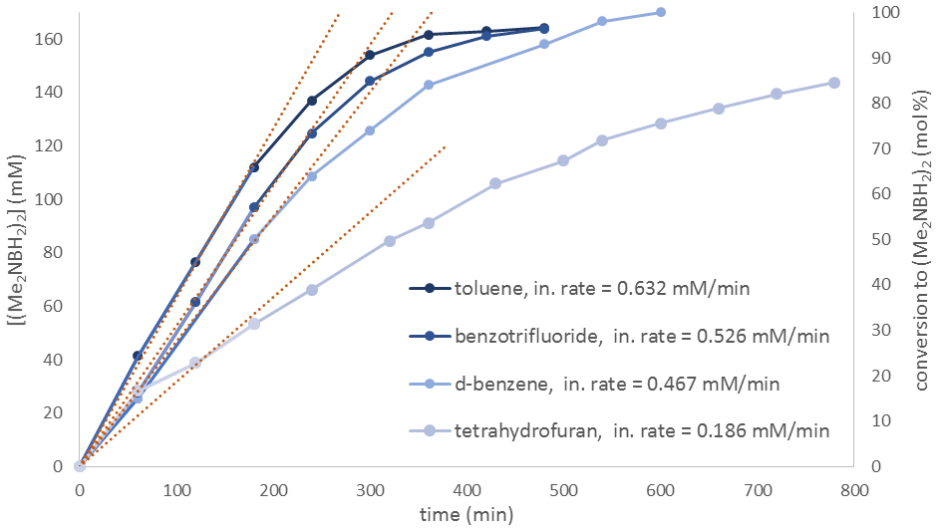


***Figure 135**: Conversion by solvent at 10 % catalyst loadings (entries **2**, **5**, **7** and **8**, Table **18**).*

Despite considerable differences in solvent polarity as displayed in Table **17**, influence of the latter on reaction progress is relatively minimal as demonstrated by their respective K_i values. Variations are likely within the margin of error, although one could speculate about the influence of quadrupole-ion interactions. Electron-rich systems such as toluene will bind to cations, *e.g.* Mg^{II}, where benzotrifluoride provides an inverse quadrupole liable to binding to anions. That being said, Mg^{II} may equally bind to the latter's CF_3 group.[448] Investigations on highly electron rich or poor systems might unearth evidence towards the influence of such interactions, paving the way towards faster Ae-catalysed dehydrocoupling.

The comparatively poor performance of thf as a reaction medium is proposed to be rooted in saturation of the active catalytic site, disadvantageously affecting substrate monomer-dimer ratios, and/ or driving the Schlenk equilibrium towards the homoleptic magnesium species.

***Table 17**: Solvent systems employed, their relative polarities and K_i values obtained.*[449,450]

Solvent	**Relative polarity**	**K_i** ($mM\ min^{-1}$)
toluene	0.099	0.632
benzotrifluoride	*ca.* 0.25	0.526
benzene	0.111	0.467
tetrahydrofuran	0.207	0.186

(iv) In Situ Halide Abstraction

Magnesium complexes featuring a reactive $[HB(C_6F_5)_3]^-$ anion have been employed in a number of chemical transformations.[76] Similarly, $[(Et_2O)_3MgN(SiMe_3)_2][B(C_6F_5)_4]$ has been reported by Bochmann *et al.* as a highly active ROP catalyst.[451] As attempts to isolate similar species were made to no avail (*v.s.* Section 2.1.2, pg. 55), experiments were carried out to determine whether *in situ* halide abstraction would yield a superior catalyst (entries **9** and **10**, Table **18**).

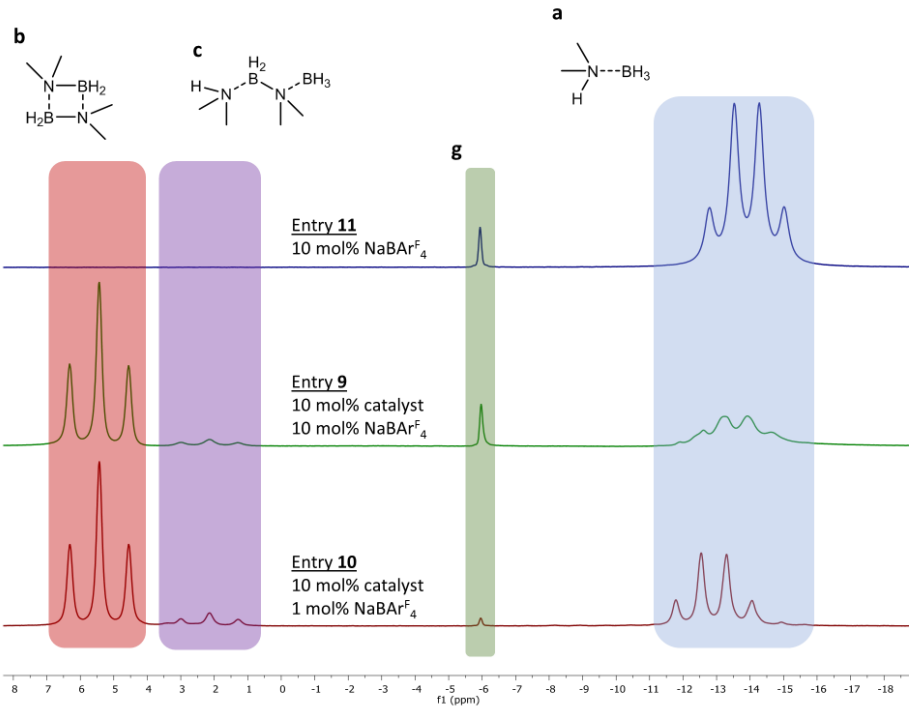


***Figure 136**: ^{11}B NMR spectra of entries **9**, **10** and **11** after 2 h at 60 °C (Table **18**).*

$NaBAr^F_4$ in the absence of catalyst showed no conversion whatsoever (heated to 60 °C for 8 h), however resulted in the appearance of a ^{11}B singlet around -6 ppm also observed in reactions involving **4** (Figure **136**). Given that the ^{11}B peak of $NaBAr^F_4$ shifts upfield with increasing coordination power of solvent, and lies at -6.8 ppm in $CDCl_3$, **g** is most likely attributed to $[BAr^F_4]^-$, with Na^+ ions solvated

by Me_2NHBH_3.† The chemical shift difference to $LMgBAr^F_4$ may not be significant enough to allow differentiation.

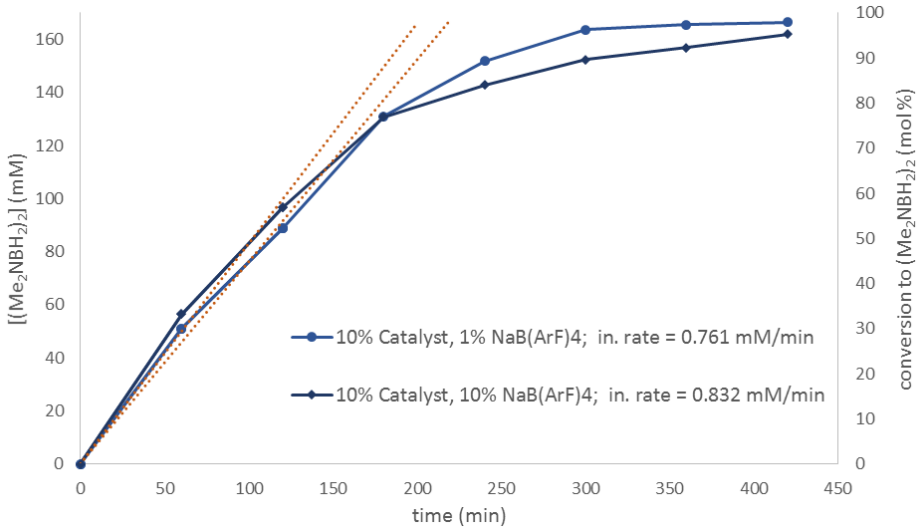


***Figure 137**: Conversion by catalyst loading and $NaBAr^F_4$ added (in C_6D_6, entries **9** and **10**, Table **18**).*

As displayed in Figure **137**, reaction rates barely differ with varying amounts of $NaBAr^F_4$, although as seen below either are faster than **4** in its own right (Figure **138**).

† $NaBAr^F_4$ is not sufficiently soluble in C_6D_6 at room temperature to observe any ^1H or ^{11}B signals whatsoever.

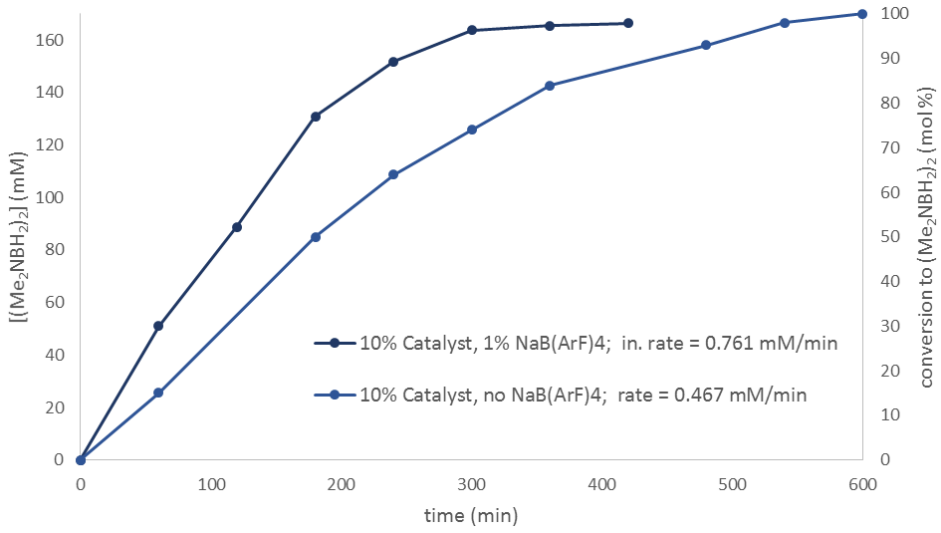


***Figure 138**: Conversion at 10% catalyst loading, with and without $NaBAr^F_4$ (in C_6D_6, entries **2** and **10**, Table **18**).*

Given that the use of $NaBAr^F_4$ only gave rise to a single additional peak, little can be inferred about its role. This would require the synthesis of $LMgBAr^F_4$ and an examination of the latter's propensity towards catalysing dehydrocoupling.

(v) Catalytic Dehydrocoupling of Ammonia Borane

To the best of my knowledge, there are no reports on the performance of magnesium complexes for the dehydrocoupling of ammonia borane in solution. Given the poor performance of thf as a solvent system observed in this work (*v.s.* Figure **129** and Figure **135**), $H_3N{\bullet}BH_3$ dehydrogenation was trialled in toluene, despite the former being apparently insoluble in the latter at room temperature (entry **17**, Table **19**).

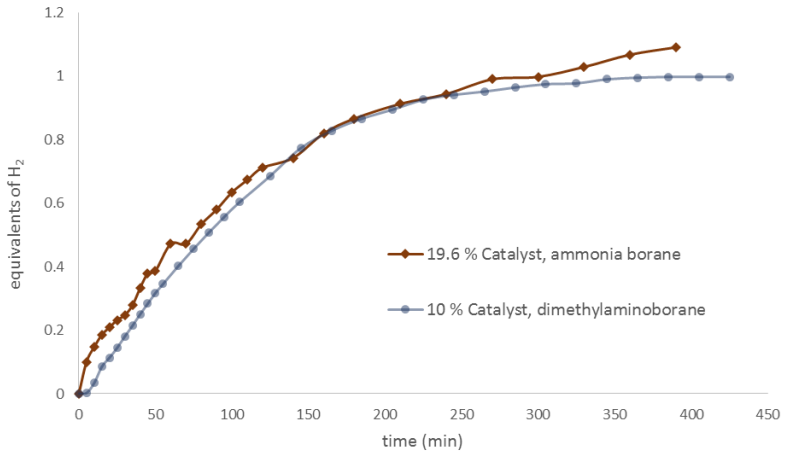


***Figure 139**: Comparison between 19.6 % catalyst loading, H_3NBH_3 and 10% catalyst loading, $Me_2NH{\cdot}BH_3$ (both in toluene, entries **17** and **14**, respectively, Table **19**).*

This resulted in the release of just over one equivalent of hydrogen within 6.5 h, which closely resembles the dehydrogenation of $Me_2NH{\cdot}BH_3$ at 10 % catalyst loading, as displayed in Figure **139**. It is unclear whether the actual dehydrocoupling mechanism is heterogeneous or homogeneous, although given the similarity in reaction profiles, a homogenous reaction appears more likely.

Upon cooling to room temperature and removal of solvent, a filtered NMR sample only showed **4** and residual toluene. In a practical context, the above consequently represents a kind of reverse phase heterogeneous catalysis. That is to say, it is the substrate rather than the catalyst which is insoluble at room temperature. This opens interesting avenues in starting material and catalyst recovery, a solution of the latter could feasibly be filtered onto fresh substrate, and the former recycled. Whether the catalyst remains active after the above experiment remains to be seen.

4.2.3. Identity of Reaction Intermediates

Despite repeated attempts, no reaction intermediates could be crystallised from stoichiometric or substoichiometric experiments. The identity and role of such species was therefore inferred from NMR spectra and comparison to literature examples.

The $^{11}BH_2$ triplet at δ 2.3 ppm (*v.s.* Figure **124**) is a unifying feature of all spectra recorded. From a survey of the literature, there are three likely candidates for the identity of this, shown in

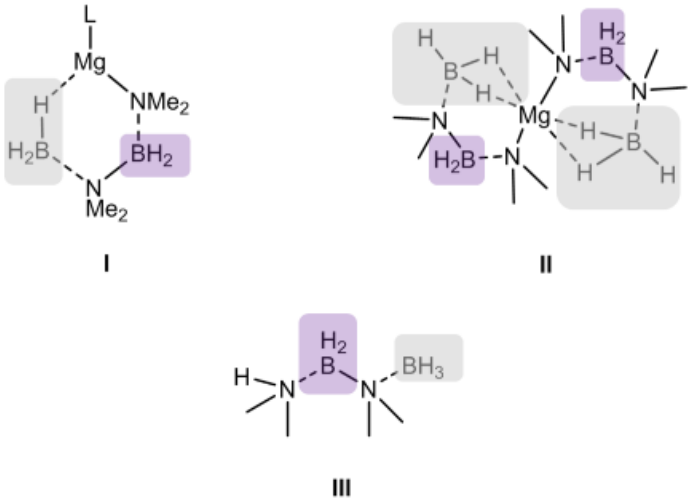


Figure 140.[90,452] All incorporate BH_3 moieties (highlighted in grey), the quartet of which is obscured by starting material **a**.

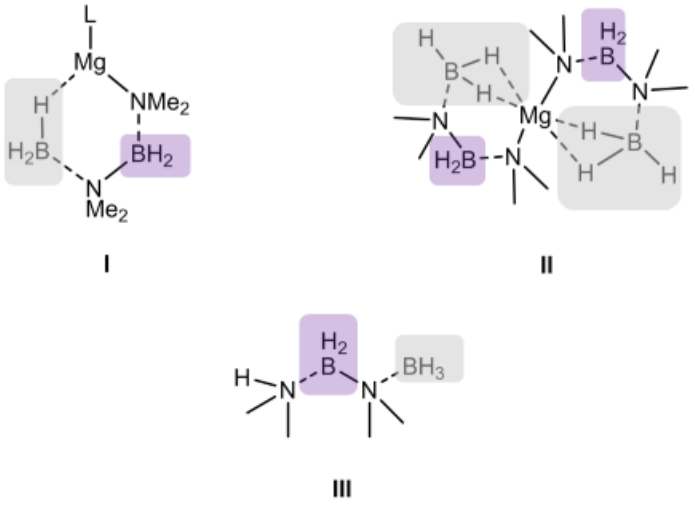


Figure 140: *Candidates for the identity of c.*

I could immediately be ruled out based on quantities of **c** observed. As depicted in Figure **141**, relative amounts of **c** exceed a 1:1 ratio of catalyst/**c**. This ratio only narrowly exceeds 1:2 at 5 % catalyst loading, rendering **II** a possible candidate. However, the thf adduct of **II** has been described by Hill *et al.*, with a ^{11}B shift of 4.2 ppm (*vs.* 2.3 ppm for **c**).[90] In contrast, spectral data of **c** very closely match that of the linear amidoborane **III**, as reported by Manners *et al.*[453] Consequently, resonance **c** most likely corresponds to **III**.†

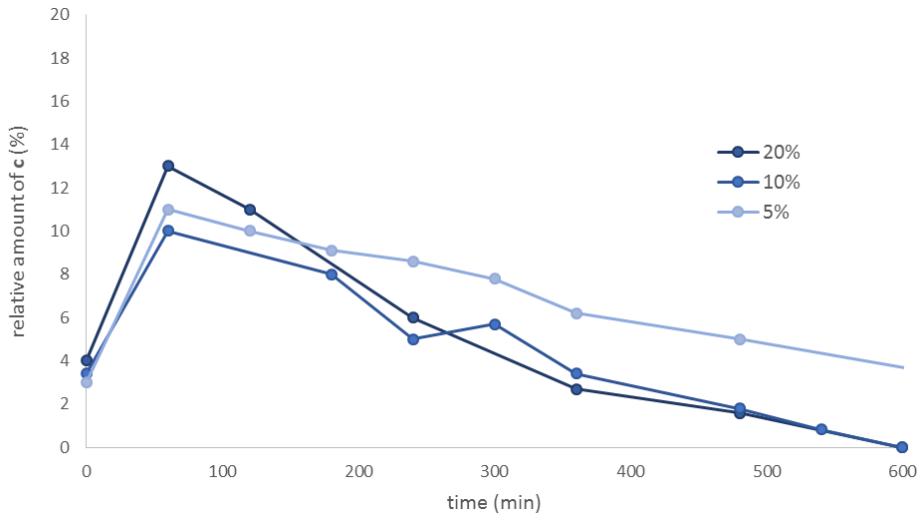


***Figure 141**: Integration ratios of ^{11}B signals at δ2.33 (t) for different catalyst loadings (entries **1-3**, Table **18**).*

Regrettably, *in situ* NMR experiments did not reveal any additional species, although very well resolved signals of **c** and **b** could be observed, as seen in Figure **142** (omitted range only shows marginal amounts of the monomeric **d**).

† Although the same signals seems to have been attributed to **I** by Hill *et al.*[90] This is likely erroneous, given the evidence collected in this work as well as the implication of **c** in the literature.[452,491] The phosphorus equivalent of **c** has also been reported as an intermediate in the dehydrogenation of Ph_2PHBH_3 by Manners *et al.*[492]

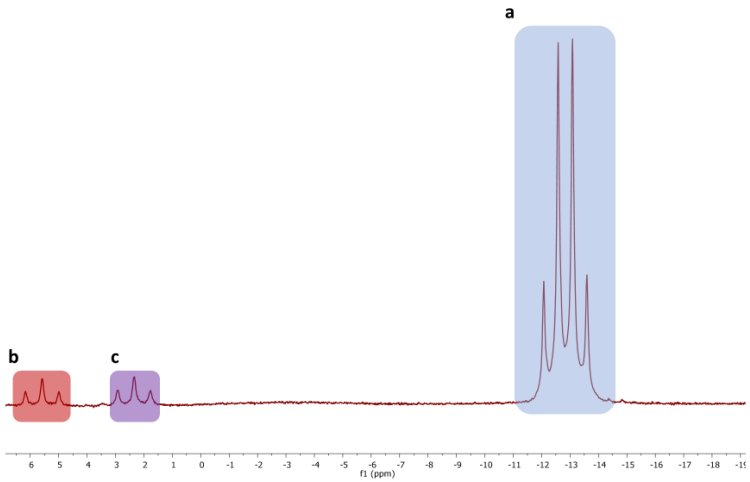


***Figure 142**: In situ NMR recorded at 60 °C after 19 min (entry **12**, Table **18**).*

As none of the above served to delineate the fate of **4** during catalytic dehydrocoupling, stoichiometric experiments were carried out in an attempt to isolate intermediates. A reaction between $Me_2NH{\bullet}BH_3$ and **4** at room temperature revealed the slow build-up of the dehydrocoupled dimer **b**, concomitant with the formation of two heavily overlapping triplets at δ 3.4 and δ 2.3 ppm (shown in yellow and purple, respectively; Figure **143**). BH_3 signals are obscured by $Me_2NH{\bullet}BH_3$ (grey section).

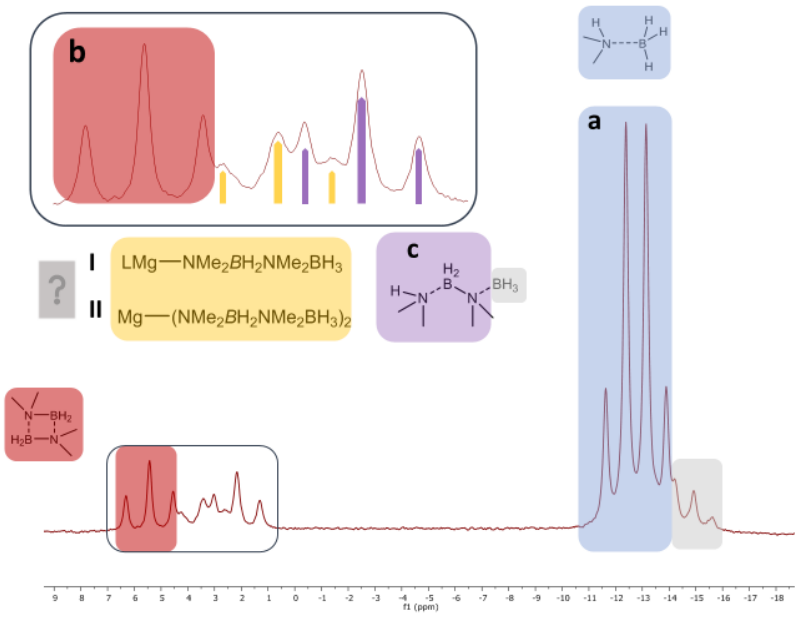


***Figure 143**: ^{11}B NMR of a stoichiometric experiment after 44h at room temperature.*

The downfield triplet now approaches the range reported for **I** and **II** (

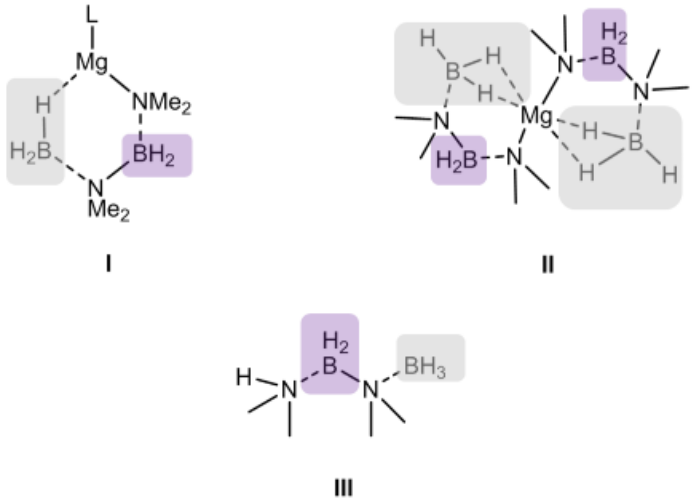


Figure 140), but cannot definitively be assigned to either without comparison to an authentic sample. As an active intermediate, **I** appears the more likely choice. If dehydrocoupling took place on **II**, similar reaction rates and selectivities would be expected irrespective of the magnesium surrogate, as there is no steric or electronic contribution from the ligand. As the performance of **4** differs considerably from literature examples of other Mg complexes, the ligands influence is likely substantial, as would be expected in the heteroleptic **I**. Subsequent heating of the above sample 60 °C resulted in disappearance of the ^{11}B δ 3.4 ppm triplet.

The fate of the iodo fragment of **4** is uncertain. Contrary to work carried out, previous publications employ LMgX systems where X is a hydrogen, hydrocarbon or $N(SiMe_3)_2$. No free *H*I (^{1}H *ca.* δ -10.4 ppm) was observed, similarly the far downfield region in which a $Me_2NH{\bullet}^{11}BIH_2$ signal would likely be found is devoid of peaks.[454] The possible identity of an "activated" **4** therefore requires the synthesis of possible intermediates, as covered below (Section **4.4**).

Although multinuclear spectra were recorded, all of the above refers to information gathered by ^{11}B NMR. This is due to the crowded nature of the aliphatic region in recorded ^{1}H NMR spectra. Hydridic peaks are broadened into the baseline, and B^1H_x signals thus unsuitable for identifying products and intermediates. Whilst N*Me*$_2$ signals are visible, these, too, frequently overlap and

exhibit broadening indicative of dynamic processes (*v.s.* Figure **123**, signals **B**). This notwithstanding, comparison of peak ratios suggest that the $^{11}BH_2$ signal of **c** (δ2.3 ppm) correlates to a ^{1}H peak at δ2.33 ppm (br s., N*Me*$_2$).

4.2.4. Observations on a Possible Mechanism

The near-absence of isolable intermediates renders the delineation of catalytic processes a challenging prospect. However, the mechanism suggested by Hill *et al.* (on the l.h.s. of Figure **144** below, *v.s.* 1.4.2(iii)) allows a comparative analysis to above results.

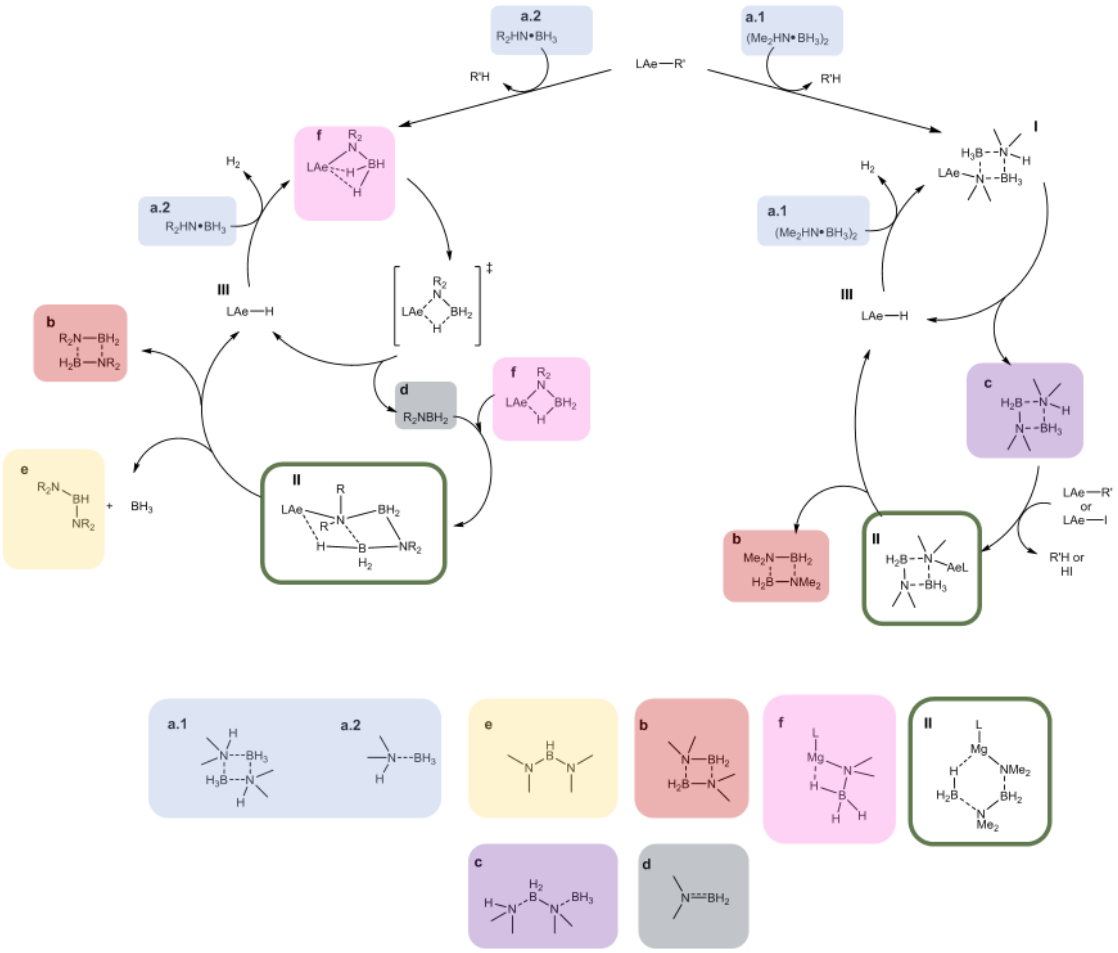


***Figure 144**: Ae dehydrocoupling mechanism as suggested by Hill et al. (left), possible origin of **c** (right), and compounds observed in this work (bottom).*

Given the amount of evidence and computational studies in support of the catalytic cycle shown on the left (Figure **144**), its applicability to Ae dehydrocoupling in general is a fair assumption. However, it does not account for the observation of **c**, the intermediate discussed above (Section **4.2.3**). Given that **f** was observed in considerable quantities in experiments conducted in thf (*v.s.* Figure **126**), it is assumed to be stable at room temperature. Thus, the absence of ^{1}H and ^{11}B NMR resonances consistent with **f** from spectra of experiments conducted in non-coordinating solvents (entries **1-3** and **7-13**, Table **18**) may have two roots: Either **f** is unstable in hydrocarbon solvent systems, and its formation and decomposition is too rapid for observation, or never formed in the first place (at least not in sufficient quantities for detection). The former explanation appears unlikely, given that **f** is the direct origin of **d**, which is only observed in small quantities. In Hill's catalytic cycle, **f** and **d** react to form **II**. Thus, the "active" dehydrocoupling species requires the reaction of a reagent not observed at all,† and one only found in very small quantities.

An alternative explanation is presented by the coexistence of the catalytic cycle shown on the right hand side in Figure **144**, which also provides a reasoning for the comparatively poor selectivity observed in thf *vs.* non-coordinating solvents (*v.s.* Figure **126** and Table **14**). Which cycle dominates is proposed to depend on solvent Lewis basicity.

In thf, **a** most likely adopts a monomeric form, **a.2**. In the latter, dimerisation would effectively saturate its coordination sphere, *i.e.* take the form of **a.1**. Where the deprotonation of **a.2** by LAeR' yields **f**, the deprotonation of **a.1** would provide compound **I**. β-hydride elimination from **I** then affords **c**, the mono-dehydrocoupled dimer observed in all NMR experiments carried out. Given that no **I** was detected, hydride elimination is likely a comparatively fast process. Deprotonation of **c** then yields **II**, the same intermediate implicated in Hill's catalytic cycle. Should **c** exist in a dimer-monomer equilibrium,

† The reaction of **f** with **d** is unlikely to be rapid, considering both are observed to coexist in thf.

dehydrocoupling in C_6D_6 may occur entirely by the catalytic cycle shown on the right.

4.3. Conclusions

Investigations have unearthed a novel magnesium complex, capable of the catalytic dehydrocoupling of $Me_2NH{\cdot}BH_3$ to Me_2NBH_2 at higher rates and better selectivity than any Ae system reported in the literature so far. The cyclic dimer is formed under relatively low catalyst loadings and mild conditions, with a full conversion of starting material. Reusability of **4** has been demonstrated.

A pronounced solvent effect on catalyst activity and selectivity was observed; a series of hydrocarbons have been shown to perform significantly better than thf. The identity of reaction intermediate **c** has been ascertained with reasonable certainty, with implications for a reaction mechanism alternative to that proposed by Hill *et al.*[90]

Differences in dehydrocoupling rates observed between measurement methods provides tantalising evidence towards the accelerating influence of a freeze-thaw process.

4 has been found to catalyse the dehydrocoupling of ammonia borane in what may be described as reverse-phase heterogeneous catalysis. The latter potentially opens new routes in facile product and catalyst recovery.

4.4. Future Work

The work carried out so far is very much a stepping stone, providing a well performing, robust catalyst shrouded in mechanistic ambiguity. There are two interlinked facets to future work: Gaining insight into intermediates, and improving catalyst performance.

The former requires the synthesis of authentic samples, chiefly the much-evoked amidoborane derivative **IV**, shown below.

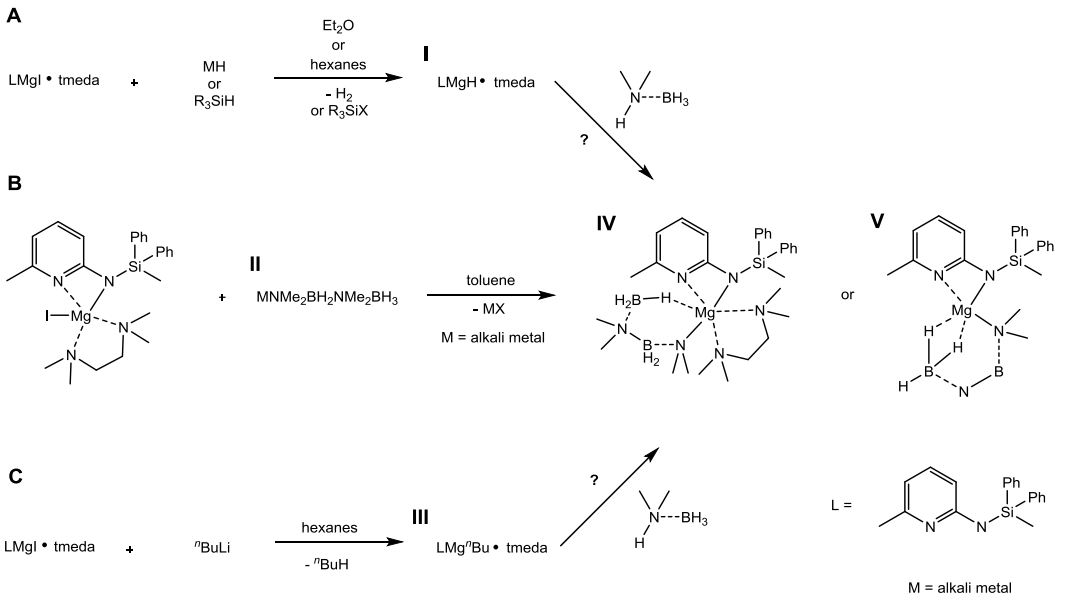


***Figure 145**: Potential routes to Mg-amidoborane intermediate.*

Three routes, **A**, **B** and **C** above (Figure **145**), are envisaged to obtain **IV**. In principle, they are all based on providing a strong driving force to allow for the rapid synthesis of **IV** at low temperatures, thus avoiding its decomposition by dehydrocoupling. This should also clarify whether the tmeda fragment remains attached (*cf.* **V**). The examination of **IV** by *in situ* variable temperature NMR may yield valuable information about the latter's stability, as well as providing evidence for the evoked LAeH species. Routes **A** and **C** are based on well-

established synthetic procedures, salt metathesis procedure **B** is based on alkali metal amidoboranes **II**, which have been synthesised by Hill *et al.*[424]

The tmeda fragment in **4** has been proven critical in stabilising the homoleptic species towards Schlenk equilibrium disproportionation (*v.s.* Section 2.1.1(ii)). However, a more loosely bound fragment, *e.g.* $Ar_2N(CH_2)_2NAr_2$, may still provide the necessary stabilisation at lower temperatures, whilst being less tightly bound and therefore allowing more facile formation of an uncongested catalytic centre. Given that the cyclic precursor to δ-hydride elimination requires a non-crowded environment, it is unlikely to occur in the presence of bound tmeda.

The possibility of freeze-thaw processes considerably accelerating dehydrocoupling rates requires systematic investigation. The required temperature differences make this process unsuitable for volumetric monitoring, particularly as comparative *in situ* NMR in the absence of a freeze-thaw presents itself as a facile method.

Monitoring reaction progress by IR spectroscopy might allow for the identification of short lived intermediates and thus aid mechanistic delineation.

Given the excellent selectivity observed, the propensity of **4** to act as a dehydrocoupling catalyst for the formation of heteronuclear element-element bonds in the areas of organic synthesis and material chemistry presents itself as a promising avenue of pursuit.

4.5. Experimental

The dehydrocoupling of dimethylaminoborane was monitored either by following reaction progress by multinuclear NMR, or hydrogen evolution. Procedures are described below; NMR samples were prepared in a glove box (*cf.* Section 5.2.1). ^{11}B FIDs were processed with backward linear prediction to eliminate the broad borosilicate ^{11}*B*–O feature.

4.5.1. Standard Procedures for Monitoring by NMR

Quantities, solvents, *etc.* are listed in Table **18**, pg. 217.

(i) Without Additive

In a Young's NMR tube, 10 mg of $Me_2NH{\bullet}BH_3$ and varying amounts of catalyst **4** were dissolved in 0.8 mL of the desired solvent. For non-deuterated solvents, a C_6D_6 insert was added. The reaction was heated to 60 °C for 1 h intervals. Progress was monitored between heating intervals by ^{1}H and/ or ^{11}B NMR.
Control experiments were carried out in all solvents in the absence of catalyst.
See entries **1** to **8**, Table **18**.

(ii) With Additive

To a 10 mol% solution of **4** in 0.8 mL C_6D_6 was added 1 or 10 mol% $NaBAr^F{}_4$, the resulting mixture vigorously shaken for 3 min, and filtered into a Young's NMR tube through a PTFE syringe filter (0.22 μm). To the clear solution was added 10 mg $Me_2NH{\bullet}BH_3$. The reaction was heated to 60 °C for 1 h intervals. Progress was monitored between heating intervals by ^{1}H and ^{11}B NMR.

In a control experiment, a suspension of 10 mg $Me_2NH{\bullet}BH_3$ and 10 mol% $NaBAr^F{}_4$ was subjected to identical conditions in the absence of **4**.
See entries **9**, **10** and **11**, Table **18**.

(iii) Monitoring by In Situ NMR

Onto a frozen 10 or 5 mol% solution of **4** in 0.4 mL C_6D_6 was added 10 mg of $Me_2NH{\bullet}BH_3$ in 0.4mL C_6D_6. The reaction was cooled to -78 °C during transit to the NMR spectrometer. The sample was transferred into the latter, which was held at 60 °C. Reaction progress was continuously monitored by ^1H and ^{11}B NMR.
See entries **12** and **13**, Table **18**.

(iv) Stoichiometric Experiment

In a Young's NMR tube, $Me_2NH{\bullet}BH_3$ (2 mg, 34.58 μmol) and **4** (20 mg, 34.58 μmol) were dissolved in 0.8 mL of C_6D_6. The reaction was monitored by ^1H and ^{11}B NMR.

***Table 18**: Quantities of reagents in NMR experiments. Substrate is $Me_2NH{\bullet}BH_3$ (10 mg, 170 µmol).*

Entry	Catalyst (NaBAr$^F_4$ in italics, where applicable)			Solvent (all 0.8mL, non-deuterated solvents with C_6D_6 insert)
	mol%	**mg**	**µmol**	
1	**20**	20	34	C_6D_6
2	**10**	10	17	C_6D_6
3	**5**	5	8.5	C_6D_6
4	**20**	20	34	thf
5	**10**	10	17	thf
6	**5**	5	8.5	thf
7	**10**	10	17	toluene
8	**10**	10	17	benzotrifluoride
9	**10** ***10***	10 15	17 17	C_6D_6
10	**10** ***1***	10 1.5	17 1.7	C_6D_6
11	- ***10***	- 1.5	- 1.7	C_6D_6
12	**10**	10	17	C_6D_6
13	**5**	5	8.5	C_6D_6

4.5.2. Standard Procedures for Monitoring by Hydrogen Evolution

Catalyst loadings and substrate quantities are listed in Table **19**, pg. 220.

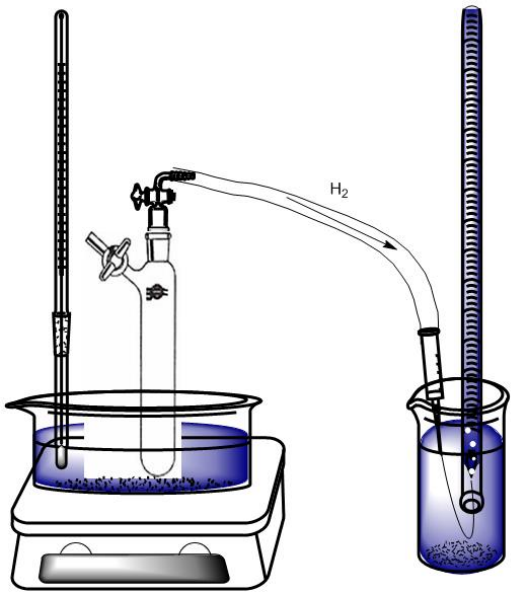


Figure 146: *Apparatus for volumetric measurements.*

(i) For the catalytic dehydrocoupling of $Me_2NH{\cdot}BH_3$

The apparatus was set up as displayed in Figure **146**. A solution of 10, 5 or 2 mol% **4** in 5 mL of toluene, stirred at 200 rpm, was heated to 60 °C until equilibrium vapour pressure was reached (*i.e.* no change in volume was observed for 15 min, typically after 45 min).† Subsequently, a solution of $Me_2NH{\cdot}BH_3$ (98.2 mg, 1.66 mmol) in 5 mL of toluene was injected, and reaction progress monitored by gas evolution. See entries **14**, **15**, and **16**, Table **19**.

† Initial screenings were undertaken employing benzene and thf as solvents. In addition to concerns about the toxicity of the former, neither system proved feasible, as no reliable static volume was reached at 60 °C. Toluene was therefore chosen as a solvent of lower toxicity, similar relative polarity to benzene, and considerably lower vapour pressure (thf: 200 hPa, benzene: 101 hPa, toluene: 29 hPa at 20 °C).[449]

(ii) Multiple cycles

The above procedure was carried out for 10 mol% **4**. After completion, the connection to the measuring burette was shut, and the Schlenk tube kept open to argon at 60 °C overnight to ensure complete consumption of any remaining starting material. The argon was then disconnected, the pressure left to equilibrate, and a further equivalent of $Me_2NH{\bullet}BH_3$ (98.2 mg, 1.66 mmol) in 2 mL of toluene injected. The procedure was repeated for a third time, with prior volume reduction *in vacuo* to *ca.* 8 mL.
See entry **16**, Table **19**.

(iii) For the catalytic dehydrocoupling of $H_3N{\bullet}BH_3$

The apparatus was set up as displayed in Figure **146**. A suspension of powdered $H_3N{\bullet}BH_3$ in 5 mL of toluene, stirred at 200 rpm, was heated to 60 °C. Equilibrium vapour pressure was reached after 35 min. To the turbid suspension was then added a solution of 20 mol% **4** (96.3 mg, 0.166 mmol) in 5 mL of toluene, and reaction progress monitored by gas evolution.
See entry **17**, Table **19**.

***Table 19**: Quantities of reagents in volumetric experiments. Solvent is 10mL toluene. (a) 3 consecutive injections of substrate, (b) repeated twice.*

Entry	Catalyst			Substrate		
	mol%	mg	µmol	Identity	mg	µmol
14	**10** [a]	96.3	166	$Me_2NH{\bullet}BH_3$	98.2	1666
15	**5** [b]	48.2	83.0	$Me_2NH{\bullet}BH_3$	98.2	1666
16	**2**	19.3	33.3	$Me_2NH{\bullet}BH_3$	98.2	1666
17	**19.6**	96.3	166	$H_3N{\bullet}BH_3$	25.7	833

Chapter 5

General Experimental

5.1. General Experimental Techniques

5.1.1. Manipulation of Air- and Moisture Sensitive Compounds

The extreme oxophilicity of s-block compounds renders them susceptible to degradation, lest exposure to air and moisture be prevented. Rigorous exclusion of the latter is best achieved by employing Schlenk line and glove box techniques. Over thirty years after its publication, "The Manipulation of Air Sensitive Compounds" authored by Shriver and Drezdzon still represents the most comprehensive publication on the subject, the reader is referred to this excellent text for more detailed information.[455]

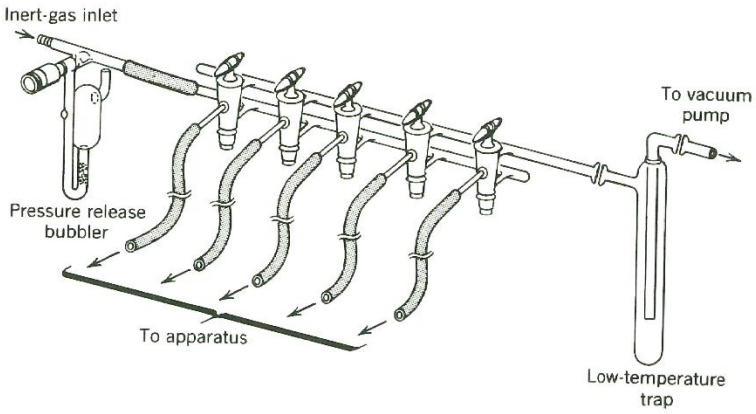


Figure 147: *Schlenk line apparatus.*[455]

The manipulation of small quantities of s-block coordination compounds was undertaken employing a Schlenk line such as that depicted above in Figure **147**, a pyrex glass dual manifold connected to an argon cylinder and dynamic vacuum (~10^{-4} mbar). The vacuum was achieved with an Edwards RV5 rotary vane two-stage mechanical vacuum pump and pressures monitored with an Edwards Pirani10 thermal conductivity vacuum gauge. Detrimental exposure of the pump to volatiles was prevented with a liquid nitrogen trap. Commercially available argon

(99.998%, *BOC Pureshield*) was further dried by passing inert gas through a drying column containing a copper-based catalyst and 4 Å molecular sieves, which was regularly regenerated.[456] Inert gas flow was monitored, and large overpressures avoided, by use of a mercury bubbler. Glassware employed in the manipulation of air-sensitive compounds was evacuated to *ca.* 10^{-3} mbar, flame-dried, and purged by three successive vacuum-argon cycles upon cooling.

Anhydrous and air-sensitive materials as well as NMR solvents were stored in an MBraun Labmaster glove box, operated under 1-4 mbar N_2 overpressure to avoid ingress of air and moisture. Anaerobic conditions of < 0.1 ppm O_2 and H_2O were maintained by constant recirculation of inert gas through a drying column comparable to that used for argon in Schlenk line techniques; materials entering the glove box were subjected to four vacuum-nitrogen cycles.

5.1.2. Solvents and Reagents

Owing to the aforementioned sensitivity of Group II complexes, reagents and solvents in particular require thorough drying prior to use. Hexanes and pentanes were dried by passing through a column of activated alumina; diethyl ether and thf were pre-dried over Na wire prior to distillation from Na/K alloy and sodium-benzophenone ketyl respectively. Toluene was heated to reflux for a week over potassium prior to distillation. tmeda and benzotrifluoride were distilled from CaH_2 and stored over 4 Å molecular sieves. All solvents were degassed before use. Solvents were stored over in ampoules over potassium mirrors, with the exception of thf, tmeda and benzotrifluoride, which were stored over 4 Å molecular sieves.

D_6-benzene was dried over potassium and stored over a mirror of the same, D_8-thf was dried over CaH_2 and stored over sodium; both were subjected to three freeze-pump-thaw cycles prior to use.

Group II and XII halides were heated to 300°C *in vacuo* overnight, bis-trimethylsilyl amides were dried under vacuum overnight. Group I hydrides were washed with dry hexanes before drying *in vacuo*. $^{n}Bu_2Mg$ and MeMgI were purchased as solutions, the solvents removed *in vacuo* and both compounds stored and used as solids. All synthesised proligands were dried *in vacuo* for a minimum time period of 16 h after purification. Purified compounds were transferred to the glove box and stored under dried nitrogen.

Activated magnesium (Mg*) was synthesised both by reduction of magnesium chloride with lithium naphthalide,[457,458] as well as the thermal decomposition of anthracene-magnesium.[459] Activated magnesium bromide ($MgBr_2$*) was obtained from the reaction of 1,2-dibromoethane with magnesium metal under elimination of ethylene,[9] triphenylbismuth from phenylmagnesium bromide and bismuth trichloride,[460] $NaBAr^{F}_4$ from sodium tetrafluoroboride and the corresponding Grignard reagent.[461]

5.2. Physical Measurements

5.2.1. NMR Spectroscopy

Samples of air and moisture sensitive compounds were prepared in the glove box employing Young's tap NMR tubes. Spectroscopic data were collected on Bruker DPX300, DPX400, AV400, AV(III)400, AV(III)400HD or AV(III)600 spectrometers. Chemical shifts are quoted in parts per million (ppm) relative to neat trimethylsilane (^{1}H, $^{13}C\{^{1}H\}$ and $^{29}Si\{^{1}H\}$), LiCl in D_2O ($^{7}Li\{^{1}H\}$), $BF_3{\bullet}OEt_2$ (^{11}B and $^{11}B\{^{1}H\}$) and $CFCl_3$ (^{19}F). Residual solvent signals were used as internal references for ^{1}H and $^{13}C\{^{1}H\}$measurements. Where necessary, assignments were verified by DEPT 90, 135 as well as ^{1}H-^{1}H and ^{1}H-^{13}C correlation experiments.

5.2.2. Mass Spectrometry

ESI-MS samples were prepared in high dilution of the samples in analytical grade methanol. Air and moisture sensitive samples were prepared under a nitrogen atmosphere in the glove box in sealed capillary tubes; EI Mass Spectrometry was carried out both in-house by Dr Mick Cooper on a Bruker ApexIV FT-ICRMS instrument using a heptacosafluorotributylamine (FC43) calibrant spectrometer, and at the EPSRC National Centre, Swansea.

5.2.3. Elemental Microanalysis

The analysis of air stable compounds was performed by Dr Tong Liu using a CE-440 Elemental Analyser (Exeter Analytical); samples of s-block complexes were prepared under inert atmosphere and sealed in glass ampoules employing Schlenk line techniques. These were analysed by Mr Stephen Boyer,

Microanalysis Service, London Metropolitan University.

The extremely reactive nature of species investigated frequently precluded the acquisition of reliable data. Repeated elemental analysis of crystalline samples with clean ^{1}H spectra and integration ratios entirely consistent with the proposed species provided inconsistent elemental microanalysis results, a commonly encountered problem in s-block chemistry.[149,462]

5.2.4. Crystallographic Method

The suitability of crystals for X-ray diffraction was ascertained optically and by brief screening, *i.e.* the collection of a small number of frames. These were mounted on polymer-tipped dual-stage glass fibre MicroMount™ (MiTeGen) using YR-1800 perfluoropolyether oil, and cooled rapidly to 120 K under a stream of nitrogen controlled by an Oxford Cryostreams open flow cryostat.[463] Diffraction data were collected on either Agilent SuperNova or SuperNovaII diffractometers (mirror-monochromated Cu-K_α radiation source; λ = 1.54184 Å; ω scans) equipped with Atlas, AtlasS2 or Titan CCD detectors. Absorption corrections were carried out employing a Gaussian numerical method with beam profile correction (CrysAlisPro).[464] The position of non-H atoms was determined by direct or iterative methods within the OLEX2 software package, and refined by full matrix least-squares with anisotropic displacement parameters.[465–467] Hydrogen atoms were placed and refined using a geometric riding model. CIF checking was undertaken with checkCIF[468] and by Dr William Lewis at the University of Nottingham.

Bibliography

1 R. E. Krebs, *The History and Use of Our Earth's Chemical Elements: A Reference Guide*, Greenwood Publishing Group, 2006.

2 E. von Frankland, *Ann. der Chemie und Pharm.*, 1849, **71**, 171–213.

3 S. Reformatsky, *Berichte der Dtsch. Chem. Gesellschaft*, 1887, **20**, 1210–1211.

4 P. Barbier, *Compt. Rend.*, 1899, **128**, 110–111.

5 V. Grignard, *Ann. Chim. Phys.*, 1901, **24**, 433–490.

6 J. J. Eisch, *Organometallics*, 2002, **21**, 5439–5463.

7 V. Grignard, *Compt. Rend.*, 1900, **130**, 1322–1324.

8 V. Grignard, *Noble Prize Lect.*

9 G. S. Silverman and P. E. Rakita, *Handbook of Grignard Reagents*, CRC Press, 1996.

10 T. J. Kealy and P. L. Pauson, *Nature*, 1951, **168**, 1039–1040.

11 T. P. Hanusa, *Chem. Rev.*, 1993, **93**, 1023–1036.

12 R. A. Williams, K. F. Tesh and T. P. Hanusa, *J. Am. Chem. Soc.*, 1991, **113**, 4843–4851.

13 A. Almenningen, A. Haaland and J. Lusztyk, *J. Organomet. Chem.*, 1979, **170**, 271–284.

14 R. Zerger and G. Stucky, *J. Organomet. Chem.*, 1974, **80**, 7–17.

15 T. P. Hanusa, *Organometallics*, 2002, **21**, 2559–2571.

16 J. Langer, S. Krieck, R. Fischer, H. Görls and M. Westerhausen, *Zeitschrift für Anorg. und Allg. Chemie*, 2010, **636**, 1190–1198.

17 F. A. Cotton, *Advanced Inorganic Chemistry*, Wiley, 1980.

18 F. G. N. Cloke, P. B. Hitchcock, M. F. Lappert, G. A. Lawless and B. Royo, *J. Chem. Soc. Chem. Commun.*, 1991, **18**, 724.

19 M. Westerhausen, *Angew. Chem. Int. Ed. Engl.*, 2001, **40**, 2975–2977.

20 T. P. Hanusa, *Coord. Chem. Rev.*, 2000, **210**, 329–367.

21 S. Krieck, L. Yu, M. Reiher and M. Westerhausen, *Eur. J. Inorg. Chem.*, 2010, **2010**, 197–216.

22 M. Driess and H. Nöth, Eds., *Molecular Clusters of the Main Group Elements*, Wiley-VCH Verlag GmbH & Co. KGaA, Weinheim, FRG, 2004.

23 X. Wang and L. Andrews, *J. Phys. Chem. A*, 2004, **108**, 11500–11510.

24 R. Köppe, P. Henke and H. Schnöckel, *Angew. Chem. Int. Ed. Engl.*, 2008, **47**, 8740–4.

25 I. Resa, E. Carmona, E. Gutierrez-Puebla and A. Monge, *Science*, 2004, **305**, 1136–8.

26 D. del Río, A. Galindo, I. Resa and E. Carmona, *Angew. Chem. Int. Ed. Engl.*, 2005, **44**, 1244–7.

27 A. Schnepf and H.-J. Himmel, *Angew. Chem. Int. Ed. Engl.*, 2005, **44**, 3006–8.

28 S. P. Green, C. Jones and A. Stasch, *Science*, 2007, **318**, 1754–1757.

29 S. Krieck, H. Görls, L. Yu, M. Reiher and M. Westerhausen, *J. Am. Chem. Soc.*, 2009, **131**, 2977–85.

30 H. Braunschweig, R. D. Dewhurst, K. Hammond, J. Mies, K. Radacki and A. Vargas, *Science*, 2012, **336**, 1420–1422.

31 C. Jones, A. Sidiropoulos, N. Holzmann, G. Frenking and A. Stasch, *Chem. Commun.*, 2012, **48**, 9855.

32 Y. Wang, Y. Xie, P. Wei, R. B. King, H. F. Schaefer, P. V. R. Schleyer and G. H. Robinson, *J. Am. Chem. Soc.*, 2008, **130**, 14970–14971.

33 K. C. Mondal, H. W. Roesky, M. C. Schwarzer, G. Frenking, B. Niepötter, H. Wolf, R. Herbst-Irmer and D. Stalke, *Angew. Chemie - Int. Ed.*, 2013, **52**, 2963–2967.

34 Y. Li, K. C. Mondal, H. W. Roesky, H. Zhu, P. Stollberg, R. Herbst-Irmer, D. Stalke and D. M. Andrada, *J. Am. Chem. Soc.*, 2013, **135**, 12422–12428.

35 S. J. Bonyhady, C. Jones, S. Nembenna, A. Stasch, A. J. Edwards and G. J. McIntyre, *Chem. - A Eur. J.*, 2010, **16**, 938–955.

36 M. Arrowsmith, M. S. Hill, G. Kociok-Köhn, D. J. MacDougall, M. F. Mahon and I. Mallov, *Inorg. Chem.*, 2012, **51**, 13408–13418.

37 M. Arrowsmith, H. Braunschweig, M. A. Celik, T. Dellermann, R. D. Dewhurst, W. C. Ewing, K. Hammond, T. Kramer, I. Krummenacher, J. Mies, K. Radacki and J. K. Schuster, *Nat. Chem.*, 2016, **8**, 890–894.

38 P. P. Power, *Nature*, 2010, **463**, 171–177.

39 W. D. Buchanan, D. G. Allis and K. Ruhlandt-Senge, *Chem. Commun.*, 2010, **46**, 4449.

40 J. S. Alexander and K. Ruhlandt-Senge, *Eur. J. Inorg. Chem.*, 2002, 2761–2774.

41 F. Ortu, G. J. Moxey, A. J. Blake, W. Lewis and D. L. Kays, *Inorg. Chem.*, 2013, **52**, 12429–39.

42 M. M. Gillett-Kunnath, J. G. MacLellan, C. M. Forsyth, P. C. Andrews, G. B. Deacon and K. Ruhlandt-Senge, *Chem. Commun.*, 2008, 4490.

43 J. Tammiku-Taul, P. Burk and A. Tuulmets, *J. Phys. Chem. A*, 2004, **108**, 133–139.

44 M. Westerhausen, M. Gärtner, R. Fischer and J. Langer, *Angew. Chem. Int. Ed. Engl.*, 2007, **46**, 1950–6.

45 A. Bom, M. Bradley, K. Cameron, J. K. Clark, J. Van Egmond, H. Feilden, E. J. Maclean, A. W. Muir, R. Palin, D. C. Rees and M. Zhang, *Angew. Chemie Int. Ed.*, 2002, **41**, 265–271.

46 H. G. Richey, *Grignard reagents: new developments*, Wiley, 1999.

47 J. Cossy, *Grignard reagents and transition metal catalysts: formation of C-C bonds by cross-coupling*, Walter de Gruyter GmbH & Co KG, 2016.

48 P. Knochel, W. Dohle, N. Gommermann, F. F. Kneisel, F. Kopp, T. Korn, I. Sapountzis and V. A. Vu, *Angew. Chemie - Int. Ed.*, 2003, **42**, 4302–4320.

49 R. E. Mulvey, *Acc. Chem. Res.*, 2009, **42**, 743–55.

50 C.-J. Li, *Tetrahedron*, 1996, **52**, 5643–5668.

51 R. Taylor, *Tetrahedron Lett.*, 1975, **16**, 435–436.

52 N. S. Narasimham and R. Ammanamanchi, *J. Chem. Soc. Chem. Commun.*, 1985, 1368.

53 J. García-Álvarez, E. Hevia and V. Capriati, *European J. Org. Chem.*, 2015, **2015**, 6779–6799.

54 C. Vidal, J. García-Álvarez, A. Hernán-Gõmez, A. R. Kennedy and E. Hevia, *Angew. Chemie - Int. Ed.*, 2014, **53**, 5969–5973.

55 H. Zong, H. Huang, J. Liu, G. Bian and L. Song, *J. Org. Chem.*, 2012, **77**, 4645–4652.

56 L. Cicco, S. Sblendorio, R. Mansueto, F. M. Perna, A. Salomone, S. Florio and V. Capriati, *Chem. Sci.*, 2016, **7**, 1192–1199.

57 A. Stasch and C. Jones, *Dalton Trans.*, 2011, **40**, 5659–72.

58 A. Stasch, *Chemistry*, 2012, **18**, 15105–12.

59 H. H. Brintzinger, D. Fischer, R. Mülhaupt, B. Rieger and R. M. Waymouth, *Angew. Chemie Int. Ed. English*, 1995, **34**, 1143–1170.

60 P. Margl, L. Deng and T. Ziegler, *J. Am. Chem. Soc.*, 1999, **121**, 154–162.

61 J. Arnold and P. Scott, *Dalt. Trans.*, 2011, **40**, 7665.

62 S. Harder, *Chem. Rev.*, 2010, **110**, 3852–76.

63 S. Arndt and J. Okuda, *Chem. Rev.*, 2002, **102**, 1953–1976.

64 F. T. Edelmann, *Chem. Soc. Rev.*, 2012, **41**, 7657–72.

65 M. R. Crimmin and M. S. Hill, in *Organometallics*, ed. S. Harder, Springer Berlin Heidelberg, Berlin, Heidelberg, 2013, vol. 45, pp. 191–241.

66 M. Arrowsmith, in *Encyclopedia of Inorganic and Bioinorganic Chemistry*, John Wiley & Sons, Ltd, Chichester, UK, 2015, pp. 1–26.

67 a. G. M. Barrett, M. R. Crimmin, M. S. Hill and P. a. Procopiou, *Proc. R. Soc. A Math. Phys. Eng. Sci.*, 2010, **466**, 927–963.

68 M. S. Hill, D. J. Liptrot and C. Weetman, *Chem. Soc. Rev.*, 2016, **45**, 972–988.

69 R. Rochat, M. J. Lopez, H. Tsurugi and K. Mashima, *ChemCatChem*, 2016, **8**, 10–20.

70 D. J. Liptrot, P. M. S. Hill and M. F. Mahon, *Angew. Chemie - Int. Ed.*, 2014, **53**, 6224–6227.

71 D. J. Liptrot, in *Group 2 Mediated Dehydrocoupling*, Springer-Verlag, 2016, pp. 131–145.

72 X. Zhang, T. J. Emge and K. C. Hultzsch, *Angew. Chemie*, 2012, **124**, 406–410.

73 M. Arrowsmith, W. M. S. Shepherd, M. S. Hill and G. Kociok-Köhn, *Chem. Commun.*, 2014, **50**, 12676–12679.

74 M. R. Crimmin, A. G. M. Barrett, M. S. Hill, P. B. Hitchcock and P. A. Procopiou, *Organometallics*, 2007, **26**, 2953–2956.

75 M. D. Anker, M. Arrowsmith, P. Bellham, M. S. Hill, G. Kociok-Köhn, D. J. Liptrot, M. F. Mahon and C. Weetman, *Chem. Sci.*, 2014, **5**, 2826–2830.

76 M. D. Anker, M. Arrowsmith, R. L. Arrowsmith, M. S. Hill and M. F. Mahon, *Inorg. Chem.*, 2017, **56**, 5976–5983.

77 M. Szwarc, *Nature*, 1956, **178**, 1168–1169.

78 N. Hadjichristidis, M. Pitsikalis, S. Pispas and H. Iatrou, *Chem. Rev.*, 2001, **101**, 3747–3792.

79 J.-F. Carpentier and Y. Sarazin, in *Alkaline-Earth Metal Compounds*, Springer, Berlin, Heidelberg, 2013, pp. 141–189.

80 T. Narita, T. Yasumura and T. Tsuruta, *Polym. J.*, 1973, **4**, 421–425.

81 A. Weeber, S. Harder, H. H. Brintzinger and K. Knoll, *Organometallics*, 2000, **19**, 1325–1332.

82 D. F. J. Piesik, K. Häbe and S. Harder, *Eur. J. Inorg. Chem.*, 2007, 5652–5661.

83 S. Harder and F. Feil, *Organometallics*, 2002, **21**, 2268–2274.

84 C. a Wheaton, P. G. Hayes and B. J. Ireland, *Dalton Trans.*, 2009, **9226**, 4832–46.

85 B. Lian, C. M. Thomas, O. L. Casagrande, T. Roisnel and J.-F. Carpentier, *Polyhedron*, 2007, **26**, 3817–3824.

86 J. Wu, Y. Chen, W. Hung and C. Lin, *Organometallics*, 2008, **27**, 4970–4978.

87 X. Xu, Y. Chen, G. Zou, Z. Ma and G. Li, *J. Organomet. Chem.*, 2010, **695**, 1155–1162.

88 J. Spielmann, M. Bolte and S. Harder, *Chem. Commun.*, 2009, 6934.

89 J. Spielmann, G. Jansen, H. Bandmann and S. Harder, *Angew. Chemie - Int. Ed.*, 2008, **47**, 6290–6295.

90 D. J. Liptrot, M. S. Hill, M. F. Mahon and D. J. MacDougall, *Chem. - A Eur. J.*, 2010, **16**, 8508–8515.

91 P. Bellham, M. D. Anker, M. S. Hill, G. Kociok-Köhn and M. F. Mahon, *Dalt. Trans.*, 2016, **45**, 13969–13978.

92 V. Butera, N. Russo and E. Sicilia, *Chem. - A Eur. J.*, 2014, **20**, 5967–5976.

93 R. Dallanegra, A. B. Chaplin and A. S. Weller, *Angew. Chemie - Int. Ed.*, 2009, **48**, 6875–6878.

94 P. Bellham, M. S. Hill, G. Kociok-Köhn and D. J. Liptrot, *Dalt. Trans.*, 2013, **42**, 737–745.

95 M. S. Hill, M. Hodgson, D. J. Liptrot and M. F. Mahon, *Dalt. Trans.*, 2011, **40**, 7783.

96 L. Euzenat, D. Horhant, Y. Ribourdouille, C. Duriez, G. Alcaraz, M. Vaultier, N. L. Pickett, W. P. Power and A. J. Scott, *Chem. Commun.*, 2003, **98**, 2280–2281.

97 H. Schumann, S. Schutte, H. J. Kroth and D. Lentz, *Angew. Chemie - Int. Ed.*, 2004, **43**, 6208–6211.

98 J. A. . Clyburne and N. McMullen, *Coord. Chem. Rev.*, 2000, **210**, 73–99.

99 D. L. Kays, *Chem. Soc. Rev.*, 2016, **45**, 1004–1018.

100 M. P. Coles, *Coord. Chem. Rev.*, 2015, **297–298**, 2–23.

101 M. P. Coles, *Coord. Chem. Rev.*, 2015, **297–298**, 24–39.

102 S. P. Sarish, S. Nembenna, S. Nagendran and H. W. Roesky, *Acc. Chem. Res.*, 2011, **44**, 157–170.

103 L. Bourget-Merle, M. F. Lappert and J. R. Severn, *Chem. Rev.*, 2002, **102**, 3031–66.

104 J. Barker and M. Kilner, *Coord. Chem. Rev.*, 1994, **133**, 219–300.

105 F. T. Edelmann, *Chapter 3: Advances in the Coordination Chemistry of Amidinate and Guanidinate Ligands*, 2008, vol. 57.

106 C. Jones, *Coord. Chem. Rev.*, 2010, **254**, 1273–1289.

107 T. Chlupatý and A. Růžička, *Coord. Chem. Rev.*, 2016, **314**, 103–113.

108 N. M. Scott, T. Schareina, O. Tok and R. Kempe, *Eur. J. Inorg. Chem.*, 2004, **2004**, 3297–3304.

109 R. Kempe, *Eur. J. Inorg. Chem.*, 2003, **2003**, 791–803.

110 S. Deeken, G. Motz and R. Kempe, *Zeitschrift für Anorg. und Allg. Chemie*, 2007, **633**, 320–325.

111 A. Noor, S. Schwarz and R. Kempe, *Organometallics*, 2015, **34**, 2122–2125.

112 M. Hafeez and M. Riaz, *Appl. Petrochemical Res.*, 2016, **6**, 307–340.

113 A. Spannenberg, H. Fuhrmann, P. Arndt, W. Baumann and R. Kempe, *Angew. Chemie - Int. Ed.*, 1999, **37**, 3363–3365.

114 S. Deeken, G. Motz, V. Bezugly, H. Borrmann, F. R. Wagner and R. Kempe, *Inorg. Chem.*, 2006, **45**, 9160–9162.

115 R. Kempe, H. Noss and T. Irrgang, *J. Organomet. Chem.*, 2002, **647**, 12–20.

116 A. R. Chakravarty, F. A. Cotton and D. A. Tocher, *Inorg. Chem.*, 1984, **23**, 4030–4033.

117 L. M. Engelhardt, G. E. Jacobsen, P. C. Junk, C. L. Raston, B. W. Skelton and A. H. White, *J. Chem. Soc. Dalt. Trans.*, 1988, 1011.

118 L. M. Engelhardt, G. E. Jacobsen, P. C. Junk, C. L. Raston and A. H. White, *J. Chem. Soc. Chem. Commun.*, 1990, 89.

119 A. Noor, F. R. Wagner and R. Kempe, *Angew. Chemie - Int. Ed.*, 2008, **47**, 7246–7249.

120 H. K. Lee, C. H. Lam, S.-L. Li, Z.-Y. Zhang and T. C. W. Mak, *Inorg. Chem.*, 2001, **40**, 4691–4695.

121 L. M. Engelhardt, G. E. Jacobsen, W. C. Patalinghug, B. W. Skelton, C. L. Raston and A. H. White, *J. Chem. Soc. Dalt. Trans.*, 1991, 2859.

122 A. Noor, W. Kretschmer and R. Kempe, *Eur. J. Inorg. Chem.*, 2006, **2006**, 2683–2689.

123 S. Aldridge, R. J. Calder, D. L. Coombs, C. Jones, J. W. Steed, S. Coles and M. B. Hursthouse, *New J. Chem.*, 2002, **26**, 677–686.

124 W. J. Grigsby, C. L. Raston, V.-A. Tolhurst, B. W. Skelton and A. H. White, *J. Chem. Soc. Dalt. Trans.*, 1998, 2547–2556.

125 C. L. Raston, B. W. Skelton, V.-A. Tolhurst and A. H. White, *Polyhedron*, 1998, **17**, 935–942.

126 J. Baldamus, M. L. Cole, U. Helmstedt, E.-M. Hey-Hawkins, C. Jones, P. C. Junk, F. Lange and N. A. Smithies, *J. Organomet. Chem.*, 2003, **665**, 33–42.

127 S. C. F. Kui, H.-W. Li and H. K. Lee, *Inorg. Chem.*, 2003, **42**, 2824–2826.

128 H. Noss, M. Oberthür, C. Fischer, W. P. Kretschmer and R. Kempe, *Eur. J. Inorg. Chem.*, 1999, **1999**, 2283–2288.

129 X.-E. Duan, S.-F. Yuan, H.-B. Tong, S.-D. Bai, X.-H. Wei and D.-S. Liu, *Dalt. Trans.*, 2012, **41**, 9460.

130 K. W. Henderson, R. E. Mulvey, W. Clegg and P. A. O'Neil, *Polyhedron*, 1993, **12**, 2535–2538.

131 K. W. Henderson, R. E. Mulvey, W. Clegg and P. A. O'Neil, *J. Organomet. Chem.*, 1992, **439**, 237–250.

132 Z. Zheng, M. K. Elmkaddem, C. Fischmeister, T. Roisnel, C. M. Thomas, J.-F. Carpentier and J.-L. Renaud, *New J. Chem.*, 2008, **32**, 2150.

133 F. Ortu, University of Nottingham, 2014.

134 J.-H. Cho, Y.-S. Ryu, S.-H. Oh, J.-K. Kwon and E.-K. Yum, *Bull. Korean Chem. Soc.*, 2011, **32**, 2461–2464.

135 W. Chrisman, M. J. Tanga and M. G. Knize, *J. Heterocycl. Chem.*, 2008, **45**, 1641–1649.

136 T. Shinozuka, K. Shimada, S. Matsui, T. Yamane, M. Ama, T. Fukuda, M. Taki, Y. Takeda, E. Otsuka, M. Yamato and S. Naito, *Bioorg. Med. Chem.*, 2006, **14**, 6807–6819.

137 M. K. Elmkaddem, C. Fischmeister, C. M. Thomas and J.-L. Renaud, *Chem. Commun.*, 2010, **46**, 925–927.

138 A. F. Pozharskii, V. V. Kuz'menko, V. A. Azimov and L. N. Yakhontov, *Chem. Heterocycl. Compd.*, 1973, **9**, 1119–1125.

139 in *Comprehensive Organic Name Reactions and Reagents*, John Wiley & Sons, Inc., Hoboken, NJ, USA, 2010.

140 J. Langer, H. Görls and M. Westerhausen, *Organometallics*, 2010, **29**, 2034–2039.

141 M. L. Cole, D. J. Evans, P. C. Junk and L. M. Louis, *New J. Chem.*, 2002, **26**, 1015–1024.

142 B. Conway, E. Hevia, A. R. Kennedy, R. E. Mulvey and S. Weatherstone, *Dalt. Trans.*, 2005, 1532–1544.

143 C. Loh, C. Glock, S. Ziemann, H. Görls, S. Krieck and M. Westerhausen, *Zeitschrift für Naturforsch. B*, 2013, **68b**, 518–532.

144 M. A. Guino-o, E. Baker and K. Ruhlandt-Senge, *J. Coord. Chem.*, 2008, **61**, 125–136.

145 M. Geissler, J. Kopf and E. Weiss, *Chem. Ber.*, 1989, **122**, 1395–1402.

146 C. E. Housecroft and A. G. Sharpe, *Inorganic chemistry*, Pearson Prentice Hall, 2005.

147 H. Blaser, *Adv. Synth. Catal.*, 2002, **344**, 17.

148 A. Pfaltz and W. J. Drury, *Proc. Natl. Acad. Sci.*, 2004, **101**, 5723–5726.

149 W. Vargas and K. Ruhlandt-Senge, *Eur. J. Inorg. Chem.*, 2003, 3472–3479.

150 H. Schumann, J. Gottfriedsen and J. Demtschuk, *Chem. Commun.*, 1999, 2091–2092.

151 A. Torvisco, A. Y. O'Brien and K. Ruhlandt-Senge, *Coord. Chem. Rev.*, 2011, **255**, 1268–1292.

152 J. A. Flores, J. G. Andino, N. P. Tsvetkov, M. Pink, R. J. Wolfe, A. R. Head, D. L. Lichtenberger, J. Massa and K. G. Caulton, *Inorg. Chem.*, 2011, **50**, 8121–31.

153 K. Searles, A. K. Das, R. W. Buell, M. Pink, C.-H. Chen, K. Pal, D. G. Morgan, D. J. Mindiola and K. G. Caulton, *Inorg. Chem.*, 2013, **52**, 5611–5619.

154 P. Crewdson, S. Gambarotta, G. P. A. Yap and L. K. Thompson, *Inorg. Chem.*, 2003, **42**, 8579–8584.

155 F. H. Allen, *Acta Crystallogr. Sect. B Struct. Sci.*, 2002, **58**, 380–388.

156 J. G. Andino, J. a. Flores, J. a. Karty, J. P. Massa, H. Park, N. P. Tsvetkov, R. J. Wolfe and K. G. Caulton, *Inorg. Chem.*, 2010, **49**, 7626–8.

157 W. E. Noland, K. P. Cole and D. Britton, *Acta Crystallogr. Sect. C Cryst. Struct. Commun.*, 2003, **59**, o263–o267.

158 S. J. Schmidtke, L. A. MacManus-Spencer, J. J. Klappa, T. A. Mobley, K. McNeill and D. A. Blank, *Phys. Chem. Chem. Phys.*, 2004, **6**, 3938–3947.

159 J. J. Klappa, S. A. Geers, S. J. Schmidtke, L. A. MacManus-Spencer and K. McNeill, *Dalt. Trans.*, 2004, 883–891.

160 B. Neumann, C. Krinninger and I.-P. Lorenz, *Eur. J. Inorg. Chem.*, 2007, **2007**, 472–480.

161 S.-F. Liu, Q. Wu, H. L. Schmider, H. Aziz, N.-X. Hu, Z. Popović and S. Wang, *J. Am. Chem. Soc.*, 2000, **122**, 3671–3678.

162 A. a Dissanayake and A. L. Odom, *Chem. Commun.*, 2012, **48**, 440–442.

163 T. Duan, T.-K. Chang, Y. Chi, J.-Y. Wang, Z.-N. Chen, W.-Y. Hung, C.-H. Chen and G.-H. Lee, *Dalt. Trans.*, 2015, **44**, 14613–14624.

164 K.-Y. Lu, H.-H. Chou, C.-H. Hsieh, Y.-H. O. Yang, H.-R. Tsai, H.-Y. Tsai, L.-C. Hsu, C.-Y. Chen, I.-C. Chen and C.-H. Cheng, *Adv. Mater.*, 2011, **23**, 4933–4937.

165 H. Xu, J. B. Diccianni, J. Katigbak, C. Hu, Y. Zhang and T. Diao, *J. Am. Chem. Soc.*, 2016, **138**, 4779–4786.

166 N. P. Tsvetkov, C. Chen, J. G. Andino, R. L. Lord, M. Pink, R. W. Buell and K. G. Caulton, *Inorg. Chem.*, 2013, **52**, 9511–21.

167 T. F. Mastropietro, A. Aprea, M. La Deda, I. Aiello, M. Ghedini and A. Crispini, *Cryst. Growth Des.*, 2012, **12**, 2173–2177.

168 T. F. Mastropietro, E. I. Szerb, M. La Deda, A. Crispini, M. Ghedini and I. Aiello, *Eur. J. Inorg. Chem.*, 2013, 2188–2194.

169 D. Karshtedt, J. L. McBee, A. T. Bell and T. D. Tilley, *Organometallics*, 2006, **25**, 1801–1811.

170 A. T. Luedtke and K. I. Goldberg, *Angew. Chemie - Int. Ed.*, 2008, **47**, 7694–7696.

171 J. L. McBee, J. Escalada and T. D. Tilley, *J. Am. Chem. Soc.*, 2009, **131**, 12703–13.

172 X. Liu, W. Sun, L. Zou, Z. Xie, X. Li, C. Lu, L. Wang and Y. Cheng, *Dalt. Trans.*, 2012, **41**, 1312–1319.

173 S. Schouteeten, O. R. Allen, A. D. Haley, G. L. Ong, G. D. Jones and D. a. Vicic, *J. Organomet. Chem.*, 2006, **691**, 4975–4981.

174 A. Szentkuti, J. A. Garg, O. Blacque and K. Venkatesan, *Inorg. Chem.*, 2015, **54**, 10748–10760.

175 H. Wang, Y. Zeng, J. S. Ma, H. Fu, J. Yao, A. I. Mikhaleva and B. A. Trofimov, *Chem. Commun.*, 2009, 5457.

176 J. J. Klappa, S. a Geers, S. J. Schmidtke, L. a MacManus-Spencer and K. McNeill, *Dalton Trans.*, 2004, 883–891.

177 R. G. Pearson, *J. Chem. Educ.*, 1968, **45**, 581.

178 R. G. Pearson, *J. Chem. Educ.*, 1968, **45**, 643.

179 R. G. Parr and R. G. Pearson, *J. Am. Chem. Soc.*, 1983, **105**, 7512–7516.

180 F. H. Allen, O. Kennard, D. G. Watson, L. Brammer, A. G. Orpen and R. Taylor, *J. Chem. Soc. Perkin Trans. 2*, 1987, S1.

181 X. Liu, W. Sun, L. Zou, Z. Xie, X. Li, C. Lu, L. Wang and Y. Cheng, *Dalt. Trans.*, 2012, **41**, 1312–1319.

182 Z. Zhang, J. M. Lim, M. Ishida, V. V Roznyatovskiy, V. M. Lynch, H. Gong, X. Yang, D. Kim and J. L. Sessler, *J. Am. Chem. Soc.*, 2012, **134**, 4076–4079.

183 C.-S. Hsiao, T.-Y. Wang, A. Datta, F.-X. Liao, C.-H. Hu, C.-H. Lin, J.-H. Huang and T.-Y. Lee, *J. Organomet. Chem.*, 2012, **718**, 82–88.

184 O. V. Petrova, A. I. Mikhaleva, L. N. Sobenina, E. Y. Schmidt and E. I. Kositsyna, *Mendeleev Commun.*, 1997, **7**, 162–163.

185 J. Firl, *Chem. Ber.*, 1968, **101**, 218–225.

186 K. Seki, K. Ohkura, M. Terashima and Y. Kanaoka, *Heterocycles*, 1984, **22**, 2347.

187 D. Savoia, V. Concialini, S. Roffia and L. Tarsi, *J. Org. Chem.*, 1991, **56**, 1822–1827.

188 J. P. Wibaut and E. Dingemanse, *Recl. des Trav. Chim. des Pays-Bas*, 1926, **45**, 671–673.

189 J. P. Wibaut and E. Dingemanse, *Recl. des Trav. Chim. des Pays-Bas*, 1923, **42**, 240–250.

190 J. J. Klappa, A. E. Rich and K. McNeill, *Org. Lett.*, 2002, **4**, 435–437.

191 L. A. MacManus-Spencer, S. J. Schmidtke, D. A. Blank and K. McNeill, *Phys. Chem. Chem. Phys.*, 2004, **6**, 3948–3957.

192 N. Agmon, *J. Phys. Chem.*, 2004, **109**, 1–288.

193 A. Pascual-Escudero, M. González-Esguevillas, S. Padilla, J. Adrio and J. C. Carretero, *Org. Lett.*, 2014, **16**, 2228–2231.

194 D. E. Lynch and I. McClenaghan, *Acta Crystallogr. Sect. E Struct. Reports Online*, 2002, **58**, o1150–o1151.

195 A. T. Luedtke, K. I. Goldberg and V. Uni, *Inorg. Chem.*, 2007, **46**, 8496–8498.

196 E. Weiss, *Angew. Chemie Int. Ed. English*, 1993, **32**, 1501–1523.

197 A. P. Dove, V. C. Gibson, P. Hormnirun, E. L. Marshall, J. A. Segal, A. J. P. White and D. J. Williams, *Dalt. Trans.*, 2003, 3088–3097.

198 L.-F. Hsueh, N.-T. Chuang, C.-Y. Lee, A. Datta, J.-H. Huang and T.-Y. Lee, *Eur. J. Inorg. Chem.*, 2011, **2011**, 5530–5537.

199 B. M. Day, W. Knowelden and M. P. Coles, *Dalton Trans.*, 2012, **41**, 10930–3.

200 W. Teng, M. Guino-o, J. Hitzbleck, U. Englich and K. Ruhlandt-Senge, *Inorg. Chem.*, 2006, **45**, 9531–9539.

201 J. Hitzbleck, Syracuse University, 2004.

202 J. Spielmann and S. Harder, *Chemistry*, 2007, **13**, 8928–38.

203 C. Weetman, M. D. Anker, M. Arrowsmith, M. S. Hill, G. Kociok-Köhn, D. J. Liptrot and M. F. Mahon, *Chem. Sci.*, 2016, **7**, 628–641.

204 C. R. Groom, I. J. Bruno, M. P. Lightfoot and S. C. Ward, *Acta Crystallogr. Sect. B Struct. Sci. Cryst. Eng. Mater.*, 2016, **72**, 171–179.

205 A. R. Kennedy, R. E. Mulvey, D. L. Ramsay and S. D. Robertson, *Dalt. Trans.*, 2015, **44**, 5875–5887.

206 E. C. Border, M. Maguire, J. G. MacLellan and P. C. Andrews, *Organometallics*, 2017, **36**, 1496–1504.

207 S. Molitor and V. H. Gessner, *Angew. Chemie - Int. Ed.*, 2016, **55**, 7712–7716.

208 S. Escoubet, S. Gastaldi and M. Bertrand, *European J. Org. Chem.*, 2005, 3855–3873.

209 E. F. V Scriven, in *Comprehensive Heterocyclic Chemistry*, 2009, vol. 2–7, pp. 165–314.

210 K. M. Waggoner, K. Ruhlandt-Senge, R. J. Wehmschulte, X. He, M. M. Olmstead and P. P. Power, *Inorg. Chem.*, 1993, **32**, 2557–2561.

211 Y. Tang, L. N. Zakharov, A. L. Rheingold and R. A. Kemp, *Organometallics*, 2005, **24**, 836–841.

212 M. J. C. Dawkins, E. Middleton, C. E. Kefalidis, D. Dange, M. M. Juckel, L. Maron and C. Jones, *Chem. Commun.*, 2016, **52**, 10490–10492.

213 M. Lappert, A. Protchenko, P. Power and A. Seeber, *Metal Amide Chemistry*, John Wiley & Sons, Ltd, Chichester, UK, 2008.

214 C. Glock, H. Görls and M. Westerhausen, *Inorg. Chem.*, 2009, **48**, 394–9.

215 M. F. Lappert, M. J. Slade, A. Singh, J. L. Atwood, R. D. Rogers and R. Shakir, *J. Am. Chem. Soc.*, 1983, **105**, 302–304.

216 E. Hevia, D. J. Gallagher, A. R. Kennedy, R. E. Mulvey, C. T. O'Hara and C. Talmard, *Chem. Commun.*, 2004, 2422–2423.

217 J. Hicks, T. J. Hadlington, C. Schenk, J. Li and C. Jones, *Organometallics*, 2013, **32**, 323–329.

218 T. L. Cottrell, *The Strengths of Chemical Bonds*, Butterworths Scientific Publications, 1958, vol. 2nd.

219 W. A. Wojtczak, P. F. Fleig and M. J. Hampden-Smith, Academic Press, 1996, vol. 40, pp. 215–340.

220 A. J. Boutland, D. Dange, A. Stasch, L. Maron and C. Jones, *Angew. Chemie - Int. Ed.*, 2016, **55**, 9239–9243.

221 C. Glock, C. Loh, H. Görls, S. Krieck and M. Westerhausen, *Eur. J. Inorg. Chem.*, 2013, 3261–3269.

222 G. J. Moxey, F. Ortu, L. Goldney Sidley, H. N. Strandberg, A. J. Blake, W. Lewis and D. L. Kays, *Dalt. Trans.*, 2014, **43**, 4838–4846.

223 J. Chai, H. Zhu, Q. Ma, H. W. Roesky, H. G. Schmidt and M. Noltemeyer, *Eur. J. Inorg. Chem.*, 2004, 4807–4811.

224 D. T. Carey, F. S. Mair, R. G. Pritchard, J. E. Warren and R. J. Woods, *Eur. J. Inorg. Chem.*, 2003, 3464–3471.

225 P. W. Dyer, J. Fawcett, G. A. Griffith, M. J. Hanton, C. Olivier, A. R. Patterson and S. Suhard, *Chem. Commun.*, 2005, 3835.

226 M. A. Dureen and D. W. Stephan, *Dalt. Trans.*, 2008, 4723.

227 J. A. Greer, V. L. Blair, C. D. Thompson and P. C. Andrews, *Dalt. Trans.*, 2016, **45**, 10887–10890.

228 C. Glock, H. Görls and M. Westerhausen, *Dalt. Trans.*, 2011, **40**, 8108.

229 S. Daniele, P. B. Hitchcock, M. F. Lappert, T. A. Nile and C. M. Zdanski, *J. Chem. Soc., Dalt. Trans.*, 2002, 3980–3984.

230 V. H. Gessner, S. G. Koller, C. Strohmann, A. M. Hogan and D. F. O'Shea, *Chem. - A Eur. J.*, 2011, **17**, 2996–3004.

231 J. Deschamp, C. Olier, E. Schulz, R. Guillot, J. Hannedouche and J. Collin, *Adv. Synth. Catal.*, 2010, **352**, 2171–2176.

232 C. Vidal, J. García-Álvarez, A. Hernán-Gómez, A. R. Kennedy and E. Hevia, *Angew. Chemie - Int. Ed.*, 2016, **55**, 16145–16148.

233 H. T. Al-Masri, J. Sieler and E. Hey-Hawkins, *Appl. Organomet. Chem.*, 2003, **17**, 63–67.

234 M. Arrowsmith, M. S. Hill and G. Kociok-Köhn, *Chem. - A Eur. J.*, 2013, **19**, 2776–2783.

235 S. Sarkar, K. P. McGowan, J. A. Culver, A. R. Carlson, J. Koller, A. J. Peloquin, M. K. Veige, K. A. Abboud and A. S. Veige, *Inorg. Chem.*, 2010, **49**, 5143–5156.

236 G. Paolucci, M. Bortoluzzi and V. Bertolasi, *Eur. J. Inorg. Chem.*, 2008, 4126–4132.

237 E. W. Y. Wong, T. J. Hadlington and C. Jones, *Main Gr. Met. Chem.*, 2013, **36**, 133–136.

238 H. T. Al-Masri, J. Sieler, S. Blaurock, P. Lönnecke, P. C. Junk and E. Hey-Hawkins, *Zeitschrift für Anorg. und Allg. Chemie*, 2005, **631**, 518–523.

239 J. Hicks and C. Jones, *Inorg. Chem.*, 2013, **52**, 3900–3907.

240 T. J. Hadlington, J. Li and C. Jones, *Can. J. Chem.*, 2014, **92**, 427–433.

241 T. J. Hadlington, B. Schwarze, E. I. Izgorodina and C. Jones, *Chem. Commun.*, 2015, **51**, 6854–6857.

242 M. P. Coles, P. B. Hitchcock, A. V. Khvostov, M. F. Lappert and L. Maron, *Dalt. Trans.*, 2011, **40**, 3047.

243 E. W. Y. Wong, D. Dange, L. Fohlmeister, T. J. Hadlington and C. Jones, *Aust. J. Chem.*, 2013, **66**, 1144–1154.

244 J. Hicks, E. J. Underhill, C. E. Kefalidis, L. Maron and C. Jones, *Angew. Chemie - Int. Ed.*, 2015, **54**, 10000–10004.

245 R. Bloch, *Chem. Rev.*, 1998, **98**, 1407–1438.

246 G. K. Friestad and A. K. Mathies, *Tetrahedron*, 2007, **63**, 2541–2569.

247 J. A. Ellman, T. D. Owens and T. P. Tang, *Acc. Chem. Res.*, 2002, **35**, 984–995.

248 S. Kobayashi and H. Ishitani, *Chem. Rev.*, 1999, **99**, 1069–1094.

249 J. G. Smith and C. D. Veach, *Can. J. Chem.*, 1966, 44, 2245–2257.

250 J. G. Smith and R. A. Turle, *J. Org. Chem.*, 1972, **37**, 126–131.

251 J. G. Smith and D. J. Mitchell, *J. Am. Chem. Soc.*, 1977, **99**, 5045–5050.

252 A. G. M. Barrett, M. R. Crimmin, M. S. Hill, P. B. Hitchcock, S. L. Lomas, M. F. Mahon and P. a Procopiou, *Dalton Trans.*, 2010, **39**, 7393–400.

253 F. Feil and S. Harder, *Eur. J. Inorg. Chem.*, 2005, 4438–4443.

254 D. H. Hunter, J. S. Racok, A. W. Rey and Y. Zea-Ponce, *J. Org. Chem.*, 1988, **53**, 1278–1281.

255 W.-C. Lee, J. M. Sears, R. A. Enow, K. Eads, D. A. Krogstad and B. J. Frost, *Inorg. Chem.*, 2013, **52**, 1737–1746.

256 H. Gilman and R. H. Kirby, *J. Am. Chem. Soc.*, 1933, **55**, 1265–1270.

257 C. H. Hassall and A. E. Lippman, *J. Chem. Soc.*, 1953, 1059.

258 H. Gilman and R. H. Kirby, *J. Am. Chem. Soc.*, 1941, **63**, 2046–2048.

259 G. J. P. Britovsek, M. Bruce, V. C. Gibson, B. S. Kimberley, P. J. Maddox, S. Mastroianni, S. J. McTavish, C. Redshaw, G. A. Solan, S. Strömberg, A. J. P. White and D. J. Williams, *J. Am. Chem. Soc.*, 1999, **121**, 8728–8740.

260 K. C. Gupta and A. K. Sutar, *Coord. Chem. Rev.*, 2008, 252, 1420–1450.

261 P. A. Vigato and S. Tamburini, *Coord. Chem. Rev.*, 2004, **248**, 1717–2128.

262 L. Strekowski, M. T. Cegla, D. B. Harden and S. Bin Kong, *J. Org. Chem.*, 1989, **54**, 2464–2466.

263 H. Weingarten, J. P. Chupp and W. A. White, *J. Org. Chem.*, 1967, **32**, 3246–3249.

264 M. R. Perry, L. E. N. Allan, A. Decken and M. P. Shaver, *Dalton Trans.*, 2013, **42**, 9157–65.

265 B. E. Love, T. S. Boston, B. T. Nguyen and J. R. Rorer, *Org. Prep. Proced. Int.*, 1999, 31, 399–405.

266 K. W. Anderson, M. Mendez-Perez, J. Priego and S. L. Buchwald, *J. Org. Chem.*, 2003, **68**, 9563–9573.

267 B. E. Love and J. Ren, *J. Org. Chem.*, 1993, **58**, 5556–5557.

268 Y. Liu, Q. Yang, D. Hao and W. Zhang, *Aust. J. Chem.*, 2012, **65**, 1390.

269 S. Vollbrecht and U. Klingebiel, 2015, 0–4.

270 P. A. Zhizhko, A. A. Zhizhin, O. A. Belyakova, Y. V Zubavichus, Y. G. Kolyagin, D. N. Zarubin and N. A. Ustynyuk, *Organometallics*, 2013, **32**, 3611–3617.

271 M. Wada, Y. Sakurai and K. Akiba, *Tetrahedron Lett.*, 1984, **25**, 1079–1082.

272 M. A. Brook and Jahangir, *Synth. Commun.*, 1988, 18, 893–898.

273 A. D. Dilman and S. L. Ioffe, *Chem. Rev.*, 2003, **103**, 733–772.

274 S. L. Buchwald, C. Mauger, G. Mignani and U. Scholz, *Adv. Synth. Catal.*, 2006, **348**, 23–39.

275 R. N. Salvatore, C. H. Yoon and K. W. Jung, *Tetrahedron*, 2001, 57, 7785–7811.

276 M. G. Siskos, A. Michaelides, A. K. Zarkadis, N. I. Tzerpos and S. Skoulika, *Cryst. Growth Des.*, 2008, **8**, 1966–1971.

277 M. G. Siskos, S. K. Garas, A. K. Zarkadis and E. P. Bokaris, *Chem. Ber.*, 1992, **125**, 2477–2481.

278 R. N. Salvatore, A. S. Nagle and W. J. Kyung, *J. Org. Chem.*, 2002, **67**, 674–683.

279 S. Hayat, Atta-Ur-Rahman, M. Iqbal Choudhary, K. M. Khan, W. Schumann and E. Bayer, *Tetrahedron*, 2001, **57**, 9951–9957.

280 D. R. Lide and H. V. Kehiaian, *CRC Handbook of Thermophysical and Thermochemical Data, Volume 1*, CRC Press, 1994.

281 K. Grant, 2015, Personal Communication.

282 D. J. Chadwick and S. T. Hodgson, *J. Chem. Soc., Perkin Trans. 1*, 1983, 93–102.

283 R. L. Letsinger, R. Collat and M. Magnusson, *J. Am. Chem. Soc.*, 1954, **76**, 4185–4186.

284 Y. Tang, L. N. Zakharov, A. L. Rheingold and R. A. Kemp, *Polyhedron*, 2005, **24**, 1739–1748.

285 H. Chen, R. A. Bartlett, H. V. R. Dias, M. M. Olmstead and P. P. Power, *J. Am. Chem. Soc.*, 1989, **111**, 4338–4345.

286 E. P. Wildman, J. P. A. Ostrowski, D. M. King, W. Lewis and S. T. Liddle, *Polyhedron*, 2017, **125**, 2–8.

287 Y. Tang, L. N. Zakharov, W. S. Kassel, A. L. Rheingold and R. a. Kemp, *Inorganica Chim. Acta*, 2005, **358**, 2014–2022.

288 B. M. Wolf, C. Maichle-Mössmer and R. Anwander, *Angew. Chemie - Int. Ed.*, 2016, **55**, 13893–13897.

289 M. A. Petrie, K. Ruhlandt-Senge and P. P. Power, *Inorg. Chem.*, 1993, **32**, 1135–1141.

290 A. Malassa, N. Herzer, H. Görls and M. Westerhausen, *Dalt. Trans.*, 2010, **39**, 5356.

291 B. Helferich, L. Moog and A. Jünger, *Berichte der Dtsch. Chem. Gesellschaft*, 1925, **58**, 872–886.

292 H. E. Applegate, C. M. Cimarusti, J. E. Dolfini, P. T. Funke, W. H. Koster, M. S. Puar, W. A. Slusarchyk and M. G. Young, *J. Org. Chem.*, 1979, **44**, 811–818.

293 L. H. Lühning, C. Brahms, J. P. Nimoth, M. Schmidtmann and S. Doye, *Zeitschrift für Anorg. und Allg. Chemie*, 2015, **641**, 2071–2082.

294 R. K. Kottalanka, A. Harinath, S. Rej and T. K. Panda, *Dalt. Trans.*, 2015, **44**, 19865–19879.

295 M. M. D. Roy, P. A. Lummis, M. J. Ferguson, R. McDonald and E. Rivard, *Chem. - A Eur. J.*, 2017, **23**, 11249–11252.

296 E. Lu, F. Tuna, W. Lewis, N. Kaltsoyannis and S. T. Liddle, *Chem. - A Eur. J.*, 2016, **22**, 11554–11558.

297 L. A. Paquette, *Encyclopedia of reagents for organic synthesis*, Wiley, 2009.

298 J. Busch-Petersen and E. . Corey, *Tetrahedron Lett.*, 2000, **41**, 2515–2518.

299 J. Busch-Petersen and E. . Corey, *Tetrahedron Lett.*, 2000, **41**, 6941–6944.

300 K. Hellwege and A. Hellwege, *Structure Data of Free Polyatomic Molecules*, Springer Berlin Heidelberg, Berlin, 1976.

301 C. Glidewell and D. C. Liles, *Acta Crystallogr. Sect. B Struct. Crystallogr. Cryst. Chem.*, 1978, **34**, 696–698.

302 J. F. Blount, A. Gutierrez and K. Mislow, *J. Org. Chem.*, 1982, **47**, 4359–4361.

303 C. Schade, W. Bauer and P. Von Ragué Schleyer, *J. Organomet. Chem.*, 1985, **295**, c25–c28.

304 G. R. Fulmer, A. J. M. Miller, N. H. Sherden, H. E. Gottlieb, A. Nudelman, B. M. Stoltz, J. E. Bercaw and K. I. Goldberg, *Organometallics*, 2010, **29**, 2176–2179.

305 J. F. Remenar and D. B. Collum, *J. Am. Chem. Soc.*, 1998, **120**, 4081–4086.

306 V. H. Gessner, C. Däschlein and C. Strohmann, *Chem. - A Eur. J.*, 2009, **15**, 3320–3334.

307 H. J. Reich, D. P. Green, M. A. Medina, W. S. Goldenberg, B. Ö. Gudmundsson, R. R. Dykstra and N. H. Phillips, *J. Am. Chem. Soc.*, 1998, **120**, 7201–7210.

308 F. Pauer and P. P. Power, *Lithium Chemistry*, John Wiley & Sons, Inc., New York, 1995.

309 T. M. Konrad, K. R. Grünwald, F. Belaj and N. C. Mösch-Zanetti, *Inorg. Chem.*, 2009, **48**, 369–374.

310 P. C. Andrews, S. M. Calleja and M. Maguire, *J. Organomet. Chem.*, 2005, **690**, 4343–4348.

311 M. A. Jacobson, I. Keresztes and P. G. Williard, *J. Am. Chem. Soc.*, 2005, **127**, 4965–4975.

312 C. Boudou, M. Bergès, C. Sagnes, J. Sopková-De Oliveira Santos, S. Perrio and P. Metzner, *J. Org. Chem.*, 2007, **72**, 5403–5406.

313 Y. Zhang, Z. Lu, A. Desai and W. D. Wulff, *Org. Lett.*, 2008, **10**, 5429–5432.

314 Z. Guo, X. Wei, H. Tong, J. Chao and D. Liu, *J. Organomet. Chem.*, 2015, **783**, 73–76.

315 Z. Guo, Q. Liu, X. Wei, Y. Zhang, H. Tong, J. Chao, J. Guo and D. Liu, *Organometallics*, 2013, **32**, 4677–4683.

316 M. Yus, F. Foubelo and L. R. Falvello, *Tetrahedron: Asymmetry*, 1995, **6**, 2081–2092.

317 D. Tilly, F. Chevallier, F. Mongin and P. C. Gros, *Chem. Rev.*, 2014, **114**, 1207–1257.

318 IEA, *Key World Energy Statistics 2016*, 2016.

319 European Commission, *Hydrogen Energy and Fuel Cells*, 2003.

320 B. Petroleum, *BP Statistical Review of World Energy*, 2016.

321 T. J. Wallington, J. L. Sullivan and M. D. Hurley, in *Meteorologische Zeitschrift*, Schweizerbart'sche Verlagsbuchhandlung, 2008, vol. 17, pp. 109–116.

322 UNECE, *1979 Convention On Long-Range Transboundary Air Pollution*, 1979.

323 J. D. Figueroa, T. Fout, S. Plasynski, H. McIlvried and R. D. Srivastava, *Int. J. Greenh. Gas Control*, 2008, 2, 9–20.

324 ICCT, *Real-world exhaust emissions from modern diesel cars*, 2014.

325 M. J. Molina and L. T. Molina, *J. Air Waste Manage. Assoc.*, 2004, **54**, 644–680.

326 VCA, Cars and air pollution, http://www.dft.gov.uk/vca/fcb/cars-and-air-pollution.asp, (accessed 25 April 2017).

327 J. Yang, A. Sudik, C. Wolverton and D. J. Siegel, *Chem. Soc. Rev.*, 2010, **39**, 656–675.

328 EVvolumes, The electric vehicle world sales database, http://www.ev-volumes.com/news/global-plug-in-sales-for-2016/, (accessed 25 April 2017).

329 W. Tahil, *Meridian Int. Res.*, 2008, 1–54.

330 C. Bertini, T. Berhan, G. Egziabher, L. Haddad, M. S. Kumar, S. L. Hendriks, A. De Janvry, R. Maluf, M. M. Aly, C. Perez, D. Castillo, R. Rabbinge, H. Tang, I. Tikhonovich, N. Wongchinda, J. Wilkinson, S. Afiff, M. Carriquiry, C. Jumbe, T. Searchinger and V. Gitz, *HLPE Project Team members Coordinator of the HLPE*, 2013.

331 Green Car Congress, Panasonic develops new higher-capacity 18650 Li-ion cells; application of silicon-based alloy in anode, http://www.greencarcongress.com/2009/12/panasonic-20091225.html, (accessed 25 April 2017).

332 L. Schlapbach and A. Züttel, *Nature*, 2001, **414**, 353–358.

333 European Commission, Cleaner urban transport with hydrogen buses, https://ec.europa.eu/programmes/horizon2020/en/news/cleaner-urban-transport-hydrogen-buses, (accessed 25 April 2017).

334 L. Shao, B. T. Low, T.-S. Chung and A. R. Greenberg, *J. Memb. Sci.*, 2009, **327**, 18–31.

335 J. D. Holladay, J. Hu, D. L. King and Y. Wang, *Catal. Today*, 2009, **139**, 244–260.

336 L. Barreto, A. Makihira and K. Riahi, *Int. J. Hydrogen Energy*, 2003, **28**, 267–284.

337 G. A. Deluga, J. R. Salge, L. D. Schmidt and X. E. Verykios, *Science*, 2004, **303**, 993–997.

338 Web of Science [v.5.24] - Result Analysis for 'hydrogen storage', http://wcs.webofknowledge.com/RA/analyze.do, (accessed 18 May 2017).

339 Hydrogen Fuel Cell Engines and Related Technologies, *Module 1: Hydrogen Properties*, 2001.

340 M. Felderhoff, C. Weidenthaler, R. von Helmolt and U. Eberle, *Phys. Chem. Chem. Phys.*, 2007, **9**, 2643.

341 A. F. Dalebrook, W. Gan, M. Grasemann, S. Moret and G. Laurenczy, *Chem. Commun.*, 2013, **49**, 8735.

342 R. von Helmolt and U. Eberle, *J. Power Sources*, 2007, **165**, 833–843.

343 Washington State University, Hydrogen Properties for Energy Research (HYPER) Laboratory, https://hydrogen.wsu.edu/hydrogen-storage/, (accessed 3 May 2017).

344 M. Ardenne, G. Musiol and U. Klemradt, *Effekte der Physik und ihre Anwendungen*, Deutsch, 2005, vol. 3.

345 C. R. Baker and R. L. Shaner, *Int. J. Hydrogen Energy*, 1978, **3**, 321–334.

346 L. J. Murray, M. Dinca and J. R. Long, *Chem. Soc. Rev.*, 2009, **38**, 1294–1314.

347 A. C. Dillon, K. M. Jones, T. a. Bekkedahl, C. H. Kiang, D. S. Bethune and M. J. Heben, *Nature*, 1997, **386**, 377–379.

348 M. Hirscher, M. Becher, M. Haluska, U. Dettlaff-Weglikowska, A. Quintel, G. S. Duesberg, Y.-M. Choi, P. Downes, M. Hulman, S. Roth, I. Stepanek and P. Bernier, *Appl. Phys. A Mater. Sci. Process.*, 2001, **72**, 129–132.

349 M. G. Nijkamp, J. E. M. J. Raaymakers, A. J. Van Dillen and K. P. De Jong, *Appl. Phys. A*, 2001, **72**, 619–623.

350 R. Ströbel, J. Garche, P. T. Moseley, L. Jörissen and G. Wolf, *J. Power Sources*, 2006, **159**, 781–801.

351 G. Férey, *Chem. Soc. Rev.*, 2008, **37**, 191–214.

352 S. S. Kaye, A. Dailly, O. M. Yaghi and J. R. Long, *J. Am. Chem. Soc.*, 2007, **129**, 14176–14177.

353 A. Züttel, *Naturwissenschaften*, 2004, **91**, 157–172.

354 B. Bogdanović and M. Schwickardi, *J. Alloys Compd.*, 1997, **253–254**, 1–9.

355 B. Sakintuna, F. Lamaridarkrim and M. Hirscher, *Int. J. Hydrogen Energy*, 2007, **32**, 1121–1140.

356 A. Steinfeld, *Int. J. Hydrogen Energy*, 2002, **27**, 611–619.

357 W. H. Johnson, *Proc. R. Soc. London*, 1874, **23**, 168–179.

358 J. Song and W. A. Curtin, *Nat. Mater.*, 2012, **12**, 145–151.

359 A. DeQuasie, *The green flame : surviving government secrecy*, American Chemical Society, 1991.

360 H. I. Schlesinger and H. C. Brown, *J. Am. Chem. Soc.*, 1953, **75**, 219–221.

361 H. I. Schlesinger, H. C. Brown, J. R. Gilbreath and J. J. Katz, *J. Am. Chem. Soc.*, 1953, **75**, 195–199.

362 H. I. Schlesinger, H. C. Brown and E. K. Hyde, *J. Am. Chem. Soc.*, 1953, **75**, 209–213.

363 H. I. Schlesinger, H. C. Brown, A. E. Finholt, J. R. Gilbreath, H. R. Hoekstra and E. K. Hyde, *J. Am. Chem. Soc.*, 1953, **75**, 215–219.

364 D. J. Heldebrant, A. Karkamkar, J. C. Linehan and T. Autrey, *Energy Environ. Sci.*, 2008, **1**, 156.

365 P. Wang and X. Kang, *Dalt. Trans.*, 2008, 5400.

366 M. E. Bluhm, M. G. Bradley, R. Butterick, U. Kusari and L. G. Sneddon, *J. Am. Chem. Soc.*, 2006, **128**, 7748–7749.

367 D. W. Himmelberger, W. Y. Chang, M. E. Bluhm, P. J. Carroll and L. G. Sneddon, *J. Am. Chem. Soc.*, 2009, **131**, 14101–14110.

368 C. W. Hamilton, R. T. Baker, A. Staubitz and I. Manners, *Chem. Soc. Rev.*, 2009, **38**, 279–93.

369 NREL, *Go/No-Go Recommendation for Sodium Borohydride for On-Board Vehicular Hydrogen Storage: Independent Review*, 2007.

370 N. J. Hess, G. K. Schenter, M. R. Hartman, L. L. Daemen, T. Proffen, S. M. Kathmann, C. J. Mundy, M. Hartl, D. J. Heldebrant, A. C. Stowe and T. Autrey, , DOI:10.1021/jp900839c.

371 R. Hoffmann, *J. Chem. Phys.*, 1964, **40**, 2474–2480.

372 H. Nöth and H. Beyer, *Chem. Ber.*, 1960, **93**, 928–938.

373 M. F. Hawthorne, *J. Am. Chem. Soc.*, 1961, **83**, 831–833.

374 M. F. Hawthorne, *J. Am. Chem. Soc.*, 1961, **83**, 833–834.

375 United States Geological Survey, *BORON [ADVANCE RELEASE]*, US DOI & GS, 2015.

376 Boren - National Boron Research Institute, Boron Production, http://www.boren.gov.tr/en/boron/production-of-boron, (accessed 1 June 2017).

377 A. G. W. Cameron, *Space Sci. Rev.*, 1973, **15**, 121–146.

378 N. N. Greenwood and A. Earnshaw, *Chemistry of the elements*, Butterworth-Heinemann, 2nd edn., 1997.

379 ETİ MINE, *TURKEY AS THE GLOBAL LEADER IN BORON EXPORT*, 2013.

380 T. W. Graham, C. W. Tsang, X. Chen, R. Guo, W. Jia, S. M. Lu, C. Sui-Seng, C. B. Ewart, A. Lough, D. Amoroso and K. Abdur-Rashid, *Angew. Chemie - Int. Ed.*, 2010, **49**, 8708–8711.

381 M. Chandra and Q. Xu, *J. Power Sources*, 2006, **156**, 190–194.

382 A. Staubitz, A. P. M. Robertson and I. Manners, *Chem. Rev.*, 2010, **110**, 4079–4124.

383 S. Bhunya, T. Malakar, G. Ganguly and A. Paul, *ACS Catal.*, 2016, **6**, 7907–7934.

384 G. Wolf, J. Baumann, F. Baitalow and F. . Hoffmann, *Thermochim. Acta*, 2000, **343**, 19–25.

385 M. G. Hu, R. A. Geanangel and W. W. Wendlandt, *Thermochim. Acta*, 1978, **23**, 249–255.

386 A. C. Stowe, W. J. Shaw, J. C. Linehan, B. Schmid and T. Autrey, *Phys. Chem. Chem. Phys.*, 2007, **9**, 1831.

387 M. Bowden, T. Autrey, I. Brown and M. Ryan, *Curr. Appl. Phys.*, 2008, **8**, 498–500.

388 R. A. Geanangel and W. W. Wendlandt, *Thermochim. Acta*, 1987, **113**, 383–385.

389 W. J. Shaw, J. C. Linehan, N. K. Szymczak, D. J. Heldebrant, C. Yonker, D. M. Camaioni, R. T. Baker and T. Autrey, *Angew. Chemie - Int. Ed.*, 2008, **47**, 7493–7496.

390 J. F. Kostka, R. Schellenberg, F. Baitalow, T. Smolinka and F. Mertens, *Eur. J. Inorg. Chem.*, 2012, 49–54.

391 R. Waterman, *Chem. Soc. Rev.*, 2013, **42**, 5621–5980.

392 C. A. Jaska, K. Temple, A. J. Lough and I. Manners, *Chem. Commun.*, 2001, 962–963.

393 M. C. Denney, V. Pons, T. J. Hebden, D. M. Heinekey and K. I. Goldberg, *J. Am. Chem. Soc.*, 2006, **128**, 12048–12049.

394 I. Göttker-Schnetmann, P. White and M. Brookhart, *J. Am. Chem. Soc.*, 2004, **126**, 1804–1811.

395 C. A. Jaska and I. Manners, *J. Am. Chem. Soc.*, 2004, **126**, 9776–9785.

396 A. Paul and C. B. Musgrave, *Angew. Chemie - Int. Ed.*, 2007, **46**, 8153–8156.

397 T. J. Clark, C. A. Russell and I. Manners, *J. Am. Chem. Soc.*, 2006, **128**, 9582–9583.

398 R. J. Keaton, J. M. Blacquiere and R. T. Baker, *J. Am. Chem. Soc.*, 2007, **129**, 1844–1845.

399 D. Enders, K. Breuer, G. Raabe, J. Runsink, J. H. Teles, J. -P Melder, K. Ebel and S. Brode, *Angew. Chemie Int. Ed. English*, 1995, **34**, 1021–1023.

400 A. Rossin and M. Peruzzini, *Chem. Rev.*, 2016, **116**, 8848–8872.

401 V. Pons, R. T. Baker, N. K. Szymczak, D. J. Heldebrant, J. C. Linehan, M. H. Matus, D. J. Grant and D. A. Dixon, *Chem. Commun.*, 2008, 6597.

402 H. A. Kalviri, F. Gärtner, G. Ye, I. Korobkov and R. T. Baker, *Chem. Sci.*, 2015, **6**, 618–624.

403 N. Blaquiere, S. Diallo-Garcia, S. I. Gorelsky, D. A. Black and K. Fagnou, *J. Am. Chem. Soc.*, 2008, **130**, 14034–14035.

404 M. Käß, A. Friedrich, M. Drees and S. Schneider, *Angew. Chemie - Int. Ed.*, 2009, **48**, 905–907.

405 B. L. Conley and T. J. Williams, *Chem. Commun.*, 2010, **46**, 4815.

406 M. A. Esteruelas, A. M. Lopez, M. Mora and E. Onate, *ACS Catal.*, 2015, **5**, 187–191.

407 M. A. Esteruelas, P. Nolis, M. Oliván, E. Oñate, A. Vallribera and A. Vélez, *Inorg. Chem.*, 2016, **55**, 7176–7181.

408 M. E. Sloan, A. Staubitz, T. J. Clark, C. A. Russell, G. C. Lloyd-Jones and I. Manners, *J. Am. Chem. Soc.*, 2010, **132**, 3831–3841.

409 R. T. Baker, J. C. Gordon, C. W. Hamilton, N. J. Henson, P.-H. Lin, S. Maguire, M. Murugesu, B. L. Scott and N. C. Smythe, *J. Am. Chem. Soc.*, 2012, **134**, 5598–5609.

410 A. Gluer, M. Forster, V. R. Celinski, J. Schmedt auf der G?nne, M. C. Holthausen and S. Schneider, *ACS Catal.*, 2015, **5**, 7214–7217.

411 T.-P. Lin and J. C. Peters, *J. Am. Chem. Soc.*, 2013, **135**, 15310–15313.

412 S. Todisco, L. Luconi, G. Giambastiani, A. Rossin, M. Peruzzini, I. E. Golub, O. A. Filippov, N. V Belkova and E. S. Shubina, *Inorg. Chem.*, 2017, **56**, 4296–4307.

413 Z. Tang, X. Chen, H. Chen, L. Wu and X. Yu, *Angew. Chemie - Int. Ed.*, 2013, **52**, 5832–5835.

414 M. M. Hansmann, R. L. Melen and D. S. Wright, *Chem. Sci.*, 2011, **2**, 1554.

415 H. J. Cowley, M. S. Holt, R. L. Melen, J. M. Rawson and D. S. Wright, *Chem. Commun.*, 2011, **47**, 2682–2684.

416 Z. Lu, L. Schweighauser, H. Hausmann and H. A. Wegner, *Angew. Chemie - Int. Ed.*, 2015, **54**, 15556–15559.

417 Z. Z. Fang, P. Wang, T. E. Rufford, X. D. Kang, G. Q. Lu and H. M. Cheng, *Acta Mater.*, 2008, **56**, 6257–6263.

418 A. J. M. Miller and J. E. Bercaw, *Chem. Commun.*, 2010, **46**, 1709.

419 A. M. Chapman, M. F. Haddow and D. F. Wass, *J. Am. Chem. Soc.*, 2011, **133**, 8826–8829.

420 M. Klahn, D. Hollmann, A. Spannenberg, A. Bruckner and T. Beweries, *Dalt. Trans.*, 2015, **44**, 12103–12111.

421 X. Kang, L. Ma, Z. Fang, L. Gao, J. Luo, S. Wang and P. Wang, *Phys. Chem. Chem. Phys.*, 2009, **11**, 2507.

422 H. V. K. Diyabalanage, R. P. Shrestha, T. A. Semelsberger, B. L. Scott, M. E. Bowden, B. L. Davis and A. K. Burrell, *Angew. Chemie - Int. Ed.*, 2007, **46**, 8995–8997.

423 R. McLellan, A. R. Kennedy, S. A. Orr, S. D. Robertson and R. E. Mulvey, *Angew. Chemie - Int. Ed.*, 2017, **56**, 1036–1041.

424 P. Bellham, M. S. Hill and G. Kociok-Köhn, *Dalt. Trans.*, 2015, **44**, 12078–12081.

425 A. Harinath, S. Anga and T. K. Panda, *RSC Adv.*, 2016, **6**, 35648–35653.

426 R. A. Geanangel and W. W. Wendlandt, *Thermochim. Acta*, 1985, **86**, 375–378.

427 V. S. Nguyen, M. H. Matus, D. J. Grant, M. T. Nguyen and D. A. Dixon, *J. Phys. Chem. A*, 2007, **111**, 8844–8856.

428 A. Staubitz, M. Besora, J. N. Harvey and I. Manners, *Inorg. Chem.*, 2008, **47**, 5910–5918.

429 S. Hausdorf, F. Baitalow, G. Wolf and F. O. R. L. Mertens, *Int. J. Hydrogen Energy*, 2008, **33**, 608–614.

430 R. V. Orye and J. M. Prausnitz, *Ind. Eng. Chem.*, 1965, **57**, 18–26.

431 G. Brauer, *Handbuch der Präparativen Anorganischen Chemie*, Band 2., 1978.

432 C. Reller and F. O. R. L. Mertens, *Angew. Chemie - Int. Ed.*, 2012, **51**, 11731–11735.

433 Z. Huang and T. Autrey, *Energy Environ. Sci.*, 2012, **5**, 9257.

434 M. T. Mock, R. G. Potter, D. M. Camaioni, J. Li, W. G. Dougherty, W. S. Kassel, B. Twamley and D. L. DuBois, *J. Am. Chem. Soc.*, 2009, **131**, 14454–14465.

435 M. T. Mock, R. G. Potter, M. J. O'Hagan, D. M. Camaioni, W. G. Dougherty, W. S. Kassel and D. L. DuBois, *Inorg. Chem.*, 2011, **50**, 11914–11928.

436 P. V. Ramachandran and P. D. Gagare, *Inorg. Chem.*, 2007, **46**, 7810–7817.

437 A. D. Sutton, B. L. Davis, K. X. Bhattacharyya, B. D. Ellis, J. C. Gordon and P. P. Power, *Chem. Commun.*, 2010, **46**, 148–149.

438 B. L. Davis, D. A. Dixon, E. B. Garner, J. C. Gordon, M. H. Matus, B. Scott and F. H. Stephens, *Angew. Chemie - Int. Ed.*, 2009, **48**, 6812–6816.

439 P. G. Jessop, F. Joó and C.-C. Tai, *Coord. Chem. Rev.*, 2004, **248**, 2425–2442.

440 A. D. Sutton, A. K. Burrell, D. A. Dixon, E. B. Garner, J. C. Gordon, T. Nakagawa, K. C. Ott, J. P. Robinson and M. Vasiliu, *Science*, 2011, **331**, 1426–1429.

441 J.-P. Schirmann and P. Bourdauducq, in *Ullmann's Encyclopedia of Industrial Chemistry*, Wiley-VCH Verlag GmbH & Co. KGaA, Weinheim, Germany, 2001.

442 H. Williams, 2016, Personal Communication.

443 A. Preetz, H.-J. Drexler, C. Fischer, Z. Dai, A. Börner, W. Baumann, A. Spannenberg, R. Thede and D. Heller, *Chem. - A Eur. J.*, 2008, **14**, 1445–1451.

444 A. A. Mikhailine, M. I. Maishan, A. J. Lough and R. H. Morris, *J. Am. Chem. Soc.*, 2012, **134**, 12266–12280.

445 N. Takenaka, A. Ueda, T. Daimon, H. Bandow, T. Dohmaru and Y. Maeda, *J. Phys. Chem.*, 1996, **100**, 13874–13884.

446 J. C. Ma and D. A. Dougherty, *Chem. Rev.*, 1997, **97**, 1303–1324.

447 P. Bellham, M. S. Hill and G. Kociok-Köhn, *Organometallics*, 2014, **33**, 5716–5721.

448 G. B. Deacon, P. C. Junk and R. P. Kelly, *Aust. J. Chem.*, 2013, **66**, 1288–1296.

449 C. Reichardt, *Solvents and Solvent Effects in Organic Chemistry*, Wiley-VCH Verlag GmbH & Co. KGaA, Weinheim, FRG, 2002.

450 J. Catalán, V. López, P. Pérez, R. Martin-Villamil and J.-G. Rodríguez, *Liebigs Ann.*, 1995, **1995**, 241–252.

451 Y. Sarazin, M. Schormann and M. Bochmann, *Organometallics*, 2004, **23**, 3296–3302.

452 A. Staubitz, M. E. Sloan, A. P. M. Robertson, A. Friedrich, S. Schneider, P. J. Gates, I. Manners and J. Schmedt auf der Guenne, *J. Am. Chem. Soc.*, 2010, **132**, 13332–13345.

453 M. E. Sloan, A. Staubitz, T. J. Clark, C. A. Russell, G. C. Lloyd-Jones and I. Manners, *J. Am. Chem. Soc.*, 2010, **132**, 3831–3841.

454 R. R. Gupta and M. D. Lechner, Eds., *Chemical Shifts and Coupling Constants for Boron-11 and Phosphorus-31*, Springer-Verlag, Berlin/Heidelberg, 1997, vol. 35A.

455 D. F. Shriver and M. A. Drezdzon, *The manipulation of air-sensitive compounds*, Wiley, 2nd edn., 1986.

456 C. R. McLlwrick and C. S. Phillips, *J. Phys. E.*, 1973, **6**, 1208–1210.

457 R. D. Rieke and S. E. Bales, *J. Chem. Soc. Chem. Commun.*, 1973, 879.

458 R. D. Rieke, P. T.-J. Li, T. P. Burns and S. T. Uhm, *J. Org. Chem.*, 1981, **46**, 4323–4324.

459 B. Bogdanovic, *Acc. Chem. Res.*, 1988, **21**, 261–267.

460 L. D. Freedman and G. O. Doak, *Chem. Rev.*, 1982, **82**, 15–57.

461 N. A. Yakelis and R. G. Bergman, *Organometallics*, 2005, **24**, 3579–3581.

462 M. L. Hays, T. P. Hanusa and T. A. Nile, *J. Organomet. Chem.*, 1996, 514, 73–79.

463 J. Cosier and A. M. Glazer, *J. Appl. Crystallogr.*, 1986, **19**, 105–107.

464 CrysAlisPRO, *Oxford Diffr. /Agilent Technol. UK Ltd, Yarnton, England.*

465 O. V. Dolomanov, L. J. Bourhis, R. J. Gildea, J. A. K. Howard and H. Puschmann, *J. Appl. Crystallogr.*, 2009, **42**, 339–341.

466 G. M. Sheldrick, *Acta Cryst*, 2015, **71**, 3–8.

467 G. M. Sheldrick, *Acta Crystallogr. Sect. A Found. Crystallogr.*, 2008, **64**, 112–122.

468 http://checkcif.iucr.org/.

469 P. L. Watson, *J. Am. Chem. Soc.*, 1983, **105**, 6491–6493.

470 R. Waterman, *Organometallics*, 2013, **32**, 7249–7263.

471 S. Harder and D. Naglav, *Eur. J. Inorg. Chem.*, 2010, **2010**, 2836–2840.

472 H. P. Fritz, *Angew. Chemie*, 1989, **101**, 810–810.

473 J. A. McCleverty and T. J. Meyer, *Comprehensive coordination chemistry II: from biology to nanotechnology*, Elsevier Pergamon, 2004.

474 S. Youssif, *Arkivoc*, 2001, 242.

475 B. Lecointre, R. Azzouz and L. Bischoff, *Tetrahedron Lett.*, 2014, **55**, 1913–1915.

476 M. Vamos and N. D. P. Cosford, *J. Org. Chem.*, 2014, **79**, 2274–2280.

477 J. Yin, B. Xiang, M. A. Huffman, C. E. Raab and I. W. Davies, *J. Org. Chem.*, 2007, **72**, 4554–4557.

478 J. A. S. C. J. Woltermann, *Fine Chem.*, 2002, 5–8.

479 P. Gros, S. Choppin, J. Mathieu and Y. Fort, *J. Org. Chem.*, 2002, **67**, 234–237.

480 G. Berthon-Gelloz, M. A. Siegler, A. L. Spek, B. Tinant, J. N. H. Reek and I. E. Markó, *Dalt. Trans.*, 2010, **39**, 1444–1446.

481 D. A. Straus, C. Zhang and T. D. Tilley, *J. Organomet. Chem.*, 1989, **369**, C13–C17.

482 R. R. Fraser, T. S. Mansour and S. Savard, *J. Org. Chem.*, 1985, **50**, 3232–3234.

483 M. Harmata, in *Encyclopedia of Reagents for Organic Synthesis*, John Wiley & Sons, Ltd, Chichester, UK, 2001.

484 A. M. Boesgaard and G. Steigman, *Annu. Rev. Astron. Astrophys.*, 1985, **23**, 319–378.

485 H. Reeves, *Annu. Rev. Astron. Astrophys.*, 1974, **12**, 437–470.

486 H. Reeves, *Rev. Mod. Phys.*, 1994, **66**, 193–216.

487 K. Croswell, *New Sci.*, 1991, 132.

488 E. M. Leitao, T. Jurca and I. Manners, *Nat. Chem.*, 2013, **5**, 817–29.

489 R. L. Melen, *Chem. Soc. Rev.*, 2016, **45**, 775–788.

490 US Pat., 4.801.439, 1989.

491 A. Friedrich, M. Drees and S. Schneider, *Chem. - A Eur. J.*, 2009, **15**, 10339–10342.

492 H. Dorn, R. A. Singh, J. A. Massey, J. M. Nelson, C. A. Jaska, A. J. Lough and I. Manners, *J. Am. Chem. Soc.*, 2000, **122**, 6669–6678.